JOURNAL OF CONDENSED MATTER NUCLEAR SCIENCE

Experiments and Methods in Cold Fusion

VOLUME 9, September 2012

JOURNAL OF CONDENSED MATTER NUCLEAR SCIENCE

Experiments and Methods in Cold Fusion

JOURNAL OF CONDENSED MATTER NUCLEAR SCIENCE

Volume 9, September 2012

 ISSN 2227-3123

Orders, claims, author inquiries and journal inquiries

Please contact the Editor in Chief, CMNSEditor@iscmns.org or webmaster@iscmns.org

J. Condensed Matter Nucl. Sci. 9 (2012) 1–127
 ISSN 2227-3123

JOURNAL OF CONDENSED MATTER NUCLEAR SCIENCE

Volume 9 2012

CONTENTS

PREFACE

This is the ninth volume of the *Journal of Condensed Matter Nuclear Science*. I am very happy that the pace of publication of new volumes is increasing steadily with more quality papers. This is a good indication that the field is growing faster. This new volume comprises nine papers of major importance.

As the editor-in-chief of the journal, I have to make some decisions regarding the quality of the papers. However, sometimes, it is difficult to decide when there is a disagreement between the author and the referee. It seemed to me wiser to let the reader make his own opinion. In this volume I had to face two such situations.

On one side, Edmund Storms proposes "An explanation of Low-energy Nuclear Reactions" based on a review of the experimental facts observed so far. This is not a theoretical model per se, but anyway, it is an interesting approach to the field. The referee had objections about the paper, but it appeared to me that it would be nonetheless worthwhile to publish it as such and let other readers criticize the work, by sending comments that will be published in another volume of the journal.

On the other site the paper "Are Ni + H Nuclear Reactions Possible" by Akito Takahashi was not accepted as such by the referee. After many exchanges between the author and the referee, we took together the decision to publish the paper along with the comments of the referee and the responses of the author in an appendix. This is not the usual way of publications in scientific journals, but it seemed to me that this exchange of points of view will enrich the debate amongst theoreticians.

Jean-Paul Biberian
September 2012

J. Condensed Matter Nucl. Sci. 9 (2012) 1–9

Research Article

Study on the Phenomenon Reported "Neutron Generation at Room Temperature in a Cylinder Packed with Titanium Shavings and Pressurized Deuterium Gas" (2)

Takayoshi Asami *

Research Institute of Innovative Technology for the Earth (retired), 9-2 Kizugawadai, Kizu-cho, Soraku-gun, Kyoto 619-0292, Japan

Noriaki Sano

Department of Chemical Engineering, Graduate School of Engineering, Kyoto University, Katsura, Nishikyo-Ku, Kyoto, 615-8510, Japan

Abstract

Following the previous study of the state of deuterium atoms in the titanium crystal (*J. Condensed Matter Nucl. Sci.* **5** (2011) 7), in this paper, the authors have analyzed the state of the deuterium atom in a tetrahedron cage, using the first principle molecular orbital calculation. In the simulation analysis of the tetrahedron cage, it is indicated that the titanium pair causes the deuterium atom to have ligancy 2 in the cage with two hydrogen atoms. If neutron generation occurs, we can deduce from the past experimental results that it occurs after a small increase of kinetic energy of deuterium atoms. This suggests that the quantity of neutron generated may increase if we can give kinetic energy to the adsorbed deuterium atoms in the titanium crystal by another means other than a temperature rise, at a suitable temperature and pressure. The authors propose a new experimental apparatus which appears to promote and increase the neutron generation.
 ISSN 2227-3123

Keywords: Deuterium, Neutron generation, Proposed apparatus, Tetrahedron cage, Titanium

1. Introduction

In the previous paper [1], the author studied the experiment of neutron generation, using titanium shavings and deuterium gas packed in a cylinder [2,3], taking into account the factors which are related to it and the example of the first principle molecular orbital calculation.

Following the previous study of the state of deuterium atoms in the titanium crystal, the authors have here intended to study the state of deuterium atoms in the tetrahedron cage of titanium crystal and to analyze its mechanism mainly

*E-mail: takaysami@yahoo.co.jp

 ISSN 2227-3123

based on the first principle molecular orbital calculation. Furthermore, the method to promote the neutron generation is studied.

2. Assumed Tetrahedron Cage Model of Titanium Crystal with the Deuterium Atom

It is said that one of the locations where a deuterium atom is able to be located under suitable conditions is in the tetrahedral interstice. To study the state of the deuterium atom in the tetrahedron cage in detail, the electronic structure of the titanium–hydrogen (Ti–H) cluster models instead of titanium–deuterium (Ti–D) cluster models have been studied by the first principle molecular orbital calculation. It seems that the calculation results of both of these are almost the same and the convergence in the calculation of the former case is faster than that of the latter case.

Prepared cluster models are as follows.

The first is a regular tetrahedron cluster model (hereafter referred to as "model 1") indicated in Fig. 1 and the second is a cluster model which is composed of the tetrahedron cluster surrounded by minimum titanium atoms (hereafter referred to as "model 2") indicated in Fig. 2 (a).

The following explains why model 2 was prepared. The nearest distance from the deuterium atom to any titanium atom in model 1 is of equal distance apart, providing that the location of a deuterium atom is in the center of gravity. However, as there is the possibility of influence to the Ti–H cluster by the surrounding surplus titanium atoms, model 2 has been constructed.

If we calculate the parameters, such as Mulliken atomic charge, etc., indicating the combined state between the titanium atoms and the deuterium atom, the difference in numbers of total titanium atoms by adding titanium atoms to model 1 may be revealed in the simulation result. In the actual experiment, it seems that it is almost impossible for the deuterium atom in the cage to collide and react with another deuterium atom in the other tetrahedron cage, therefore we determined to analyze models 2 and 3.

Under the specified state, the combination between titanium atoms and hydrogen atoms may indicate stable ligancy 2 in the simulation. Under this assumption, the Mulliken atomic charge value based on the Mulliken density analysis and atom–atom overlap-weighted NAO bond order (hereafter referred to as "weighted bond order") [4] calculated are indicated in the development drawings of models 2 and 3. Model 3 is the modified model 2 with a hydrogen atom just outside of the tetrahedron cage in the center of it, see Figs. 3 and 4, respectively. In these figures, each circled number indicates the named number of each atom. In Fig. 3 for the cluster model 2 and in Fig. 4 for the cluster model 3.

Estimated results regarding model 2 are indicated in Fig. 3 by numerical value. Although it seems that the distance between the deuterium atom and the nearest titanium atoms in the assumed model 3 is equal to one another, the Mulliken atomic charge value based on Mulliken density analysis (hereafter referred to as "atomic charge value") for each titanium atom is not the same. These differences in combination are observed in the parameters indicated in Figs. 3 and 4.

The simulation of the cluster model 2 indicates that the titanium atoms do not clearly cause the deuterium atom in the cage to have ligancy 2. The atomic charge values of each titanium atom in the cage become almost the same value except Ti(1) (Fig. 3). On the other hand, the atomic charge value of hydrogen is negative and its absolute value is small. It is observed that the hydrogen atom partially co-owns the electron of titanium atoms. However, in Fig. 4, as a hydrogen atom is added to the titanium atoms outside of the cage in cluster model 2, the atomic charge value of Ti(16) indicates higher values than that in Fig. 3. The atomic charge value of Ti(1) changes little and is almost equal to the value of Ti(16). As these titanium atoms cause the nearest hydrogen atoms to have ligancy 2, it seems that the atomic charge values of Ti(1) and Ti(16) will indicate higher values than those of Ti(4) and Ti(5).

Moreover, weighted bond orders, Ti(1)-H(31) and Ti(16)-H(31) become bigger compared to those indicated in Fig. 3. This suggests that the formation of the hydrogen bond in ligancy 2 is as described in our previous paper [1].

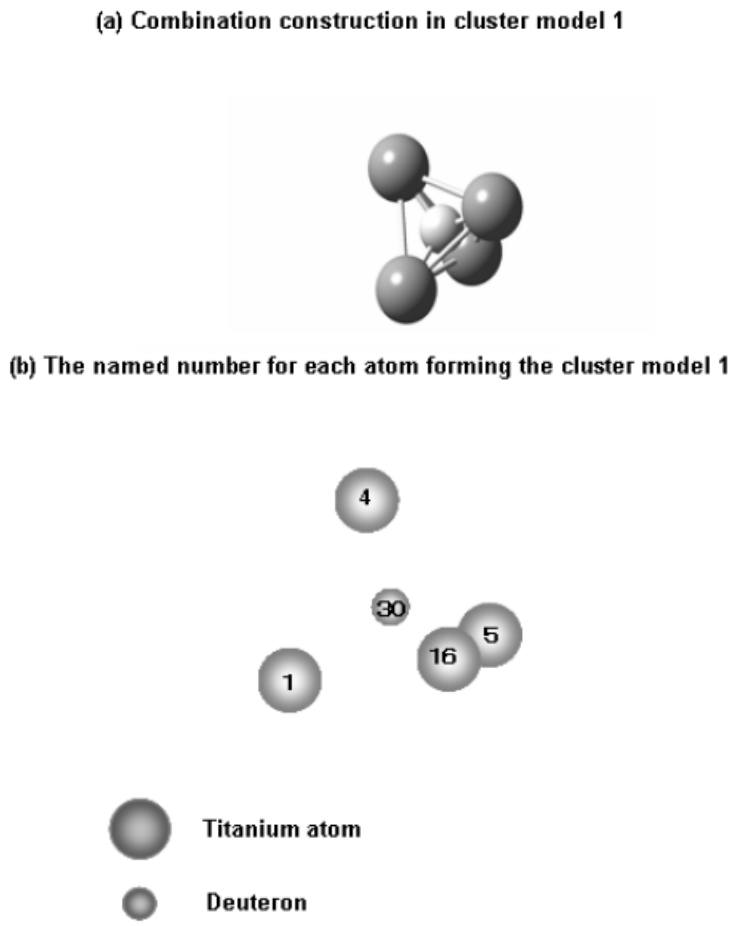

Figure 1. The cluster model 1, regular tetrahedron cage, (a) and (b).

3. The Study of the Experimental Apparatus to Cause Promotion of the Neutron Generation

From the result of the past experiments [2,3], it is observed that the conditions for neutron generation to occur are composed of the following items.

(1) Preparation of titanium shavings in the stainless steel cylinder which have fully adsorbed deuterium gas at a low temperature under a pressurized condition.
(2) About a 160–220 K temperature rise from liquid nitrogen under pressurized or evacuation condition in the above-mentioned cylinder.

Item (2) mentioned above, appears to trigger the process of neutron generation. It means an increase of kinetic energy of the deuterium atoms in the titanium crystal.

If the nuclear fusion occurs by the collision of deuterium atoms in the cage of titanium crystal, the increase of kinetic energy of the deuterium atoms adsorbed in the titanium crystal may be able to promote it and thus increase the

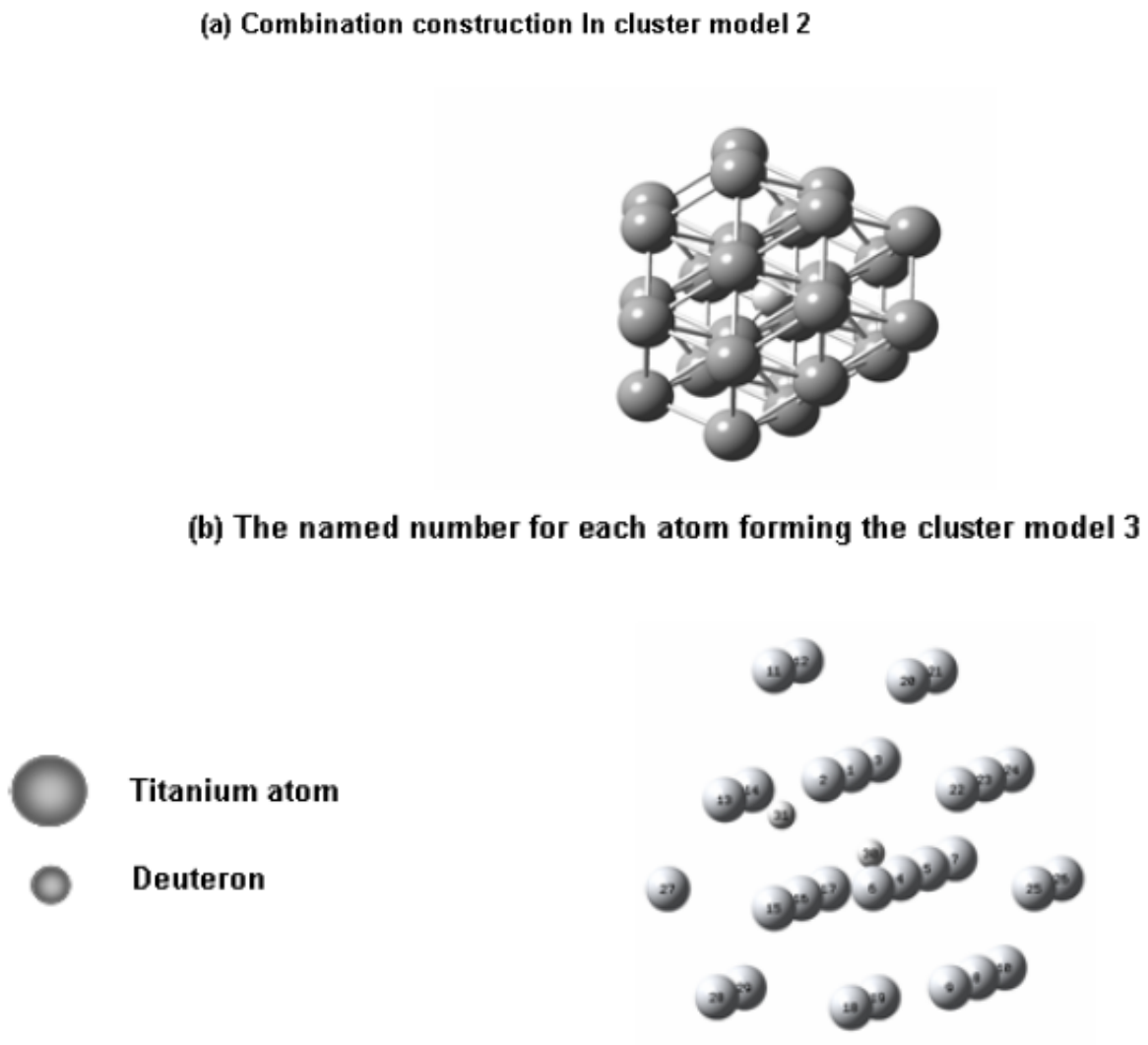

Figure 2. The cluster models 2 and 3, model 2 is the tetrahedron cage with surrounding minimum titanium atoms and a deuterium atom in it. Model 3 is the modified model 2 with a deuterium atom outside the cage, (a) and (b).

neutron generation. We intend to study the reason of neutron generation in accordance with the analogical principle compared to chemical reaction. In the chemical reaction, it is said that the factors influencing the reaction condition are temperature, pressure and the catalytic function to promote the reaction.

Regarding temperature and pressure in the experiments [2,5], the conditions of both of them are almost the same, although the operational conditions are different. The only difference between these experiments is that one occurs in the active period run by depressurizing (at desorption phase from liquid nitrogen temperature warming to room temperature) and the other occurs at warming to room temperature with pressurized condition after thawing terms and

cooling cycles.

The notable condition is that the neutron generation in both experiments always occurs at the warming term in the process after enough adsorption of deuterium gas to titanium shavings. Regarding temperature change, it is approximately a 160–220 K temperature rise from liquid nitrogen temperature, mentioned above. Also, the kinetic energy of a free deuterium atom at 80 and 300 K are 6.9 and 25.9 meV, respectively.

If such a small energy change by temperature rise makes nuclear fusion occur, we conclude that titanium atoms surrounding deuterium atoms act as an effective catalyst for nuclear fusion. Judging from the result of the first principle molecular orbital calculation indicated in Figs. 3 and 4, it seems that the combination of titanium and deuterium atoms locally form a kind of polar compound. Although titanium atoms combined to the deuterium atom can not move freely, they form local dipole (hereafter referred to as "Ti-d p-compound").

If titanium and deuterium atoms locally form a polar compound, then one of the methods to consider for utilizing the electromagnetic wave, is to increase the kinetic energy of the deuterium atoms combined to the titanium atoms in the crystal. If titanium and adsorbed deuterium atoms in titanium crystal form the local polar compound, even if it is in local portion, it seems that we can utilize the characteristics of a polar compound, therefore we can utilize the electromagnetic wave to give it the energy.

If the Ti–d p-compound is positioned in an alternating electromagnetic field, the polarization of it will occur and the deuterium atom will move following the frequency change. It seems that some portion of deuterium atoms in the combined state of ligancy 2, vibrate as if they were the swing of a pendulum in the vicinity of the axis with the two titanium atoms at both ends. Some of these atoms may then be able to enter into the cage and collide with the deuterium atom in the cage.

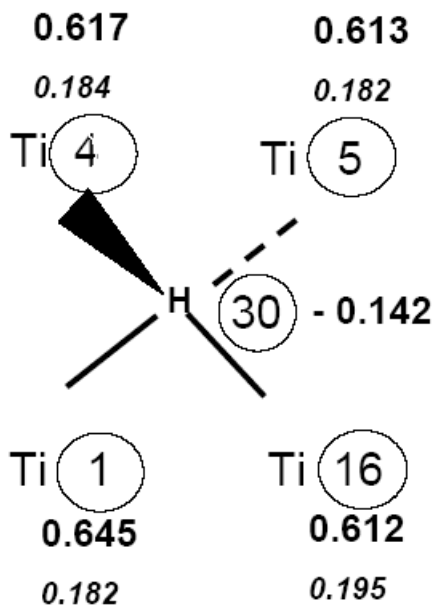

Figure 3. Atomic charge value (*bold*) and weighted bond order (*italic*) in the cluster model 2 are indicated in the development drawing of cluster model 2.

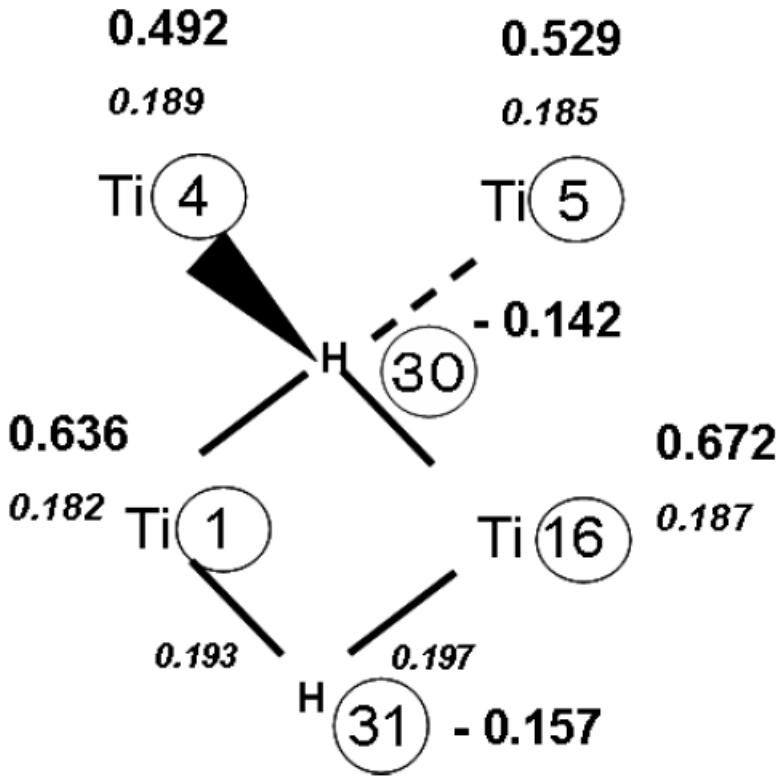

Figure 4. Atomic charge value (*bold*) and weighted bond order (*italic*) in the cluster model 3, are indicated in the development drawing of the cluster model 3. Two hydrogen atoms are located inside and outside the cage, respectively.

For example, if the direction of the electromagnetic wave is equal to the locus line from D(31) to D(30) indicated in Fig. 5, D(31) will be able to have a chance to enter into the tetrahedron cage.

The direct objective of the irradiation of the electromagnetic wave to the cylinder is not to heat the Ti–d p-compound but to increase the kinetic energy of deuterium atoms combined to titanium atoms. So the experiment by this apparatus should be executed in keeping with the planned suitable pressure and temperature condition so as not to decompose the deuterium bonds in ligancy 2. In Japan, two kinds of frequency are thought to be in accordance with the difference in the number of frequency when utilizing the electromagnetic wave. One is mainly for the use of small energy and its frequency is 2450 MHz, and the other is 915 MHz mainly for industrial use. If the deuterium atoms in Ti–d p-compound can move in the same way as hydrogen atoms in water molecules in food in microwave ovens i.e. following an alternating electromagnetic fields, we can expect an increase of kinetic energy of the deuterium atoms combined to the titanium atoms.

Although titanium atom in Ti–d p-compound cannot move as freely as that of oxygen and hydrogen atoms in a water molecule, we think that the microwave heating device mentioned above is applicable in the irradiation in the experiment, providing that the local polarization occurs in Ti–d p-compound and deuterium atoms will be able to move as hydrogen atoms in the water molecule. In treating hydrogen and deuterium gas, we think that it is important to take

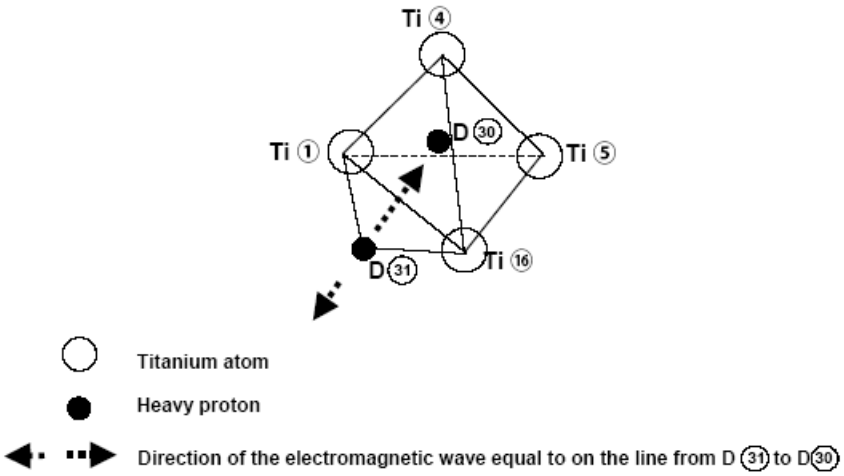

Figure 5. Preferable irradiation direction model of the electromagnetic wave.

into account of these characteristics. At low temperature, it is observed that the state of temperature equilibrium of deuterium is para form as same as that of normal hydrogen.

At temperatures below 100 K, essentially all ortho-hydrogen molecules are in the lowest ortho-rotational energy state (J: rotational quantum number, $J = 1$) and all para-hydrogen molecules are in the lowest rotational energy state ($J = 0$). The lowest ortho-state is associated with approximately 337 cal./mol more than the lowest para-state [6].

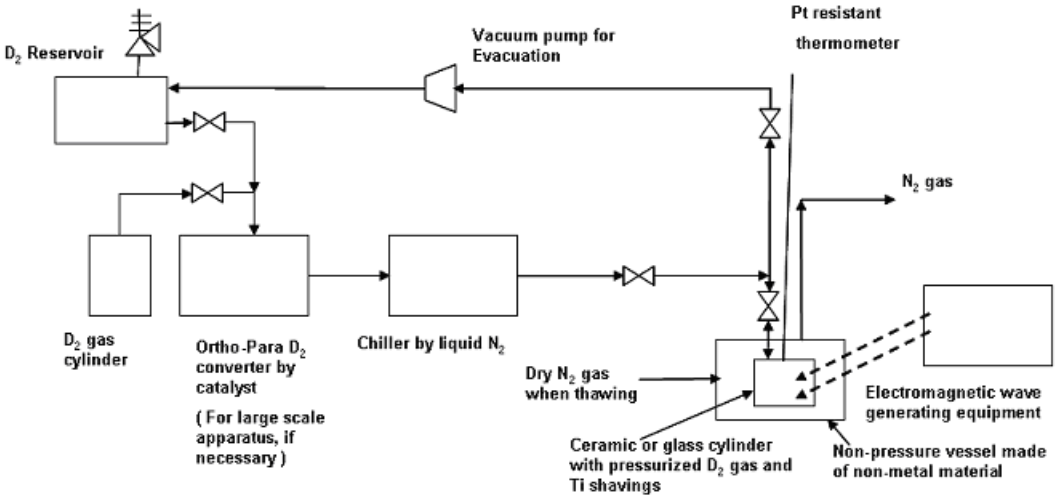

Figure 6. Block diagram of proposed neutron generation experimental apparatus.

This means that, at cryogenic temperature, this amount of energy is released as a result of the conversion of 1 mol of ortho-hydrogen to the para-form. So, to avoid the cold loss by the change of ortho–para equilibrium and to maintain the para-form, it is better to equip the ortho–para deuterium converter in the flow of a large scale apparatus. Referring to the deuterium separation apparatus by liquefied hydrogen distillation in the past, the ortho–para deuterium converter had also been equipped in the apparatus [7,8]. Taking the above into consideration, the block diagram of the proposed neutron generation experimental apparatus to increase kinetic energy of deuterium atoms is indicated in Fig. 6.

4. Discussion and Conclusion

Following the previous paper, we have simulated and intended to confirm the possibility of the existence of assumed cluster models, applying the first principle molecular orbital calculation. As a result, the cluster model 3 which has a hydrogen atom inside and outside of the cage respectively, has indicated that a titanium atom pair causes the hydrogen atom outside of the cage to have ligancy 2. In this connection, the estimated distance H(30)-H(31) in Fig. 4 is about 2.09 Å.

If the collision occurs in the tetrahedron cage, the driving force for deuterium atoms to collide may be the kinetic energy by vibration of polarized deuterium atoms in Ti–d p-compound. If the concept of room temperature nuclear fusion is correct, the observed phenomenon will also occur in an experiment from the liquid nitrogen temperature to the warming process of the deuterium adsorbed metal, which is electron deficient. It has suitable crystal construction and has adsorbed sufficient deuterium atoms.

As previously mentioned, the kinetic energy of a free deuterium atom at 300 K, the energy is about 25.9 meV. If we get the same energy quantity above mentioned by the radiation of ray, the wave length estimated by the formula based on Planck's law ($E = h\nu$) is about 48 μm. This wave length is within the range of infrared ray (0.8–1000 μm). So if we intend to utilize the electromagnetic wave in the experiment, it is preferable that its wave length should be shorter than 48 μm. By this selection of wave length, if the Ti–d p-compound is positioned in an alternating electromagnetic field, we presume that we will be able to expect from the result of past experiments both the necessary energy for the deuterium atom to collide each other and its vibration as the swing of a pendulum.

If we can give the kinetic energy under the specified low temperature and high pressure without decomposing the deuterium bonds in ligancy 2, for example by the irradiation of the electromagnetic wave, the vibration energy of the deuterium atoms combined with titanium atom in the crystal may increase and the chance of their collision in the crystal will also increase. As a result, it should make the quantity of neutron generation increase. For reference, it is necessary to take into account when irradiating in an experiment, that the efficiency of the microwave heating device to input electric energy is about 15%.

At present, we cannot theoretically estimate the necessary equivalent electromagnetic energy to generate the neutron per unit deuterium gas quantity in the specified condition. However, we deduce that the condition to generate neutrons is as follows. First, we should make the repulsion barrier around the deuterium nuclei thin by the nearer influence of the outer surrounding electrons under the low temperature and high pressure without destroying the titanium crystal lattice and deuterium bonds in ligancy 2.

Secondly, to prepare the condition of a non-equilibrium state by giving energy from the outer side. We think that one of the more effective means to prepare this condition than simple warming, is to irradiate the electromagnetic waves under the low temperature and high pressure and the reproducibility of the neutron generation in the experiment will be also improved. The authors would like to further analyze other suitable cluster models for nuclear fusion reaction.

Addendum

In the preparation of titanium shavings, it is preferable to shave the titanium bar or plate using a sharp-edged tool in a glove-box sealed by argon gas. The prepared titanium shavings should be packed in a ceramic or special glass cylinder without ever contacting air. This is to prevent titanium oxide from forming on the surface of the titanium shavings. According to the author's experience of titanium plate welding, there are major workmanship differences in the standard of welded seams between shaved plate surfaces and unshaved plate surfaces. Please note that the cylinder packed with titanium shavings should be made of ceramic or special glass when we irradiate the electromagnetic wave to the cylinder in the experiment, as a metal plate reflects the electromagnetic wave.

It is preferable to use nonmagnetic materials in the fabrication of all the equipment and apparatus. This is to prevent the converted para-deuterium form from changing to the ortho-deuterium form. It is also preferable that the design pressure of all the parts of the experimental apparatus is designed in a maximum working pressure. This is to simplify the flow of apparatus and to be able to decrease the total number of fittings.

If we intend to prepare the experimental apparatus, we think that there are several ideas in planning the part of the electromagnetic wave irradiation. In the other simple experiment, there is the example in which the simply altered microwave oven on the market is used for the irradiation of microwave [9].

References

[1] T, Asami, *J. Condensed Matter Nucl. Sci.* **5** (2011) 7–16.

[2] A. De Ninno, A. Frattolillo, G. Lollobattista, L. Martinis, M. Martone, L. Mori, S. Podda and F. Scaramuzzi, Evidence of emission of neutrons from a Titanium–deuterium System, *Europhys. Lett.* **9**(3) (1989) 221–224, ENEA, Dipartimento TIB, U.S. Fisica Applicata, Centro Ricerche Energia Frascati, C.P. 65-00044 Frascati, Rome, Italy, 1st June (1989).

[3] A. De Ninno, F. Scaramuzzi, ENEA-Area Energia e Innovazione, Dip. Sviluppo Tecnologie di Punta, Centro Ricerche Energia Frascati, CP 65, I-00044 Frascati, Italy, *AIP Conference Proceedings*, Vol. 228, Anomalous Nuclear Effects in Deuterium/Solid Systems, PROVO, UT (1990) (*Emission of Neutron Bursts from a Titanium–deuterium Gas System in a High-efficiency Low-background Experimental Setup*), pp. 122–129.

[4] Y. Wasada and H. Wasada, Molecular orbital calculation program Gaussian 03 (Bunshi-kidohohkeisan puroguramu Gaussian 03), *Information Technology Center News*, Nagoya university **7**(1) (2008) 72–87.

[5] H.O. Menlove, M.M. Fowler, E. Garcia, A. Mayer, M.C. Miller, R.R. Ryan (Los Alamos National Laboratory) and S.E. Jones (Bringham Young University), Highlights of Papers Presented at the Workshop on Cold Fusion Phenomena, The Measurement of Neutron Emissions from Ti plus D_2 Gas , Santa Fe, New Mexico, May 23–25 (1989), p. 13.

[6] G.E. Schmauch, J.F. Kucirka and R.G. Clark, Activity data on improved para–ortho conversion catalysts, Air Products and Chemicals Inc., Allentown, Penn., *Chem. Eng. Progress* **59**(8) (1963) 55–60.

[7] Helmuth Hausen and Hermann Linde, Tieftemperaturtechnik Erzeugung sehr tiefer Temperaturen, *Gasverfluissigung und Zerlegung von Gasgemischen, Zweite, voellig neubearbeitete Auflage*, Springer-Verlag, Berlin, Heidelberg, New York, Tokyo (1985) pp, 436–439.

[8] F. Schmeissner and z.Z. Europaedishe Organsation fuir Kernforschung (CERN) in Genf, und W. Wiedemann Kommission fuir Tieftemperaturforschung der Bayerischen Akademie der Wissenschaften, Muinchen, Wasserstoff-verfluissigungsanlage fuir Laboratoriumszwecke mit ortho-para-umwandlung, Kaeltetechnik, 14 Jahrgang, Heft **9** (1962) 270–273.

[9] M. Suzaki, K. Hayashi and H. Ueda, (Osaka Prefecture University College of Technology), Development of Temperature-Controlled Microwave Heating Method and its Application to Crystal Growth of $CuGaSe_2$, *Oyobutsurigaku-kankeirengokai Conference Proceedings*, Vol. 52, No. 3, JST data No. Y0054A, March 29 (2005), p. 1626.

J. Condensed Matter Nucl. Sci. 9 (2012) 10–20

Research Article

Instrumentation Relevant to Electrochemical Measurements in Condensed Matter Nuclear Reactions

John O'M Bockris *

10515 SW 55th Place, Gainesville, FL 32608, USA

Abstract

The typical electrochemical cell consists of four potentials. One of these is spurious: it should be eliminated from the measurement. A method of doing this is described. The major recommendation is that a third or, so called reference electrode, should be involved in all measurements from which structural information is to be taken from the working electrode. This is then attached to the reference electrode and a high resistance volt meter measures the potential of the working electrode with respect to the reference electrode. Alternative reference electrodes are described.
 ISSN 2227-3123

Keywords: Anode, Cells, Cathode, IR Drop, Potentiostat

1. Introduction

One of the instruments involved in investigating condensed matter nuclear reactions is the electrochemical cell. Fleischmann and Pons [1], my group of electrochemists in Texas A&M University [2], and work going on in Los Alamos National Laboratory under Ed Storms [3], were the first works to identify a specific nuclear reaction in the cold: they all used electrochemical cells.

About 100 physicists stumbled about in 1989 trying to respond to an edict put out by the head of DOE (Admiral Watkins) who told those who were interested in nuclear reactions from his department, that they should be present at a meeting in Sante Fe May 23–25, 1989 [4].

Nigel Packham, in my group at Texas A&M, was the first to report that his electrolytic vessel had given tritium in August 4, 1989 [4]. A very active group at Bhabha Atomic Research in India with more than 50 people working on it [5], also obtained tritium in 1989. Ed Storms and Carol Talcott at Los Alamos National Laboratory published a detailed study of tritium evolution in 1991 [5].

In 2011, it was discovered that Speri and Zorzi [6], two Italian engineers, had received an Italian patent for producing nuclear reactions from D which they considered was present in the hydrocarbons with which they were working (spark

*E-mail: jbockris@cox.net

 ISSN 2227-3123

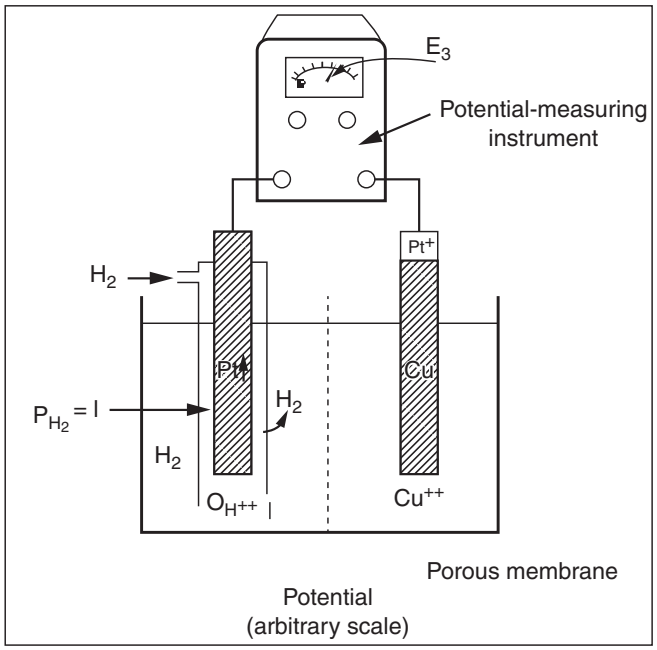

Figure 1. A galvanic cell composed of a copper electrode in cupric ion solution and a standard hydrogen electrode (a) gives a measurable potential difference E_3 (b). (From *Modern Electrochemistry,* Vol. IIA, 2000, Plenum, New York.)

effect causing explosions). Speri and Zorzi obtained a patent in 1978 for this work which was carried out in 1974. Their paper was published in 1989 in an obscure medium [7].

The objective of this paper is to present specialist information which is needed so that the electrochemical cell can be exploited to its full capacity. Other methods are available and some involve Fourier-transform, infrared spectroscopy [8] from which one may obtain information on the surface of an electrode whilst in solution. Another method which was pioneered in the Texas A&M laboratory in 1990 was the work of Marek Scklarzyck [9] who was able to observe *individual atoms* on the surface of an electrode. (Paper peer reviewed in the *J. Electrochemical Society*.)

2. The Electrochemical Cell

A basic electrochemical cell is shown in Fig. 1. On the left is what is called the "working electrode" – the electrode on which the objective of the study takes place. The solution most prevalent at this time for studies of condensed matter nuclear science was that containing lithium deuteroxide in D_2O. Whatever reaction it is wished to be carried out will be done on the "working electrode."

The cell (Fig. 1) shown is for explanatory purposes. The actual cells used by other experimentation aimed at excess heat were different than that in Figs. 1 and 2. A central electrode here was the working electrode and around it was an anode consisting of a platinum wire (see below).

Thus, on the right of the cell in Fig. 1, there is a second electrode "the counter electrode." During electrolysis with the solution as D_2O, the anode evolves oxygen.

Many using an electrochemical cell and wanting to refer to its potential take the difference between the two electrodes. However, there are two more potentials in understanding an electrochemical cell. Very often, in such cells,

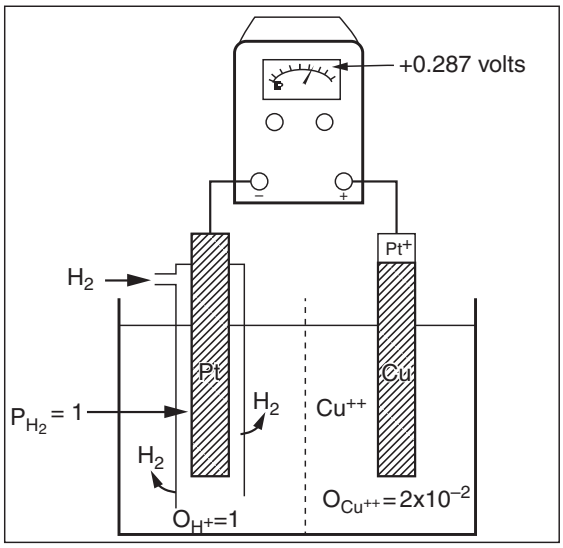

Figure 2. If the activity of cupric ions is changed, e.g., to 2×10^{-2} mol/l, the voltage of the cell should decrease to 0.287 V, as can be calculated from the Nernst equation. (From *Modern Electrochemistry*, Vpl. IIA, Plenum, 2000, New York.)

there is a different material at the cathode (left electrode) and the anode. Of course, connections to two metals must meet. When they meet, there is a contact potential generated and this is included in the potential difference between the two electrodes.

These potentials, (p.d.'s) are the basic ones which make up the cell potential and which are measured. There is a fourth potential difference which is unwanted. This potential is the so called "IR drop" between the cathode and anode (through the solution) when the cell is passing a current, this IR drop is not a valid part of the machinery which gives rise to the "cell potential." If one is to obtain the true cell potential, elimination of the IR drop is necessary. It will be dealt with in a section below although it is pertinent to say here that there are some simple methods for *reducing* the IR drop; e.g. bringing the cathode and anode as close together as possible. However, it may not contribute to the aims of the experimenter to allow the deuterium and oxygen to mix together. It is necessary sometimes to measure the deuterium and other gases which may be being produced at the cathode, without any oxygen from the anode.

In order to obtain a closer distance between the electrodes, some electrochemists use a porous membrane and then one has to judge the advantage of the nearer electrodes versus the resistance which the membrane itself brings in. Manufacturers are striving to make membranes which have a minimal resistance to the cell current.

3. Errors Made in Using Electrochemical Cells

The first and most frequent error is in reporting the data of the cell itself (Fig. 2) instead of the electrode which is evolving deuterium. The cell potential is influenced by the IR drop which should be eliminated. There are the two other potentials. One is at the junction of the anode and solution and the other potential difference is at the junction between the two electrodes of differing materials. All of these p.d.'s have to be understood in working with the cell.

Let us, for a moment, focus upon two imaginary workers: Dr. A and Dr. B are both using different electrochemical cells and examining the same reaction. Dr. A reports that his cell is working at 5.8 V (the total potential); Dr. B says his is working at 4.9 V. Comparing the current densities and the electrodes, they find they have the same current density

and yet the difference in the cell potential is relatively large – about 0.9 V. Why is that?

First of all, the IR drop can be different although the current density is the same. The distance between cathode and anode in A's and B's cells may differ. But those with experience in the use of these cells sometimes know how to diminish the IR drop. Taking this away, the two workers still find that there is a significant difference in their cell potentials. But this may be due to the materials of the anode. Some people use a platinum anode and some a nickel oxide anode or something else. Of course, Dr. A and Dr. B are measuring the cell and if different anodes are used, the whole cell will give a different potential for the same current density. Lastly, there is the contact pd between two electrodes of different materials into account.

What is the condition one needs to make if one is working with a cell? First of all, I would concentrate on the working electrode as we will see in the next section, when we see how to isolate it.

Another thing the two cells which Dr. A and Dr. B are comparing is to recall that the palladium electrodes may be indeed pure palladium 99.99%, but there is another aspect which will contribute its electrochemical properties and that is the annealing of the palladium while this is made from the liquid state. Metals cool down at different rates. This can be eliminated by letting them cool down in a temperature controlled thermostat. The vital reduction of the electrode material under cooling conditions of annealing is an important part of preparing an electrode and should be looked after if Dr. A and Dr. B want to have cells with the same performance of these cells.

Apart from this, there is the surface of the electrode which has to be prepared. It cannot be simply taken from the drawer and put into the solution. There are various methods of preparing the surfaces of the electrode which is too much detail for me to give here but it can be easily obtained [10].

Lastly, there is the question of vacancies in the electrode. Every metal has a number of vacancies which depends on this preparation and the temperature. Assuming that Dr. A and Dr. B are working at the same temperature, the annealing rate changes the number of vacancies.

4. Pitfalls of Platinum

Many electrochemical cells use a platinum counter electrode. The operator may forget that platinum has a potential at which it dissolves at potentials above 1.188 V on the hydrogen scale.

During the use of an anode in the cell, its potential may be substantially more positive so that this co-dissolution of Pt may occur. And what happens to the Pt^{++}? They diffuse over to the cathode. After this, you no longer have a palladium surface – it is of platinum.

I suspect that some people who read this will think that there are plenty of alternatives to noble metal anodes but that is not so because evolving oxygen is highly destructive. In looking for a suitable electrode which is going to be less susceptible to dissolution than platinum, it should be an oxide. The counterpoint is that most oxides do not have a large enough electronic conductivity so that they start adding to the IR drop in the cell and that is not what is wanted. Perhaps one may coat a thin layer of an oxide which isn't subject to further oxidation and does have sufficient electronic conductivity to be used without setting up a significant IR drop.

One anode worth considering is nickel oxide which I found to be a good anode but you may find something better once you look for it. Above all, it must not dissolve during anodic operation as does platinum although significantly only at higher anodic potentials.

You may wonder whether the new anode you choose is sound. That would be possible if you have a method to examine the surface of the palladium while it is in solution. I used infrared spectroscopy. The method must be usable when the solution is present. Most of the ordinary methods have to have a vacuum and the FT method will work through the solution and thus can be used but does need a fairly expensive instrument.

A cheaper method, if less informative, would be to run through an evolution of hydrogen on the palladium to see

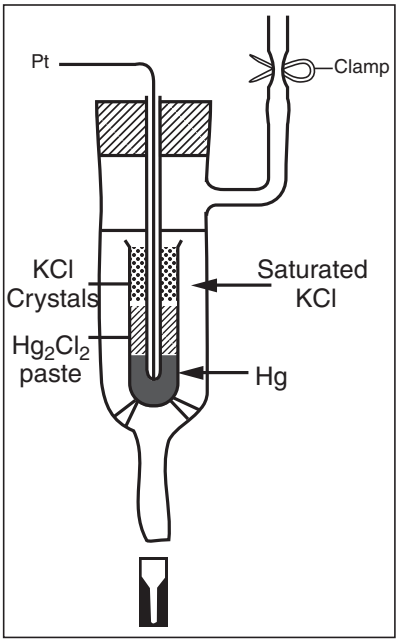

Figure 3. The calomel electrode. (One must be careful to avoid currents passing across the interface sufficient to form HgO, for this irreversibly spoils the electrode's reversible function. (From *Modern Electrochemistry,* IIA, Plenum, 2000, New York, p. 1110.)

if it fits other peoples' graphs for evolution of hydrogen on pure palladium and if it does not, then it is already coated with platinum.

5. The Isolation of the Working Electrode (See Figs. 3–5)

Some things have been explained about the properties of using an electrochemical cell. Attention should be on the working electrode as this gives the information germane to the problem. All the rest of the cell and what is happening there should be eliminated. The method involves using an auxiliary electrode – a thermodynamically reversible reference electrode.[a]

We add this small auxiliary cell (Fig. 3) which connects up the working electrode to another cell which contains a reference electrode (Figs. 3 and 4).

What thermodynamically reversible electrode should be used? Many workers would use the reversible hydrogen electrode because that is a well-known standard but it is quirky in preparation. Another reversible electrode is the calomel electrode and its potential on the standard hydrogen scale is 0.281. In this new circuit, a potentiostat is interposed (which I will describe in a separate section). A potentiostat is sensitive to the potential of the working electrode and allows the potential of this to be set and kept at the desired value during the operation of the cell. This has an advantage because from now on it is not necessary to know any more about those other potentials. The information one needs is that of the working electrode.

[a]In using any reversible electrode, the possibility of unwanted ions diffusing over from it and affecting the surface of the working electrode should be considered. If there is concern with this, a liquid junction connection can be interposed between the working electrode and reference electrode.

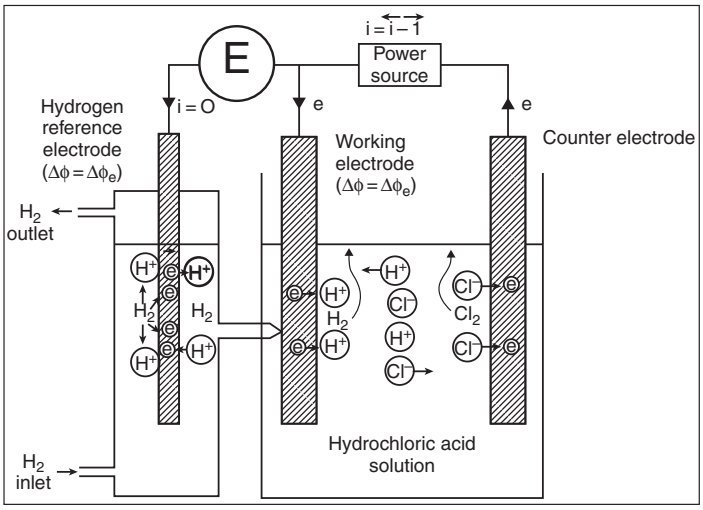

Figure 4. The three-electrode system required to measure electrode over-potentials, or use potentiostat. The potential between the working electrode and the reference electrode when both $\Delta\phi$ and $\Delta\phi_e$ correspond to the same reaction is equal to the over-potential η. The tube joining the reference electrode and the working electrode is called a Luggin capillary. It helps diminish the inclusion of an illicit IR drop in the measurement. (Reprinted from *Modern Electrochemistry*, Vol. IIA, Plenum, 2000, New York, p. 1105.)

There is an alternate reference electrode often used – the silver-silver chloride electrode. The potential of that is 0.222 on the standard H scale. These other values have to be converted to the hydrogen scale if everything else is to be measured in respect to that. But that is a matter of changing the reference electrode from whatever is being used to values for the corresponding standard hydrogen electrode (e.g., 0.222 for the silver-silver chloride reference electrode).

6. The Potensiostat

Now let us go then to the potentiostat. As the name indicates, the potentiostat keeps the *potential* of the electrode constant. The working electrode potential can be set to a given value and then some transient work which can be carried out at that constant potential. A jump up of the current is seen while the double layer is being charged and that fades away exponentially with time. It becomes a steady state potential in a short time (seconds).

How does the potentiostat work? It must be sensitive to the potential of the working electrode in order to do its job. If the potentiostat measures something too positive, the *cathodic* current is increased through the main current until the working electrode is at the desired value. Correspondingly if it is too negative, the current through the main circuit is changed until the potentiostat is at the desired value.

7. A Way towards the Elimination of IR Drops

I have referred already to the need of getting rid of IR drops, diminishing them down to 10 mV or less.

The following is a method for getting rid of all IR drops but its problem is the apparatus which is needed is not commercially available so you have to build it yourself and this can be done with minimal electronic skills.

The basis of this approach to the IR drop elimination is that the decay of the IR drop itself is very rapid (micro second) after the current through the cell has been turned off. To check my statement, one must have a quick acting measuring instrument with a micro second range and then try measuring the cell potential there with this instrument

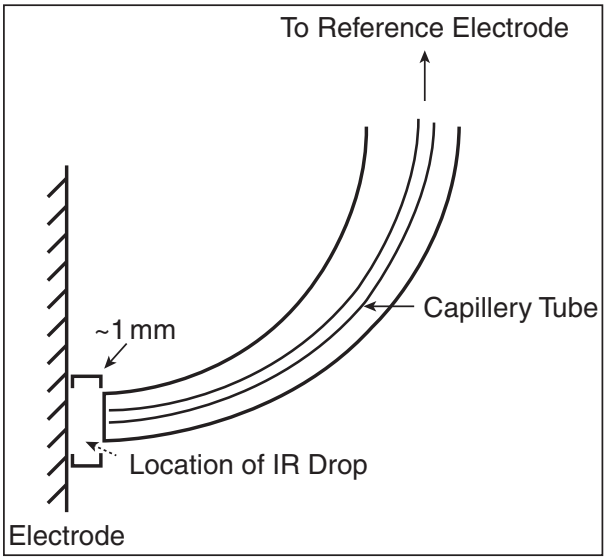

Figure 5. A closer look at a Luggin capillary (Reprinted from *Modern Electrochemistry*, Vol. IIA, Plenum, 2000, New York, p. 1108).

while at the same time switching off the current and you will see a rapid change of the measuring instrument showing that the IR drop has faded away in less than 10 μs.

Now, one is interested in the potential of the working electrode. The dependence on time for this is *much slower than the IR drop*. In order of magnitude terms, the IR drop will fade away in 1 or 2 μs and the electrode potential will remain within 10% of its original value in milliseconds. The numbers I am putting out here (1–10 μs and a few milliseconds) will vary with the system so it would be necessary to check them out in your equipment. Important is that the IR drop decays 95% away, by the time electrode potential is switched in. The current is only off for, say, a millisecond. The cathode potential should not change more than a few percent in that time for this.

Clearly then, the measurement of the electrode potential should be done when the main current is off, no IR drop but it must be made quickly because the electrode potential also decays (but more slowly) after the current has been interrupted.

8. The Metal–Metal Pd (Contact Pd)

One assumes that the electrochemical potentials of the electrons are equal on both sides of the junctions:

$$\overline{\mu}_{\mathrm{e}}^{\alpha} = \overline{\mu}_{\mathrm{e}}^{\beta}$$

$$\mu_{\mathrm{e}}^{\alpha} - nF\varphi^{\alpha} = \mu_{\mathrm{e}}^{\beta} - nF\varphi^{\beta}$$

$$\varphi^{\beta} - \varphi^{\alpha} = \frac{\mu_{\mathrm{e}}^{\beta}}{nF} - \frac{\mu_{\mathrm{e}}^{\alpha}}{nF}$$

This is the contact p.d. between two metals at equilibrium.

If different material are being used for the cathode and the reference electrode, the metal–metal pd will be significant. Consider two metals in contact, and assume they are in equilibrium. This means then that the electrochemical potentials, a symbol for which is $\bar{\mu}$, are equal on both sides of the metal–metal junction.

An Individual Electrode and its Potentials [10]

The working electrode potential is shared between the metal–solution inner potential difference and the chemical potential of the electron on the phase concerned.

$$^{M}\Delta^{s}\varphi - \frac{\mu_{e}^{M}}{nF}.$$

Then, if we leave out the IR drop (see above), a whole cell, made up of the working electrode and a reversible reference electrode would look:

$$\left(^{M}\Delta^{s}\varphi^{M} - \frac{\mu_{e}^{M}}{nF}\right) - \left(^{\mathrm{Rev}}\Delta^{s}\varphi^{\mathrm{Ref}} - \frac{\mu_{e}^{\mathrm{Ref}}}{nF}\right).$$

This is about as fundamental as one can get. Fundamental electrochemists call the $\Delta\varphi$ term a Galvani potential difference, μ terms refer to the chemical potential of the phase indicated.

This expression would apply to Fig. 4. This side circuit joins the reference electrode, whichever kind you choose.

There is another phenomenon which should be examined in all of these condensed matter nuclear reactions and that is the breakdown of the interior of the electrode. This has been established in recent work and may be an important aspect of what is in the future in this field [14].

One other thing I would like to draw attention to at this time and that is there is known as early as the 1960s, work done in France in which transmutation seems easy to do in bio systems and this field is now being carried out vigorously in Russia, 2010 (Vysotski and Kornilowa). These happen more easily than electrochemical transmutation reactions. This may be a future method to lead to a transmutation obtaining precious metals from those of lower costs.

9. Rate in Chemical Catalysis and in Electrochemistry

Current density is the current divided by the area of the electrode. In chemistry the rate of a surface reaction is measured in moles per second per unit area. The corresponding quantity in electrochemistry is: A cm^2/nF, therefore is the same meaning if divided by nF though in a different language. So any current density one has is converted to moles per second per cm^{-2} by dividing by nF which n is the number of electrons in the act of the overall reaction; F, is 96,500 C/mol.

10. Some Extra Techniques may Come

In developing the instrumentation in the next twenty years, we shall be looking at surfaces in detail and I think we should be looking at atoms [9]. We already know from the work of Marek Scklarzyck carried out in my laboratory in 1990 that you can look at certain atoms on surfaces. The instrument used was a scanning tunneling microscope.

Another experiment that we should be looking at is penetration by electron microscopes into the interior of the electrode and following happenings thereon. This is because deuterium atoms not only diffuse into the palladium, but apparently damage the structure there..

11. Summary

Electrochemical cells were poorly understood in the early stages of work on the condensed matter nuclear reactions. Cells consist of two electrodes and their potentials must be separated. What was little realized by workers is that when

one has two different metals as a cathode and anode, the resultant metal–metal pd has to be added to the analysis of the overall cell potential. Further, there is an IR drop between the electrodes in the solution and this should be eliminated because although it is the highest and dominates the cell potential, it is of no electrochemical value. The actual cell potential excluding the IR drop, was written out in the last section.

Use of platinum in anodes may cause errors because platinum dissolves at potentials greater than 1.19 V. and deposits on the Pd electrode. NiO_2. or other oxides which shows sufficient electronic conductivity and stability with O_2 may be a substitute.

Isolation of the working electrode can be achieved by coupling it with a thermodynamically reversible electrode. The potential of the working electrode is controlled at a designed value by means of a potentiostat.

The potentiostat is a device sensitive to the potential of the working electrode. When the potentiostat registers a potential more positive than the chosen value it gives rise to a corrective change in current through the main current to bring the working electrode potential back to the original chosen value.

Potentiostats are commercially available for lab scale work. For industrial sized plants, if needed, the potentiostat has to be made to special order.

IR drops can be eliminated by using the short time in which the IR's decay compared with the much longer time for the electrode potential which can be measured up to, say, 0.1 ms.

Acknowledgements

I am indebted to Dr. Digby MacDonald of the Pennsylvania State University for a critical reading of this document.

Appendix A. How to Use this Paper

The use of this paper should be step by step.

(1) The first thing would be to get rid of this IR drop, i.e., the ohmic potential which exists between electrodes in the solution.

To show you how much this can distort the answer, let me quote you a recent author who wrote to me with some details about his work. He says that the potential drop between the electrodes in his cell was about 5–6 V. After he had calculated the approximate IR drop and subtracted it, he was left at 1.5 V as the real potential between the two electrodes, leaving out the useless IR drop.

You can get within a few percent of the real answer by assuming that the passage way between the cathode and the anode is a cylinder. Now, the formula which calculates an IR drop is given by an equation:

$$R = \frac{1}{\sigma}\frac{L}{A},$$

where L is the distance between electrodes, and A the cross-sectional area between it and is the specific resistance of the solution and has to be looked up in tables and varies with the electrolyte and concentration. Finally, when one has calculated the resistance one multiplies this by the current (not the current density) and there is the IR drop which you then subtract from the reading that you are getting from the two electrodes of the cell.

It is not much use using in communication with other colleagues because there are various specific differences of people's cells which we will hear as we go through this appendix, and what I have said is the first step, and speaking numerically, is also the biggest step because the IR drop between electrodes is sometimes three-quarters of the whole potential that you are getting when you look at your high resistance volt meter.

Now, a much better method for overcoming this IR drop is quite complicated and I will delay telling you about it until we are near the end of the appendix.

(1) After the IR drop has been removed, you still have before you the potential of the whole cell with an IR drop removed

The next thing we have to do is isolate the working electrode which if you look at the diagrams, the one on the left in Figs. 1 and 2. Thus, in order to isolate the working electrode, the main way to do it is to use a third electrode which is a thermodynamically reversible electrode at equilibrium so that no current passes in it and one knows exactly what its potential is so that if one measures the working electrode potential versus the reference electrode potential, then one is free of all IR drop and also other problems such as the fact that the anode had its own potential which you'd like to thrust aside and there is another potential when one metal touches platinum and meets another metal such as palladium, there is a p.d.set up between the two of them, and you have to reckon that one too.

(1) Figure 5 shows the Luggin Capillary. This leads from the reversible reference electrode on the extreme left of Fig. 4 to the working electrode and the reason for having it is to avoid including a little IR drop in the solution near the working electrode
(2) The fourth step would bring the author into the sophisticated measurement because he will be taking into account everything which gives him the information that he wants, which is the behavior of the working electrode protected from the influence of other things such as the current going over to the anode and the metal–metal p.d which we mentioned.
(3) If you have been through Steps 1–4, you are producing data which is worth recording in a paper because everybody's paper has different IR drops and different anodes and different metal–metal p.d.'s but if you wipe all those and look only at the potential of the working electrode, and you can compare your results with those of any other experimenter who has taken the same steps.
(4) I strongly advise experiments which examine damage inside the electrode.

For example, in those two papers which I published, in 2000, and in 2011, we found that at 0.35 V for the over potential, there was a beginning of a breakup inside the palladium. This breakup starts the reactivity in respect to tritium which we have been trying to produce for the last 100 hours begins, i.e., no tritium for 100 h.

List of Symbols

$\overline{\mu}^{\alpha}$	the electrochemical potential of the phase α
n	the number of electrons which take part in the overall reaction with you are examining, e.g. = 2
F	96,500 C/gmol of univalent ions
μ^{α}	the chemical potential of the phase α
φ^{α}	the inner potential of the phase α
${}^{\alpha}\Delta^{s}\varphi$	the inner potential difference between the bulk of the interior of the metal and the bulk of the interior of the solution

References

[1] M. Fleischman and S. Pons, *J. Electroanalytical Chem.* **261** (1989) 301.
[2] N.J. C. Packham, R.C. Kainthla and J.O'M. Bockris, *J. Electroanalytical Chem.* **279** (1989) 481.
[3] E. Storms and C. Talcott-Storms, *Fusion Technol.* **20** (1991) 246.

[4] DOE Meeting on Cold Fusion, Santa Fe, NM., May 23–25, 1989; about 100 people,: Major Discussions Session, evening of 23rd, chaired by John O'M. Bockris; N.J.C. Packham, R.C. Kainthla, J.O'M. Bockris, *J. Electroanal. Chem*. **279** (1989) 481, 485.
[5] N. Iyenger and N. Srinivasen, Collection of contributions to early cold fusion work, from Bhabha atomic research, in press.
[6] S. Speri and F. Zorzi, *Proceedings of the Foundation of Mathematics and Physics*, Perugia, Italy,1989.
[7] Reference 6 and Patent No. 1024274.
[8] J.O'M. Bockris, P. Zeleney and M.A. Habib, *J. Electrochem. Soc*. **131** (1984) 2164.
[9] Marek Szklarzcyk and J.O'M. Bockris, *J. Electrochem. Soc.* **137** (1990) 452.
[10] J.O'M. Bockris and S.U.M. Khan, *Surface Electrochemistry*, Plenum, London and New York, 1993, p. 53.
[11] J. O'M. Bockris, A.K. Reddy and Maria Gamboa-Aldeco, *Modern Electrochemistry*, Plenum, New York and London, Vol. IIA, 2000, pp. 838–840.
[12] Luggin Capillary. E. Gileadi, Wiley-VCH, Berlin, 2012.
[13] J.O'M. Bockris and Z. Minevski, *Int. J. Hydrogen Energy* **35** (2000) 747.
[14] J.O'M. Bockris, *J. Condensed Matter Nucl. Sci.* **7** (2011) 1.
[15] J.O'M. Bockris and S.U.M. Khan, *Surface Electrochemistry*, Plenum, New York, 1993, pp. 74–78.

J. Condensed Matter Nucl. Sci. 9 (2012) 21–29

Research Article

Evidence for the Induction of Nuclear Activity in Polarized Pd/H–H_2O System

Stanislaw Szpak *

SPAWAR Systems Center San Diego, San Diego, CA 92152, USA

Jack Dea†

4809 Clairemont Drive, San Diego, CA 92117, USA

Abstract

In cells employing cathodes prepared by the co-deposition process, the polarized Pd/D–D_2O system becomes nuclear active when the concentration of deuterium, expressed as D/Pd atomic ratio, is equal to or greater than one. In contrast, to activate the polarized Pd/H–H_2O system, action of an external magnetic field, modulation of cell current or both, are required. Evidence for the nuclear active state in the Pd/H–H_2O system namely deuterium production, particle emission and catastrophic thermal event, is presented.
 ISSN 2227-3123

Keywords: Co-deposition, Coupled reaction, Magnetic field, Pd/H–H_2O system

1. Introduction

Recently Widom and Larsen [1] presented a novel approach to explain the induction of a nuclear active state in the polarized Pd/D–D_2O system. In their approach, an electron capture by the deuteron is responsible for the system's behavior. Their model implies that, under the same conditions, the energetically less demanding Pd/H–H_2O system should show signs of nuclear activity, but this has not been reported. To resolve this issue, we reviewed [a] the available empirical evidence and concluded that the proper course of action is to examine in detail the content and meaning of the reaction

$$e^- + p^+ \rightarrow n + \nu. \tag{1}$$

Nuclear reactions of this type can be treated as chemical reactions [2,3]. Consequently it is not difficult to write down the thermodynamic conditions for the reaction to proceed, namely the inequality $\mu(e^-) > \mu(n) - \mu(p^+) > 0$.

*Retired. Present address: 3498 Conrad Ave., San Diego, CA 92117, USA.
†E-mail: eepsd@yahoo.com
[a]Division of labor: JD – data collection, SS – data interpretation.

 ISSN 2227-3123

Since the neutrinos are not retained by matter, the chemical potential of the neutrinos will not appear in the equation of equilibrium or reaction kinetics. Equation (1) provides only limited information, namely it is the statement of conservation of mass, energy and charge. Since the initial and final states are not specified, it simply means that the system consists of unbounded particles in the sense that there is a continuous range of possible energies. All protons located in the reaction volume interact with the Pd lattice to a various degree. The chemical potential of interacting protons p_l^+ is of the form $\mu(p_l^+) = \mu(p^+) + u(r)$, where $u(r)$ denotes the energy of interaction. To evaluate the $u(r)$ function, we consider the relation $\mu(p) = \varepsilon(-p)$, i.e. the chemical potential of a particle p is its negative binding energy In this representation the $u(r)$ function indicates that a part of the interacting site is incorporated into the proton itself, i.e. it represents the degree of an overlap which, in turn, determines whether or not the electron capture by proton can occur. For an electron capture by a proton to occur, the quantity $\mu(n) \ -\mu(p_l^+)$ must be positive Since light water electrolysis does not produce a nuclear active state, it follows that $\mu(p_l^+)$, is greater than that of the neutron, $\mu(n)$, i.e. irrespective of its energy the electron capture reaction cannot occur. In Section 2 of this communication, we describe the procedure that reduces the interaction energy of the palladium/lattice defect, in Section 3 we present evidence for nuclear activity in Section 4 we offer interpretation of a few selected cases using methods and terminology commonly employed in chemical research.

2. Effect of an External Magnetic Field

The interaction of a magnetic field with electrochemical systems can be divided into three main areas: (i) magneto-hydrodynamic effects, i.e. those affecting mass transport via the reduction of the diffusion layer thickness, (ii) magneto-mechanical effects, i.e. those that involve the shape change of micro-globules as well as complex macro-molecules, and (iii) non-specific interactions of electronic nature, i.e. those affecting dynamics of the highly concentrated hydrogen in the Pd lattice. These effects are attributed to forces generated by the gradients of magnetic energy density, i.e. by forces that arise from non-homogeneity of the paramagnetic entity and those associated with non-uniformity of the magnetic field. Of interest to the present communication is the effect on the structure of the deposit, the magneto-mechanical effect, and on the process(es), the non-specific interactions.

2.1. Magneto-mechanical effects

The effect of an external magnetic field, (ca 0.2 T) on a single globule and on the deposit, including the interphase, is briefly discussed.

2.1.1. *Single micro-globule*

In the absence of an external magnetic field, the SEM photograph shows that the Pd/H deposit has a “cauliflower” structure consisting of almost spherical micro-globules, Fig. 1a. When placed in an external magnetic field, its structure changes. The almost spherical micro-globules are flattened to form a “star-like” appearance, Fig. 1b.

2.1.2. *The Pd/H deposit and the interphase*

As a general information, we note that when the Pd/H deposit is placed in an external magnetic field the magnetic “order” of one layer (interphase) affects the “order” of another layer (bulk) being in contact with the first. The change in the deposit morphology affects the distribution of absorbed hydrogen. Any motion of hydrogen within the interphase generates stresses that, in turn, produce dislocation and other types of interaction sites. That it is to say within the interphase exists a state of dynamic equilibrium which governs the distribution of hydrogen interacting with

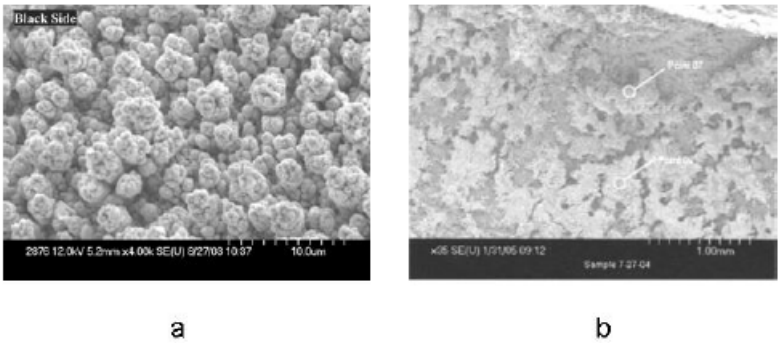

Figure 1. (a) SEM photo of electrode surface with no magnetic field applied. (b) Electrode surface with applied magnetic field.

the palladium lattice which means that some interaction sites are formed, other disappear thus releasing the interacting protons and making them available for the electron capture reaction.

2.2. Non-specific interactions

In general: When the "host/guest" complexes (where the Pd lattice defect acts as the host for the guest $p_l^+e^-$ complexes) are exposed to magnetic field, deformation of their structure is very likely to occur due to magnetic torque. Here, we address the effect of magnetic field on strength of Pd/lattice defect interaction and rate of transport.

2.2.1. *Sequence of events and strength of interaction*

The sequence of events leading to the initiation of the nuclear active state is shown in Fig. 2. Here, the events within the metal side of the interphase are: an exchange between the adsorbed and absorbed hydrogen, H_{ad} H_{ab} the transition from atomic to nuclear state denoted $H_{ab} \rightarrow p^+$, followed by $p^+ \rightarrow p_l^+$, the latter identifies a proton interacting strongly with

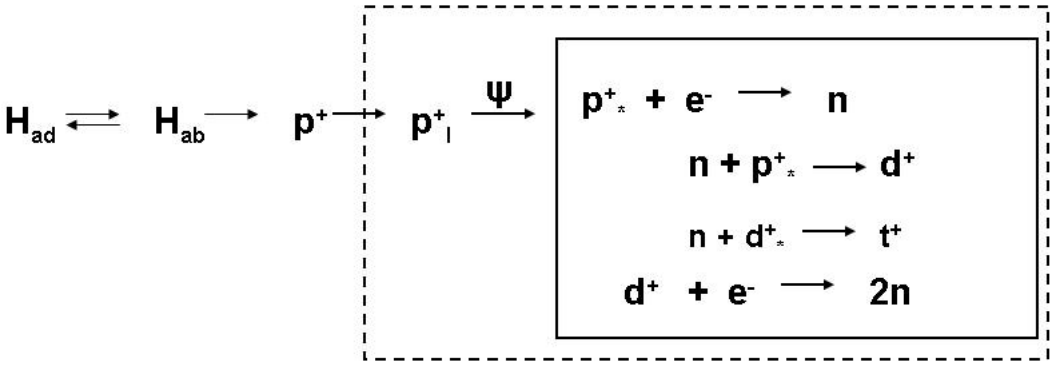

Figure 2. Schematic diagram showing events within the interphase. Enclosed by *broken line* are processes affected by an external field; by *solid line* coupled nuclear reactions.

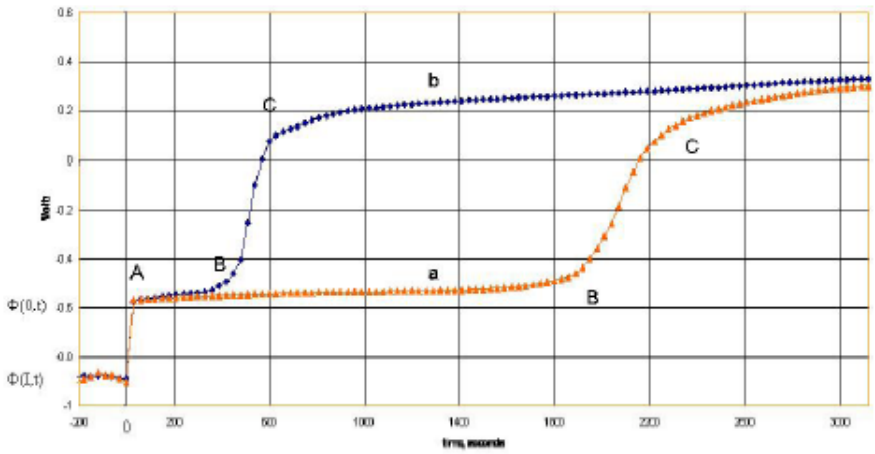

Figure 3. Hydrogen desorption rates. *Curve a* in the absence of magnetic field. *Curve b* in the presence of external field.

the Pd lattice. When an external magnetic field, ψ is applied, a new set of processes can be identified, viz weakening of the interaction, $p_l^+ \rightarrow p_*^+$ electron capture by proton $e^- + p_*^+ \rightarrow n$, with neutrons either escaping or reacting with proton to yield deuteron, $n + p_*^+ \rightarrow d^+$ and an electron capture by deuteron yielding two neutrons $e^- + d^+ \rightarrow 2n$.

2.2.2. *Rate of transport (desorption)*

The data presented in Fig. 3 show a typical potential/time curve for the desorption of hydrogen from the electrode having structure shown in Fig. 1b, in the absence and presence of an external magnetic field, curves a and b, respectively. Here, the electrode potential/time relation, $\Phi(t)$, shows that the time for the transition from transport to surface controlled desorption of hydrogen, segments AB and BC, is substantially shorter when an external magnetic field was applied. Such behavior indicates that magnetic field weakens the proton/Pd defect interaction, i.e. $\mu(p_l^+) > \mu(p_*^+)$.

3. Evidence of Nuclear Activity

In what follows, we present description of experimental protocol, evidence of nuclear activity based on deuterium production, neutron emission and catastrophic thermal behavior.

3.1. Experimental protocol

A rectangular vessel, made of clear plastic, served as the electrochemical cell, Fig. 4. The cathode assembly is shown in Fig. 4a. A stock of two CR-39 chips is attached to a plastic strip and one placed outside the cell. A platinum wire, in the indicated shape, served as a substrate for the co-deposited Pd/H film. The assembled cathode is inserted into the cell. The fabrication of cathodes involves co-deposition. The co-deposition is a process whereby the palladium is deposited in the presence of evolving hydrogen from a Pd^{2+}salt solution onto a substrate that does not absorb hydrogen. The structure of the electro-deposited palladium is controlled by the solution composition and the cell current profile. To assure acceptable deposits, one starts at current density less than its diffusion controlled value. Here, for the co-deposition from a solution of 0.03 M $PdCl_2$ and 0.3 M LiCl dissolved in H_2O, the current profile was as follows:

$i = -1.0$ mA cm^{-2} for the first 24 h followed by $i = -3.0$ mA for the time required to reduce all the Pd^{2+} ions; (b) a 3–4 h stabilization period at $i = 30$ mA. When the co-deposition is completed the cell is placed in an external magnetic field as shown in Fig. 3. Upon placing an operating cell in a magnetic field the electrochemical compression of absorbed hydrogen was put under computer controlled regime with $i = -400$ mA for 90 s and $i = 5.0$ mA for 5 s.

3.2. Deuterium detection

The mass spectrograph was used to analyze for deuterium. The Pd/H film co-deposited onto a thin coiled palladium wire was employed to assure retention of the electrochemically compressed hydrogen isotopes (Fig. 4b). This electrode design was selected to meet the requirements imposed by mass spectrograph. To minimize the desorption of hydrogen isotopes the following procedure was adapted (a) remove the cell from magneto-static field, (b) stop the cell current flow, (c) take out the cathode, (d) cut-off the coiled part of the cathode, (e) place the sample in mass spectrograph, (f) evacuate to ca 10^{-5} torr, (g) turn on mass spectrograph, (h) set the atomic number of interest, and (i) print results. The mass spectroscopic analysis, performed upon completion of a run, showed the presence of all hydrogen isotopes. Qualitatively, deuterium was the dominant isotope with negligible amounts of tritium. Typically, the D/H atomic ratio greater than one, with a value as high as 5.1, was recorded. Needless to say that the presence of deuterium in the cathode is of utmost importance because it might provide decisive insight into the mechanism of nuclear reactions in condensed matter. As a rule, mass spectroscopic analysis yields results that are unambiguous. However if additional verification is required, then this can be done by measuring the D/H atomic ratios following electrolysis of water with known concentration of D_2O [4], a method used by us.

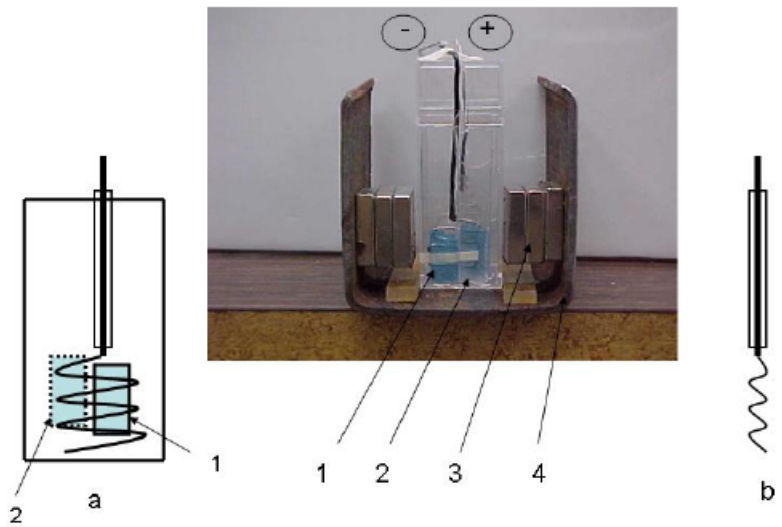

Figure 4. Electrochemical cell. (1) Outside CR-39 detector, (2) double CR-39 stock located inside cell, (3) neodymium magnets, (4) magnet holder Cathode assembly designed for, (a) neutron detection, 1–CR-39 chips inside the cell, 2–CR-39 outside the cell; (b) for determination of deuterium content.

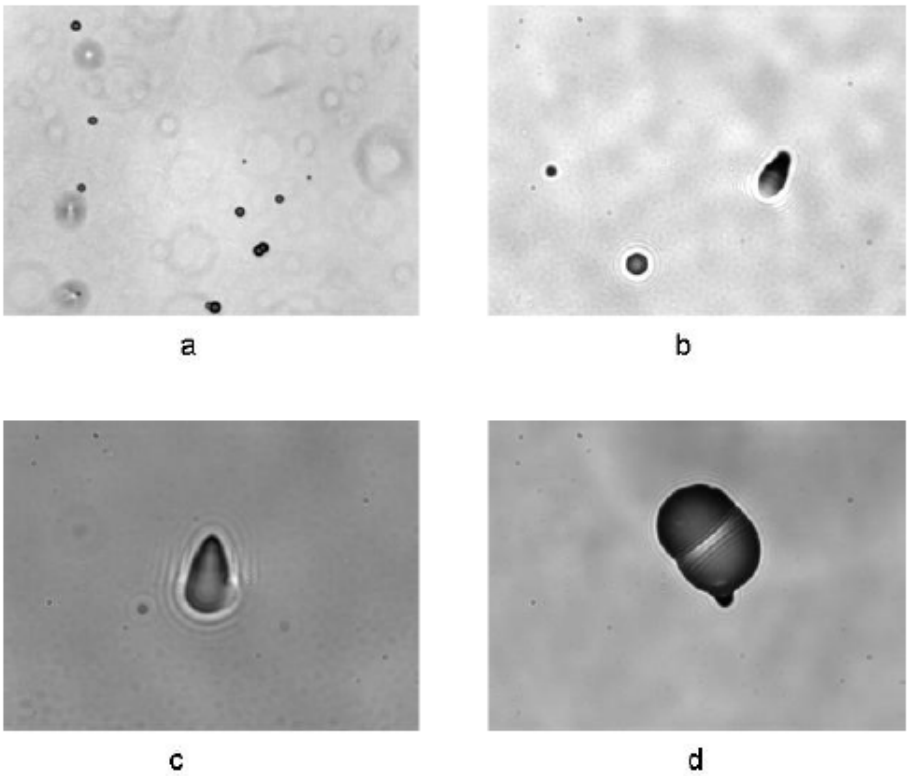

Figure 5. Images of tracks in CR-39 detectors created in the course of an experiment: (a) distribution of tracks at 40×, (b) illustrates the angle of impingement at 500×, (c) shows a single track at 1000×, and (d) image of a double track at 500×.

3.3. Neutron detection

Figure 5 shows typical images of tracks recorded on CR-39 chips. The examination of the CR-39 chips, located inside and outside, indicates no difference in the type of tracks but in their number, the latter being highest on the CR-39 detector facing the cathode and the lowest on the chip located outside the cell. In particular, Fig. 5a shows a typical distribution of images of circular and elliptical tracks, Fig. 5b and 5c illustrate the case of ionizing particle entering either perpendicular to the detector's surface or at an oblique angle, and Fig. 5d a double track. The physical meaning of the images recorded by CR-39 detectors is discussed in detail by Mosier-Boss et al. [5].

3.4. Catastrophic thermal events

Several catastrophic thermal events were observed (three out of ten). In one case, after three days of electrolysis with cell current varying between −300 and 5 $mA\,cm^{-2}$, a catastrophic thermal event has occurred that resulted in cell deformation, loss of electrolyte due to evaporation and leaking through a punctured cell bottom (Fig. 6). The damage, about 1/3 of total area, viewed from the outside, Fig. 6a, and inside the cell, Fig. 6b, is consistent with placing a very hot object in contact with plastic material. The intensity of the heat source can be estimated from the temperature raise of the electrolyte during the last 170 min of cell operation Fig. 7. In a another run, a cell, charged with 3.0 ml of 0.03 M

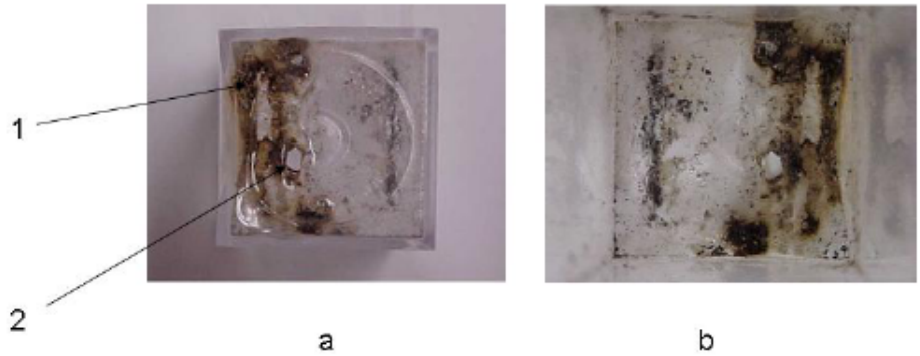

Figure 6. Damaged cell bottom: (a) outside view, (b) inside view. *Arrows* indicate the well-defined damage areas (1–embedded particles, 2–hole).

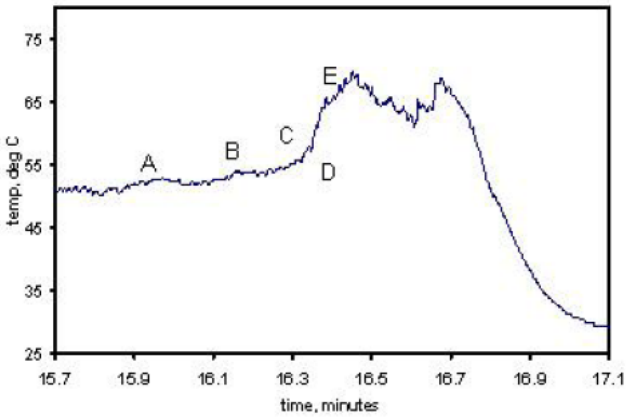

Figure 7. Temperature profile during thermal run-away

$PdCl_2$ and maintained at a constant volume of 5.0 ml, was operated for two days before recording the temperature with the thermocouple located below the cathode. Within the last 160 min the electrolyte temperature remained constant (at 50°C) followed by, at first, a slow raise for the next four minutes, section ABC, followed by a rapid increase at 2.6°C/s, section DE. During the next 3–4 min, the electrolyte evaporated and the temperature returned to ambient. For this run, the intensity of the heat source, based on the heat generated by the minute amount of the PD/H film and transferred to the electrolyte, can be estimated to be more than 10 eV/Pd atom, i.e. outside the limits of chemical reaction. Furthermore the temperature raise of the source of ca 250°C/s. means that substantial amount of the electrolyte was lost by "film boiling".

3.5. Mechanism of the Pd/H film separation

A probable, but speculative, mechanism of Pd/H film separation from the Pt substrate can be deduced using photograph, Figs. 8a and 8b. The separation shown in Fig. 8 illustrates the separation of a Pd/D deposit in another set of experiments.

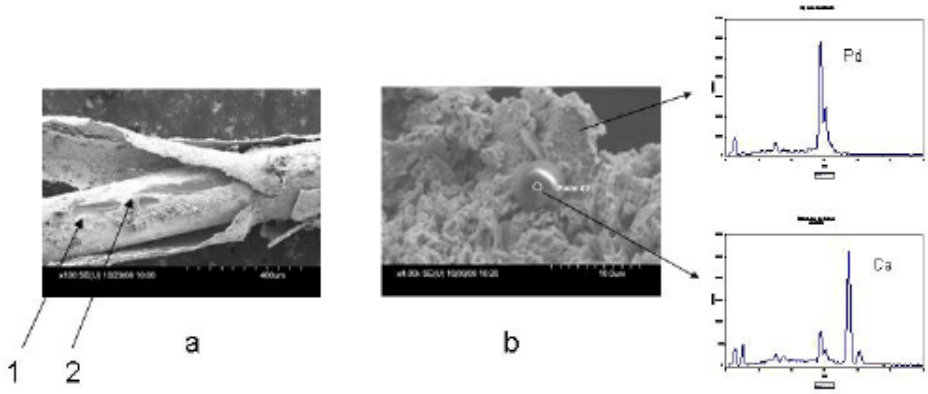

Figure 8. (a) SEM/EDX SEM photograph illustrating separation of a Pd/H film during a mild run-a-way run. (b) SEM photograph showing single reaction site; *top chart*–EDX of Pt substrate; *bottom chart*–EDX showing localized transmutation.

In particular examination of Fig. 8a suggests the following: (i) a number of localized reactions at the Pt/Pd/D interface, indicated by an arrow, forced the separation of the Pd/D deposit from the Pt substrate (ii) the SEM/EDX analysis of reaction sites contains participation of a nuclear event (transmutation) is involved in forcing film separation. The Pd/H film separation shown in Fig. 8 occurred during a mild thermal run-away during electrolysis of light water is almost identical to that heavy water, thus suggesting the same mode of separation.

The film separation may be explosive. The damage, shown in Figs. 8a and 8b, indicates that a Pd/H sleeve after separation was propelled away from the cathode and came in contact with the cell bottom. The high temperature and the amount of thermal energy necessary to generate the observed damage implies that thermal activity did not terminate upon separation from the cathode but persisted during flight as well as after landing at the cell bottom.

4. Closing Remarks

We prepared this communication to disclose that it is possible to extend the Fleischmann–Pons effect to the Pd/H–H_2O system. This extension is reproducible provided that the described procedure is followed and, in particular, that the Pd/H co-deposition is done carefully Because of its introductory nature, some interpretations of experimental evidence are certain other are speculative.

4.1. Cases of certain interpretation

There are two cases where the interpretation appears to be certain, namely: (i) the $e^- + p^+ \rightarrow n$ reaction starts the induction of the nuclear active state in the Pd/H–H_2O system and (ii) the transition $p_l^+ \rightarrow p_*^+$ is the low-energy process that generates the condition for the reaction $e^- + p_*^+ \rightarrow n$ to occur.

4.2. Case of speculative interpretation

One of the unresolved problems, associated with the Fleischmann–Pons effect, is the origin of the catastrophic thermal run-a-way There is little factual information on which to arrive at a probable model. In an attempt to get some understanding, from the many reported cases, we selected two involving the Pd/D–D_2O and one a mixed

Pd/D//Pd/H –H_2O systems. The first, at the University of Utah in Prof. Pons laboratory [6], the second described by Biberian [7] and the third reported in this communication. The available factual information: In the first case – cathode size (volume) 1.0 cm^3 explosion occurred at night; damage: cell destroyed, a hole in the laboratory bench, light damage to laboratory floor. On the second case – cathode volume 0.11 cm^3; damage experimental set-up destroyed. In the third case – cathode volume 0.01 cm^3; minor damage (cf. Fig. 6). It appears that the severity of damage correlates with the amount of palladium.

The puzzling question: What causes these explosions Are they inherent to the system or a result of the formation of new entities because .... *there are appropriate thermodynamic conditions for the formation of large clusters of hydrogen nuclei or of regions of the lattice containing ordered arrays of hydrogen nuclei at high H/Pd ratios* [8]. A limited discussion, suggesting that the explosive character is due to a chain reaction, was advanced by Biberian [7]. It is reasonable to assume that a set of events preceded the chain reaction. This assumption appears to be consistent with the data in Fig. 7, sections A B C, and can be further developed if, as the concentration of deuterium increases, the Pd/H–H_2O system transits to the Pd/D–D_2O system. Conditions associated with this transition can be obtained by examining the kinetics of the set of coupled reactions: $e^- + p_*^+ \rightarrow n$; $n + p_*^+ (\text{or } p_l^+) \rightarrow d^+$; $e^- + d^+ \rightarrow 2n$ This, however, is outside of the scope of this communication.

References

[1] A. Widom and L. Larsen, *Eur. Phys. J.* **C46** (2006) 107–117.

[2] H. Remy, *Treatise on Inorganic Chemistry*, Elsevier, Amsterdam, Vol. II, p. 563, 1956. [*Nuclear reaction may be represented by equations which correspond exactly to those employed in chemical reactions. This section of nuclear physics which deals particularly with transmutation of the elements, occurring in nuclear reactions has appropriately been termed nuclear chemistry.* It goes on to say: *The essential goal of nuclear physics is to interpret the nature of nuclear forces. One important approach to this objective is the study of transmutations occurring in nuclear reactions, and the magnitude of energy liberated in such processes.*]

[3] L.D. Landau and E.M. Lifshitz, *Statistical Phys.*, Vol. 5, Part 1, Pergamon, Oxford, 1957, pp. 318–319. *It is not diffcult to write down the thermodynamic conditions which govern the "one chemical equilibrium" of the nuclear reaction, which may be symbolically written as* $A_Z + e^- \rightarrow A_{Z-1} + \nu$, *where* A_Z *denotes nucleus of atomic weight A and charge Z,* e^- *an electron and* ν *a neutrino. The neutrinos are not retained by matter and leave the body.*

[4] H.W, Washburn, C.E. Berry and H.G. Hall, *Anal. Chem.* **25** (1953)130.

[5] P.A. Mosier-Boss, S. Szpak, F.E. Gordon and L.P.G. Forsley, *Naturwissenschaften* **96** (2008) 135–142.

[6] M. Fleischmann, private communication.

[7] J.-P. Biberian, *J. Condensed Matter Nucl. Sci.* **2** (2009) 1.

[8] M. Fleishmann, S. Pons and G. Peparata, *Il Nuovo Cimento* **107 A** (1994) 143.

J. Condensed Matter Nucl. Sci. 9 (2012) 30–49

Research Article

Pulse and Amplitude Approximation for the Lossy Spin–Boson Model

Peter L. Hagelstein *

Research Laboratory of Electronics, Massachusetts Institute of Technology, Cambridge, MA 02139, USA

Irfan U. Chaudhary

Department of Computer Science and Engineering, University of Engineering and Technology. Lahore, Pakistan

Abstract

The lossy spin-boson model is of interest to us since it predicts efficient energy exchange between identical two-level systems and an oscillator when the transition energy is a large (odd) multiple of the the oscillator energy. This model is not so easy to solve directly in the strong coupling regime, so we have developed approximate versions of the model that are easier to analyze. Here we introduce the pulse and amplitude approximation which compares very well with exact numerical solutions when the coupling is strong, and when the characteristic oscillator energy is much less than the transition energy. We examine discrete and continuum versions of the approximation, and find that they give good results for the solutions and for the self-energy. We show that the indirect coupling matrix element can be estimated from differences in the eigenvalue of the pulse optimization constraint for solutions with different phases.
 ISSN 2227-3123

Keywords: Fleischmann–Pons effect, Lossy spin–boson model, Phonon exchange, Quantum fractionation

1. Introduction

In previous publications we introduced the lossy spin–boson model [1–5], which has the interesting property that it describes efficient coherent energy exchange between a set of identical two-level systems and and oscillator under conditions where the transition energy of the two-level systems is very much greater than the oscillator energy. The fractionation of a large quantum into a great many small quanta constitutes a new physical effect that may have applications in different fields, and for this reason alone merits further study. Our motivation for pursuing the model comes from trying to understand excess heat production in the Fleischmann–Pons experiment [6,7].

*E-mail: plh@mit.edu

 ISSN 2227-3123

The model predicts that the dimensionless coupling constant g must be large in order to fractionate a two-level quantum into more oscillator quanta. The associated scaling parameter for this process in the model is $g/\Delta n^2$, where Δn is the number of oscillator quanta that make up the transition energy ΔE

$$\Delta E = \Delta n \hbar \omega_0, \tag{1}$$

where $\hbar\omega_0$ is the characteristic oscillator energy. To fractionate a large quantum into ten times as many oscillator quanta requires a dimensionless coupling constant larger by one hundred. We view this scaling as relatively gentle, suggesting that in a physical system for which the model applies, it should be "easy" to fractionate the two-level system quantum.

In the analysis reported previously, we developed a simplified version of the model that we were able to solve using a combination of numerical and analytical methods. In this work we examine the approximate solution for the eigenfunctions and eigenvalues using a separable eigenfunction; the ideas behind this approach were described briefly previously [5]. Our goal here is to provide a more systematic version of the approximation. This analysis is useful for the lossy spin–boson model with infinite loss, and perhaps more importantly lays the foundation for a systematic approximation that we can use for more complicated models based on three and more levels in place of the two-level system model.

2. Basic Model

The sector Hamiltonian for the lossy spin–boson model is [1]

$$\hat{H} = \frac{\Delta E}{\hbar}\hat{S}_z + \hbar\omega_0 \hat{a}^\dagger \hat{a} + V(\hat{a}^\dagger + \hat{a})\frac{2\hat{S}_x}{\hbar} - i\frac{\hbar\hat{\Gamma}(E)}{2}. \tag{2}$$

This model in general is very difficult to solve, especially in the strong coupling limit which is of interest to us since we would like to study coherent energy exchange under conditions where the large quantum of the two-level system is fractionated. A great simplification comes about in perturbation theory calculations if we assume that the loss is infinitely large for basis states with energies less than E; such states are removed from the problem with this assumption since their occupation probability becomes vanishingly small as the loss goes to infinity.

2.1. Local approximation

We are interested in the eigenfunctions and eigenvalues of the Schrödinger equation

$$E\Psi = \hat{H}\Psi. \tag{3}$$

If we use a basis expansion of the form

$$\Psi = \sum_m \sum_n c_{m,n} |S, m\rangle |n\rangle, \tag{4}$$

then the expansion coefficients $c_{m,n}$ satisfy

$$Ec_{m,n} = \left(\Delta E m + \hbar\omega_0 n - i\frac{\hbar}{2}\Gamma(E)\right)c_{m,n} + V\sqrt{n+1}\sqrt{(S-m)(S+m-1)}c_{m+1,n+1}$$

$$+V\sqrt{n}\sqrt{(S-m)(S+m-1)}c_{m+1,n-1}+V\sqrt{n+1}\sqrt{(S+m)(S-m+1)}c_{m-1,n+1}$$

$$+V\sqrt{n}\sqrt{(S+m)(S-m+1)}c_{m-1,n-1}. \tag{5}$$

In the limit of large n and large $\sqrt{S^2-m^2}$, the different factors of the interaction terms become nearly the same, which suggests that we might make progress by studying a version of the problem in which the coefficients are all the same. This problem can be written as

$$Ec_{m,n} = \left[\Delta Em+\hbar\omega_0 n - i\frac{\hbar}{2}\Gamma(E)\right]c_{m,n}$$

$$+V\sqrt{n}\sqrt{S^2-m^2}\left(c_{m+1,n+1}+c_{m+1,n-1}+c_{m-1,n+1}+c_{m-1,n-1}\right). \tag{6}$$

We term this the local approximation [4].

2.2. Periodic model

If we assume that the system is in resonance

$$\Delta E = \Delta n\hbar\omega_0 \tag{7}$$

with integer Δn, then the model becomes periodic under energy conserving translations. This allows us to make use of Bloch's theorem, which has the practical consequence of reducing a two-dimensional calculation to a set of calculations in one dimension. We can implement Bloch's theorem by adopting a solution of the form

$$\Psi = \sum_m\sum_n e^{im\phi}v_{n+m\Delta n}|S,m\rangle|n\rangle. \tag{8}$$

The v expansion coefficients satisfy [4]

$$E(\phi)v_n = \left[n\hbar\omega_0 - i\frac{\hbar}{2}\hat{\Gamma}(E)\right]v_n$$

$$+g\Delta E\left[e^{i\phi}(v_{n+\Delta n+1}+v_{n+\Delta n-1})+e^{-i\phi}(v_{n-\Delta n+1}+v_{n-\Delta n-1})\right], \tag{9}$$

where the dimensionless coupling constant g is defined as

$$g = \frac{V\sqrt{n}\sqrt{S^2-m^2}}{\Delta E}. \tag{10}$$

2.3. Implementing loss as a hard boundary

In the limit of infinite loss, we eliminated the basis states in perturbation theory with an energy less than E. In the strong coupling limit, the self-energy is sufficiently large that it becomes difficult to implement such a scheme. It ends up being simpler to eliminate basis states below a fixed basis state energy, which we can implement here by adopting a hard boundary in n. It is convenient in this limit to work with a relative n that is zero just above the boundary. This leads to an eigenvalue equation of the form [5]

$$E(\phi)v_n = n\hbar\omega_0 + g\Delta E\left[\mathrm{e}^{i\phi}(v_{n+\Delta n+1} + v_{n+\Delta n-1}) + \mathrm{e}^{-i\phi}(v_{n-\Delta n+1} + v_{n-\Delta n-1})\right] \tag{11}$$

with the condition

$$v_n = 0 \qquad \text{for } n < 0. \tag{12}$$

2.4. Indirect coupling coefficients and system dynamics

The system dynamics can be approximated using a model based on indirect coupling between sequential nearly degenerate states. For coherent energy exchange when Δn is large, the associated rate is determined by the indirect coupling coefficient between states that differ according to

$$(m, n) \rightarrow (m \pm 1, n \mp \Delta n). \tag{13}$$

Since the indirect coupling is strongest between these states, we can estimate the indirect coupling matrix element V_{eff} from the level splitting [3]

$$V_{\text{eff}} = \frac{E(0) - E(\pi)}{4}. \tag{14}$$

The system dynamics developed from Ehrenfest's theorem for the classical average $m(t)$ when the states are degenerate satisfy [2]

$$\frac{\mathrm{d}^2}{\mathrm{d}t^2}m(t) = \frac{2}{\hbar^2}\frac{\mathrm{d}}{\mathrm{d}m}.V_{\text{eff}}^2(m). \tag{15}$$

Consequently, our primary focus is on the determination of the indirect coupling matrix elements V_{eff} in what follows.

3. Pulse and Envelope Approximation

Even though the various approximations we have introduced simplify the problem considerably, the eigenvalue equation for the v_n expansion coefficients can still be difficult to solve when the coupling is strong. We are interested in developing an approximate product solution that will model the shape of individual "pulses" separately from the "envelope".

3.1. Energy

Although we obtained approximate equations previously for the pulse shape and amplitude, here we would like to be more systematic. The starting point for our analysis is total energy, which we write as

$$\langle v_n|\hat{H}|v_n\rangle \;=\; \hbar\omega_0 \sum_n n|v_n|^2$$
$$+g\Delta E \sum v_n^* \Big[\mathrm{e}^{i\phi}(v_{n+\Delta n+1} + v_{n+\Delta n-1}) + \mathrm{e}^{-i\phi}(v_{n-\Delta n+1} + v_{n-\Delta n-1}) \Big]. \tag{16}$$

Ideally, we would like to implement our approximation to derive a new energy relation in terms of a pulse shape and amplitudes, and then minimize the energy to obtain variational equations for the pulse and amplitudes.

3.2. Approximate product solutions for $\phi = 0$ and $\phi = \pi$

We adopt approximate product solutions given by (see the solutions for the expansion coefficients in [5])

$$v_n \;=\; \sum_m (-1)^m a_m u_{n-m\Delta n} \qquad (\phi = 0), \tag{17}$$

$$v_n \;=\; \sum_m a_m u_{n-m\Delta n} \qquad (\phi = \pi). \tag{18}$$

The idea is that a single pulse is modeled using the u_n within a range of Δn indices, and successive pulses are scaled with the amplitude a_m (where the m index keeps track of the pulse). We include the phase factor for the $\phi = 0$ case since successive pulses are observed to alternate in sign in numerical calculations.

The energy expression in both cases is the same algebraically; we may write

$$\langle v_n|\hat{H}|v_n\rangle \;=\; \Delta E \sum_m m a_m^2 \;+\; \hbar\omega_0 \sum_n n u_n^2$$
$$-g\Delta E \sum_m a_m(a_{m+1} + a_{m-1}) \sum_n u_n(u_{n+1} + u_{n-1}), \tag{19}$$

where we have assumed that

$$\sum_n u_n^2 \;=\; 1, \qquad \sum_m a_m^2 \;=\; 1. \tag{20}$$

3.3. Optimization of the pulse and envelope

We can optimize the pulse shape u_n by minimizing the energy subject to the constraint that the associated probability is constant to obtain

$$\lambda_u u_n \;=\; \frac{n}{\Delta n} u_n - g\Big[\sum_m a_m(a_{m+1} + a_{m-1}) \Big](u_{n+1} + u_{n-1}). \tag{21}$$

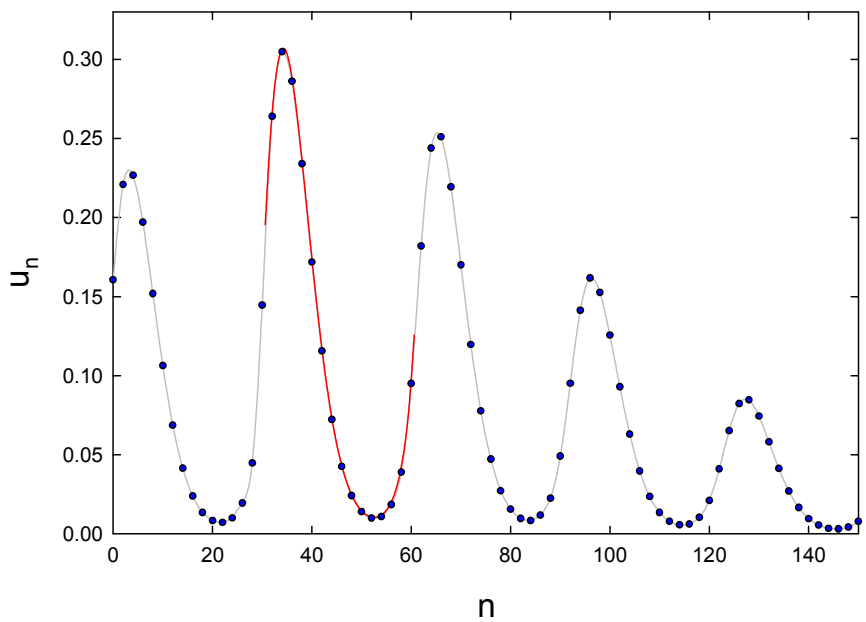

Figure 1. Expansion coefficients for $\Delta n = 31$, $g = 2$, and $\phi = \pi$ (*blue points*); optimized product solution for the pulse (*red line*).

The boundary conditions for the u_n for the two cases within this approximation are

$$u_n = -u_{n+\Delta n} \quad (\phi = 0), \tag{22}$$

$$u_n = u_{n+\Delta n} \quad (\phi = \pi). \tag{23}$$

A similar argument can be used to optimize the envelope a_m to obtain

$$\lambda_a a_m = m a_m - g\left[\sum_n u_n(u_{n+1} + u_{n-1})\right](a_{m+1} + a_{m-1}). \tag{24}$$

The boundary conditions appropriate are

$$a_{-m} = 0 \quad (m = 1, 2, \cdots), \tag{25}$$

$$\lim_{m\to\infty} a_m = 0. \tag{26}$$

3.4. Evaluation of the discrete pulse and envelope model

The formulation that we have outlined above allows us to optimize pulse shapes and amplitudes systematically, and provides a route for the computation of the total energy. In principle, all we need to do is to carry out such computations in order to develop approximate results for the energy splitting needed to estimate the indirect coupling. The approach works pretty well, as we can see from comparing with a test problem.

Consider the specific example of $\Delta n = 31$ and $g = 2$. We can see how good the approximate pulse solution is by comparing it to a numerically exact solution in Fig. 1. The optimized approximate pulse shape compares well with the exact solution. The optimized amplitudes are shown in comparison with the exact solution for the expansion coefficients in Fig. 2, where one sees again that the agreement is good.

The total energies for the numerically exact solution are

$$E(0) = -5.0856160\,\Delta E, \qquad E(\pi) = -5.0859317\,\Delta E. \tag{27}$$

The total energies for the approximate solution are evaluated from the total energy expression of Eq. (19)

$$E(0) = -5.0723289\,\Delta E, \qquad E(\pi) = -5.0726649\,\Delta E. \tag{28}$$

The approximate self-energies are reasonably close to the numerically exact results (see Fig. 3). The indirect coupling matrix element in the numerically exact calculation is

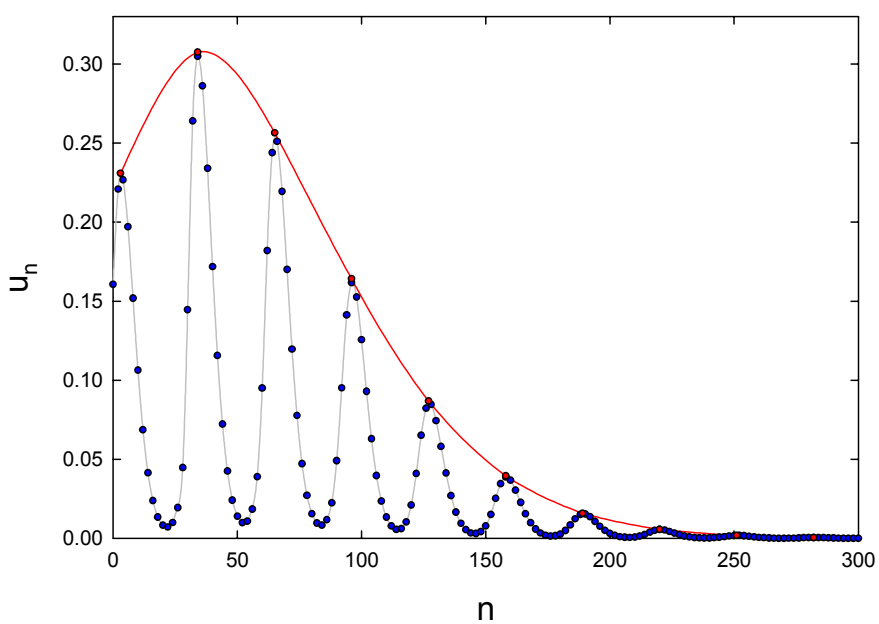

Figure 2. Expansion coefficients for $\Delta n = 31$, $g = 2$, and $\phi = \pi$ (*blue points*); optimized product solution for the amplitude (*red points*).

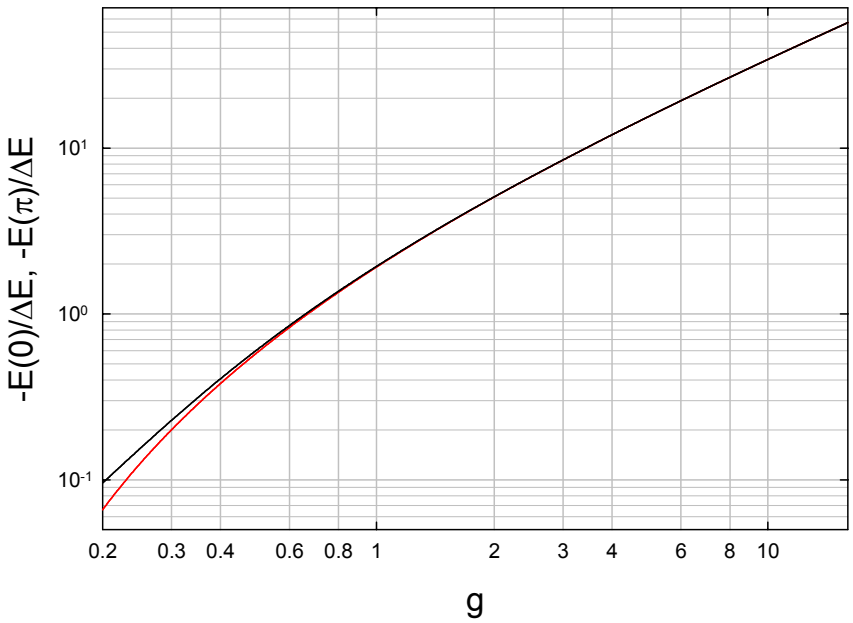

Figure 3. Self-energy as a function of g for $\Delta n = 31$; numerically exact results (*black*), and results computed from optimized pulse and amplitudes (*red*).

$$\frac{V_{\text{eff}}}{\Delta E} = 7.89137 \times 10^{-5}. \tag{29}$$

For the approximation, we get

$$\frac{V_{\text{eff}}}{\Delta E} = 8.40067 \times 10^{-5}, \tag{30}$$

which from our perspective is reasonable, since this quantity changes rapidly with g as can be seen in Fig. 4. The approximate indirect coupling matrix element begins to diverge from the exact result at small g, which might be expected as the solution in this regime is dominated by a single narrow pulse.

Our basic conclusion is that the pulse and amplitude approximation works pretty well for this problem.

4. Continuum Pulse and Discrete Envelope Approximation

We are interested in lossy spin–boson models and their generalizations under conditions where Δn is very large, in which case we would like to use a continuum approximation for the pulse. For now, we will keep the envelope discrete as in the model of the previous section.

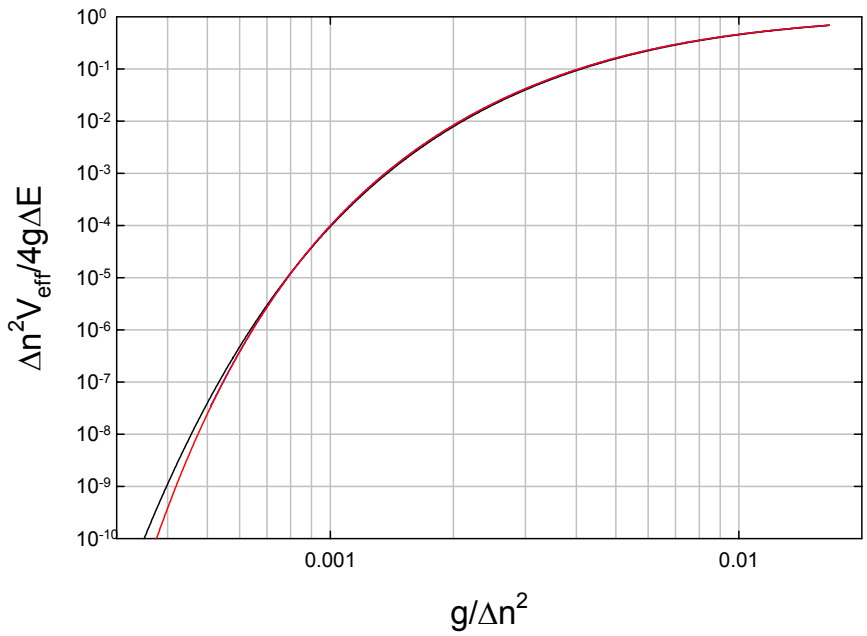

Figure 4. Scaled indirect coupling matrix element as a function of g for $\Delta n = 31$; numerically exact result (*black*), and scaled matrix element computed from optimized discrete pulse and amplitudes (*red*).

4.1. Pulse continuum approximation

We begin by defining a continuum variable associated with the n index

$$\frac{n}{\Delta n} \rightarrow z \tag{31}$$

and then allow the pulse to be a continuous functions

$$u_n \rightarrow u(z). \tag{32}$$

The energy expression with a continuous pulse can be written as

$$\langle v_n|\hat{H}|v_n\rangle = \Delta E \sum_m m a_m^2 + \Delta E \int_0^1 z u^2(z)\,\mathrm{d}z$$
$$-g\Delta E \sum_m a_m(a_{m+1} + a_{m-1}) \int_0^1 u(z)\left[u\left(z + \frac{1}{\Delta n}\right) + u\left(z - \frac{1}{\Delta n}\right)\right]\mathrm{d}z, \tag{33}$$

where we assume that

$$\sum_m a_m^2 \;=\; 1, \tag{34}$$

$$\int_0^1 u^2(z)\,\mathrm{d}z \;=\; 1. \tag{35}$$

4.2. Large Δn limit

Although it is possible to develop a continuum model based on the energy expression above, the resulting optimization of the pulse will involve a difference-differential eigenvalue constraint that is not particularly easy to solve. We would prefer a differential eigenvalue equation. The continuum approximation would be used for problems where many indices n are involved, which occurs when Δn is large. So, it seems reasonable to assume that Δn will be large, and we may approximate

$$u\left(z+\frac{1}{\Delta n}\right)+u\left(z-\frac{1}{\Delta n}\right) \;=\; 2u(z)+\frac{1}{\Delta n^2}\frac{\mathrm{d}^2}{\mathrm{d}z^2}u(z)+\cdots \tag{36}$$

If a second order approximation is sufficient, then the integral in the energy expression can be recast as

$$\begin{aligned}\int_0^1 u(z)\left[u\left(z+\frac{1}{\Delta n}\right)+u\left(z-\frac{1}{\Delta n}\right)\right]\mathrm{d}z \;&=\; \int_0^1 u(z)\left[2u(z)+\frac{1}{\Delta n^2}\frac{\mathrm{d}^2}{\mathrm{d}z^2}u(z)\right]\mathrm{d}z\\ &=\; 2+\frac{1}{\Delta n^2}\int_0^1 u(z)\frac{\mathrm{d}^2}{\mathrm{d}z^2}u(z)\,\mathrm{d}z.\end{aligned} \tag{37}$$

We can write

$$\int_0^1 u(z)\frac{\mathrm{d}^2}{\mathrm{d}z^2}u(z)\,\mathrm{d}z \;=\; u(z)\frac{\mathrm{d}}{\mathrm{d}z}u(z)\bigg|_0^1-\int_0^1\left[\frac{\mathrm{d}}{\mathrm{d}z}u(z)\right]^2\mathrm{d}z. \tag{38}$$

Since our boundary conditions are periodic for $\phi=\pi$, we have

$$u(z)\frac{\mathrm{d}}{\mathrm{d}z}u(z)\bigg|_0^1 \;=\; 0. \tag{39}$$

Since $u^2(z)$ is periodic when $\phi=0$, this condition then holds for both cases of interest.

As a result, we can rewrite the energy expression as

$$\begin{aligned}\langle v_n|\hat{H}|v_n\rangle \;=\; \Delta E\sum_m m a_m^2 \;+\; \Delta E\int_0^1 z u^2(z)\,\mathrm{d}z\\ -\,2g\Delta E\sum_m a_m(a_{m+1}+a_{m-1})\left[1-\frac{1}{2\Delta n^2}\int_0^1\left[\frac{\mathrm{d}}{\mathrm{d}z}u(z)\right]^2\mathrm{d}z\right].\end{aligned} \tag{40}$$

4.3. Optimization of the pulse and amplitude

We optimize the pulse by minimizing the energy to obtain

$$\lambda_u u(z) \;=\; zu(z) - g\sum_m a_m(a_{m+1}+a_{m-1})\frac{1}{\Delta n^2}\frac{\mathrm{d}^2}{\mathrm{d}z^2}u(z) \tag{41}$$

with the boundary condition

$$u(z+1) = -u(z) \quad (\phi = 0), \tag{42}$$

$$u(z+1) = u(z) \quad (\phi = \pi). \tag{43}$$

Optimization of the amplitude leads to the constraint

$$\lambda_a a_m \;=\; -ma_m - g\left[1 - \frac{1}{2\Delta n^2}\int_0^1 \left[\frac{\mathrm{d}}{\mathrm{d}z}u(z)\right]^2 \mathrm{d}z\right](a_{m+1}+a_{m-1}). \tag{44}$$

Subject to the same boundary conditions as before

$$a_{-m} \;=\; 0 \quad (m = 1, 2, \cdots), \tag{45}$$

$$\lim_{m\to\infty} a_m \;=\; 0. \tag{46}$$

4.4. Results

The pulse and amplitudes predicted by this model are very good, similar to those considered in Section 4.3. However, if we calculate the indirect coupling matrix element based on the total energy expression, the results are not particularly satisfactory as illustrated in Fig. 5. At low $g/\Delta n^2$ for this model, the model result appears to diverge from the numerically exact result. The reason for this is that there occur minor differences in the amplitude in this model for $\phi = 0$ and $\phi = \pi$ at low g which has a big impact on the relative total energy. We can eliminate this effect by using instead an estimate based on the pulse eigenvalues

$$\frac{V_{\mathrm{eff}}}{\Delta E} \;=\; \frac{\lambda_u(0) - \lambda_u(\pi)}{4}. \tag{47}$$

The indirect matrix element computed in this way is much better, as can be seen in Fig. 5.

5. Continuum Pulse and Continuum Amplitude Model

At larger Δn, the dimensionless coupling parameter g must be even larger for significant indirect coupling to occur, which results in a much larger number of pulses appearing. To address this, we would like to develop a continuum approximation for the amplitudes.

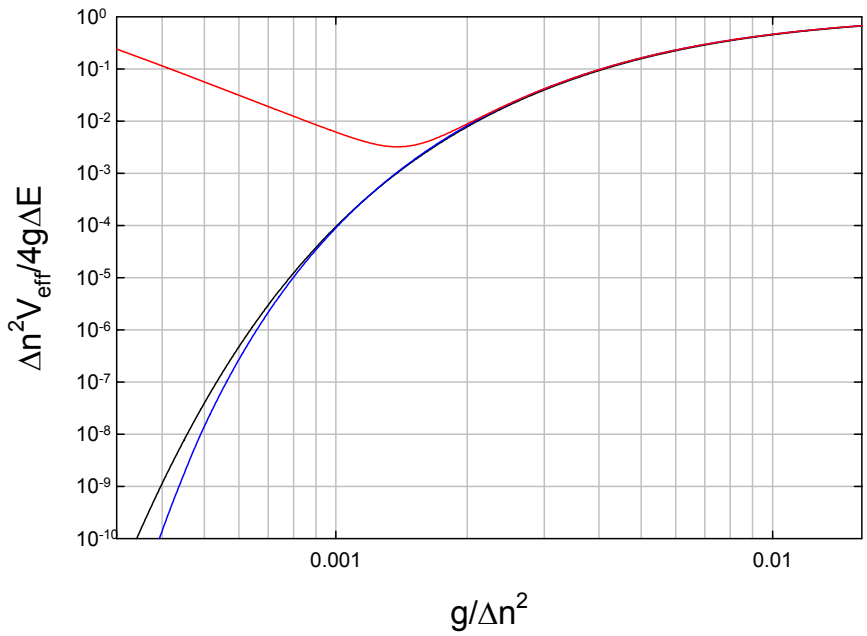

Figure 5. Scaled indirect coupling matrix element as a function of g for $\Delta n = 31$; numerically exact result (*black*), scaled matrix element computed from the total energy expression (*red*); scaled matrix element computed from the difference in pulse eigenvalues (*blue*).

5.1. Amplitude continuum approximation

We adopt a continuous variable in place of the index m

$$m \rightarrow y \tag{48}$$

and then use a continuous version of the envelope amplitudes

$$a_m \rightarrow a(y). \tag{49}$$

The energy expression in this model becomes

$$\langle v_n|\hat{H}|v_n\rangle = \Delta E \int_0^\infty y a^2(y)\,\mathrm{d}y + \Delta E \int_0^1 z u^2(z)\,\mathrm{d}z$$
$$- 2g\Delta E \int_0^\infty a(y)[a(y+1)+a(y-1)]\,\mathrm{d}y \left[1 - \frac{1}{2\Delta n^2}\int_0^1 \left[\frac{\mathrm{d}}{\mathrm{d}z}u(z)\right]^2 \mathrm{d}z\right], \tag{50}$$

where we assume that

$$\int_0^1 u^2(z)\,\mathrm{d}z \;=\; 1, \tag{51}$$

$$\int_0^\infty a^2(y)\,\mathrm{d}y \;=\; 1. \tag{52}$$

5.2. Large g approximation

We would prefer to work with a differential eigenvalue equation for the optimization of the amplitudes, so we use a Taylor series to approximate

$$a(y+1)+a(y-1) \;=\; 2a(y)+\frac{\mathrm{d}^2}{\mathrm{d}y^2}a(y)+\cdots \tag{53}$$

Once again, if a second-order approximation is good enough, then we may write

$$\int_0^\infty a(y)[a(y+1)+a(y-1)]\,\mathrm{d}y \;=\; 2+\int_0^\infty a(y)\frac{\mathrm{d}^2}{\mathrm{d}y^2}a(y)\,\mathrm{d}y. \tag{54}$$

We can use integration by parts to write

$$\int_0^\infty a(y)\frac{\mathrm{d}^2}{\mathrm{d}y^2}a(y)\,\mathrm{d}y \;=\; a(y)\frac{\mathrm{d}}{\mathrm{d}y}a(y)\bigg|_0^\infty-\int_0^\infty\left[\frac{\mathrm{d}}{\mathrm{d}y}a(y)\right]^2\mathrm{d}y. \tag{55}$$

We expect that the amplitudes decay to zero as $y\to\infty$, but the amplitudes and the first derivative does not vanish at $y=0$; hence

$$\int_0^\infty a(y)\frac{\mathrm{d}^2}{\mathrm{d}y^2}a(y)\,\mathrm{d}y \;=\; -a(0)a'(0)-\int_0^\infty\left[\frac{\mathrm{d}}{\mathrm{d}y}a(y)\right]^2\mathrm{d}y. \tag{56}$$

The energy expression in this approximation becomes

$$\begin{aligned}\langle v_n|\hat{H}|v_n\rangle \;=\; &\Delta E\int_0^\infty ya^2(y)\,\mathrm{d}y \;+\; \Delta E\int_0^1 zu^2(z)\,\mathrm{d}z\\ &-4g\Delta E\left[1-\frac{a(0)a'(0)}{2}-\frac{1}{2}\int_0^\infty\left[\frac{\mathrm{d}}{\mathrm{d}y}a(y)\right]^2\mathrm{d}y\right]\left[1-\frac{1}{2\Delta n^2}\int_0^1\left[\frac{\mathrm{d}}{\mathrm{d}z}u(z)\right]^2\mathrm{d}z\right].\end{aligned} \tag{57}$$

5.3. Optimization of the pulse and amplitudes

We can optimize the pulse $u(z)$ to obtain

$$\lambda_u u(z) \;=\; zu(z) - \frac{2g}{\Delta n^2}\left[1 - \frac{a(0)a'(0)}{2} - \frac{1}{2}\int_0^\infty \left[a'(y)\right]^2 \,\mathrm{d}y\right]\frac{\mathrm{d}^2}{\mathrm{d}z^2}u(z) \tag{58}$$

subject to the boundary conditions

$$u(0) \;=\; -u(1) \quad (\phi = 0), \tag{59}$$

$$u(0) \;=\; u(1) \quad (\phi = \pi). \tag{60}$$

The amplitudes are optimized to give the constraint

$$\lambda_a a(y) \;=\; ya(y) - 2g\left[1 - \frac{1}{2\Delta n^2}\int_0^1 [u'(z)]^2 \,\mathrm{d}z\right]\frac{\mathrm{d}^2}{\mathrm{d}y^2}a(y) \tag{61}$$

subject to the boundary conditions

$$\lambda_a a(0) \;=\; -2g\left[1 - \frac{1}{2\Delta n^2}\int_0^1 [u'(z)]^2 \,\mathrm{d}z\right]\left[a(1) - 2a(0)\right], \tag{62}$$

$$\lim_{y\to\infty} a(y) \;=\; 0. \tag{63}$$

The first of these was selected (as giving the best self-energy) from numerous possible similar boundary conditions based on the ways of estimating the slope at the boundary; this one is adapted from the relation between the discrete amplitude approximation for a_m with $m = 0$. We note that there are relations between the eigenvalue and the factors that appear in these optimization equations, as given in the Appendix.

5.4. Airy function solution for the amplitudes

Note that we can solve analytically for the amplitude function in terms of Airy functions

$$a(y) \;=\; C\,\mathrm{Ai}\left(\beta(y - y_0)\right), \tag{64}$$

where C is a normalization constant, and β satisfies

$$\frac{1}{\beta^3} \;=\; 2g\left[1 - \frac{1}{2\Delta n^2}\int_0^1 [u'(z)]^2 \,\mathrm{d}z\right]. \tag{65}$$

The eigenvalue λ_a for this solution is

$$\lambda_a \;=\; y_0. \tag{66}$$

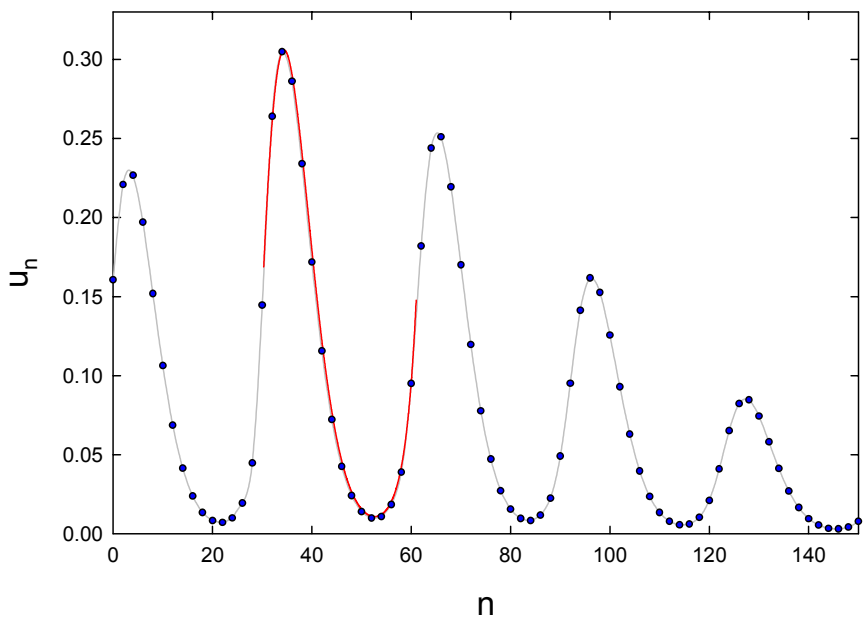

Figure 6. Expansion coefficients for $\Delta n = 31$, $g = 2$, and $\phi = \pi$ (*blue points*); optimized product continuum solution for the pulse (*red line*).

The boundary condition at $y = 0$ is satisfied by

$$\lambda_a \mathrm{Ai}\,(-\beta y_0) \;=\; -2g\left[1 - \frac{1}{2\Delta n^2}\int_0^1 [u'(z)]^2\,\mathrm{d}z\right]\left[\mathrm{Ai}\left(\beta(1-y_0)\right) - 2\mathrm{Ai}\,((-\beta y_0)\right], \tag{67}$$

$$\frac{\mathrm{Ai}\left(\beta(1-y_0)\right)}{\mathrm{Ai}\,(-\beta y_0)} \;=\; 2 - \frac{y_0}{2g\left[1 - \dfrac{1}{2\Delta n^2}\displaystyle\int_0^1 [u'(z)]^2\,\mathrm{d}z\right]}. \tag{68}$$

5.5. Evaluation of the continuum pulse and envelope model

Two distinct approximations are made in the continuum model described in the sections above; modeling the pulse as a continuum, and modeling the amplitudes as a continuum. For our test problem with $\Delta n = 31$ and $g = 2$, we find that the pulse (Fig. 6) and amplitudes (Fig. 7) once again are well approximated by the continuum approximation. In general, the continuum approximation seems to be closer for the self-energy than the discrete approximation described previously, as shown in Fig. 8. The indirect matrix element computed from the total energy, and from the pulse eigenvalues, are shown in Fig. 9. One sees that the problem with the total energy expression is now more severe, but the alternate approach of using the pulse eigenvalues seems to give an estimate not too far from the numerically exact result.

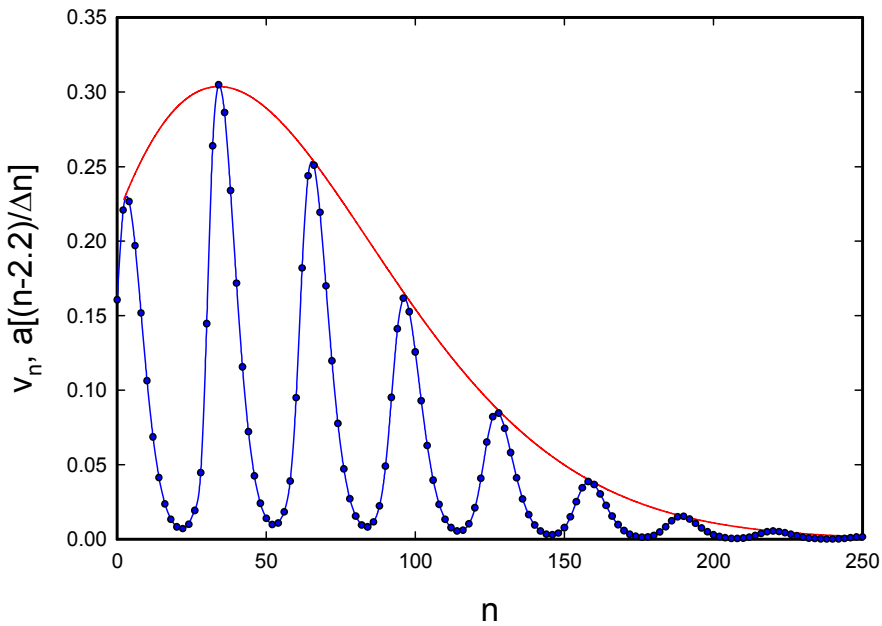

Figure 7. Expansion coefficients for $\Delta n = 31$, $g = 2$, and $\phi = \pi$ (*blue points*); optimized product solution for the amplitude (*red line*). We offset the $a(y)$ here to match the peaks of the different pulses (since the first peak does not occur at $n = 0$).

We expect that the pulse and amplitude model comes closer to the exact numerical result when the dimensionless coupling strength is larger, and that the continuum approximation will be better when Δn is larger. We can see that this is the case from results for the indirect coupling matrix element shown in Fig. 10.

6. Discussion and Conclusions

The lossy spin–boson model is important in our view as the first example of a class of models which demonstrates efficient energy conversion between a two level system and an oscillator when the transition energy ΔE is a large integer multiple of the oscillator frequency. In spite of the apparent simplicity of the model Hamiltonian, a direct solution of the model when Δn is large in the strong coupling regime is not easy. We have developed approximate versions of the model which can be solved much more easily, as described in Section 2

The idea of a pulse and amplitude separation was introduced in earlier work, and it was used to obtain a scaling law in the strong coupling regime. In this paper we revisited the pulse and amplitude model, and developed it much more systematically. This model appears to give good results for both the pulses and amplitudes for the cases studied, as well as for the self-energies. It is in general much more difficult to estimate the indirect coupling matrix element accurately, so that we can get a sense of how good each version of the model is by how well the indirect coupling matrix elements are reproduced.

In the case of the discrete pulse and discrete amplitude approximation, we find the best agreement. When we introduce the continuum approximation for the pulse, we find that estimating the indirect coupling matrix element from

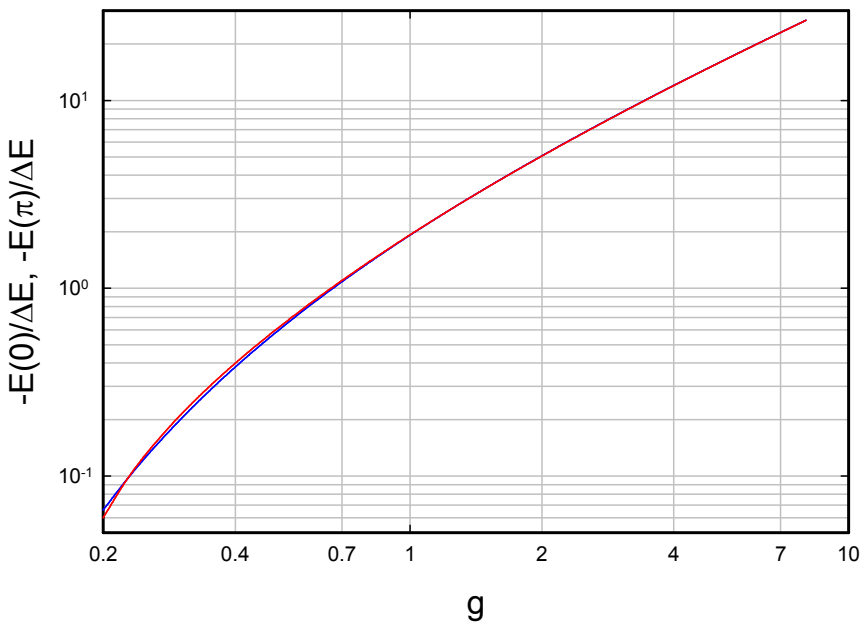

Figure 8. Self-energy as a function of g for $\Delta n = 31$; numerically exact results (*blue*), and results computed from optimized pulse and amplitudes (*red*).

the total energy is unreliable in the weak coupling regime. In this case, good results can be recovered if we rely on the difference between the pulse eigenvalues λ_u computed for both the $\phi = 0$ and $\phi = \pi$ cases under the assumption that the amplitude is fixed (we chose the $\phi = \pi$ case). In the model where both the pulse and amplitude are continuous, once again the indirect coupling matrix element obtained from the total energy is unreliable in the weak coupling regime, but the results are pretty good if we again use the pulse eigenvalues. If we go back to the discrete pulse and discrete amplitude model and examine the indirect coupling matrix element computed with the pulse eigenvalues, we find that they are very close (the lines overlap on the resulting plots) to those computed with the total energy.

The pulse and amplitude approximation helps to make the lossy two-level model much more understandable. We can see the effect of the amplitudes on the difference in the pulse eigenvalues which approximately determines the splitting. For example, in the strong coupling approximation of Ref. [5], the pulse eigenvalue equation used can be written as

$$\lambda_u u(z) \;=\; z u(z) - \frac{2g}{\Delta n^2}\frac{\mathrm{d}^2}{\mathrm{d}z^2}u(z), \tag{69}$$

while in the pulse and amplitude approximation we may write

$$\lambda_u u(z) \;=\; z u(z) - \frac{2g}{\Delta n^2}\left[1 + \frac{1}{2}\int_0^\infty a(y)a''(y)\,\mathrm{d}y\right]\frac{\mathrm{d}^2}{\mathrm{d}z^2}u(z). \tag{70}$$

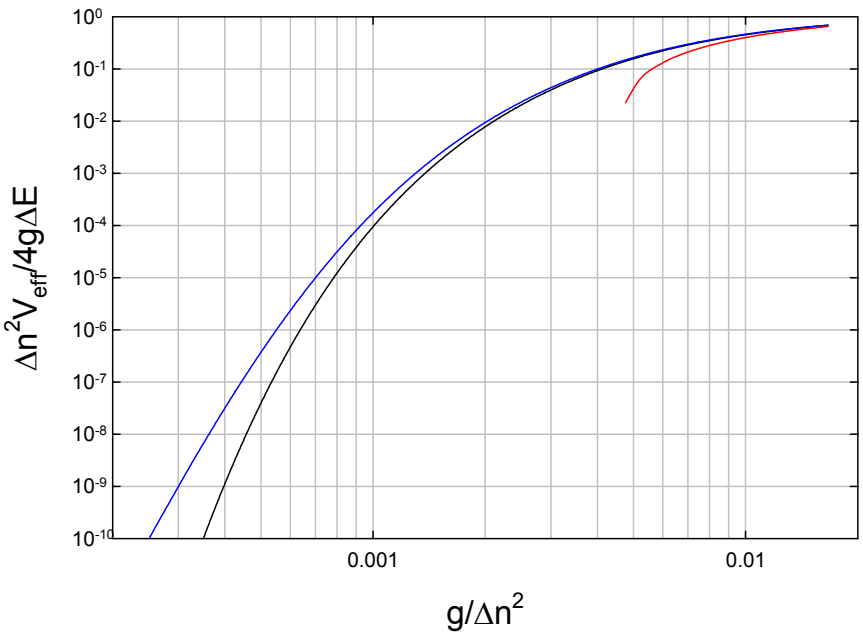

Figure 9. Scaled indirect coupling matrix element as a function of g for $\Delta n = 31$; numerically exact result (*black*), scaled matrix element computed from the total energy expression (*red*); scaled matrix element computed from the difference in pulse eigenvalues (*blue*).

Deviations from the strong coupling limit for the pulse come about because the amplitudes are not constant (or linear), and this results in a decrease (since the integral is negative) in the indirect coupling matrix element.

The pulse and amplitude approximation is very powerful, and has applications beyond the lossy spin–boson model. We have found that the approach works well in the case of the generalization of the model to three-level systems.

Appendix A. Connection between Eigenvalues and Integrals

Once the eigenvalues are found, they can be used to evaluate terms that appear in the energy expression. This is helpful in avoiding the explicit computation of an integral that appears in the other eigenvalue equation, and in the energy expression. We begin by noting

$$\lambda_u \int_0^1 u^2(z)\,\mathrm{d}z = \int_0^1 z u^2(z)\,\mathrm{d}z - \frac{2g}{\Delta n^2}\left[1 - \frac{a(0)a'(0)}{2} - \frac{1}{2}\int_0^\infty \left[a'(y)\right]^2 \mathrm{d}y\right]\int_0^1 u(z)\frac{\mathrm{d}^2}{\mathrm{d}z^2}u(z)\,\mathrm{d}z. \tag{A.1}$$

We can rewrite this using the normalization condition as

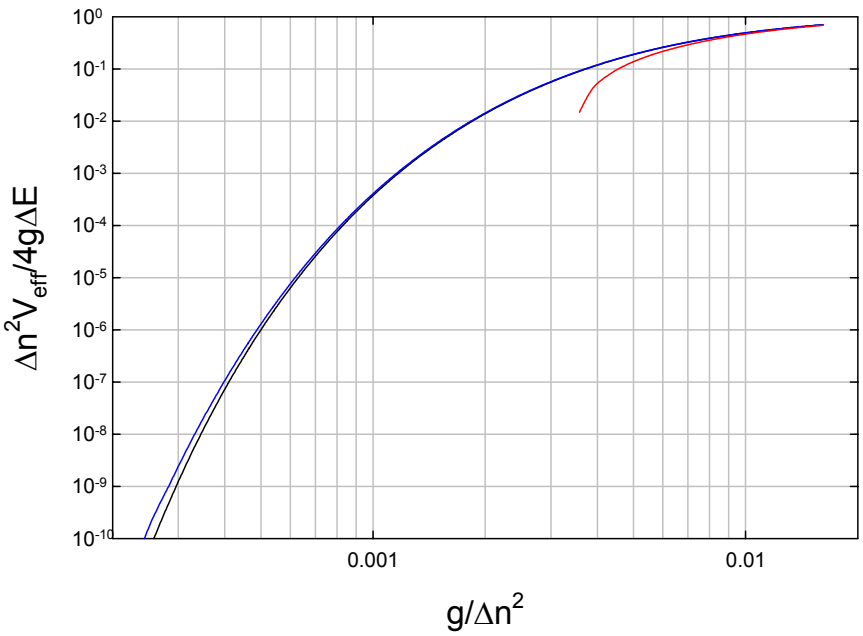

Figure 10. Scaled indirect coupling matrix element as a function of g for $\Delta n = 61$; numerically exact result (*black*), scaled matrix element computed from the total energy expression (*red*); scaled matrix element computed from the difference in pulse eigenvalues (*blue*).

$$\frac{1}{2\Delta n^2}\int_0^1 [u'(z)]^2\,\mathrm{d}z = \frac{1}{4g}\frac{\lambda_u - \int_0^1 z u^2(z)\,\mathrm{d}z}{\left[1 - \frac{a(0)a'(0)}{2} - \frac{1}{2}\int_0^\infty \left[a'(y)\right]^2\,\mathrm{d}y\right]}. \tag{A.2}$$

Similarly, we may write

$$\lambda_a \int_0^\infty a^2(y)\,\mathrm{d}y = \int_0^\infty y a^2(y)\,\mathrm{d}y - 2g\left[1 - \frac{1}{2\Delta n^2}\int_0^1 [u'(z)]^2\,\mathrm{d}z\right]\int_0^\infty a(y)\frac{\mathrm{d}^2}{\mathrm{d}y^2}a(y)\,\mathrm{d}y, \tag{A.3}$$

$$-2g\left[1 - \frac{1}{2\Delta n^2}\int_0^1 [u'(z)]^2\,\mathrm{d}z\right]\int_0^\infty a(y)\frac{\mathrm{d}^2}{\mathrm{d}y^2}a(y)\,\mathrm{d}y = \lambda_a - \int_0^\infty y a^2(y)\,\mathrm{d}y, \tag{A.4}$$

$$-\frac{1}{2}\int_0^\infty a(y)\frac{\mathrm{d}^2}{\mathrm{d}y^2}a(y)\,\mathrm{d}y = \frac{a(0)a'(0)}{2} + \frac{1}{2}\int_0^\infty [a'(y)]^2\,\mathrm{d}y$$

$$= \frac{1}{4g}\frac{\lambda_a - \int_0^\infty ya^2(y)\,\mathrm{d}y}{\left[1 - \frac{1}{2\Delta n^2}\int_0^1 [u'(z)]^2\,\mathrm{d}z\right]}. \tag{A.5}$$

References

[1] P.L. Hagelstein and I.U. Chaudhary, Energy exchange in the lossy spin–boson model, *J. Cond. Mat. Nucl. Sci.* **5** (2011) 52.

[2] P.L. Hagelstein and I.U. Chaudhary, Dynamics in the case of coupled degenerate states, *J. Cond. Mat. Nucl. Sci.* **5** (2011) 72.

[3] P.L. Hagelstein and I.U. Chaudhary, Second-order formulation and scaling in the lossy spin–boson model, *J. Cond. Mat. Nucl. Sci.* **5** (2011) 87.

[4] P.L. Hagelstein and I.U. Chaudhary, Local approximation for the lossy spin–boson model, *J. Cond. Mat. Nucl. Sci.* **5** (2011) 102.

[5] P.L. Hagelstein and I.U. Chaudhary, Coherent energy exchange in the strong coupling limit of the lossy spin–boson model, *J. Cond. Mat. Nucl. Sci.* **5** (2011) 116.

[6] M. Fleischmann, S. Pons and M. Hawkins, *J. Electroanal. Chem.* **261** (1989) 301; errata **263** (1990) 187.

[7] M. Fleischmann, S. Pons, M.W. Anderson, L.J. Li and M. Hawkins, *J. Electroanal. Chem.* **287** (1990) 293.

J. Condensed Matter Nucl. Sci. 9 (2012) 50–63

Research Article

Coupling between a Deuteron and a Lattice

Peter L. Hagelstein *

Research Laboratory of Electronics, Massachusetts Institute of Technology, Cambridge, MA 02139, USA

I.U. Chaudhary†

Department of Computer Science and Engineering, University of Engineering and Technology, Lahore, Pakistan

Abstract

We recently put forth a new fundamental lattice Hamiltonian based on an underlying picture of electrons and deuterons as elementary Dirac particles. Within this model there appears a term in which lattice vibrations are coupled to internal nuclear transitions. This is interesting as it has the potential to provide a connection between experiment and models that describe coherent energy transfer between two-level systems and an oscillator. In this work we describe a calculation of the coupling matrix element in the case of the deuteron based on the old empirical Hamada–Johnston model for the nucleon–nucleon interaction. The triplet S and D states of the the deuteron in the rest frame couples to a singlet P state through this new interaction. The singlet P state in this calculation is a virtual state with an energy of 125 MeV, and a coupling matrix element for z-directed motion given by $2.98 \times 10^{-3}\ M_J c \hat{P}_z$.
 ISSN 2227-3123

Keywords: $\mathbf{a} \cdot c\mathbf{P}$ interaction, Deuteron, Fleischmann–Pons effect, Quantum fractionation, Phonon exchange matrix element

1. Introduction

We recently obtained a new Hamiltonian for a lattice which includes interactions with internal nuclear degrees of freedom [1]. We started with a Dirac model for electrons and for nucleons on equal footing, then allowed the nuclei to be described by a finite basis expansion, and finally developed an approximation appropriate for low nuclear velocity. Our original motivation for this was to obtain a model capable of describing the mass shift associated with excited nuclear states in a configuration interaction calculation. However, the new model unexpectedly contains a new coupling term which provides for a direct interaction between lattice vibrations and nuclear transitions.

On the face of it, this new interaction term looks like it should allow for the strongly-coupled transitions that we have sought [2] in connection with the generalized lossy spin-boson models [3–8] that we proposed to account for some of the anomalies (such as excess heat [9–12] and collimated X-ray emission [13–17]) that have been reported in

*E-mail: plh@mit.edu
†E-mail: irfanc@mit.edu

 ISSN 2227-3123

experiments in recent years. What is needed at this point is an explicit calculation for some nuclear system to see how it works, what states are coupled to, and how big the interaction is.

In general nuclear structure models are much more complicated than atomic structure models due to the more complicated strong force interaction. We would like to work with empirical strong force models derived from scattering experiments and few-body bound state binding energies. In recent years these models have achieved impressive results [18,19]; however, some of these strong force models involve a fair amount of work to implement. If we go back a few decades we can find simpler versions of strong force models that are easier to work with, and are sufficiently accurate to clarify the issues of interest here. In the computations that follow we will focus on the old Hamada–Johnston potential model [20]. Without question the simplest compound nucleus which should show the effects of interest is the deuteron, and so we will focus on this system in what follows.

In this formulation we have modeled the nucleons as elementary Dirac particles. As nucleons are made up of strongly interacting quarks, we know that they are not elementary Dirac particles. To do better in the case of coupling with the deuteron, we would require a description in terms of the six constituent quarks. We would expect from such a model a coupling matrix element likely somewhat different from what we calculated in this work. Even so, it makes sense here to pursue this simpler deuteron model based on simple Dirac nucleons as a step forward in the modeling process.

2. Basic Model

In a recent paper we discussed the derivation of a finite basis approximation for a moving nucleus in the many-particle Dirac model which leads to the new coupling that we are interested in. We begin with the (relativistic) finite basis model that we obtained.

2.1. Finite basis approximation

In [1], we developed finite basis eigenvalue relations in the form

$$Ec_n = \sqrt{(M_n c^2)^2 + c^2|\mathbf{P}|^2}c_n + \sum_{m\neq n} H_{nm}c_m, \tag{1}$$

where the off-diagonal matrix elements were written as

$$H_{nm} = \overline{\alpha}_{nm} \cdot (c\mathbf{P}) + V_{nm}. \tag{2}$$

Here V_{nm} is the relative coupling matrix element

$$V_{nm} = \left\langle \Phi_n \middle| \sum_j \alpha_j \cdot c\hat{\pi}_j + \sum_j \beta_j m_j c^2 + \sum_{j<k} \hat{V}_{jk}(\xi_k - \xi_j) \middle| \Phi_m \right\rangle. \tag{3}$$

We defined $\overline{\alpha}_{nm}$ as

$$\overline{\alpha}_{nm} = \left\langle \Phi_n \middle| \sum_j \frac{m_j}{M}\alpha_j \middle| \Phi_m \right\rangle. \tag{4}$$

The notation for the two-body version of the problem is a bit different than what we used for the many-particle problem. It is useful to recast the relative matrix element as

$$V_{nm} = \left\langle \Phi_n \middle| (\alpha_2 - \alpha_1) \cdot c\hat{\mathbf{p}} + \beta_1 m_1 c^2 + \beta_2 m_2 c^2 + \hat{V}(\mathbf{r}) \middle| \Phi_m \right\rangle. \tag{5}$$

The relative part of the off-diagonal matrix element corresponds to the rest frame interaction terms, which might come about from strong force interactions as in the development above for the nonrelativistic deuteron problem. What is new is the coupling with the center of mass momentum $\mathbf{P}$ that appears in $\overline{\alpha}_{nm} \cdot (c\mathbf{P})$. We are interested in these new matrix elements.

2.2. Nonrelativistic reduction of the new interaction term

In [1], we discussed the reduction of the new interaction matrix element to the nonrelativistic case. The results can be expressed as

$$\begin{aligned}\left\langle \Phi_f \middle| \sum_j \frac{m_j}{M} \alpha_j \cdot c\hat{\mathbf{P}} \middle| \Phi_i \right\rangle \rightarrow\ & \frac{(E - Mc^2)}{2Mc^2} \left\langle \Phi_f \middle| \sum_j \frac{\hat{\pi}_j \cdot \hat{\mathbf{P}}}{m_j} \middle| \Phi_i \right\rangle \\ & + \frac{1}{2Mc^2} \left[\left\langle \Phi_f \middle| \sum_j (\sigma_j \cdot c\hat{\mathbf{P}}) \left[\frac{1}{2m_j c^2} \sum_{k<l} \hat{V}_{kl}(\xi_l - \xi_k) \right] (\sigma_j \cdot c\hat{\pi}_j) \middle| \Phi_i \right\rangle \right. \\ & \left. + \left\langle \Phi_f \middle| \sum_j (\sigma_j \cdot c\hat{\pi}_j) \left[\frac{1}{2m_j c^2} \sum_{k<l} \hat{V}_{kl}(\xi_l - \xi_k) \right] (\sigma_j \cdot c\hat{\mathbf{P}}) \middle| \Phi_i \right\rangle \right].\end{aligned} \tag{6}$$

As above, this is written for the many-particle problem, and we wish to recast it in terms of the two-body problem; we may write

$$\begin{aligned}\left\langle \Phi_f \middle| \sum_j \frac{m_j}{M} \alpha_j \cdot c\hat{\mathbf{P}} \middle| \Phi_i \right\rangle \rightarrow\ & \frac{(E - Mc^2)}{2Mc^2} \left(\frac{1}{m_2} - \frac{1}{m_1} \right) \left\langle \Phi_f \middle| \hat{\mathbf{p}} \cdot \hat{\mathbf{P}} \middle| \Phi_i \right\rangle \\ & - \frac{1}{2Mc^2} \left[\left\langle \Phi_f \middle| (\sigma_1 \cdot c\hat{\mathbf{P}}) \left[\frac{1}{2m_1 c^2} \hat{V}(\mathbf{r}) \right] (\sigma_1 \cdot c\hat{\mathbf{p}}) \middle| \Phi_i \right\rangle \right. \\ & \left. + \left\langle \Phi_f \middle| (\sigma_1 \cdot c\hat{\mathbf{p}}) \left[\frac{1}{2m_1 c^2} \hat{V}(\mathbf{r}) \right] (\sigma_1 \cdot c\hat{\mathbf{P}}) \middle| \Phi_i \right\rangle \right] \\ & + \frac{1}{2Mc^2} \left[\left\langle \Phi_f \middle| (\sigma_2 \cdot c\hat{\mathbf{P}}) \left[\frac{1}{2m_2 c^2} \hat{V}(\mathbf{r}) \right] (\sigma_2 \cdot c\hat{\mathbf{p}}) \middle| \Phi_i \right\rangle \right. \\ & \left. + \left\langle \Phi_f \middle| (\sigma_2 \cdot c\hat{\mathbf{p}}) \left[\frac{1}{2m_2 c^2} \hat{V}(\mathbf{r}) \right] (\sigma_2 \cdot c\hat{\mathbf{P}}) \middle| \Phi_i \right\rangle \right].\end{aligned} \tag{7}$$

2.3. Equal mass approximation

It is possible to split up this new interaction term into a contribution that takes the nucleon masses to be equal, and a small correction term that depends on the difference between the nucleon masses. In what follows our focus will be on the larger equal mass terms, which is equivalent to making an equal mass approximation. In this case we may write

$$\left\langle \Phi_f \left| \sum_j \frac{m_j}{M} \alpha_j \cdot c\hat{\mathbf{P}} \right| \Phi_i \right\rangle \rightarrow -\left(\frac{1}{2Mc^2}\right)\left(\frac{1}{2m_{av}c^2}\right)\left[\left\langle \Phi_f \left| (\sigma_1 \cdot c\hat{\mathbf{P}})\left[\hat{V}(\mathbf{r})\right](\sigma_1 \cdot c\hat{\mathbf{p}}) \right| \Phi_i \right\rangle \right.$$
$$\left. + \left\langle \Phi_f \left| (\sigma_1 \cdot c\hat{\mathbf{p}})\left[\hat{V}(\mathbf{r})\right](\sigma_1 \cdot c\hat{\mathbf{P}}) \right| \Phi_i \right\rangle \right]$$
$$+ \left(\frac{1}{2Mc^2}\right)\left(\frac{1}{2m_{av}c^2}\right)\left[\left\langle \Phi_f \left| (\sigma_2 \cdot c\hat{\mathbf{P}})\left[\hat{V}(\mathbf{r})\right](\sigma_2 \cdot c\hat{\mathbf{p}}) \right| \Phi_i \right\rangle \right.$$
$$\left. + \left\langle \Phi_f \left| (\sigma_2 \cdot c\hat{\mathbf{p}})\left[\hat{V}(\mathbf{r})\right](\sigma_2 \cdot c\hat{\mathbf{P}}) \right| \Phi_i \right\rangle \right], \tag{8}$$

where we have assumed that

$$m_1 = m_2 = m_{av}. \tag{9}$$

In this approximation there is no longer an explicit dependence on the state energy E.

2.4. Nonrelativistic approximation

It is possible to develop a nonrelativistic approximation using

$$\sqrt{(M_n c^2)^2 + c^2|\mathbf{P}|^2} \rightarrow M_n c^2 + \frac{|\mathbf{P}|^2}{2M_n}. \tag{10}$$

In this case, a finite basis model that includes center of mass dynamics to lowest order could be developed starting from a nonrelativistic Hamiltonian of the form

$$\hat{H} = \hat{M}c^2 + \frac{|\hat{\mathbf{P}}|^2}{2\hat{M}} + \frac{|\hat{\mathbf{p}}|^2}{2\mu} + \hat{V}(\mathbf{r}) + \hat{\mathbf{a}} \cdot c\hat{\mathbf{P}}, \tag{11}$$

where $\hat{M}$ is an operator that returns the rest mass energy of the nuclear state, and where $\hat{\mathbf{a}} \cdot c\hat{\mathbf{P}}$ in the equal mass approximation is

$$\hat{\mathbf{a}} \cdot c\hat{\mathbf{P}} \rightarrow \left(\frac{1}{2Mc^2}\right)\left(\frac{1}{2m_{av}c^2}\right)\left[(\sigma_2 \cdot c\hat{\mathbf{P}})\hat{V}(\sigma_2 \cdot c\hat{\mathbf{p}}) + (\sigma_2 \cdot c\hat{\mathbf{p}})\hat{V}(\sigma_2 \cdot c\hat{\mathbf{P}})\right.$$
$$\left. - (\sigma_1 \cdot c\hat{\mathbf{P}})\hat{V}(\sigma_1 \cdot c\hat{\mathbf{p}}) - (\sigma_1 \cdot c\hat{\mathbf{p}})\hat{V}(\sigma_1 \cdot c\hat{\mathbf{P}})\right]. \tag{12}$$

3. Finite-basis Model for the Deuteron

We know from the literature that the deuteron at rest can be modeled using a triplet S and triplet D state, since the tensor interaction mixes the two. Since the kinetic energy and potential terms preserve J and M_J, each of the triplet S states mixes with a triplet D state that has the same J and M_J.

3.1. Mixing with ^{1}P states

The new interaction term causes these states to mix with singlet P states. In general, the new term does not preserve M_J, so that we would require a finite basis approximation that distinguishes the different sublevels. However, it is possible to focus on a special case of the new interaction which does preserve M_J. This occurs if we restrict our attention to

$$\hat{\mathbf{P}} = \hat{\mathbf{i}}_z \hat{P}_z. \tag{13}$$

We find in this case that mixing occurs for $M_J = \pm 1$, but not for $M_J = 0$. In response, we might write

$$\Psi = \Psi_{^3\mathrm{S}} + \Psi_{^3\mathrm{D}} + \Psi_{^1\mathrm{P}} \tag{14}$$

with the understanding that

$$\Psi_{^1\mathrm{P}}(M_J = 0) \rightarrow 0. \tag{15}$$

3.2. Basis state construction

Nuclear state construction is usually carried out in the isospin scheme, with antisymmetry enforced through the application of the generalized Pauli principle. The two-body problem is particularly simple in this regard, with spin, isospin and spatial components restricted to being either symmetric (s) or antisymmetric (a); we may write for the three states

$$\Psi_{^3\mathrm{S}} = R(\mathrm{s})S(\mathrm{s})T(\mathrm{a}), \tag{16}$$

$$\Psi_{^3\mathrm{D}} = R(\mathrm{s})S(\mathrm{s})T(\mathrm{a}), \tag{17}$$

$$\Psi_{^1\mathrm{P}} = R(\mathrm{a})S(\mathrm{a})T(\mathrm{a}). \tag{18}$$

The antisymmetric spin and isospin terms $S(\mathrm{a})$ and $T(\mathrm{a})$ are singlets, and the symmetric spin and isospin terms $S(\mathrm{s})$ and $T(\mathrm{s})$ are triplets.

3.3. Triplet S state

The S state is a triplet spin state, so we may write it as

$$\Psi_{^3\mathrm{S}} = \Psi_{^3\mathrm{S}}(S = 1, M_S; T = 0, M_T = 0; l = 0, m = 0)$$

$$= \frac{u(r)}{r} Y_{00}(\theta, \phi)\, |1, M_S\rangle_S\, |0, 0\rangle_T. \tag{19}$$

The $Y_{lm}(\theta, \phi)$ are spherical harmonics; we choose $l = 0$ and $m = 0$ since we are working with an S state. The $|S, M_S\rangle_S$ are spin functions for the neutron and proton spins; the $|T, M_T\rangle_T$ are isospin functions, and we have used an isospin singlet function here.

3.4. Triplet D state

We can develop a D state by applying the tensor $\hat{S}_{12}$ operator on an S state. This approach was used early on as a convenient way of generating few-body wavefunctions for variational calculations in nuclear physics. We may write

$$\Psi_{^3\mathrm{D}} = \frac{1}{\sqrt{8}}\hat{S}_{12}\left[\frac{v(r)}{r}Y_{00}(\theta,\phi)|1, M_S\rangle_S\,|0,0\rangle_T\right]. \tag{20}$$

This construction is convenient since

$$\hat{S}_{12}\Psi_{^3\mathrm{D}} = \sqrt{8}\left[\frac{v(r)}{r}Y_{00}(\theta,\phi)|1, M_S\rangle_S\,|0,0\rangle_T\right] - 2\Psi_{^3D}. \tag{21}$$

3.5. Singlet P state

The singlet P state for a particular calculation can be specified using

$$\begin{aligned}\Psi_{^1\mathrm{P}} &= \Psi_{^1\mathrm{P}}(S=0, M_S=0; T=0, M_T=0; l=1, m)\\ &= i\frac{w(r)}{r}Y_{1m}(\theta,\phi)\,|0,0\rangle_S\,|0,0\rangle_T.\end{aligned} \tag{22}$$

Including an i here leads to real coupling coefficients in what follows.

3.6. Normalization

We can evaluate the normalization integral for these states simply; we write

$$\begin{aligned}\langle\Psi|\Psi\rangle &= \langle\Psi_{^3\mathrm{S}}|\Psi_{^3\mathrm{S}}\rangle + \langle\Psi_{^3\mathrm{D}}|\Psi_{^3\mathrm{D}}\rangle + \langle\Psi_{^1\mathrm{P}}|\Psi_{^1\mathrm{P}}\rangle\\ &= \int_0^\infty |u(r)|^2 + |v(r)|^2 + |w(r)|^2 dr.\end{aligned} \tag{23}$$

3.7. Expectation value of Hamiltonian terms

We are interested in developing coupled channel equations that include the new interaction. For the problem in the rest frame, this is most easily accomplished by developing an expression for the total energy and then using the variational principle. We can use the same basic approach here for the moving frame version of the problem. We begin with

$$\begin{aligned}&\left\langle\Psi\left|\frac{\mathbf{p}^2}{2\mu} + \hat{V} + (\mathbf{a}\cdot c\hat{\mathbf{P}})_z\right|\Psi\right\rangle\\ &= \left\langle\Psi_{^3\mathrm{S}}\left|\frac{\mathbf{p}^2}{2\mu} + \hat{V}\right|\Psi_{^3\mathrm{S}}\right\rangle + \left\langle\Psi_{^3\mathrm{D}}\left|\frac{\mathbf{p}^2}{2\mu} + \hat{V}\right|\Psi_{^3\mathrm{D}}\right\rangle + \left\langle\Psi_{^1\mathrm{P}}\left|\frac{\mathbf{p}^2}{2\mu} + \hat{V}\right|\Psi_{^1\mathrm{P}}\right\rangle\\ &+ \left\langle\Psi_{^3\mathrm{S}}\left|\hat{V}\right|\Psi_{^3\mathrm{D}}\right\rangle + \left\langle\Psi_{^3\mathrm{D}}\left|\hat{V}\right|\Psi_{^1\mathrm{S}}\right\rangle + \left\langle\Psi_{^1\mathrm{P}}\left|(\mathbf{a}\cdot c\hat{\mathbf{P}})_z\right|\Psi_{^1\mathrm{S}}\right\rangle\\ &+ \left\langle\Psi_{^1\mathrm{P}}\left|(\mathbf{a}\cdot c\hat{\mathbf{P}})_z\right|\Psi_{^3\mathrm{D}}\right\rangle + \left\langle\Psi_{^3\mathrm{S}}\left|(\mathbf{a}\cdot c\hat{\mathbf{P}})_z\right|\Psi_{^1\mathrm{P}}\right\rangle + \left\langle\Psi_{^3\mathrm{D}}\left|(\mathbf{a}\cdot c\hat{\mathbf{P}})_z\right|\Psi_{^1\mathrm{P}}\right\rangle.\end{aligned} \tag{24}$$

3.8. Diagonal matrix elements

We can evaluate the diagonal matrix elements directly using Mathematica to obtain

$$\left\langle \Psi_{^3\mathrm{S}} \left| \frac{\mathbf{p}^2}{2\mu} + \hat{V} \right| \Psi_{^3\mathrm{S}} \right\rangle = \int_0^\infty u(r) \left[-\frac{\hbar^2}{2\mu} \frac{\mathrm{d}^2}{\mathrm{d}r^2} - 3v_C^{et}(r) \right] u(r)\,\mathrm{d}r, \tag{25}$$

$$\left\langle \Psi_{^3\mathrm{D}} \left| \frac{\mathbf{p}^2}{2\mu} + \hat{V} \right| \Psi_{^3\mathrm{D}} \right\rangle = \int_0^\infty v(r) \left[-\frac{\hbar^2}{2\mu} \frac{\mathrm{d}^2}{\mathrm{d}r^2} - 3v_C^{et}(r) + 6v_T^{et}(r) - 3v_{LS}^{et}(r) - 3v_{LL}^{et}(r) \right] v(r)\,\mathrm{d}r. \tag{26}$$

$$\left\langle \Psi_{^1\mathrm{P}} \left| \frac{\mathbf{p}^2}{2\mu} + \hat{V} \right| \Psi_{^1\mathrm{P}} \right\rangle = \int_0^\infty w(r) \left[-\frac{\hbar^2}{2\mu} \frac{\mathrm{d}^2}{\mathrm{d}r^2} + 9v_C^{os}(r) - 2v_{LL}^{os}(r) \right] w(r)\,\mathrm{d}r. \tag{27}$$

3.9. Off-diagonal potential matrix elements

In the case of the Hamada-Johnston potential, there occur off-diagonal matrix elements between the triplet S and triplet D states, which are given by

$$\left\langle \Psi_{^3\mathrm{S}} \left| \hat{V} \right| \Psi_{^3\mathrm{D}} \right\rangle = \left\langle \Psi_{^3\mathrm{D}} \left| \hat{V} \right| \Psi_{^3\mathrm{S}} \right\rangle = -3\sqrt{8} \int_0^\infty u(r) v_T^{et} v(r)\,\mathrm{d}r. \tag{28}$$

The superscript *et* in the associated potentials here is connected with the even triplet channel, since the Hamada-Johnston potentials are fit for the different channels separately.

3.10. Off-diagonal matrix elements for the new interaction

For the off-diagonal matrix elements of the new interaction, we have used Mathematica to compute

$$
\begin{aligned}
\langle \Phi_{^1\mathrm{P}} | (\mathbf{a} \cdot c\hat{\mathbf{P}})_z | \Phi_{^3\mathrm{S}} \rangle \;=\; & M_J \left(\frac{1}{2Mc^2} \right) \left(\frac{1}{2m_{av}c^2} \right) (\hbar c)(c\hat{P}_z) \\
& \Bigg\{ -2\sqrt{3} \int_0^\infty w(r) \left[\frac{\mathrm{d}}{\mathrm{d}r} v_C^{eT}(r) \right] u(r)\,\mathrm{d}r \\
& + 12\sqrt{3} \int_0^\infty w(r) v_T^{eT}(r) \left[\frac{\mathrm{d}}{\mathrm{d}r} u(r) + \frac{u(r)}{r} \right] \mathrm{d}r \\
& + 8\sqrt{3} \int_0^\infty w(r) \left[\frac{\mathrm{d}}{\mathrm{d}r} v_T^{eT}(r) \right] u(r)\,\mathrm{d}r \\
& + \frac{2}{\sqrt{3}} \int_0^\infty w(r) v_{LS}^{eT}(r) \left[\frac{\mathrm{d}}{\mathrm{d}r} u(r) - \frac{u(r)}{r} \right] \mathrm{d}r \\
& - 2\sqrt{3} \int_0^\infty w(r) v_{LL}^{eT}(r) \left[\frac{\mathrm{d}}{\mathrm{d}r} u(r) - \frac{u(r)}{r} \right] \mathrm{d}r \Bigg\},
\end{aligned} \tag{29}
$$

$$
\begin{aligned}
\langle \Phi_{^1\mathrm{P}} | (\mathbf{a} \cdot c\hat{\mathbf{P}})_z | \Phi_{^3\mathrm{D}} \rangle \;=\; & M_J \left(\frac{1}{2Mc^2} \right) \left(\frac{1}{2m_{av}c^2} \right) (\hbar c)(c\hat{P}_z) \\
& \Bigg\{ -\sqrt{6} \int_0^\infty w(r) \left[\frac{\mathrm{d}}{\mathrm{d}r} v_C^{eT}(r) \right] v(r)\,\mathrm{d}r \\
& + 6\sqrt{6} \int_0^\infty w(r) v_T^{eT}(r) \left[\frac{\mathrm{d}}{\mathrm{d}r} v(r) + \frac{v(r)}{r} \right] \mathrm{d}r \\
& + 4\sqrt{6} \int_0^\infty w(r) \left[\frac{\mathrm{d}}{\mathrm{d}r} v_T^{eT}(r) \right] v(r)\,\mathrm{d}r \\
& - \sqrt{\frac{8}{3}} \int_0^\infty w(r) v_{LS}^{eT}(r) \left[\frac{\mathrm{d}}{\mathrm{d}r} v(r) + 2\frac{v(r)}{r} \right] \mathrm{d}r \\
& - \sqrt{6} \int_0^\infty w(r) \left[\frac{\mathrm{d}}{\mathrm{d}r} v_{LS}^{eT}(r) \right] v(r)\,\mathrm{d}r \\
& - 2\sqrt{6} \int_0^\infty w(r) v_{LL}^{eT}(r) \left[\frac{\mathrm{d}}{\mathrm{d}r} v(r) + 2\frac{v(r)}{r} \right] \mathrm{d}r \\
& - \sqrt{6} \int_0^\infty w(r) \left[\frac{\mathrm{d}}{\mathrm{d}r} v_{LL}^{eT}(r) \right] v(r)\,\mathrm{d}r \Bigg\},
\end{aligned} \tag{30}
$$

$$
\begin{aligned}
\langle \Phi_{^3\mathrm{S}} | (\mathbf{a}\cdot c\hat{\mathbf{P}})_z | \Phi_{^1\mathrm{P}} \rangle \;=\; & M_J \left(\frac{1}{2Mc^2}\right)\left(\frac{1}{2m_{av}c^2}\right)(\hbar c)(c\hat{P}_z) \\
& \Bigg\{ -2\sqrt{3}\int_0^\infty u(r)\left[\frac{\mathrm{d}}{\mathrm{d}r}v_C^{eT}(r)\right]w(r)\,\mathrm{d}r \\
& + 12\sqrt{3}\int_0^\infty u(r)v_T^{eT}(r)\left[-\frac{\mathrm{d}}{\mathrm{d}r}w(r)+\frac{w(r)}{r}\right]\mathrm{d}r \\
& - 4\sqrt{3}\int_0^\infty u(r)\left[\frac{\mathrm{d}}{\mathrm{d}r}v_T^{eT}(r)\right]w(r)\,\mathrm{d}r \\
& + \frac{2}{\sqrt{3}}\int_0^\infty w(r)v_{LS}^{eT}(r)\left[-\frac{\mathrm{d}}{\mathrm{d}r}u(r)-\frac{u(r)}{r}\right]\mathrm{d}r \\
& - \frac{2}{\sqrt{3}}\int_0^\infty u(r)\left[\frac{\mathrm{d}}{\mathrm{d}r}v_{LS}^{eT}(r)\right]w(r)\,\mathrm{d}r \\
& - 2\sqrt{3}\int_0^\infty w(r)v_{LL}^{eT}(r)\left[-\frac{\mathrm{d}}{\mathrm{d}r}u(r)-\frac{u(r)}{r}\right]\mathrm{d}r \\
& + 2\sqrt{3}\int_0^\infty u(r)\left[\frac{\mathrm{d}}{\mathrm{d}r}v_{LL}^{eT}(r)\right]w(r)\mathrm{d}r\Bigg\}
\end{aligned}
\tag{31}
$$

$$
\begin{aligned}
\langle \Phi_{^3\mathrm{D}} | (\mathbf{a}\cdot c\hat{\mathbf{P}})_z | \Phi_{^1\mathrm{P}} \rangle \;=\; & M_J \left(\frac{1}{2Mc^2}\right)\left(\frac{1}{2m_{av}c^2}\right)(\hbar c)(c\hat{P}_z) \\
& \Bigg\{ -\sqrt{6}\int_0^\infty v(r)\left[\frac{\mathrm{d}}{\mathrm{d}r}v_C^{eT}(r)\right]2(r)\,\mathrm{d}r \\
& + 6\sqrt{6}\int_0^\infty v(r)v_T^{eT}(r)\left[-\frac{\mathrm{d}}{\mathrm{d}r}w(r)+\frac{w(r)}{r}\right]\mathrm{d}r \\
& - 2\sqrt{6}\int_0^\infty v(r)\left[\frac{\mathrm{d}}{\mathrm{d}r}v_T^{eT}(r)\right]w(r)\,\mathrm{d}r \\
& - \sqrt{\frac{8}{3}}\int_0^\infty w(r)v_{LS}^{eT}(r)\left[-\frac{\mathrm{d}}{\mathrm{d}r}v(r)+2\frac{v(r)}{r}\right]\mathrm{d}r \\
& - \sqrt{\frac{2}{3}}\int_0^\infty w(r)\left[\frac{\mathrm{d}}{\mathrm{d}r}v_{LS}^{eT}(r)\right]v(r)\,\mathrm{d}r \\
& - 2\sqrt{6}\int_0^\infty w(r)v_{LL}^{eT}(r)\left[-\frac{\mathrm{d}}{\mathrm{d}r}v(r)+2\frac{v(r)}{r}\right]\mathrm{d}r \\
& + \sqrt{6}\int_0^\infty w(r)\left[\frac{\mathrm{d}}{\mathrm{d}r}v_{LL}^{eT}(r)\right]v(r)\mathrm{d}r\Bigg\}.
\end{aligned}
\tag{32}
$$

4. Coupled-channel Equations

We have specified a finite basis problem with three channels, which would produce three complicated coupled-channeled equations if we decided to treat the different basis states on equal footing. However, since the momentum **P** that we are interested in for applications of this model is small, the triplet S and D channels are then best considered to constitute

the unperturbed deuteron problem, and the singlet P channel will contain the weak response of the deuteron to the $\mathbf{a}\cdot c\mathbf{P}$ perturbation.

In this case, it seems appropriate to develop the coupled triplet S and D channels consistent with the rest frame deuteron problem. Once the associated wavefunctions are known, then we can use them to approximate the occupation of the singlet P channel.

4.1. Rarita–Schwinger equations

Given the approach outlined above, we can optimize the channel wave functions $u(r)$ and $v(r)$ by minimizing the rest frame energy

$$\begin{aligned}\left\langle \Psi_{^3\mathrm{S}} \left| \frac{\mathbf{p}^2}{2\mu} + \hat{V} \right| \Psi_{^3\mathrm{S}} \right\rangle + \left\langle \Psi_{^3\mathrm{D}} \left| \frac{\mathbf{p}^2}{2\mu} + \hat{V} \right| \Psi_{^3\mathrm{D}} \right\rangle + \left\langle \Psi_{^3\mathrm{S}} \left| \hat{V} \right| \Psi_{^3\mathrm{D}} \right\rangle + \left\langle \Psi_{^3\mathrm{D}} \left| \hat{V} \right| \Psi_{^3\mathrm{S}} \right\rangle \\ = \int_0^\infty u(r)\left[-\frac{\hbar^2}{2\mu}\frac{\mathrm{d}^2}{\mathrm{d}r^2} - 3v_C^{et}(r)\right]u(r)\,\mathrm{d}r \\ + \int_0^\infty v(r)\left[-\frac{\hbar^2}{2\mu}\frac{\mathrm{d}^2}{\mathrm{d}r^2} + \frac{6\hbar^2}{2\mu r^2} - 3v_C^{et}(r) + 6v_T^{et}(r) - 3v_{LS}^{et}(r) - 3v_{LL}^{et}(r)\right]v(r)\,\mathrm{d}r \\ - 6\sqrt{8}\int_0^\infty u(r)v_T^{et}v(r)\,\mathrm{d}r. \end{aligned} \tag{33}$$

The minimization of this rest frame energy leads to the constraints

$$E_r u(r) = \left[-\frac{\hbar^2}{2\mu}\frac{\mathrm{d}^2}{\mathrm{d}r^2} - 3v_C^{et}(r)\right]u(r) + \left[-3\sqrt{8}v_T^{et}(r)\right]v(r), \tag{34}$$

$$\begin{aligned} E_{\mathrm{r}} v(r) = \left[-\frac{\hbar^2}{2\mu}\frac{\mathrm{d}^2}{\mathrm{d}r^2} + \frac{6\hbar^2}{2\mu r^2} - 3v_C^{et}(r) + 6v_T^{et}(r) - 3v_{LS}^{et}(r) - 3v_{LL}^{et}(r)\right] v(r) \\ + \left[-3\sqrt{8}v_T^{et}(r)\right]u(r), \end{aligned} \tag{35}$$

where E_{r} is the relative energy. We recognize these as the Rarita–Schwinger equations based on the Hamada–Johnston potential model.

4.2. Rest frame triplet S and D channel wave functions

We have solved the Rarita–Schwinger equations to obtain the channel wave functions plotted in Fig. 1. The triplet S channel wave function $u(r)$ is larger and extends out to a relatively large radial separation, and the triplet D channel wave function $v(r)$ is smaller and localized to much smaller radial separation. We can see the effect of the hard core potential in the zero boundary condition at the cut-off radius.

4.3. Optimization of the singlet P channel

In the perturbation theory approach outlined above, we can approximate the occupation of the singlet P channel in terms of known triple S and D channel wavefunctions. The associated constraint on the channel wavefunction can be written as

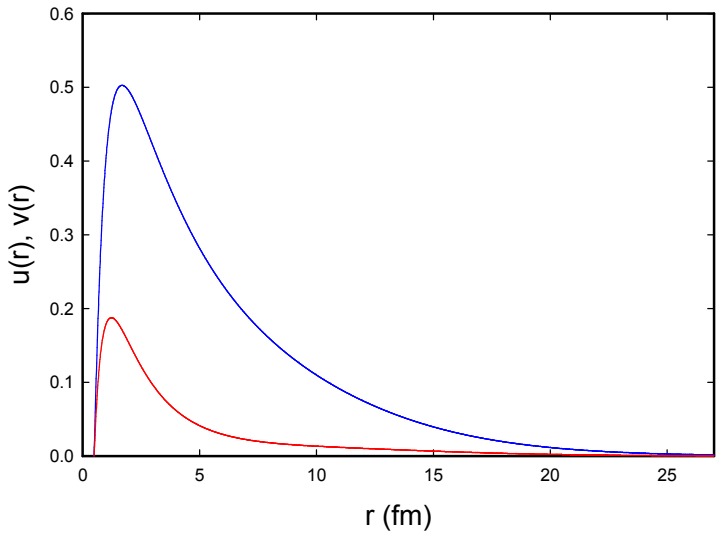

Figure 1. Numerical solutions of the Rarita–Schwinger equations for the deuteron using the Hamada-Johnston potential. The solution for the S state $[u(r)]$ is shown in blue; the solution for the D state $[v(r)]$ is shown in red.

$$
\begin{aligned}
&\left[-\frac{\hbar^2}{2\mu}\frac{\mathrm{d}^2}{\mathrm{d}r^2}+\frac{2\hbar^2}{2\mu r^2}+9v_C^{os}(r)-2v_{LL}^{os}(r)\right]w(r)\\
&=M_J\left(\frac{1}{2Mc^2}\right)\left(\frac{1}{2m_{av}c^2}\right)(\hbar c)(c\hat{P}_z)\\
&\times\left\{-2\sqrt{3}\left[\frac{\mathrm{d}}{\mathrm{d}r}v_C^{eT}(r)\right]u(r)+12\sqrt{3}v_T^{eT}(r)\left[\frac{\mathrm{d}}{\mathrm{d}r}u(r)+\frac{u(r)}{r}\right]+8\sqrt{3}\left[\frac{\mathrm{d}}{\mathrm{d}r}v_T^{eT}(r)\right]u(r)\right.\\
&\left.+\frac{2}{\sqrt{3}}v_{LS}^{eT}(r)\left[\frac{\mathrm{d}}{\mathrm{d}r}u(r)-\frac{u(r)}{r}\right]-2\sqrt{3}v_{LL}^{eT}(r)\left[\frac{\mathrm{d}}{\mathrm{d}r}u(r)-\frac{u(r)}{r}\right]\right\}\\
&+M_J\left(\frac{1}{2Mc^2}\right)\left(\frac{1}{2m_{av}c^2}\right)(\hbar c)(c\hat{P}_z)\left\{-\sqrt{6}\left[\frac{\mathrm{d}}{\mathrm{d}r}v_C^{eT}(r)\right]v(r)\right.\\
&+6\sqrt{6}v_T^{eT}(r)\left[\frac{\mathrm{d}}{\mathrm{d}r}v(r)+\frac{v(r)}{r}\right]+4\sqrt{6}\left[\frac{\mathrm{d}}{\mathrm{d}r}v_T^{eT}(r)\right]v(r)-\sqrt{\frac{8}{3}}v_{LS}^{eT}(r)\left[\frac{\mathrm{d}}{\mathrm{d}r}v(r)+2\frac{v(r)}{r}\right]\\
&\left.-\sqrt{6}\left[\frac{\mathrm{d}}{\mathrm{d}r}v_{LS}^{eT}(r)\right]v(r)-2\sqrt{6}v_{LL}^{eT}(r)\left[\frac{\mathrm{d}}{\mathrm{d}r}v(r)+2\frac{v(r)}{r}\right]-\sqrt{6}\left[\frac{\mathrm{d}}{\mathrm{d}r}v_{LL}^{eT}(r)\right]v(r)\right\}. \qquad (36)
\end{aligned}
$$

We have solved this equation numerically assuming that $u(r)$ and $v(r)$ are fixed solutions of the Rarita-Schwinger equations, and the resulting normalized solution for $w(r)$ is shown in Fig. 2.

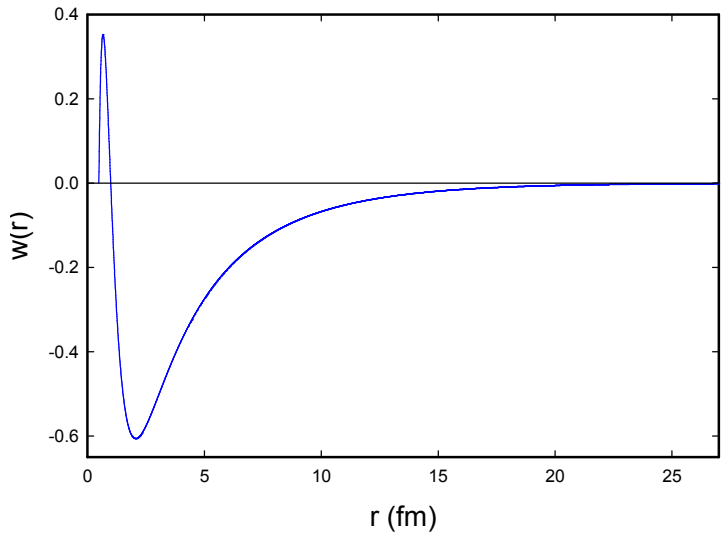

Figure 2. Numerical solution for the normalized singlet P radial wavefunction.

4.4. Equivalent two-level model parameters

From the computation outlined above we can derive an equivalent two-level system model in the form

$$E \begin{pmatrix} c_1 \\ c_2 \end{pmatrix} = \begin{pmatrix} H_{11} & H_{12} \\ H_{21} & H_{22} \end{pmatrix} \begin{pmatrix} c_1 \\ c_2 \end{pmatrix}. \tag{37}$$

We compute

$$H_{11} = -2.245 \text{ MeV}, \tag{38}$$

$$H_{22} = 125.4 \text{ MeV}, \tag{39}$$

$$H_{12} = H_{21} = 2.98 \times 10^{-3} \, M_J (c\hat{P}_z). \tag{40}$$

The off-diagonal coupling matrix elements are somewhat smaller than we were hoping for, and future work will be needed to understand if this coupling is sufficiently large to account for experimental results. In addition, we have found that these off-diagonal matrix element depend on the nuclear spin, which suggests that the system may respond to net spin alignment.

5. Discussion and Conclusions

We recently proposed a new fundamental Hamiltonian for condensed matter lattice problems that includes coupling to nuclear internal degrees of freedom. From our perspective this new coupling seems to be what is needed to account for the excess heat effect in the Fleischmann–Pons experiment. What has been needed in order to evaluate the models that result is an estimate for the coupling matrix element.

The development of an estimate for this matrix element is challenging for a variety of reasons. We have presumed in the derivation of the fundamental Hamiltonian that it is sufficient to model the nucleons as elementary Dirac particles. However, we know that nucleons are composite particles made up of quarks and gluons, and that it is unlikely that using a Dirac model as we have done is going to give accurate results. To do better we probably need to go back and develop a better fundamental Hamiltonian based on quarks and electrons. If it is possible to obtain reasonable nucleon models from empirical potentials, then we may be able to develop a better estimate for the deuteron coupling matrix element. Working directly with bound state QCD at this stage does not seem to be an attractive option.

Once we have decided on the simpler model that adopts an elementary Dirac particle model for nucleons, then it is an issue of whether to use a relativistic or nonrelativistic model, and further it is an issue of what potential to use. Since these computations involve a fair amount of work, it seemed sensible to adopt a nonrelativistic model since it is simpler, and to work with an older relatively simple nuclear model. The Hamada–Johnston potential fits the bill in this regard, as it is sufficiently simple that we are able to complete a calculation in relatively short order. Perhaps the most work in this computation was the evaluation of the spin, isospin, and angular momentum algebra; for this we relied on brute force Mathematica calculations.

In the end, we have developed a model for the coupling between the different nuclear spin states of the ground state deuteron and lattice-induced coupling to a highly excited singlet P virtual state. The energy of this virtual state is about 125 MeV in this model, which is consistent with our expectations. The coupling matrix element fell short of what we had hoped for by about an order of magnitude. We will need to clarify in future calculations if this is sufficiently large to be relevant to experimental results.

The coupling matrix element in this model is proportional to M_J, which is interesting in connection with the reported dependence of excess heat on the strength of an applied magnetic field. Two of the deuteron spin states couple in the case of z-direct motion, so that there is the possibility of increasing the overall coupling if population can be moved out of the non-interacting $M_J = 0$ state and into the other two $M_J = \pm 1$ states.

References

[1] P. L. Hagelstein and I. U. Chaudhary, Including nuclear degrees of freedom in a lattice Hamiltonian, *J. Cond. Mat. Nucl. Sci.* (in press).

[2] P. L. Hagelstein, Bird's eye view of phonon exchange models for excess heat in the Fleischmann-Pons experiment, *J. Cond. Matter Nucl. Sci.* (in press).

[3] P.L. Hagelstein and I.U. Chaudhary, Energy exchange in the lossy spin-boson model, *J. Cond. Matter Nucl. Sci.* **5** (2011) 52.

[4] P.L. Hagelstein and I.U. Chaudhary, Second-order formulation and scaling in the lossy spin-boson model, *J. Cond. Matter Nucl. Sci.* **5** (2011) 87.

[5] P.L. Hagelstein and I.U. Chaudhary, Local approximation for the lossy spin-boson model, *J. Cond. Matter Nucl. Sci.* **5** (2011) 102.

[6] P.L. Hagelstein and I.U. Chaudhary, Coherent energy exchange in strong coupling limit of the lossy spin-boson model, *J. Cond. Matter Nucl. Sci.* **5** (2011) 116.

[7] P.L. Hagelstein and I.U. Chaudhary, Generalization of the lossy spin-boson model to donor and receiver systems, *J. Cond. Matter Nucl. Sci.* **5** (2011) 140.

[8] P.L. Hagelstein and I.U. Chaudhary, Errata and comments on a recent set of papers in Journal of Condensed Matter Nuclear Science, *J. Cond. Matter Nucl. Sci.* (in press).

[9] M. Fleischmann, S. Pons and M. Hawkins, *J. Electroanal Chem.* **201** (1989) 301; errata, **263** (1990) 187.
[10] M. Fleischmann, S. Pons, M.W. Anderson, L.J. Li and M. Hawkins, *J. Electroanal. Chem.* **287** (1990) 293.
[11] M.C.H. McKubre, S. Crouch-Baker, R.C. Rocha-Filho, S.I. Smedley, F. L. Tanzella, T.O. Passell, J. Santucci, *J. Electroanal. Chem.* **368** (1994) 55.
[12] E. Storms, *Science of Low Energy Nuclear Reaction: A comprehensive compilation of evidence and explanations about cold fusion*, World Scientific Publishing Co, Singapore (2007).
[13] A.B. Karabut, X-ray emission in the high-current glow discharge experiments, *Condensed Matter Nuclear Science, Proc. ICCF9*, edited by Xing Z. Li, p. 155 (2002).
[14] A. B. Karabut and S. A. Kolomeychenko, "Experiments characterizing the x-ray emission from a solid-state cathode using a high-current glow discharge," *Condensed Matter Nuclear Science, Proc. ICCF10*, P.L. Hagelstein and S.R. Chubb (Eds.), p. 585 (2003).
[15] A.B. Karabut, Research into characteristics of x-ray emission laser beams from solid state cathode medium of high-current glow discharge, *Condensed Matter Nuclear Science, Proc. ICCF11*, J.P. Biberian (Ed.), p. 253 (2004).
[16] A.B. Karabut, Study of energetic and temporal characteristics of x-ray emission from solid state cathode medium of high-current glow discharge, *Condensed Matter Nuclear Science, Proc. ICCF12*, by A. Takahashi, K.-I. Ota and Y. Iwamura (Eds.), p. 344 (2005).
[17] A. B. Karabut, E. A. Karabut, P. L. Hagelstein, " Spectral and temporal characteristics of x-ray emission from metal electrodes in a high-current glow discharge," *J. Cond. Mat. Nucl. Sci.* **6** (2011) 217.
[18] H. Kamada, A. Nogga, W. Glöckle, E. Hiyama, M. Kamimura, K. Varga, Y. Suzuki, M. Viviani, A. Kievsky, and S. Rosati, Benchmark test calculation of a four-nucleon bound state, *Phys. Rev. C* **64** (2001) 044001.
[19] R. Machleidt and D. R. Entem, Chiral effective field theory and nuclear forces, *Phys. Reports* **503** (2011) 1.
[20] T. Hamada and I.D. Johnston, A potential model representation of two-nucleon data below 315 MeV, *Nucl. Phys.* **34** (1962) 382.

J. Condensed Matter Nucl. Sci. 9 (2012) 64–71

Research Article

Excess Energy Release During Na Metal Dissolution in a Dilute Epsom ($MgSO_4 \cdot 7H_2O$) Solution

Arunachalam Lakshmanan *

Saveetha Engineering College, Chennai 602105, India

Abstract

During sodium metal dissolution in aqueous Epsom salts, it was accidentally discovered that a massive explosion occurs in 0.85 M Epsom solution on the completion of Na dissolution. Borosil glass vaporizes at temperatures >1000°C. This fact indicated that a very high temperature has indeed been reached in this experiment. The timing of the explosion (20–25 s after Na addition) indicated that hydrogen somehow got trapped in cavitation induced meta-stable nano-crystals. The excess energy release could not be explained by conventional hydrogen combustion in air. One must therefore look elsewhere for an explanation of the process behind the excess energy release.
 ISSN 2227-3123

Keywords: Cavitation crystallization, Epsom solution, Excess energy release, Explosion, Hydrogen trapping, Na dissolution

1. Introduction

One of the reasons molten sodium (Na) metal is used as a coolant in fast-breeder nuclear reactors is its high thermal conductivity. Unlike water, its atomic number is relatively high and hence its moderation capacity of neutrons is low. It is also unlike other coolants, which usually contain low Z materials such as water or graphite. Therefore, nuclear fission of fissile materials can be carried out with fast neutrons resulting in a higher neutron production (closer to 3) per fission of a fissile nucleus when compared to the fission at thermal neutron energies. At fast neutron energies, the excess neutrons not only sustain a chain fission reaction but also they can be used to breed other non-fissile materials such as ^{232}Th into fissile materials (i.e. ^{233}U), when the non-fissile materials are used as a blanket surrounding the reactor core. The transfer of heat from sodium to water leads to the formation of steam, which is used to produce electricity. The major problem with sodium coolant is its vigorous chemical reactivity with water. Usually in fast reactors, thin walls of stainless steel separate the sodium coolant pipeline from water/steam carrying pipeline. Any leakage in sodium pipeline can lead to major sodium fire and even explosion due to hydrogen production during the highly exothermic Na–H_2O reaction. Firefighting a sodium fire with conventional extinguishers using a water-based fluid is ruled out. Presently, dry chemical powder ($NaHCO_3$) is used. This merely serves as a blanket against atmospheric oxygen. It poses its own

*E-mail: arunachalamlakshmanan@yahoo.com

 ISSN 2227-3123

problems those include poor visibility, inability to apply from distance, etc. Sodium when cooled to room temperature solidifies and sticks to reactor components. During the routine operations, cleaning of reactor components containing residual sodium is essential. Presently used methods such as removal of Na by melting it with acetylene torch have proved to be highly cumbersome and ineffective in many situations. To address these problems, we developed an aqueous system based on Epsom salt ($MgSO_4 \cdot 7H_2O$). Concentrated aqueous solutions of this salt were found to be highly effective in dissolving Na metal peacefully. When applied through a high-speed water jet, the Epsom solution easily removes Na sticking to metal components. This solution could also serve as an effective liquid fire extinguisher in Na firefighting. Tiny droplets of this salt solution were found to be very effective in neutralizing Na aerosol generated during Na fire. The byproducts obtained during this application, namely $Mg(OH)_2$ and Na_2SO_4 are highly ecofriendly (unlike the case with the presently used 10 M NaOH solution) and hence the entire firefighting or cleaning operation could be carried out in air in open conditions. The only precaution to be taken is the production of hydrogen whose concentration should be controlled through proper ventilation or by other means.

Following the lead of France in fast-breeder reactors, most countries use 10 M NaOH solution for Na disposal during decommissioning of fast reactors. The rationale behind selecting NaOH was the end product obtained due to Na–H_2O reaction is also NaOH, which is water soluble, so no new byproduct is formed. But this work must be carried out in closed environment since NaOH is highly corrosive. In any case it cannot be used for Na-firefighting in open conditions because NaOH solution is highly alkaline and corrosive [1].

While the application of concentrated aqueous Epsom solution ($\gg$1.3 M) under stirring conditions or through high-speed water jets was found to be highly effective in dissolving Na metal peacefully, very dilute solutions ($\ll$0.7 M) resulted in an instant explosion due to the hydrogen released through highly exothermic Na–H_2O reaction. Intermediate salt concentrations (0.7–1.3 M) offer challenging possibilities of hydrogen production by Na–H_2O as well as Mg–H_2O reactions and the trapping of hydrogen. This occurred at a critical Epsom salt concentration in cavitation-induced nano-crystals in a glass beaker. It is the subject of this paper, and a matter of great interest.

The paper is divided into two parts. The first part describes the experiment, which involves the dissolution of Na metal in aqueous Epsom solution at different salt concentrations. The second part describes the plausible theory behind excess energy release and its applications for electrical power production.

2. Experimental Results

Dissolution of Na metal in aqueous salt solution is tricky because Na usually floats in the solution. When comes in contact with air, molten Na catches fire and produces Na aerosols, both of which are highly dangerous. An encyclopedia report suggests that Na metal wets effectively solid powders in molten condition under stirring condition provided us the clue to overcome this problem. First of all, stirring a liquid solution is easy. Secondly, reaction of Na metal and Na_2O with water is exothermic and hence no external heating is essential. For example the thin Na_2O layer surrounding Na metal reacts with water exothermically to heat up Na metal and melt it through the reaction, $Na_2O + H_2O \Leftrightarrow 2NaOH$. Stirring helps in distributing the heat uniformly in solution. Thus Na metal dissolution could be easily carried out under vigorous stirring condition ($\sim$800–1000 rpm) in a glass beaker containing Epsom solution. A commercial Remi external mixer was used for stirring purposes. Figure 1 shows the typical experimental set-up used. Before stirring, the Epsom solution (2 M) is crystal clear. After stirring the solution turns milky due to tiny bubbles formed by entrapped air and dissolved gas. The tiny bubbles caused by vaporous cavitation and occurring extremely rapidly, in a microsecond time scale are not visible to naked eye especially under turbid conditions. Elsewhere, such cavitation bubbles generated by a 193 nm ArF excimer laser beam delivered with a specially designed tip into absorbing NaCl solution were found to have a life time of 80 μs with a maximum bubble diameter of about 1 mm when imaged with flash photomicrography with CCD camera [2]. Cavitation depends on the purity of water. Pure water can withstand considerable low pressure without undergoing cavitation. However, in salt water, cavitation inception occur easily at

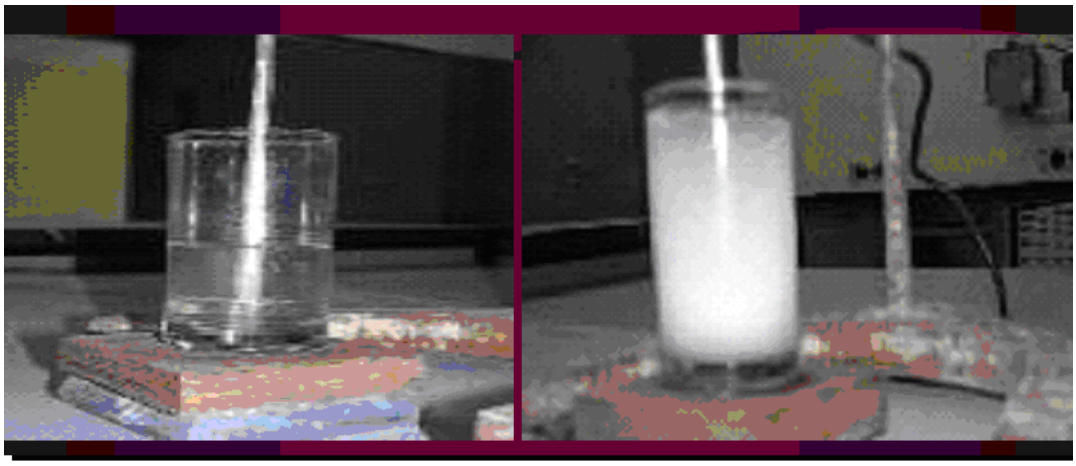

Figure 1. Typical experimental set-up used for peaceful Na dissolution in concentrated Epsom (2 M) solution. This salt concentration is about 85% of its solubility limit. The salt solution in the glass beaker is crystal clear before stirring (*left*). But after stirring the solution turns milky due to tiny bubbles formed by entrapped air and dissolved gas (*right*).

reduced pressures (encountered in a column of fast moving fluid) due to presence of ions which break the hydrogen bond between water molecules.

Figure 2 shows the results obtained on Na metal dissolution in Epsom (*right*) as well as NaOH (*left*) solutions. The solution temperature was constantly monitored with a Ch–Al thermocouple wire inserted into the solution in such a way that it does not disturb the stirring. In both cases the solution temperature raises during Na dissolution carried out under stirring condition in air. Hydrogen gas is released in both cases and a blue flame due to hydrogen burning in air over the beaker is witnessed at times. In the case of NaOH solution, the rise in solution temperature is faster with increasing water content. This is only to be expected because Na reacts with water and hence with increasing water content, the Na dissolution rate is faster. The Na dissolution rate is very slow if the water content is low as seen from the very slow rise in solution temperature (Fig. 2a, *left*). In fact the Na metal could be seen to rotate for more than a minute till it is dissolved completely in the latter case. In contrast, Na dissolution is quite swift with Epsom solution at all concentrations above a threshold limit as witnessed from the quick rise in solution temperature irrespective of its water content (Fig. 2a, *right*). This result shows that the mechanisms of Na metal dissolution in the two solutions are quite different.

Another notable difference between the NaOH and Epsom solutions was on the sodium solubility limits. In an Epsom solution, for a given water content (∼100 mL), the amount of sodium that could be dissolved peacefully increased from 6 to 10.5 g when the molar concentration was increased from 1.4 to 1.8 M. The above solubility limits were arrived at on the basis of observation of sodium fire initiated by sodium–air reaction with further addition of sodium. In contrast in the NaOH solution, for a given water content (∼120 mL), the Na solubility was found to decrease from about 30 to 15 g when the molar concentration was increased from 8 to 12 M as expected from the reduced availability as well as reduced thermodynamic activity of water at such high salt concentrations. The sodium solubility limit in this case was arrived at on the basis of NaOH salt reaching its solubility limit in water, i.e., further sodium addition resulted in NaOH precipitation. More details of this work can be obtained from reference [1].

Na dissolution was also carried out in several other aqueous salt solutions and the results obtained are as follows. In concentrated $Zn(NO_3)_2{\cdot}6H_2O$, Zn_2SO_4 and $CuCl_2{\cdot}2H_2O$ (85% solubility limit, molarity = 3) solutions, sodium

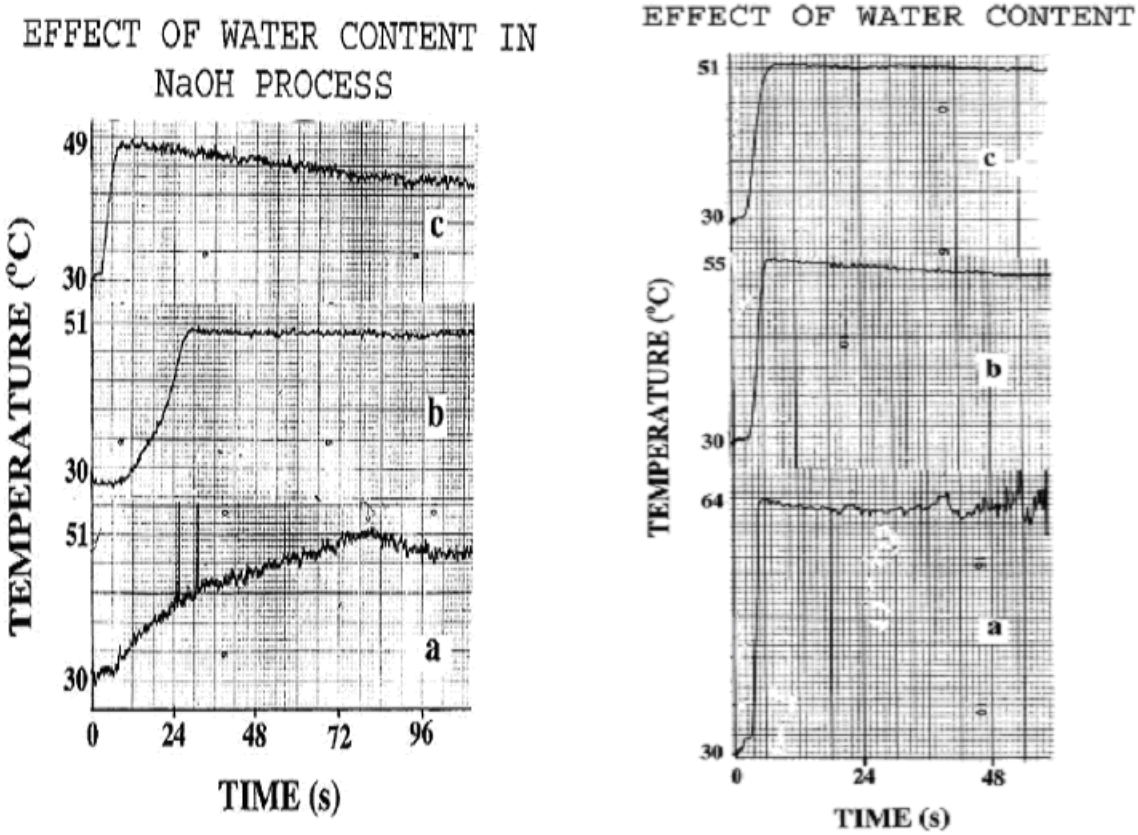

Figure 2. The dependence of solution temperature since the addition of sodium on the water content in NaOH solution (*left*) and in Epsom solution (*right*). The molarity of the solutions (M) were: NaOH: 14(a), 10.1 (b) and 8.1 (c); Epsom: 2.13 (a), 1.57 (b) and 1.25 (c).

dissolution turned very violent. Intense sodium sputtering, sodium fire and sodium aerosol release were observed in all three cases. When the concentration of the $Zn(NO_3)_2{\cdot}6H_2O$ solution was decreased to 45% of its solubility limit (molarity = 2), intense explosion was observed once sodium was added to the solution under stirring condition since Na reacted freely with water to produce intense hydrogen. A common feature with the above salts is that those metals, i.e., Cu and Zn do not react with water, unlike Mg, and thus sodium–cation exchange reactions becomes energetically unfavorable. This view is confirmed from the fact that in $MnSO_4$ and $NiSO_4$ aqueous salt solutions, sodium dissolution

rate is peaceful but the rate of dissolution is quite low even at low salt concentrations (1.7–3.8 M) since Mn and Ni react very slowly with water. Based on a detailed study with many salt solutions, it was concluded that high enthalpy of formation of crystal and high molarity are two other factors, which favor peaceful dissolution of Na [3].

On the suggestion of a reactor chemist to cut down the cost, we tried a dilute Epsom solution (0.85 M) to dissolve Na. The Na dissolution indeed proceeded peacefully as with 2 M solution for about 20–30 s since Na addition. The formation of a small quantity of white $Mg(OH)_2$ precipitate in the glass beaker could be seen visually thereby confirming the Na dissolution process. However, at the end of Na dissolution, i.e., 30 s after Na addition, an intense and massive explosion occurred, accompanied with Na aerosol release and a shock wave as well as vaporization of Borosil glass beaker containing salt solution. The explosion attracted the attention of everyone in the building due to its high intensity, even people in rooms far from the one where the experiment was carried out. Molten glass needles flew all around, making holes too small to be seen with the naked eye in two plastic water bottles at two different locations about 2 m from the explosion. I was standing 4–5 m from the cell when it exploded. The needles scratched my hand. Borosil glass vaporizes at temperatures $>1000^{\circ}$C. This fact indicates that a very high temperature has indeed been reached in this experiment. The timing of the explosion (20–25 s after Na addition) is *prima facie* evidence that hydrogen somehow got trapped in the solution. A normal hydrogen explosion occurs within 5–10 s after Na addition in dilute salt solutions, and the intensity of a normal explosion is not sufficient to vaporize the glass beaker. It merely breaks it into a few pieces. This situation was quite different. Despite the massive energy release, the stirrer was not damaged. It continued to rotate, which indicated that the energy was released outwardly. It was also noted that the bottom of the glass beaker which was placed on a wooden stool did not vaporize. This showed that the plasma-like condition was reached only on the side walls of the glass beaker, since a container free condition could be reached only on its sides. At the bottom, this condition could not be reached due to the presence of the wooden stool which acted as a heat absorber. Therefore, in future, experiments researchers should take note of the geometry and material of the container. Another parameter which needs to be standardized is the Epsom salt concentration. This is critical. An excess of salt would result in peaceful Na dissolution while a lack of salt concentration would result in premature Na–H_2O reaction. It was found that to trigger the excess energy release, the 2Na $\Leftrightarrow$ Mg exchange reaction in cavitation induced crystals as well as Na–H_2O reaction should take place with equal probability. That can occur only at a critical Epsom salt concentration which exactly coincided with the salt concentration (0.85 M) used in the experiment. The role of serendipity (accidental discovery) in the development of science cannot be overlooked. Such a massive release of energy, which could not be explained away easily by chemical means, calls for a close scrutiny of the process behind it.

> One can imagine a series of successive experiments done at 1.9 M, 1.8 M, ... The thought is that one might see an increase in energy release along the way prior to where the system explodes. If so, then this might be important in that it could provide a "safe" version of the experiment which begins to show anomalous behavior.

3. Discussion

3.1. Peaceful Na dissolution in concentrated Epsom solution

The fact that the amount of sodium that could be dissolved peacefully increases with the salt content in an Epsom solution is a clear indication that sodium is dissolved mainly in the salt rather than in water. If sodium–water is the major or only mode of reaction, sodium solubility should not depend on the salt content at these relatively low molar concentrations. In contrast, in the NaOH solution, in which sodium reacts with water at all salt concentrations, for a given water content, the sodium solubility has been found to decrease with increasing salt content. This is expected from the reduced availability as well as reduced thermodynamic activity of water at such high salt concentrations. In an Epsom solution, a chief reason why sodium prefers to displace host metal rather than reacting directly with water is the difference in the rates of these two reactions. The Na–metal exchange reaction rate in Epsom is fast at the crystalloid

embryo level which grows quickly to nano- or even micro-crystals due to stimulation by cavitation. In comparison, the Na–H_2O reaction rate is slowed down because the water molecules are continuously engaged in hydrolyzing these crystalloids formed while stirring the solution. If an ionic solid is to dissolve, some energy is needed to overcome the force of inter-ionic attraction. If water is the solvent, this energy is supplied by the interaction of water molecules with the ions of the solute.

3.2. Cavitation-induced crystallization

There remains a question as how such tiny (micro- or nano-sized) Epsom crystalloids are formed in under-saturated solution. It is known that a reduction in pressure by rotation can cause water to boil even at room temperature, leading to cavitation-induced crystals. Such cavitation events occurring in ship propellers damage the propeller. Crystal formation due to cavitation has been attributed to a number of factors such as: (i) local temperature increase, (ii) pressure changes leading to rapid cooling rates (10^7–10^{10} K s^{-1}) and iii) concomitant shockwaves [4]. Local hot spots can vaporize the solution and can turn an under-saturated solution into a super-saturated one, thereby promoting crystal formation. However, the application of Bernoulli's equation in this case has shown that cavitation occurs in the Epsom solution not because of stirring but because of exothermicity arising during the exothermic reaction of Na_2O layer surrounding the Na metal, followed by exothermic sodium metal dissolution. These local boiling spots are distributed throughout the solution by the stirring. Due to the small size of the stirrer blades (a few centimeters) the pressure drop is too small to cause boiling of water at room temperature despite the high speed (1000 rpm). In contrast, rotation of water stream for e.g., by a ship propeller of 8 m diameter with a tip velocity higher than 40 m s^{-1} creates a high vacuum (> -27.5 inch Hg) due to its larger length (a few meters); this pressure drop is large enough to cause boiling even at room temperature, despite the relatively low speed of rotation (100 rpm). This is conventional cavitation. But in this experiment, the highly exothermic Na reactions cause local hot spots which lead to cavitation-induced meta-stable crystals. This is known as steam cavitation. A recent study shows that if a steam bubble is introduced in a cold-water pool, due to a fast condensation of the steam from the surface of this bubble, a phenomena similar to the cavitational collapse of the bubble occurs. The steam bubble cavitation process was found to be more efficient compared to conventional processes because of the elimination of intermediate energy [5]. A recent study confirms that gas bubbles formed by absorbing the heat of vaporization from surrounding environment can be used to tailor the kinetics of the nucleation and growth of inorganic nano-crystals in a colloidal synthesis [6]. In this experiment, gas bubbles generated from boiling solvents under atmospheric pressure (or under vacuum) were shown to facilitate the formation of iron oxide nano-crystals. Artificial argon bubbles could also replace the solvent gas bubbles in controlling the nucleation and growth of iron oxide nano-crystals.

It should be emphasized that cavitation in this work primarily causes the formation of metastable crystals, and not in the production of high temperatures directly. This is unlike earlier work in which it was postulated that cavitation alone (during the process of gas bubble implosion using ultrasonic sound waves) can directly lead to the generation of very high temperatures required for nuclear fusion [7]. The fact that Na dissolution proceeds peacefully in Epsom solution clearly indicates that the Na–H_2O reaction rate is slowed down by the cavitation process and the hydrogen production rate is controlled with controlled release of Mg atoms from the crystals by 2Na $\Leftrightarrow$ Mg exchange reaction as shown in Table 3a,b. Before the Na–H_2O reaction commences, or during its early onset, the cation-exchange reaction becomes the predominant mode of Na-dissolution in a concentrated Epsom solution. Although the rate of reaction of Mg with water is slow when compared to Na, all the Mg atoms expelled do not react with water instantly since a portion of Mg atoms released could get trapped again and again in the $MgSO_4$ crystalloids, additively similar to what happens to the sodium atoms in Na_2SO_4 crystals formed due to cavitation, as depicted in Table 3c. Such a retrapping process would slow down the release of Mg atoms into the salt solution. The Mg atoms displaced will react relatively slowly with water to form $Mg(OH)_2$ and hydrogen until all the Mg atoms are released into the solution. Thus the sodium dissolution

Table 1. A simplified picture of the Epsom salt solution before ($10MgSO_4$ - (a)) and after sodium dissolution ($8MgSO_4.2Na_2SO_4$ – (b)) in the 2 M standard solution under vigorous rotation recommended for sodium disposal. Exchange of Na with Mg takes place by 2Na–Mg exchange reaction. The dissolution process of Mg atoms in $MgSO_4$ in what is known as additive reaction (c) slows down the reaction rate and that is how Na dissolution proceeds peacefully in 2M Epsom solution.

(a)						**(b)**			
Mg^{2+}	SO_4^{2-}	Mg^{2+}	SO_4^{2-}			Mg^{2+}	SO_4^{2-}	Na^+	SO_4^{2-}
SO_4^{2-}	Mg^{2+}	SO_4^{2-}	Mg^{2+}			SO_4^{2-}	Na^+	x	Mg^{2+}
Mg^{2+}	SO_4^{2-}	Mg^{2+}	SO_4^{2-}			Mg^{2+}	SO_4^{2-}	Mg^{2+}	SO_4^{2-}
SO_4^{2-}	Mg^{2+}	SO_4^{2-}	Mg^{2+}			SO_4^{2-}	Na^+	x	Mg^{2+}
Mg^{2+}	SO_4^{2-}	Mg^{2+}	SO_4^{2-}			Mg^{2+}	SO_4^{2-}	Na^+	SO_4^{2-}
						SO_4^{2-}	Mg^{2+}	SO_4^{2-}	Mg^{2+}
(c)			Mg^{2+}	SO_4^{2-}	Mg^{2+}	e^- e^-			
			SO_4^{2-}	Mg^{2+}	SO_4^{2-}	Mg^{2+}			
			Mg^{2+}	e^- e^-	Mg^{2+}	SO_4^{2-}			
			SO_4^{2-}	Mg^{2+}	SO_4^{2-}	Mg^{2+}			
			Mg^{2+}	SO_4^{2-}	Mg^{2+}	SO_4^{2-}			

proceeds in a controlled and peaceful manner in concentrated Epsom solution. In pure 2 M aqueous Epsom solution, the above reaction lasts for about 15–20 s as evidenced from the hydrogen released, which usually ignites in air above the glass beaker in which sodium is dissolved. But for the above slow and controlled release of Mg atoms from the crystalloids into the solution, the Mg–H_2O reaction would also have proceeded quite quickly, resulting in an explosion similar to that of Na–H_2O reaction.

3.3. Na dissolution in dilute Epsom solution and hydrogen trapping

The situation with the massive explosion in 0.85 M solution on the completion of Na dissolution (20–25 s after Na addition) is completely different and calls for a different explanation. First of all, the massive energy burst was an accidental discovery – serendipity! At high Epsom concentration (>1.6 M), 2Na–Mg cation exchange reaction and at low concentration (<0.7 M) Na–H_2O reaction occur. At 0.85 M Epsom concentration both the reactions mentioned above are shown to take place with equal probability [3]**.** Borosil glass vaporizes at temperatures >1000˚C. This fact indicated that a very high temperature has indeed been reached in this experiment. The timing of the explosion indicated that hydrogen somehow got trapped in the cavitation induced metastable nanocrystals. This means that instead of a 2Na–Mg cation exchange, a 2H–Mg exchange seems to have taken place. *A cage meant to trap a massive elephant (Na^+ ions) instead trapped the elusive panthers (H^+ ions).* Towards the end of sodium dissolution in the 0.85 M Epsom solution, i.e ∼25 s from the start, the original aim of dissolving sodium in a dilute aqueous solution of Epsom salt at room temperature appears to have been almost achieved at less cost than in the standard solution.

As 2.4×10^{22} hydrogen atoms/molecular ions (0.04 mol) are involved in the present case, the burning of hydrogen would release 9.57 kJ which is less than the energy needed to vaporize the salt solution (260 kJ). So the crucial questions before us now are: Why did the cavitation induced crystal structure containing sodium and hydrogen collapse the moment it solidified, setting in motion a chain reaction resulting in the observed violent explosion? And: What is the mechanism behind the release of such excess energy? These questions will be addressed in the theoretical part of this paper.

4. Conclusion

Sodium metal dissolves peacefully in concentrated Epsom solution (>1.6 M) when it is stirred in open air. This technique offers several advantages for alkali metal dissolution as well as for alkali metal (Na, K, Li, etc.) firefighting since the end products are ecofriendly. Sodium dissolution in dilute Epsom solutions ($\ll 0.7$ M) can, however, be hazardous due to the onset of highly exothermic and violent Na–H_2O reaction. Intermediate concentrations offer interesting possibilities of hydrogen trapping in cavitation induced metastable nano-crystals. The massive explosion witnessed in 0.85 M Epsom solution accompanied by the vaporization of the entire glass beaker containing the solution at the end of sodium metal dissolution could not be explained away by simple hydrogen combustion; the massive excess energy released as a burst deserves to be understood in detail.

The evidence presented here is circumstantial. We will not know for sure how much energy is produced until the experiment is reproduced many times and the energy release is measured with adequate calorimetry. The energy balance assembled in this work is useful only in as much as it provides a reference energy balance under the interpretation provided. This is not proof that the energy matches the numbers, or in fact is anomalous at all. There is the need to carry out the experiment in an appropriate calorimeter. The author is hoping to get support from funding agencies to carry out appropriate replication experiments in the future; and that such follow on experiments are very important to confirm that the energy produced really is anomalous. There is also the need to confirm if the anomalous energy release occurs only at a particular (0.85 M) salt concentration. If the increase in energy release is gradual as the salt concentration is decreased from 2 to 0.85 M, it could provide a "safe" version of the experiment in the concentration at which the anomalous behavior begins. A still better approach would be to develop a fuel cell with a continuous flow of Epsom solution having appropriate salt concentration with another flow of molten Na metal to produce continuous excess heat energy similar to the heat production in Ni–H systems reported by Focardi et al. [8].

References

[1] A.R. Lakshmanan, M.V.R. Prasad, D. Ponraju and H. Krishnan. *J. Solid State Chem.* **177** (2004) 3460.
[2] T. Turovets, D. Palanker, Yu. Kokotov, I. Heno and A. Lewis. *J. Appl. Phys.* **79**(5) (1996) 2689.
[3] A.R. Lakshmanan, *Infinite Energy* **81** (2008) 41.
[4] A.V. Mahulkar, P.S. Bapat, A.B. Pandit and F.M. Lewis. Steam bubble cavitation, *AIChE J.* **54** (7) (2008) 1711.
[5] P.R. Gogate, R.K. Tayal and A.B. Pandit, Cavitation: A technology on the horizon, *Current Sci.* **91**(1) (2006) 35.
[6] Jared Lynch, Jiaqi Zhuang, Tie Wang, Derek LaMontagne, Huimeng Wu and Y. Charles Cao, Gas-Bubble Effects on the Formation of Colloidal Iron Oxide Nanocrystals (dx.doi.org/10.1021/ja2032597/*J. Am. Chem. Soc.* **133** (2011) 12664–12674..
[7] R.P. Taleyarkhan, C.D. West, J.S. Cho, R.T. Lahey, R.J. Nigamutin and R.C. Block, *Science* **295** (5561) (2002) 1868–1873.
[8] S. Focardi, V. Gabbani, V. Montalbano, F. Piantelli and S. Veronesi, Large excess heat production in Ni–H systems. *IL Nuovo Cimento* **111** A (11) (1998) 1233–1142.

J. Condensed Matter Nucl. Sci. 9 (2012) 72–85

Research Article

Anomalous Heat Energy Released through Cavitation-Coulombic Repulsion Oscillations Following Sodium Metal Dissolution in a Dilute Epsom Solution – Plausible Mechanisms

Arunachalam Lakshmanan *

Saveetha Engineering College, Chennai 602105, India

Abstract

Plausible mechanisms are discussed for explaining the sudden burst of energy released from 0.85 M Epsom ($MgSO_4 \cdot 7H_2O$) aqueous solution following sodium metal dissolution which led to the vaporization of the entire system including the glass beaker. Exothermic reactions lead to micro/nano-metastable crystal formation due to steam cavitation. ${H_2}^+$ molecular ions trapped at Mg^{2+} ion lattice sites in cavitation-induced metastable crystals were considered as precursors for energy release. In principle, for charge compensation, two protons should occupy one Mg^{2+} lattice site in these crystals. Therefore, cavitation crystal formation brings in the two protons in molecular ions closer. This process is, however, opposed by Coulombic repulsion between the two protons which results in the collapse of the nanocrystal containing hydrogen. This leads to the release of hydrogen ions into the solution resulting in the release of hydration energy during the formation of H_3O^+, hydronium ions and in local heating. Stirring distributes the heat energy uniformly in the solution. Local heating, however, leads to the promotion of cavitation – this time with more vigor since additional energy input has occurred. Thus reformation of the crystal takes place quickly and the hydrogen ions are brought together more closer than during the previous occasion which increases the electrostatic repulsive force. As a result, the crystal collapses faster leading to the release of more hydration energy. This is how cavitation gains energy from repulsion. The above cavitation Coulombic repulsion oscillation (CCRO) cycle continues leading to an exponential build-up of the pressure and oscillation speed of the precursors and a decrease in inter-proton separation leading to their collision. Finally a sudden burst of energy witnessed occurs due to cavitation collapse. *It remains to be ascertained if the energy release is a consequence of p–p fusion, or other mechanisms proposed which include volume casimir effect, miniature black holes and lattice phonon amplification. The fact that increase in the oscillation speed of the two protons in the proposed ${H_2}^+$ species is exponential without an upper limit till the end-point is reached should determine the logistics of the underlying mechanism causing the energy release.* The p–p fusion should, however, be accompanied by positron emission whose presence could be verified by its annihilation gamma rays or with 5.5 MeV gamma rays produced from HD fusion reactions if energetic deuterium is formed from p–p fusion in amounts commensurate with the energy produced but this fusion process is mediated by weak interaction process and hence is less probable. No other proposal explains burst of energy observed better than the collapse of miniature black holes.
 ISSN 2227-3123

Keywords: Anomalous heat energy release, Cavitation-Coulombic repulsion oscillation, Collision of protons, Exponential build-up

© 2012 ISCMNS. All rights reserved. ISSN 2227-3123

of energy, Lattice phonon amplification, Miniature black holes, p–p fusion, Volume casimir effect

1. Introduction

A consideration of present and future energy scenario related to nuclear technology indicates that nuclear fission suffer from issues related to radioactive waste, fuel (uranium) shortage and nuclear security related to proliferation of radioactive materials and other nuclear devices into unauthorized personnel. The feasibility of harnessing nuclear fusion technology in the near future seems to be doubtful since it involves high-energy input resulting in low production efficiency (energy output/energy input) meaning high cost. Another major technological issue related to fusion is hot plasma containment. However, the present work will show for the first time that a pulsed heat energy source can be achieved relatively easily by internal accumulation of phonon energy through cavitation-Coulombic repulsion oscillation (CCRO) in condensed matter following sodium metal dissolution in a dilute Epsom ($MgSO_4 \cdot 7H_2O$) solution. The advantages with the proposed system are: (i) production of green energy – only heat release, no radioactive or radiation release or carbon pollution, (ii) infinite amount of fuel in the form of hydrogen in water, (iii) feasible technology with better understanding and finally (iv) the high-efficiency (energy output/energy input) of proposed system.

It has been shown in part I of this paper [1] that in concentrated aqueous Epsom solution, Na dissolution proceeds peacefully through cation exchange process in cavitation-induced crystals and the Na–H_2O reaction rate is slowed down by the above cavitation process and the hydrogen production rate is controlled with controlled release of Mg atoms from the crystals by 2Na $\Leftrightarrow$ Mg exchange reaction. Intermediate salt concentrations (0.7–1.3 M) offer challenging possibilities of hydrogen production by Na–H_2O as well as Mg–H_2O reactions and the trapping of hydrogen produced at a critical Epsom salt concentration in cavitation-induced metastable nanocrystals which is the subject matter of the present study.

2. Sodium Dissolution in 0.85 M Epsom Solution

When a reactor scientist suggested to cut down the salt concentration to save cost, we tried to dissolve Na in 0.85 M Epsom solution. For Epsom concentrations >1.2 M, Na dissolves into Epsom crystals peacefully by $2Na^+ - Mg^{2+}$ exchange reaction. Below <0.6 M, Na–H_2O reaction dominates and solution explodes instantly on Na addition. In 0.6–1.2 M range both these reactions occur. Specifically, an intense explosion accompanied with a shock wave and vaporization of Borosil glass beaker containing salt solution was witnessed in 0.85 M Epsom solution on the completion of sodium dissolution, i.e., nearly 25 s after Na addition. There was Na aerosol everywhere in the room. No trace of the glass beaker was seen. Subsequent search, however, revealed that the bottom of the beaker, which was in contact with the wooden stool on which it was placed did not evaporate but broke into pieces. This was understood on the basis that for reaching plasma like conditions a container free condition is essential. Such a condition could be reached only on the sidewalls of the glass beaker. The intense explosion brought safety personnel from far away rooms in the building to book a complaint against us stating that we are doing unsafe experiment while we were still amazed at the turn of the events. At 0.85 M Epsom concentration, both the reactions mentioned above are shown to take place with equal probability. Glass vaporizes at temperatures $>1000^\circ$C. This fact indicated that a very high temperature has indeed been reached in this experiment. During the explosion, ultra thin molten glass needles flew all around. One such glass needle scratched the finger of the author, who stood at a distance of about 4 m from the beaker. Due to this injury blood oozed out of the author's finger and the scratching mark is visible even now. The glass needles also pierced invisible holes in two plastic water bottles kept around (2–3 m away from the explosion site) after which they could not

*E-mail: arunachalamlakshmanan@yahoo.com

pump out water on squeezing. Despite intense explosion, the stirrer blade made of stainless steel did not get damaged and continued to rotate which indicated that the energy is released outwardly. The fact that no radiation related injury occurred indicates that no nuclear reaction involving fission, fusion or transmutation occurred in the above case. But the involvement of nucleus occurs indirectly in CCRO, since it is the oscillation involving protons in H_2^+ions which lead to the accumulation of hydration energy.

Sodium dissolution in water or in very dilute Epsom solutions ($\ll 0.6$ M) leads to Na–H_2O reaction and the hydrogen released mix with atmospheric oxygen to cause hydrogen explosion resulting in breaking of the glass beaker rather than its vaporization. Additionally, the above explosion occurs within 5 s after Na addition. However, in the above experiment involving 0.85 M Epsom solution, the explosion occurs 25 s after Na addition. Both these factors clearly indicated that the explosion is not a result of detonation of hydrogen in the presence of oxygen.

The intensity and timing of the explosion witnessed above clearly indicated that the hydrogen released during Na–H_2O and Mg–H_2O reactions in 0.85 M Epsom solution somehow got trapped *in situ* in the cavitation-induced Epsom crystals. It is a case where a cage meant for trapping a massive elephant (Na^+ ions), instead, trapping more efficiently the elusive panthers (H^+ ions). The reactions involved are described below.

3. Hydrogen Production and Hydrogen Trapping Mechanisms

If we assume that hydrogen released from Na–H_2O reaction escapes, then the crystalline structure that remain on sodium dissolution in the explosive solution should be considerably unstable and may not even be formed as it assumes one sulphate anion vacancy for every Mg^{2+} ion present [2,3]. In this case it is assumed that 50% of sodium dissolved reacts with water while the remaining 50% get dissolved into Epsom crystal. Alternately, if the NaOH formed from Na–H_2O reaction converts the remaining $MgSO_4$ to $Mg(OH)_2$, then hydrogen trapping would not have been possible and no intense explosion would have resulted. Therefore, hydrogen trapping in the cavitation-induced crystals takes place as per the reactions described below.

The 2Na atoms get into the $MgSO_4$ crystal while one Mg atom is expelled into the solution as a result of cation exchange. The Mg atoms released react with water to produce hydrogen:

- $2Na \leftrightarrow Mg$
- Na donates electrons to a Mg^{2+} ion
- $2Na^+$ will replace a Mg^{2+} ion

$$Mg + 2H_2O \rightarrow Mg(OH)_2 + H_2 \tag{1}$$

- 50% Na added simultaneously reacts with water:

$$2Na + 2H_2O \rightarrow 2NaOH + H_2 \ \text{(to produce more hydrogen)} \tag{2}$$

- Hydrogen donates electrons to a Mg^{2+} ion

$$H_2 + Mg^{2+} \rightarrow {H_2}^{2+} + Mg^0 \tag{3}$$

(Due to ion exchange reaction between hydrogen and Mg, ${H_2}^{2+}$gets into the crystal while Mg is released into the solution).

- Reactions (1) and (2) are primary reactions taking place simultaneously with equal probability.

$$Mg^0 + 2H_2O \rightarrow Mg(OH)_2 + H_2 \tag{4}$$

Mg atoms released through reaction (3) react with water to produce MgOH, a confirmed by product which could be visually seen as a white precipitate from a distance and release further hydrogen which again get trapped in the precursor as hydrogen molecules as shown in Fig. 1a since there are no more Mg left in the crystal. This is a secondary reaction and temporally delayed when compared to the ${H_2}^{2+}$ incorporation through reaction (3).

Calculations reveal that the nanocrystal now contains only Na^+, ${SO_4}^{2-}$ and ${H_2}^{2+}$ ions bonded to the water molecules [3]. This necessitates the creation of ${SO_4}^{2-}$ anion vacancies for charge compensation in which H_2O molecules sit as shown in Fig. 1(a). Electrons donated by nearby water molecules stabilize the two hydrogen ions near a Mg^{2+} cation lattice site.

Additional trapping of hydrogen atoms/molecules near oxygen atom in the water molecule as shown in Fig.1(a) will compensate for the electron density loss created by the pulling of the electronic cloud towards the hydrogen ions needed for their co-existence near Mg^{2+} ion lattice site.

4. $(H_4O)^{2+}$ and $(H_6O)^{2+}$ Species

The formation of a divalent species, like H_4O^{2+} shown in Fig.1(a), would be normally energetically not favored in water because two positive charges are being pushed together on the same water molecule. But in the above case the water molecules act as a carrier of two hydrogen ions with the help of two independent dative bonds formed between the two lone pair electrons in the oxygen and the two hydrogen ions. The divalent crystal lattice energy demands the positioning of two protons at a single Mg^{2+} ion lattice site and hence the energy needed to overcome the electrostatic repulsion of the two protons is provided by the ionic crystal lattice energy. The existence of H_4O^{2+} ions in other systems such as sulfolane solution is known [4]. During oscillatory reactions, a hydrogen ion has to be separated from one of the hydronium ion in the solution and attached with another hydronium ion so as to form the H_4O^{2+}species shown in the crystalline nanoprecursor. The energy required for both the above reactions should come basically from cavitation. Apart from crystallization, dissociation of chemical species in liquids due to cavitation is well known.

Since equal probability of Na–H_2O reaction and Mg–H_2O reaction is proposed, the number of hydrogen atoms generated by the latter reaction would be exactly equal to the number of hydrogen atoms released by the former reaction and so the additional hydrogen generated could get trapped in a structure shown in Fig. 1(a). The hydrogen budget is thus accounted for. Adsorption of hydrogen atoms in such systems is well known. As a result, the structure shown in Fig. 1(a) forms which can be represented as $[H_6O]^{2+}$ with an overall +2 charge as that required at a Mg^{2+} site.

5. Oscillator/Substance (O/S) Theory and Molecular Hydrogen Ion

The O/S theory proposed by Dean Sinclair postulates that the formation of molecular monocation (H_2^+) is more likely rather than hydrogen molecular di-cation (${H_2}^{2+}$) [5]. Without making any other change, this idea can be fused into the mechanism proposed above. In the alternate proposal shown in Fig.1(b), two ${H_2}^{+}$ ions replace one ${H_2}^{2+}$ion. The exchange reactions in this case may be described as follows:

$$2H_2 + Mg^{2+} \rightarrow 2{H_2}^{+} + Mg^0 \tag{5}$$

Due to exchange reaction between hydrogen and Mg, H_2^+ions gets into the crystal while one Mg atom is released into the solution

$$2Mg^0 + 2H_2O \rightarrow 2MgOH + H_2 \tag{6}$$

Mg released reacts with water to produce MgOH, a confirmed by product

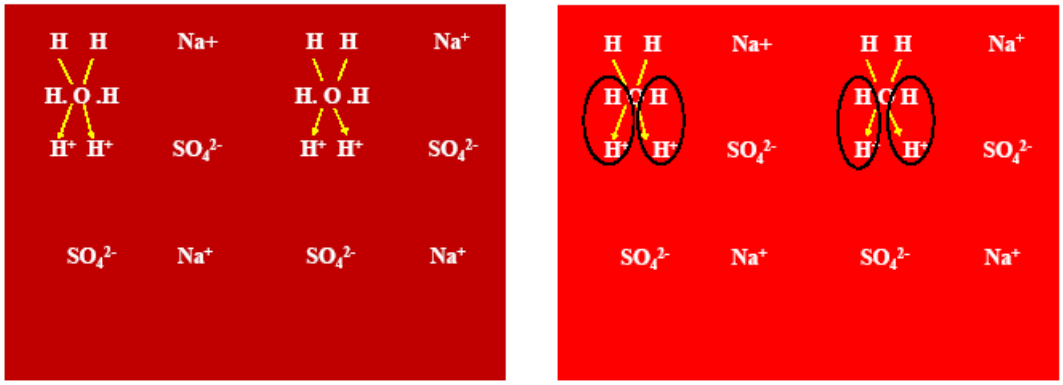

(a) (b)

Figure 1. *Original proposal* – Precursor state of the explosive solution after the sodium dissolution. In (a) the electrons are donated to hydrogen ions by water molecules. But in (b), the electrons are part and parcel of the molecular monocation $H_2{}^+$. *Alternate proposal* – O/S (oscillator/substance) theory presumes the formation molecular monocation ($H_2{}^+$) shown within the oblong circles rather than hydrogen molecular Di-cation (H^+H^+) shown in (a) as more likely. Figure (a) could well be the precursor of (b). See text for more details of the two figures.

On cavitation collapse, $2H_2{}^+$ ions are released into the solution:

$$2H_2{}^+ \rightarrow 2H^+ + H_2 \tag{7}$$

$$2H^+ + 2H_2O \rightarrow 2H_3O^+ \quad \text{(Hydration energy release)} \tag{8}$$

Figures 1(a) and (b) are essentially same. Only the concepts differ. Except for the replacement of two $H_2{}^+$ ions in the place of one $H_2{}^{2+}$ion, both concepts invoke cavitation collapse under high pressures.

6. Cavitation-Coulombic Repulsion Oscillation (CCRO)

In principle, for charge compensation, two protons should occupy one Mg^{2+} lattice site. Therefore, cavitation crystal formation brings in the two protons (and the two electrons attached to them) closer. This process is, however, opposed by Coulombic repulsion between the two protons which results in the collapse of the nanocrystal containing hydrogen.

Hydration energy is released during the formation of $2H_3O^+$, hydronium ions (Fig. 2). This once again leads to the promotion of cavitation – this time with more vigor since additional energy input has occurred. Thus reformation of the crystal takes place quickly and the hydrogen ions are brought together more closer than during the previous occasion which increases the electrostatic repulsive force. As a result, the crystal collapses faster leading to the release of more hydration energy. The above cycle continues leading to increasing oscillation speed with time and pressure build-up on the p–e–p species. The oscillation of the p–e–p species can be compared to a spring action as depicted in Fig. 3. The more the spring is squeezed, the faster it recoils. The beauty with the Cavitation-Coulombic Repulsion Oscillation (CCRO) process lies in the fact that the oscillation can continue indefinitely unhindered (perpetual oscillations!) till the end point is reached. There is no upper limit to the number of oscillations. This means the kinetic energies of protons can reach to very high levels (TeV?) leading to their head-on collisions through exponential accumulation of internally

released chemical energy! The forced end point in this case is of course the vaporization of the system. But for the vaporization, the CCRO would have continued further. The crucial question before us is what causes the vaporization?

In the CCRO process, the electrostatic repulsive force between protons which has been a stumbling block so far in bringing together protons is turned in its favor. Martial art uses this principle by deflecting cleverly the energy possessed by the opponent against the enemy himself. Indian Epic "Ramayana" also describes a character Vanara Vali who possess the power of capturing 50% of the power of the opponent facing him so he could defeat the enemy. It is due to the repulsive electrostatic force, the crystal collapses and it is due this collapse hydration energy is released. This is how cavitation gains energy from repulsion. Eventually the cavitation force wins over the electrostatic repulsive force by increasing the oscillation speed and bringing in the two protons to closer distances by deriving energy from the coulombian repulsion itself. Despite this fact, p–p fusion is unlikely to be the cause of the massive energy release witnessed in the above experiment since nuclear fusion involving protons is mediated by weak nuclear force as one of the proton has to be converted to neutron. This is the reason why Sun is burning very slowly. The reason for it being so sluggish is because its force carriers, intermediate vector bosons, W^+, W^- and Z_0 are so massive (about 80 times higher than that of protons) that the probability of a virtual one arising is extremely small. As per Heisenberg's uncertainty principle (HUP), in view of the short range of such massive particles, during p–p (or p–e–p) nuclear fusion the protons have to approach each other to much closer distances than is the case with deuterons in D–D/D–T fusion which invoke strong nuclear force involving mesons. One must therefore look elsewhere for the cause of the excess energy release in this experiment.

As per the O/S theory, once HH^+, hydrogen molecular cation is formed, it could coalesce into deuterium ion rapidly under suitable orientations in high-pressure conditions inside an ionic solid. This theory predicts that the HH^+ ion rotate down to a proper orientation losing motion (vibrational motion) to the milieu (environment) while condensing (spinning down) into a more symmetric unit when the two protons and electron come closer and closer to a rotating circular array corresponding to a Deuterium ion, eventually coalescing into that form. As per the O/S theory, coalesion (fusion) of para-hydrogen (nuclei with opposing spins) unit HH^+ into D^+ by rotation is more likely than the coalesion of di-protonated hydronium ions or p^+p^+ species. This has been presumed to occur when the rotations of both units are aligned on the same vector, in exactly opposite senses such that the two rotations will cancel before collision occurs as shown in Fig. 4. There would be good deal of usable energy release during this process as it would not be a sudden transform but a succession of transforms which would release energy. O/S theory presumes that very high temperatures

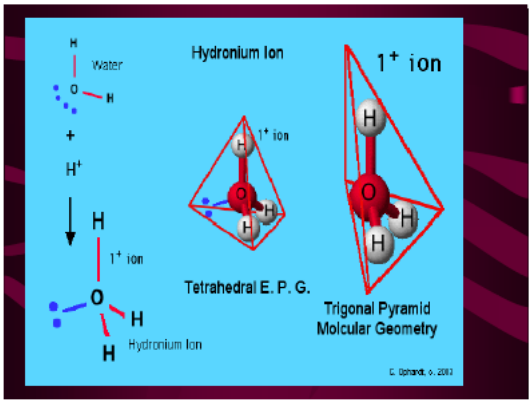

Figure 2. Formation of hydronium ion (H_3O^+) in the aqueous solution releases hydration energy. The exponential accumulation of this energy through repeated cavitation constitutes the energy input in the proposed system.

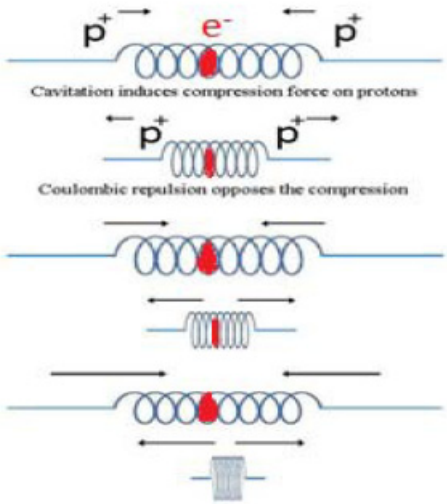

Figure 3. A simplied picture of the Cavitation-Coulombic Repulsion Oscillations of the p–e–p ($H_2{}^+$) species. Spring like action takes place due to two strong opposing forces – cavitation force and Coulombic repulsion. Note with increasing number of oscillations, the speed of oscillations increases exponentially and the distance between the protons decrease. Eventually collision of protons can occur. The crystal collapses due to Coulombic repulsion. Each time the crystal dissolves, hydration energy is released during the formation of H_3O^+, hydronium ions (Fig. 2). This once again leads to the promotion of cavitation – this time with more vigor since additional energy input has occurred. Thus reformation of the crystal takes place quickly and the hydrogen ions are brought together more closer than during the previous occasion which increases the electrostatic repulsive force. As a result, the crystal collapses faster leading to the release of more hydration energy. The above cycle continues leading to increasing oscillation speed with time and pressure build-up on the p–e–p species. The oscillation of the p–e–p species can be compared to a spring action as depicted above**.** The more the spring is squeezed, the faster it recoils.

will tear apart the HH^+ species.But high pressures can keep them intact. The situation of reaction within a solid has also the definite advantage of a lattice having many possible energy states to absorb the necessary motion, which must be removed as the entities fuse. This is harder to consider happening easily in a liquid or gas. O/S theory predicts that the formation of para-hydrogen is a necessary pre-requisite for the two hydrogen ions to come closer and that can happen only in $H_2{}^+$ molecular mono cation shown in Fig. 1(b) and not in $H_2{}^{2+}$ shown in Fig.1(a) which is an unknown species. Figure 1(a) shows that there is an additional electron attached to each of the hydrogen ion in the $H_2{}^{2+}$ species. So essentially in $H_2{}^{2+}$ species two electrons are attached while in H_2^+ ion only one electron is attached. In both the hydrogen ion species, the attached electrons stabilize the two protons near a divalent cation site. However,the symmetric para-hydrogen depicted in Figs. 4 and 5(c) is favored because in this species the electron density states get automatically squeezed in as they lie in between the two protons and the proposed CCRO basically squeezes the two protons together. *The lone pair electron donated by a nearby water molecule would convert $H_2{}^+$ ion into H_2 molecule like species thereby lending further stability to it.* The predicative values of pressure and temperature surrounding the precursors are shown in Fig. 6. Since the solution actually explodes at the end of sodium dissolution process, actual values of these two quantities are not exactly known. The merits of the arguments in O/S theory that the H_2^+ rather than $2H^+$ species could lead to the observed energy release are clear.

Dean Sinclair is of the view that the generation of the initial HH^+ unit to initiate the chain reaction may be the very slowest, least probable, step of the whole process. He is of the view that in our system there may be a film of H_2 molecules on the surface of the glass which goes into a fusion chain reaction once an initial HH^+ unit is generated.

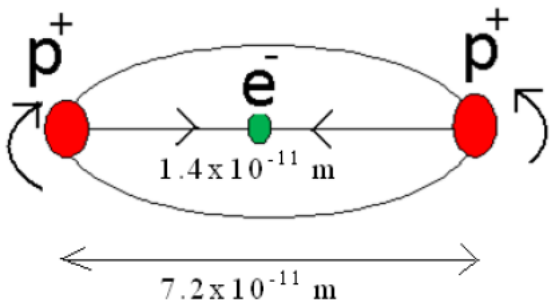

Figure 4. A symmetric para hydrogen in H_2^+ molecular cation.

Thus the arguments in favor of H_2^+ taking part in energy production are quite acceptable but it will be seen that the exact process seems to be connected to the exponential build–up of phonon energy and/or collapse of miniature black holes rather than to nuclear fusion unlike our earlier prediction [6].

7. Volume Casimir Effect

Hawking like radiation can be created in a crystal lattice through dynamic or volume casimir effect. Wilson et al. [7] have reported that a mirror moving at quarter of velocity of light prises virtual photons (always produced in pairs) apart so that instead of rapidly annihilating, the virtual photons are free to remain as real photons. The emitted photon frequency is about half that of the mirror's oscillation frequency. The reason why real photons appear in the experiment is that they lack mass. Relatively little energy is therefore required in order to excite them out of their virtual state. In

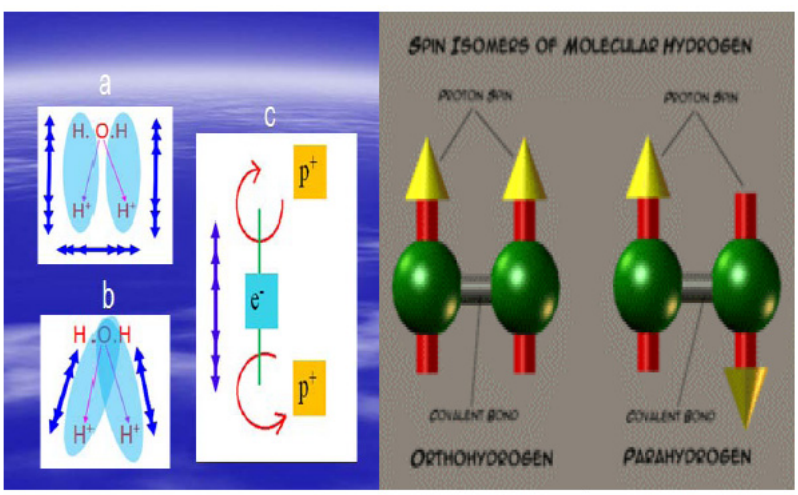

a-c d

Figure 5. (a-c, *left*). The oscillation of different hydrogen ion species during CCRO process. (d, *right*) Ortho (parallel nuclear spin) and para hydrogen (antiparallel nuclear spin).

principle, one could also create other particles from vacuum, such as electrons or protons, but that would require a lot more energy. In this case, a number of virtual photons from the vacuum are reportedly converted into a pair of real photons produced in opposite direction in the microwave region ("Casimir radiation"), while the moving metal surface loses some of its kinetic energy.

It is known that in principle high electric field generated by fast moving electrons accelerated by high-energy accelerators or high power (terra watt) lasers can prise virtual particles into real ones. But it requires enormous energy input similar to that required in hot fusion devices and therefore no practical device has been produced so far.

This work has, however, shown that in principle it is possible to accelerate/vibrate electrons to relativistic speeds through internal accumulation of energy. Through CCRO, collision of protons at high velocities trapped in cavities in ionic crystals has also been shown to be possible but whether to TeV energy range as envisaged by theorists of black hole production remains to be tested. In condensed matter the energy production mechanism requires elaborate description.

In order to prevent the scattering of electrons by gas molecules, normally electrons are accelerated in vacuum. However, electrons in stationary orbits of atoms do not face this problem. Intense energy source of real photons useful for heat production can be easily created by prising high-energy virtual photons exchanged between protons and electrons near the nucleus of an atom or ion! An added advantage with such an approach is that such electrons do not radiate energy through bremstrahlung process even at high speeds as long as they are bound to the so-called stationary orbits of the atom/ion. When the electric field build-up by the p–e–p in H_2^+ molecular ion oscillations continue unhindered and reaches a critical value extremely rapidly, high-energy virtual photons exchanged between protons and electrons at close distances will be prised to pairs of real photons and emitted as a burst. Accelerating electrons to a KE > 1.02 MeV to prise virtual photons into e^-/e^+ pair requires enormous energy input – roughly million times hydration energy which is unlikely. However, creation to a pair of real photons around 15 keV at relativistic electron speeds is feasible since their rest mass energy is zero. It is roughly only 6000 times the hydration energy released. In principle a 30 keV virtual photon could get converted into two 15 keV real photons. It appears that the kinetic energy of protons as well as electrons seem to be used up in creating the real photons in this case. Therefore, only photons

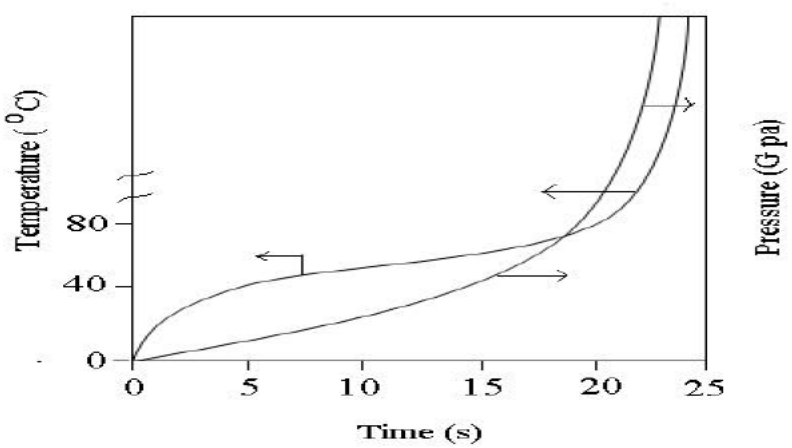

Figure 6. Solution temperature and pressure (predicative) on the hydrogen atoms/ions (HH^+ or $2H_2^+$) trapped in the metastable nanocrystal during sodium metal dissolution in a dilute aqueous Epsom solution (0.85 M). These are predicative values since the solution actually explodes at the end of sodium dissolution process. The figure depicts the scenario during the final moments of cavitation collapse in which the pressures and temperatures shoot up exponentially resulting in the burst of energy as a result of exponential increase in the release of hydration energy.

(in the keV region) appear in the experiment as a burst of energy as their rest mass is zero. The photon frequency is half of electron's oscillation frequency. No radioactivity is produced. The energy that would have otherwise remained dormant is released once the required input energies are reached internally. Since the energy is accumulated internally, the figure of merit of such devices would be very high and therefore a practical energy source is very well possible.

8. Phonon Amplification

Solids with more than one type of atom – either with different masses or bonding strengths – in the smallest unit cell, exhibit two types of phonons: acoustic phonons and optical phonons. Acoustic phonons are coherent movements of atoms of the lattice out of their equilibrium positions. Optical phonons are out of phase movement of the atoms in the lattice, one atom moving to the left, and its neighbor to the right. This occurs if the lattice is made of atoms of different charge or mass. They are called *optical* because in ionic crystals, such as sodium chloride, they are excited by infrared radiation. The electric field of the light will move every positive sodium ion in the direction of the field, and every negative chloride ion in the other direction, sending the crystal vibrating.

The possibility of phonon amplification in connection with a phonon laser was recognized in the early 1960s. Over the years people have built phonon lasers, which amplify phonons. This has been demonstrated from the MHz region up to the THz region. While low-frequency sound in the range that humans can hear (up to 20 kHz) is easy to produce in either a random or orderly fashion, things get more difficult at the terahertz (trillions of hertz) frequencies that are the regime of potential phonon laser applications. Instead of resulting in orderly, coherent phonon lasers, miniscule structures that can produce terahertz sound tend to emit phonons randomly. As an electron hops from one quantum well to the next, it produces a phonon. High-frequency phonons play an important role in thermal energy transport [8,9]. Phonon gain can cause amplification of the vibrations resulting and the build-up of CCRO can be accomplished consistent with the laws of physics *as suggested by an anonymous reviewer of this paper.*

In recent gas loading experiments in NiH, excess heat generation has been reported [10]. H or D flux in metals is expected to create high-frequency phonon excitation. Changes in pressure can lead to sudden violent energy release associated with high-frequency vibrations. CCRO mechanism would provide a route for amplification of high-frequency vibrations.

9. Miniature Black Holes

According to general relativity, a black hole should form whenever some mass is squeezed into a very small region of space. Collisions of protons with other protons at high energies (some observations show energies of hundreds of TeV which is much larger than the collision energies in particle collider experiments) should result in the formation of miniature black holes through quark interaction. However, there are models on the market suggesting that the strength of gravity could become significantly larger at very small distances, up to 10^{38} times stronger. If this is true then the Schwarzschild radius of two colliding partons becomes large enough that, at the LHC center-of-mass energy, two partons passing each other at their Schwarzschild radius is not so unlikely anymore. So, we may be able to produce microscopic black holes after all. During head-on collision of protons, a sufficiently high concentration of mass would result, and a *mini-black hole* would form. Black holes with a mass that is extremely small are extremely hot and unstable. They would evaporate nearly as soon as they are created ($\iota \sim 10^{-25}$ s) with the emission of *Hawking radiation*. Their decay would result in a sudden blast of a few energetic particles. And while such collision events with very high energy are exceedingly rare in particle accelerators, this type of collision has been going on for literally billions of years in the earth's atmosphere by the collision of Ultra High-Energy Cosmic Rays (UHECRs) with nuclei of oxygen, carbon, nitrogen and other elements present in the atmosphere., so an inordinate number of mini black holes would have formed. Since the earth has not (yet!) disappeared into one of these black holes, the much less massive man-made mini black

holes should be quite safe. As stated earlier, it is unique that there is no upper limit to the number of proton oscillations in the proposed CCRO process. This means the oscillation speed of protons and hence their kinetic energies can increase exponentially with oscillations due to phonon amplification to any desired extent with minimal energy input.

Thus the achievement proton energies of hundreds of TeV is very well possible within a very short interval of time. The distance between the protons decrease with the number of oscillations (Fig. 3). At some point, this will result in the their collision. In addition, the protons in the H_2^+ species (Fig. 4) are confined in space which increases their head-on collision probability at high energies unlike the random collisions at the particle accelerators. These two factors put together mean that the formation of miniature black holes is very well possible in the proposed system in laboratory conditions when the proton energies reach a critical point. The observed burst of energy at the conclusion of the CCRO lend further support to this hypothesis since the decay of such mini black holes is expected to result in a sudden blast of energy. No other proposal explains burst of energy observed better than the collapse of miniature black holes.

10. Energy Budget

Let us consider all possibilities of energy production in the above experiment.

10.1. Energy input

To start with the input energy to the bulk of the solution comes from the 40 W electrical stirrer (∼40 J/s) giving rise to an energy input of about 1.2 kJ in 30 s, the approximate time taken for the explosive energy release since sodium addition, which of course is extremely small compared to the energy released eventually (2 MJ).

Na–H_2O exothermic reaction ($Na + H_2O \rightarrow NaOH + 0.5\ H_2 \uparrow$) produces nearly 148 kJ/mol. Sodium added in this case (3.92 g = 0.17 mol) would then produce only about 25.2 kJ which is also quite small compared to 2 MJ.

10.2. Simple hydration

Preliminary calculation reveal that the number of hydronium-like ions formed during a single collapse of the nanoprecursor crystal in the explosive solution = 0.04 mol (2.4×10^{22} ions). Hence each time the above crystal dissolves in the solution an energy equivalent to 18.44 kJ (= 461.1 kJ/mol × 0.04 mol) is released into the solution, *which is less than the energy needed to vaporize the salt solution.* Let us assume that the solution used in the explosive mixture is equivalent to 100 cm^3 of water. Energy needed to vaporize it $\sim 100 \times 1 \times 80 \times 4.1855 + 100 \times 540 \times 4.1855 = 260$ kJ. Energy required to vaporize the glass beaker is $\sim 200 \times 1 \times 1000 \times 4.185 = 837$ kJ. Let us assume that the amount of energy vented out in the form explosion ∼1000 kJ. Then together about 2000 kJ (=2 MJ) of energy is released. The estimation of energy released, especially the amount of energy vented out in explosion is of course very crude.

10.3. Chemical combustion

As 2.4×10^{22} hydrogen ions (0.04 mol) are involved in the present case, the burning of hydrogen would release an energy of 9.57 kJ (240 kJ/mol), *which is also less than the energy needed to vaporize the salt solution.*

10.4. The p–p nuclear fusion

The first step involves the fusion of two nuclei (protons) into deuterium, releasing a positron and a neutrino as one proton changes into a neutron. It is a two-stage process; first, two protons fuse to form a diproton: ${}^1H_1 + {}^1H_1 \rightarrow {}^2He_2$ followed by the beta-plus decay of the diproton to deuterium: ${}^2He_2 \rightarrow {}^2D_1 + e^+ + \text{neutrino} + 0.42$ MeV. This first step

is extremely slow, because the beta-plus decay of the diproton to deuterium is extremely rare (the vast majority of the time, it decays back into hydrogen-1 through proton emission). The positron immediately annihilates with an electron, and their mass energy, as well as their kinetic energy, is carried off by two gamma ray photons: $e^- + e^+ \rightarrow 2\gamma$ + 1.02 MeV.

After this, the deuterium produced in the first stage can fuse with another proton to produce a light isotope of helium, ^{3}He: $^2D_1 + {}^1H_1 \rightarrow {}^3He_2 + \gamma$ + 5.5 MeV.

The fusion reaction involving hydrogen releases an energy of 6.945×10^7 kJ/g. The number of hydrogen ions incorporated in the solid solution = 0.239×10^{23}. 1 g of hydrogen will have $6.022 \times 10^{23}/2 = 3.011 \times 10^{23}$number of $H_2{}^{2+}$ ions. Fusion of these ions will release an energy of 6.945×10^7 kJ. Therefore, fusion of 0.239×10^{23} $H_2{}^{2+}$ ions in the solid solution will release an energy of 0.552×10^7 kJ (5.52×10^3 MJ). Thus the energy released during the thermo-nuclear explosion is nearly 5520 times [= (5.52 / 1) $\times$ 10^3] more than the energy required to vaporize the system. So it is no wonder that the excess energy has been vented out in the form of a massive explosion! This means that the collapse of the nanocrystals and their reformation should go on many ($\gg$ 100) times in an unhindered manner. This is less likely, since the vaporization of the system occurs after nearly 100 oscillations. Moreover, *p–p fusion invokes weak nuclear interaction and hence is extremely slow even in Sun as pointed out earlier whereas the present experiment which resulted in a massive burst of energy seems to be a result of a fast reaction.*

In any case, one way of testing it would be to look for the reaction products such as deuterium or positron (through their annihilation gammas) expected from such a fusion process or with 5.5 MeV gamma rays produced from HD fusion reactions if energetic deuterium is formed from p–p fusion in amounts commensurate with the energy produced. *Gamma ray spectra have been taken in the Piantelli NiH experiment, and there are not annihilation gammas present in amounts commensurate with the energy produced.*

10.5. The p–e–p nuclear fusion

Deuterium can also be produced by the rare pep (proton–electron–proton) reaction (electron capture): $^1H_1 + e^- + {}^1H_1 \rightarrow {}^2D_1$ + neutrino + 1.44 MeV. In the Sun, the frequency ratio of the pep reaction versus the pp reaction is 1:400. In p–p fusion most of the energy is carried away by positrons whose absorption releases heat but in p–e–p fusion, in the absence of charged particle emission, the neutrinos carry most of the energy released during fusion in a benign way. Hence p–e–p fusion in its present form cannot produce significant heat *(Ref: Proton–proton chain reaction. From Wikipedia, the free encyclopedia).*

10.6. Hawking-like radiation

Basically as per dynamical Casimir effect, the photon frequency is half of the electron oscillation frequency, say in the H_2^+ molecular ion. Let us assume that the inter-ionic (p–p) distance in it = 72 pm similar to the H_2 molecule. The frequency of a 15 keV photon = 3.5×10^{18}/s. Therefore, the electron oscillation frequency = 7×10^{18} vib/s. Let us assume that the electron travels at $1/3^{rd}$ velocity of light at the time of energy release. Therefore $v = 10^8$ m/s. Distance traveled by the electron in one oscillation = 1.4×10^{-11} m, which is about 1/5th of inter-ionic distance. Once the oscillation frequency of the electron bound to the H_2^+ molecular ion reaches the value of 7×10^{18} (electron speed = $c/3$), by the build-up of CCRO a burst of a pair 15 keV real photons will be emitted. Higher electron oscillation frequencies, would, of course result in higher photon energies. An experimental measurement of the photon spectrum would confirm this prediction.

In the above case, intense energy production occurs as a burst instead of the constant low-level energy release reported by others. Of course the systems used by others are quite different than that used by us.

Therefore, it is appropriate that modes of energy production other than fusion must be looked into while explaining heat production in CMNS.

10.7. Phonon amplification

Hydration energy is not released once but is released repeatedly with exponentially increasing rate with time since the rate of collapse of the precursor crystal should increase with increasing force of Coulombic repulsion as the two protons approach closer and closer. This means that the collapse of the nanocrystals and their reformation should go on many (nearly 100 or more) times in an unhindered manner till the pressures required for initiating the accumulated energy release through hydration process is achieved. In fact, the CCRO mechanism proposed envisages unlimited number of oscillations and hence unlimited amount of energy release through internal accumulation of energy without any major energy input. Only limitation occurs due to the limited capacity of the system to withstand the heat energy released due to phonon amplification.

Here comes the interesting question if heat energy is released due to the accumulation of hydration energy or due to phonon amplification. It is like the question which came first? Chicken or egg? Since heat dissipation occurs during stirring, heat accumulation can be discarded in favor of phonon accumulation. Moreover, heat energy transfer from lower temperature to higher temperature would invoke violation of second law of thermodynamics though in principle in small systems in short intervals of time such violation has been known to occur. Pressure build-up can lead to sudden violent energy release associated with high-frequency vibrations. CCRO mechanism would provide a route for amplification of such high-frequency vibrations from the MHz region up to the THz region.

10.8. Miniature black holes

Energy released from miniaturized black holes should be massive. The exact estimate of energy released depends on their number which remains uncertain since head-on probability of two protons in the proposed species is unknown and plasma like conditions seems to have been reached in the experiment only on the sidewalls of the glass beaker. Therefore, only a fraction of protons trapped in condensed matter seemed to have reached the desired head-on collision conditions needed for such an energy release. More detailed studies are therefore needed to verify this claim.

11. Summary

(1) Pressure build-up through accumulation of chemical energy can lead to sudden violent energy release associated with high-frequency vibrations. CCRO mechanism would provide a route for amplification of such high-frequency vibrations from the MHz region up to the THz region. Burst of energy release could occur during cavitation collapse when the build-up of pressure in the Epsom solution surrounding the nanocrystalline precursors by the unhindered p–e–p oscillations reaches a critical value extremely rapidly. Underlying mechanisms causing the explosion are, however, still speculative. A consensus, however, seems to be emerging in the sense that many of the proposed mechanisms of energy production in CMNS predict production of low-energy photons (or particles constituting Hawking radiation!) as the source of heat through high (relativistic) speed oscillations/collisions of charged particles trapped in crystal cavities. Similar views invoking cracks have been proposed to provide nuclear active environments.by Edmond Storms [11] in metal lattices. Burst of energy released from miniature black holes created in laboratory conditions due to collision of protons trapped in ionic crystal cavities appears to be quite an interesting possibility and merit serious consideration.

(2) Energy released in the experiment is nearly 200 times higher than the hydrogen combustion energy and nearly 100 times higher than the energy released by simple hydration. It is large enough to cause the observed explosion but is, however, much less (by nearly 2760 times) than the energy released by p–p nuclear fusion reactions. The p–p nuclear fusion proposal is highly speculative and is considered less probable. It could, however, be proven or disproven by the observation of 5.5 MeV gammas from secondary reactions.

Proposed experiments and challenges involved

(1) Reproduction of the explosive experiment – no other material nearby to curtail plasma.
(2) Effect of container material – should it be made of glass or other thin material?
(3) Should the container hang and not placed on a stool so plasma like condition can be reached even at its bottom?
(4) It is a pulsed energy release. This means for connecting to power grid we need to recharge a number of such fuel cells but each explosion should not disturb the other. How to achieve this?
(5) It is necessary to perform a series of successive experiments done at various Epsom concentration (1.9 M, 1.8 M, etc.) and to see if an increase in energy release along the way prior to where the system explodes. If so, then this might be important in that it could provide a "safe" version of the experiment which begins to show anomalous behavior.
(6) A still better approach would be to develop a fuel cell with a continuous flow of Epsom solution having appropriate salt concentration with continuous addition of appropriate quantity of molten Na metal to produce continuous excess heat energy similar to the heat production in Ni–H systems reported by Focardi et al. [11]. Currently there is enormous interest in the Ni–H experiments.
(7) The absence of any radiation injury suggests that heat energy release occurred without any radiation release. But measurement of radiations released, if any (0.51 MeV annihilation gammas or 5.5 MeV gamma rays produced from HD fusion) using a NaI:Tl detector would confirm or disprove the p–p nuclear fusion process. Once the reproduction is confirmed, technologists can take it over to a commercial electrical power grid level.

References

[1] Arunachalam Lakshmanan, Excess energy release during Na metal dissolution in a dilute Epsom ($MgSO_4{\cdot}7H_2O$) solution, *J. Condensed Matter Nucl. Sci.* **9** (2012) 64–71.
[2] A.R. Lakshmanan, M.V.R. Prasad, D. Ponraju and H. Krishnan, A novel method of non-violent dissolution of sodium metal in a concentrated aqueous solution of Epsom salt, *J. Solid State Chem.* **177** (2004) 3460.
[3] Arunachalam Lakshmanan, Can water serve as an infinite source of energy? *Infinite Energy* **81** (2008) 41.
[4] J.B. Bollinger, R. Faure, T. Yvernault and D. Stahl. On the existence of the protonated hydronium dication H_4O^{2+}in sulfolane solution, *Chem. Phys. Lett*. **140** (1987) 579–581.
[5] Dean Sinclair, http://groups.google.com/group/oscillatorsubstance-theory.
[6] Arunachalam.Lakshmanan, *J. Mod. Phys.* **2** (2011) 447.
[7] C. M.Wilson, G. Johansson, A. Pourkabirian, M. Simoen, J. R. Johansson, T. Duty, F. Nori and P. Delsing, Observation of the dynamical Casimir effect in a superconducting circuit, *Nature* **479** (376) 17 November 2011.
[8] V. Narayanaamurti, Phonon optics and phonon propagation in semiconductors, *Science* **213** (4509) (1981) 717–723. DOI: 10.1126/science.213.4509.717 .
[9] K. Vahala, M. Herrmann, S. Knünz, V. Batteiger, G. Saathoff, T. W. Hänschand Th. Udem·A phonon laser, *Nature Physics* **5** (2009) 682–686. Published online: 16 August 2009. doi:10.1038/nphys1367.
[10] S. Focardi, V. Gabbani, V. Montalbano, F. Piantelli and S. Veronesi, Large excess heat production in Ni–H systems, *IL Nuovo Cimento* **111** A (11) (1998) 1233–1242.
[11] Edmund Storms, An explanation of low-energy nuclear reactions (Cold Fusion), *J. Condensed Matter Nucl. Sci.* **9** (2012) 86–107.

J. Condensed Matter Nucl. Sci. 9 (2012) 86–107

Research Article

An Explanation of Low-energy Nuclear Reactions (Cold Fusion)

Edmund Storms*

KivaLabs. Santa Fe, NM 87501-6319, USA

Abstract

A plausible nuclear-active-environment in which Low-energy Nuclear Reaction (LENR) occurs is identified by ruling out various possibilities and by identifying an environment that is common to all successful methods. When this environment is combined with a plausible mechanism, many testable predictions result. These insights and proposals are offered to help clarify understanding of LENR and to suggest future studies. The common environment in which LENR occurs is proposed to be cracks of a critical size, followed by a resonance process that dissipates energy by X-ray emission based on a laser-like process. The LENR behavior has the potential to test the Standard Model of nuclear interaction.
 ISSN 2227-3123

Keywords: CMNS, Cold fusion, LENR, Theory

1. Introduction

Twenty-three years have now passed since Fleischmann and Pons (F–P) announced discovery of "cold fusion", aka Low-energy Nuclear Reaction (LENR) [1]. This phenomenon has two unique behaviors that have confounded explanation. Significant energy along with several nuclear products is produced in what appears to be ordinary materials under ambient conditions, where no nuclear reaction should be possible. And, unlike conventional nuclear reactions, release of the resulting energy does not cause emission of energetic radiation. When radiation is detected, it has relatively low energy and intensity. Even the documented nuclear products of helium-4, tritium, and various transmutation products are unexpected. To make the explanation even more challenging, the latter two products have been detected when either deuterium or light hydrogen is used. Application of extra energy from various sources and modest increases in temperature increase the reaction rate but are not required to initiate the process. In other words, the process does not act like conventional hot fusion.

The initial rejection of the claim has been shown to be unwarranted by hundreds of replications [2]. These studies show consistent patterns of energy production and various nuclear products being produced using four different methods. Many books summarize the history of this discovery [3–9], and several websites[a] provide up to date information. Ignorance is no longer an excuse for rejecting the claims.

*E-mail: storms2@ix.netcom.com
[a]See: www.LENR.org or www.coldfusionnow.org

 ISSN 2227-3123

This paper proposes to identify the location of the reactions within a material, how the process is expected to behave, and the general type of mechanism leading to the fusion and transmutation reactions. The goal is to find a productive approach to uniting and explaining all of the observations while resolving the apparent conflict with expected behavior based on conventional understanding of nuclear interaction. Of course, not all observations can be assumed correct. Nevertheless, enough well done studies are available to make rational judgment possible. Besides the acknowledged uncertainty in the behavior of LENR, flaws or gaps may also exist in conventional understanding of nuclear interaction, in particular in how the Coulomb barrier can be reduced and the role of the neutrino in the resulting reactions. As a result, demonstrating how LENR actually behaves may advance understanding of nuclear physics.

Attempts have been made by various theoreticians to propose a mechanism to explain how the Coulomb barrier can be reduced within the PdD lattice. These models generally involve changing the energy or local concentration of electrons. Initiation of a nuclear reaction in ordinary materials by such processes is prevented by chemical effects, as is shown later in the paper. Instead, the approach used here assumes a novel structure must form in the material before LENR is possible. The mechanism that causes the nuclear reactions occurs only within this structure, which is referred to as the "nuclear active environment" (NAE). Once this environment forms and is populated by any of the hydrogen isotopes, a fusion reaction follows. The challenge is to identify the NAE and create as much of it as possible. Identification can be accomplished by searching for a universal condition present during all successful production of LENR regardless of the method used or chemical system. Once the NAE is identified, search for the mechanism that produces LENR becomes easier. Many efforts to understand LENR have been unsuccessful because they reversed this process, i.e. by searching for the mechanism first within a single material, such as in PdD, while ignoring a unique NAE that would be present in all active material regardless of its composition or the method used.

2. Discussion

2.1. Nuclear active environment

The concept applies to an environment or location in which the mechanism leading to the nuclear reactions must operate. Consequently, it must form before the mechanism can start, the amount will limit the rate of energy production, and its nature will determine the mechanism that operates within it. The NAE must also be chemically independent of the normal chemical environment. Understanding and accepting these requirements are basic to what follows. Justification for this approach is provided later in the paper.

Identification of the NAE can start by finding a single condition that is present during all successful LENR studies. Requiring consistency with what is known about basic chemical behavior can set additional limits. These limits are created because electrons and nuclei in a chemical structure are arranged in tightly controlled relationships with respect to their energy and location relative to each other. Any change in this relationship will change the chemical structure and be resisted because energy is required to cause a change. This requirement cannot be avoided simply by using quantum mechanical models. Further justification for this insight is provided later in the paper.

Chemical structures, even highly modified ones at high temperatures and pressure, are known not to initiate spontaneous nuclear reactions based on experience over geological time. In other words, the nuclear mechanism rarely occurs and requires a very unique condition. The NAE is this unique condition. Its characteristics can be further limited by requiring the NAE and the nuclear mechanism to work together in a logical way. In other words, physics and chemistry have to work together to solve this problem.

LENR is proposed to involve three main events. NAE forms as the first event, the second event involves hydrogen atoms entering the NAE, and finally these atoms interact during the third event to cause a nuclear reaction. Each of these events can be described as a separate and independent process, starting with formation of the NAE. Slow formation of the NAE is proposed to cause the long delay typically experienced using the electrolytic process of F–P. Only the most general aspects of these events are outlined here, with more detail to follow in later papers.

The general principles that apply to any NAE need to be understood before a NAE can be proposed. First, the NAE must form. No matter how this happens or the final configuration, the formation process is expected to follow conventional chemical behavior and obey accepted laws governing such processes because it occurs in a chemical environment. A reduction in Gibbs energy must occur and the process that causes such reduction needs to be identified. Typical initiators of such changes involve a change in composition, a change in temperature, or accumulation of stress. In addition, the process of forming the NAE is probably endothermic. Obviously, a limit exists to how much NAE can form. Without a limit, power production would increase until the material is destroyed, which is not the case. A reason for this limit must be made part of a proposed process.

The second process, which involves insertion of hydrogen into the NAE, must also result in reduction of Gibbs Energy and the rate of insertion will be controlled by an activation energy[b]. This approach allows behavior to be predicted by applying the Laws of Thermodynamics to a collection of atoms rather than using quantum theory to describe how individual atoms might behave. In other words, focus is on the general behavior, as is typically used in chemistry, rather than on the quantum behavior of individual atoms, as is favored by physics.

The third process, involving the actual nuclear reaction, is required to be exothermic and to result in nuclear products known to occur. The details of this process will be discussed later in the paper.

Let us start by applying these basic requirements after the NAE has been created. Three major variables are expected to determine the amount of generated power.

(1) The number of sites where nuclear reactions can occur, i.e. concentration of NAE. Obviously, the greater the number of active sites, the more power is produced.
(2) The concentration of H or D in the NAE, which is related to the applied H_2 or D_2 pressure when gas is used or chemical activity when electrolysis is used. The greater the concentration of hydrogen isotopes, the more power would be produced.
(3) The energy available at the NAE, which is normally provided by temperature. Temperature is expected to have an exponential effect within a limited range, typical of its effects on ordinary chemical reactions. This energy also can be applied using lasers or other sources. The more power applied to the sites, the greater the rate of fusion at each site and the more power is produced.

Different combinations of these variables affect each method differently. For example, the electrolytic method suffers from relatively low temperatures while benefiting from a high concentration of deuterium. In contrast, the gas loading method has low hydrogen concentration while being able to benefit from high temperatures. Both have unknown and highly variable NAE concentrations. The best way to increase the amount of energy would be to maximize all three variables. Consequently, LENR does not necessarily require a high concentration of H or D to function, as is frequently assumed. The conditions only need to combine to produce a rate that can be detected using available instruments. In addition, the variables interact in complex ways. For example, increase in temperature will lower the concentration of hydrogen, all else remaining constant, causing power to decrease when the temperature exceeds a critical value. Destruction of the NAE by too high a temperature or excessive local energy production can also reduce the rate.

Once the NAE forms, the subsequent mechanism operating at the nuclear level may be very unusual, but the researcher has no influence over this reaction. It occurs spontaneously and automatically. Trying to influence the

[b]Conventional chemistry uses the relationship ($k = A\ e^{-E/RT}$). This could be applied to LENR if "k" is related to power produced by the nuclear reaction, T is the temperature in the NAE, and E is the activation energy for forming the NAE or for making H^+ (D^+) available to the NAE. This assumes an energy barrier exists in all processes that precede the nuclear reaction. If several kinds of nuclear reactions occur at the same time, each could be described by independent equations having the same form, but different activation energies. For example, failure to detect tritium while helium is produced would result partly because the tritium producing reaction would have greater activation energy, hence a lower rate, for the local conditions.

nuclear process directly would be like lighting the fuse (creating the NAE) and then trying to influence the rate of the resulting explosion. The amount of energy being created locally is simply too large to control once the process starts.[c] Consequently, knowing exactly how this mechanism functions is not useful to making the LENR more intense or reliable. Nevertheless, this understanding can help identify the NAE and the expected nuclear products, which is important.

How many kinds of NAE-mechanism combinations are expected? Are all the observed nuclear products created by the same combination? These questions are difficult to answer based on present experience because each method producing LENR involves a different gross chemical environment. Nevertheless, a process so rare and unique would be expected to involve only one or, at most, a very few different combinations. Hints about the basic nature of the NAE and where it is located can be obtained from the Fleischmann–Pons effect, which shows:

(1) Almost complete loss of helium to the gas. (Shows that helium is produced within a few microns of the surface [10].)
(2) Appearance of tritium in the electrolyte rather than in evolving gas. (Shows that tritium is produced close enough to the surface to permit exchange with the arriving D^+ ions [11].)
(3) Transmutation products located only in the surface region. (Shows that some of the reaction occurs at the surface [12,13].)
(4) Presence of melted regions on the surface. (Shows that the major energy-generating reaction is concentrated at the surface.)
(5) Ability to generate LENR using thin layers of palladium on an inert substrate. (Shows that a large amount of material is not required [14].)

These behaviors point to the surface region as the place to look for the NAE when electrolysis is used, not in the interior of the cathode. What chemical and physical conditions are present in the surface of an electrolytic cathode? Many careful analyses of such surfaces reveal a complex alloy containing lithium, platinum, oxygen, elements provided by the Pyrex container, and impurities in the electrolyte, with sometimes no palladium present at all. This impurity layer appears to be necessary to maintain a high concentration of deuterium [15] and perhaps to create the NAE as well. Measurements of the surface composition place it above D/Pd = 1.5[d] [17,18], which is well above the measured average composition [17]. Deuterium is continuously lost from this layer through cracks, causing a steady but non-uniform flux of deuterons within the layer [19]. Further complicating the interpretation, high-resolution SEM examination shows a complicated morphology consisting of dendrites, cracks, well-formed crystal structures with preferred orientation [20,21], and a very uneven topology [21–25]. Deposition of palladium using the so-called co-deposition process creates even greater complexity [26]. Just where in this tortured landscape the NAE is located is not known, although it must have a very small size because all features on such a surface are very small. The observed energy is expected to result from the sum of many active sites, with each site being independent of the others. This kind of behavior can be seen clearly in the IR images taken by Szpak et al. [27,28] showing random flashes of light as a result of sudden local heating–cooling cycles in random locations. Fogging of photographic film placed against active material shows that tritium is also produced only in random locations very near the surface. Mosier-Boss et al. [28] found this effect after electroplating Pd from D_2O, and Sankaranarayanan et al. [29] observed the same behavior by loading and deloading Ni wire with H_2. Other studies have produced tritium and detected it using autoradiography, but we cannot be sure LENR is the sole cause when discharge voltages great enough to cause some hot fusion [30,31] are used. From these observations we can conclude that the NAE has a very small size and it is not uniformly distributed within a complex

[c]Of course, denial of fuel will control the overall power, as described above.
[d]The fcc lattice of PdD does not exceed D/Pd = 1. Compositions in excess of this limit suggest formation of a crystal structure (a new phase) that can accommodate the extra D [16], similar to formation of ZrH_2 following ZrH in the Zr–H_2 system.

surface. Presumably, the observed melting can occur where concentration of NAE is especially great. In summary, these observations show that the NAE exists only near the surface, it is not pure PdD, and the measured D/Pd ratio is too large to result from beta-PdD alone. Therefore, any model must be rejected when it is based on the NAE being in the bulk of the sample and when it requires the presence of pure PdD having the measured average composition.

Arata [32] and Case [33] focused attention on the importance of small particle size. This idea was carried to extreme by attempting to place a few atoms of Pd in the small atomic cage present in Zeolite [34], but without obvious success. Arata [35,36] proposed creating nanoparticles of Pd by oxidizing an alloy of Pd + Zr. The dilute Pd–Zr alloy that remains in the final matrix of ZrO_2 appears to produce a small amount of LENR [37,38], but not enough to identify the small size of the metal particles as being the only important condition. The material Case [33] used, which is a typical chemical catalyst consisting of nanoparticles of Pd on charcoal, does not work unless special carbon is used and the material is given special treatment. My many attempts to apply finely divided Pd to various materials, including carbon, failed to produce predictable LENR. Obviously, the size of the Pd particles is not the only important variable using this method. After all, any attempt to form nanosized particles will usually create a wide range of sizes, some of which will cause LENR and detectable energy if size were the only important condition. While small size is beneficial, probably because of increased surface area, the total experience shows this is not the only important condition.

Simply causing deuterium to diffuse through palladium or other materials apparently can initiate LENR reactions at a low level. Iwamura et al. [39] diffused deuterium through alternate layers of calcium oxide (CaO) and Pd. The presence of CaO was necessary for transmutation to occur on the surface where various elements were deposited. The behavior during this study reveals an even more complex process because the CaO layers were separated from the targets on the surface by 400 Å of Pd. Did the CaO create a special species that diffused through the Pd without reacting, only to cause the deposited elements on the surface to transmute? Or did the mechanical and electronic stress introduced by the CaO cause a NAE to form at the surface? In contrast, Liu et al. [40] and Biberian and Armanet [41] were able to achieve LENR by simple diffusion of D^+ through pure Pd, again using a relatively low deuterium concentration. Possible features these studies might have in common are described later.

2.2. Additional requirements for evaluating an explanation

Behavior initiated by hot fusion needs to be identified and not used to explain LENR. Because both hot fusion and LENR can occur in the same materials and sometimes at the same time, the results of these two independent reactions need to be separated. Crack formation is known to initiate nuclear reactions in material containing deuterium. This process, called fractofusion [42–45], creates brief high voltage in the crack that can cause fusion by the hot fusion process with the expected energetic nuclear products. Because neutrons result, they are frequently detected as brief pulses, which must be carefully evaluated before they are attributed to LENR. Another example of potential hot fusion is obtained when solid materials are bombarded by energetic deuterons [46–48]. The resulting hot fusion-like reaction is sensitive to the electron concentration in the material when applied energy is low. This is not an example of LENR because the reaction products are very energetic and are the ones expected to result from conventional hot fusion, not LENR. A clear separation between how LENR and hot fusion are caused to happen must be maintained because entirely different mechanisms are apparently operating.

Two very different assumptions have been applied to the process of creating a theory. One approach assumes a spontaneous nuclear reaction can occur within a normal lattice or on the surface of normal material simply because a proposed mechanism starts to operate, usually because the deuterium concentration reaches a critical level. The other approach, which is encouraged here, assumes a significant and observable change must take place *before* LENR can occur and this results in a new environment in which the nuclear reactions take place.

This unique environment avoids conflicts with how common materials are known to behave and is consistent with just how rare and localized the behavior appears to be.[e]

Ordinary materials cannot be the location of LENR because of how chemical systems are known to behave, which can be understood several different ways. Materials are made up atoms arranged in characteristic crystal structures, the form being determined by the energy of electrons associated with the atoms and the thermal energy experienced by the crystal. These energies cannot be altered without changing the structure or, if increased enough, cause melting.[f] The electrons do not shift spontaneously from one energy level to another in any observable way in a stable chemical system unless energy is applied from outside the structure or changed conditions make the present structure unstable. When such a change takes place, it is always associated with a reduction in Gibbs energy[g]. Consequently, any proposed spontaneous change that can initiate a nuclear reaction must also show why the Gibbs energy would be reduced. In addition, the atoms act as a collective so that when any change is made in one location, this change is communicated to all parts of the crystal at well-understood rates. The Laws of Thermodynamics describe this collective behavior. Metals such as palladium or nickel and compounds such as PdD are all stable chemical systems under the conditions normally used. Even if a spontaneous change were to take place because of unexpected release of internal energy, the limited magnitude is known not to cause nuclear reactions.[h] This understanding is so basic, it cannot be ignored without clearly stated and demonstrated reasons. Indeed, the role of energy in materials is so important and well understood that arguments based on quantum mechanics or any proposed increase in energy must be consistent with this behavior.

A list of proposed requirements a theory must satisfy are summarized below.

(1) LENR does not happen in pure beta-PdD, but requires formation of a unique condition (NAE) before LENR can occur. Regardless of the condition, a high deuterium or hydrogen concentration is not the only requirement.
(2) The mechanism causing the nuclear interaction occurs only in the NAE and is logically related to the nature of the NAE.
(3) This NAE-mechanism combination must be consistent with what is known about the behavior of materials, the Laws of Thermodynamics, and basic rules governing nuclear interaction.
(4) The NAE-mechanism combination must explain all observed products of LENR, including results of fusion, transmutation, and the source of radiation.
(5) The explanation must logically explain both how LENR is initiated and how the resulting energy is dissipated without apparent radiation.

[e]As an aside, these two different approaches to finding an explanation reveal a basic difference in how different branches of science look at Nature. People trained in physics focus on mechanisms while trained chemists tend to focus on the environment and conditions. The phenomenon of LENR requires a marriage between these two fields of science, which has not yet happened. Rejection of the observations has generally resulted because a mechanism could not be imagined based on currently accepted "theory". Successful understanding will only happen after the conventional mechanisms are abandoned and a new mechanism is applied to the correct kind of material.

[f]As an example of how a typical material would behave, palladium will melt if more than 0.17 eV is applied to each palladium atom. This amount of local energy is not enough to cause a nuclear reaction. Any energy accumulating process operating within a lattice of Pd atoms would cease once the local amount had reached this level because melting would commence. As a result, energy would be absorbed from the proposed energy-accumulating process and the region in which this mechanism operates would be destroyed.

[g]Gibbs energy is defined as being equal to the enthalpy change minus the entropy change times absolute temperature: $\Delta G = \Delta H - T\,\Delta S$. The enthalpy is the measured energy given off or taken up by the reaction.

[h]An exception is found in the fractofusion process. In this case, rapid separation between atoms, resulting in a crack, creates a large voltage difference within the space that can ionize and accelerate any deuterons present to energies sufficient to cause hot fusion. This event is normally detected as a burst of neutrons.

2.3. Published explanations

What basic requirements can be accepted so far? Although the answer is incomplete, a few can be provisionally accepted and used to evaluate suggested mechanisms. Hopefully, this process will make the requirements easier to understand.

Hundreds of attempts have been made to explain the LENR effect, yet no theory has successfully shown how the effect can be made more reproducible and robust, and no theory has gained acceptance outside of a select group. Nevertheless, a few examples of published explanations will be discussed below to give an understanding of the approaches being explored and their limitations in view of the proposed requirements listed above. Rather than describe each theory, the general principles are applied to a few models to show how similar ideas might be evaluated.

2.3.1. *Role of metal atom vacancies*

Hagelstein and Chaudhary [49] propose vacancies in the palladium sub-lattice where Pd atoms are missing is the location of the NAE. This approach is based on three assumptions: (1) that a sufficient number of metal atom vacancies are present in PdD, (2) that more than two deuterons can enter such a site in a PdD lattice, and (3) that once there, the deuterons can fuse to form helium. Failure of any one of the three assumptions would invalidate the model. We start by examining each assumption separately. Flanagan et al. [50] report that metal atom vacancies introduced by cold-working palladium were removed by heating between 473 and 573 K, which would eliminate such vacancies at temperatures known to produce LENR. If metal atom vacancies are present in large concentrations in PdD, the upper phase boundary is expected to exceed D/Pd = 1. McKubre and Tanzella [51] determined this boundary at room temperature using the behavior of resistance. They found a break in slope between resistance and D/Pd to occur very close to a value of 1, indicating formation of a two-phase region at higher compositions; not a continuation of the beta phase. Norlander et al. [52] conclude, based on calculations, as many 6 D can occupy a Pd vacancy. But, even at this number, they conclude the deuterons are not close enough to fuse. The more atoms needed to be assembled in one place for a reaction to occur, the lower would be the probability of this happening. Therefore, the reaction rate would be small and the rate would be very sensitive to the applied D_2 pressure. The observations do not show a large pressure effect, but this variable needs to be studied more carefully. If fusion were to occur, another set of assumptions have to be used to explain absence of radiation. Consequently, violation of requirements Nos. 1, 4 and 5 (listed above) do not encourage use of this approach as an explanation.

2.3.2. *Role of neutrons*

Obviously, if neutrons were involved in the nuclear mechanism, the Coulomb barrier would not be an issue. Therefore, several people have proposed a source of potentially reactive neutrons. These neutrons are thought to be initially present in the material as stable clusters [53] or as stable polyneutrons [54], which are released from this stable condition by some mechanism. No direct evidence exists for trapped neutrons, neither as clusters nor as polyneutrons, being present or released in ordinary material. Indeed, if enough neutrons were present to support the large reaction rates being occasionally observed, their presence would be obvious from their effect on the density of such repositories, which has not been found. Also, just how neutrons or polyneutrons would remain in the palladium or any material after chemical purification requires use of implausible assumptions. Although a few observations are consistent with a rare and low-level nuclear process being caused by what might be polyneutrons [55], the explanation does not identify the NAE and violates requirements Nos. 4 and 5.

On the other hand, neutrons have been proposed to form [56–61] by fusion of an electron with a proton or deuteron, which requires about 0.76 MeV to be present at the time and place of the reaction. Because this explanation of LENR has gotten wide attention, it needs to be fully understood. The idea is flawed because it assumes enough energy to form a neutron can be concentrated in a chemical environment at one location. Energy is a real and basic quantity that is not

observed to accumulate spontaneously beyond well-understood limits.[i] If such large energy were to concentrate in an electron or the target nucleus, it would have to be harvested from an environment in which the average energy is much less than 0.1 eV. Consequently, packets of energy would have to spontaneously seek out and add to individual electrons in which the accumulating energy must be stored. How is this storage accomplished? The electron is a fundamental particle that cannot store energy. If it could, its rest mass would not be constant and, at the very least, the TV would not work. Perhaps energy can be stored by another process. Particles are known to store energy as increased mass if enough energy is added to accelerate them to near the speed of light. Traveling at this speed in a lattice with many electrons and nuclei in the way would seem implausible[j]. So, we are asked to imagine an electron being able to pass through a collection of atoms at near the speed of light while accumulating energy from the surrounding energy fields without losing this energy before a hydrogen nucleus is encountered. Calling this a weak interaction, introducing the concept of plasmons, or proposing a super-heavy electron provides no justification for or insight about how the process might actually work. Unless this process can be shown to actually occur, rather than assumed to be possible, formation of a neutron is not a plausible explanation for LENR. Indeed, when electrons are given the required energy and used to bombard a material containing p or d, very few, if any, neutrons are detected [62]. In addition, if so much energy could be concentrated in an electron, observed chemical effects would be expected long before the electron could make a neutron. For example, no explosive would be stable once this process started. Furthermore, if neutrons were present from any source, radiation from their own normal beta decay and gamma resulting from their interaction with various nuclei would be expected, but is not detected. In addition, the various nuclear products cannot be explained only by neutron interaction because this reaction produces a new isotope, not a new element. Subsequent radioactive decay is required to produce the observed elements, which is not observed. Consequently, even though this mechanism has gained some attention, it is not consistent with how LENR behaves or with conventional science. This explanation does not identify the NAE and violates Nos. 3–5.

On the other hand, many people have speculated about what would happen if the electron could get sufficiently close to the nucleus to form what they call a "virtual neutron". In this way, the electron might provide enough shielding for the proton or deuteron to enter a nucleus without the impossible task of creating a real neutron. Mills [63] provides a theoretical basis for allowing the electron to closely approach the nucleus, with the formation of the so-called Hydrino. Dufour et al. [64,65] proposed a structure called a Hydrex where many electrons and photons cluster together in a stable collection that might lower the Coulomb barrier. The formation of Rydberg or BEC structures could be viewed as variations on this approach. Such variations on a pseudo neutron-like structure seem worth exploring. The kind of NAE-mechanism combinations required for such structures to form and be involved in LENR has not been identified, but will be explored below. Nevertheless, the explanation violates Nos. 4 and 5.

2.3.3. *Role of phonons*

A phonon is a pseudo-particle used to describe how energy is transferred between or interacts with atoms or electrons in condensed matter. The model is used to describe how heat energy moves through a material as vibrations of atoms and electrons located within a material. When the concept is applied to LENR, these vibrations are proposed to cause a few atoms to approach one another within nuclear reaction (strong force) distance [66–69] or to cause energy to accumulate within a nucleus [70] so that the nucleus becomes unstable. In the process, a basic assumption is made – the vibration energy is focused on one nucleus and does not affect the general chemical bonds between the surrounding atoms in

[i]Such an abnormal energy distribution conflicts with the well-known Boltzmann distribution and the Second Law of Thermodynamics

[j]Electrons of this energy have a very small range in palladium because their energy is lost to the surrounding material by generating X-rays [271]. This means the mysterious transfer of energy must take place at an impossibly fast rate and a proton must be found within a small fraction of a micron after this energy has been acquired, all without generating X-rays that are not observed.

PdD. This assumption is in basic conflict with how phonons are observed to behave and the requirement that energy always moves "down hill". Indeed, phonons are proposed to provide this "down hill" transfer of energy once a nuclear reaction occurs as the released energy is communicated to the surrounding atoms. Use of this concept must show a plausible reason why phonons can produce an "up hill" transfer of energy without causing chemical changes, followed by the expected "down hill" transfer after the nuclear reaction is initiated. As a result, the explanation violates all of the proposed requirements.

2.3.4. *Role of particle-wave conversion*

The Chubbs [71] proposed that a deuteron can convert to a wave under proper conditions. As such, it can interact with another deuteron wave without a Coulomb barrier being directly involved. This interaction briefly forms a helium wave, which slowly converts to a helium particle by losing small quanta of energy to the surrounding lattice. This model solves a few problems, but it does not account for how transmutation products are produced or what unique property of the lattice encourages particle-wave conversion. Simply having a periodic array of atoms, as they propose, is not sufficient because this a universal condition existing in all materials, while nuclear reactions are rare and localized in special regions. Although this general approach could be applied to a special NAE, as is described below, the concept violates all of the proposed requirements as it is described by the authors.

2.3.5. *Role of "Strange" particles*

Explanations based on rare particles have been proposed. These include the Erzion [72] the NATTOH [73], fractionally charged particle [74], massive negative particle [75], electron cluster [76], and super-heavy nucleus [54]. While some of these particles obviously exist in Nature, how each might cause the full range of behaviors produced by LENR at the observed rates has not been explained. Remember, generation of 1 W of power by helium formation requires 10^{12} helium atoms be made per second. This would seem to be too heavy a burden for an explanation based on strange particles to carry.

2.3.6. *Role of tunneling or enhanced cross-section*

The process called "tunneling" is used when a reaction appears to require an abnormally small amount of energy compared to an expected amount. Of course, this idea assumes the full (expected) amount is known accurately for the conditions being used. Instead of using the tunneling metaphor, an unexpectedly large rate is sometimes described as resulting from an increase in cross-section. In either case, the expected energy or cross-section needs to be justified, not just why less energy is apparently required. For example, expected behavior for LENR under various conditions is based on a model obtained using the hot fusion process. The rate of the hot fusion-type reaction is measured as a function of applied energy, from which the expected barrier height is calculated. Application of this barrier height to LENR would only be valid if LENR were caused by the same mechanism, which is very unlikely to be the case. In addition, requirements Nos. 2–5 are violated. Nevertheless, early theoreticians including Preparata [77] used this incomplete description and this approach was favored by Fleischmann [78]. Many other people also have proposed the same idea [79–84].

A source of screening electrons has been suggested to exist between two materials having different work functions, the so-called swimming electron theory [85–87]. These electrons are proposed to reduce the Coulomb barrier and explain the transmutation observations reported by Miley [88,89]. Unfortunately, this theory ignores how the required number of protons can enter the available nuclei in the sample without producing radioactive isotopes, which are seldom detected. Miley et al. [90] try to avoid this problem by creating another problem. Their mechanism involves formation

of a super-nucleus of $^{306}X_{126}$ from a large cluster of H and D. This structure then experiences various fission reactions. The cluster is proposed to form as local islands of ultra dense hydrogen [91] using Rydberg-like process [92]. Why so many deuterons would spontaneously form a cluster in a lattice in apparent violation of the Laws of Thermodynamics has not been explained. Why No. 5 is not violated is not explained.

2.3.7. *Role of multi-body fusion and Bose–Einstein condensates*

Multi-body fusion was first suggested by Takahashi et al. [93] who arrived at this model using the energy spectrum of the few neutrons being emitted from an electrolytic cell while anomalous energy was detected. A later study using energetic D^+ bombardment of PdD is consistent with the neutron spectrum obtained using electrolysis [94], which suggest the neutrons might have actually resulted from a hot fusion-type reaction, as would be expected to result from the ion bombardment method. On the other hand, Iwamura et al. [95] show evidence for up to six deuterons entering a nucleus simultaneously when no extra energy is present, adding additional support to a multi-body model. Formation of such clusters [96] solves many problems, not the least of which is a method to release momentum after fusion without emitting a gamma ray. In this case, the resulting nuclear energy is distributed between a few alpha particles and many un-reacted deuterons in the cluster. However, unless the clusters were improbably large, energetic emissions would be detected [97], which has not been the case. Requirements Nos. 4 and 5 are apparently violated.

Kim [98,99] justified cluster formation by calling it a Bose–Einstein Condensate (BEC) [100,101], which would be the NAE. He proposes this type of structure is able to form on the surface of very small particles of PdD. Typically, BEC is only observed near absolute zero because the bonding energy is too small for the structure to survive higher temperatures. Formation of a BEC at the temperatures used to initiate LENR would be an amazing event even without LENR being a consequence. Nevertheless, Kim proposes special conditions exist in a lattice to stabilize a BEC. Even if BEC could initiate fusion, explaining how the resulting energy is dissipation into the lattice without detected radiation requires many assumptions, resulting in violation of No. 5.

2.3.8. *Theory of Rossi and Piantelli*

Piantelli et al. [102–112], in a series of papers, have described how energy, radiation, and transmutation result when N–Cr and Ni tubes are exposed to H_2 after extensive pretreatment. The process is proposed to involve clusters of nickel on the surface that interact with H^- ions dissolved in the metal to cause conversion of nickel to copper when the metal is heated above 350°C. The authors suggest a mechanism for this reaction.

Rossi [113] increased the amount of power over that obtained by Piantelli et al. by using specially treated nickel powder and proposed the same source of energy. Furthermore, Rossi [114] believes that positrons result from decay of the resulting radioactive copper isotopes and these generate annihilation radiation of 511 keV that is absorbed in a lead shield, thereby heating the apparatus. No evidence supports this implausible claim. Instead, Piantelli reports detecting gamma emission at 744 keV, which is not consistent with the energy from positron annihilation.

The descriptions of the process offered by Piantelli or Rossi cannot be considered a theory. The proposed process is not consistent with what is observed nor is it plausible based on the listed requirements. Transmutation cannot be a source of significant energy even if the significant Coulomb barrier could be overcome. Once an Ni nuclei has been transmuted, energy production can only continue at that site if another H or D is added to the fixed target. Such a process will eventually produce radioactive isotopes, yet these are not found. Furthermore, the amount of energy released by each transmutation reaction is small, requiring a large reaction rate to account for the measured energy[k] as well as many active sites. Explaining how so many sites can form in ordinary material is a challenge not met so far. Nevertheless,

[k]The reaction $Ni^{62} + p = Cu^{63}$ produces 5.6 MeV/event. For 1 kW of power to be generated, this reaction must occur at 10^{15} times/s or produce

both workers apparently have been successful in creating enough NAE sites to make significant energy using ordinary hydrogen.

2.4. The process of finding an explanation for LENR

In the previous sections, the requirements a theory must satisfy, the behaviors in need of explanation, and the flaws in a few explanations are discussed. The challenge now is to propose a model consistent with these requirements and behaviors.

The general features of a plausible NAE will be used to start the search. The goal is to eliminate most environments by applying these requirements and focus on the few that remain. Environments surviving this process can then be tested against proposed mechanisms to determine which combination is consistent with the most observations. The intent is to use as few assumptions as possible.

Four different kinds of NAE have been proposed by various authors.

(1) A normal arrangement of atoms and electrons that create a crystal structure, so-called bulk atoms, including vacancies in the nonmetal and metal sublattices. Cubic PdD, either pure or impure, is an example of such an environment. This violates requirement No. 1.
(2) A novel arrangement of atoms not normally present. The BEC structure, Rydberg matter [115,116], nanostructures [117–119], diamondoid or Zeolite molecules [120,121], cracks [122–124], or carbon nanotubes [125] are variations of this condition. In addition, the NAE might also be where Hydrinos [126] can form because the required catalyst is uniquely present. No requirements are violated if several plausible assumptions are used.
(3) An interface between two different structures having different energy or electron concentrations. Examples are two different crystal structures in contact at a surface. This includes contact between two different phases, including contact between a gas and a solid or contact between a liquid and a solid. This condition violates requirement No. 3 and perhaps Nos. 4 and 5 unless assumptions are applied.
(4) Absence of material, such as cracks, gaps, or voids within structures [123,127–129]. Carbon nanotubes or stress cracks in solids would be plausible examples. The dimensions and shape of such a structure would determine its behavior. This condition violates no requirement as explained below.

Involvement of particles having nanosized dimensions has been proposed but this is not considered to be a unique environment in this discussion. Such nanoparticles, at least at the size being used for LENR, differ from ordinary material only because they have a high surface area, which would create a large interface and place them in category (3). If the size is really small (submicron), they no longer act like ordinary material and would fall in category (2). Because of rapid sintering, nanoparticles do not remain in a material for long once the temperature in increased much above 150°C.

The condition No. 4 holds the greatest promise as the NAE. Most metals form cracks of various sizes when they react with hydrogen as stress is generated by increase in lattice size and is then relieved. The number of cracks has a limit determined by the treatment and material, thereby creating a natural limit to the amount of NAE. A crack or void has the potential to act as the site for a resonance process without being limited by the nature of a chemical lattice. Therefore, cracks having suitable shape and dimensions are proposed as the location of LENR. These would be rarely produced, have limited concentration, and could be formed in all materials. At the present time, success in producing LENR relies on accidental and random formation of these structures, which would account for why replication is a challenge.

8 mg/day of copper. This would result in 15 g of copper after 6 months while producing 10 kW, which would represent a significant and impossible fraction of nickel powder being transmuted during the proposed lifetime of the e-Cat.

Having identified a plausible NAE, what mechanism causes the nuclear reaction? For a search to be successful, it must follow a series of perhaps ambiguous clues in the correct logical order. The first clue in this search involves tritium and how it can form. Because it apparently forms in the same region of the material as does helium and no detectable radiation typical of hot fusion is produced, tritium and helium can be assumed to result from the same general mechanism and NAE. Absence of neutrons rules out direct D + D fusion, as would result from the hot fusion process. What other reaction might be the source? Tritium seems to be produced when both H and D [130] are present, but simple fusion would give He^3, as first proposed in 1990 by Schwinger [131]. This reaction can be ruled out because the amount of detected He^3 is only consistent with that expected to result from decay of tritium, which means tritium is formed before He^3. Tritium could form if an electron is absorbed into the fusion reaction and is later ejected by normal beta decay. Let us see if this process has a plausible general application.

If electron absorption is universal regardless of the isotopes involved, then the reactions listed in Table 1 can be predicted. In every case, except for tritium and deuterium, ejection of the electron from the product nucleus could be too rapid to detect as a half-life. In addition, like tritium, the energy of this beta could be too low to allow easy detection. In fact, were it not for the slow rate of tritium decay, this proposed addition of an electron could not be observed and might be ignored because it violates expected behavior. By accepting this clue, a general pattern for the fusion reaction can be suggested. In addition, a mechanism can be proposed that would not only add this electron by a plausible process during the fusion reaction, but explain how the resulting energy is dissipated. But first, the conflict with expected behavior needs to be addressed.

Table 1. Predicted nuclear reactions involving isotopes of hydrogen.

$d + d + e = H^4 = He^4 + e$	$Q = <23.8$ MeV
$d + p + e = T = He^3 + e$ (18.6 keV)	$Q = <4.9$ MeV (t = tritium = H^3)
$p + p + e = d$	$Q = 1.4$ MeV
$d + t + e = H^5 = He^4 + n + e$	$Q = <18.1$ MeV
$p + t + e = H^4 = He^4 + e$	$Q = <20.4$ MeV
Role of the neutrino is ignored when calculating Q	

Conflict with conventional understanding involves the role of the neutrino. Addition of an electron to a nucleus causes ejection of an electron-neutrino. Ejection of an electron as beta decay requires ejection of an antineutrino, which carries much of the energy that never appears as heat. If this interpretation were correct, the reactions listed in Table 1 would not produce the calculated energy and probably would not occur at all. However, unlike "normal" nuclear reactions, the LENR process proposed here takes place gradually, with most of the energy being released from the fusion process before the electron is absorbed by the final nucleus, thereby releasing a neutrino. Consequently, the amount of energy available to the neutrino might be very small. Nevertheless, the LENR process provides a test of how neutrinos are generated and emitted. In other words, LENR might provide a test of the Standard Model, similar to the studies being done at Caltech using a different nuclear reaction[1]. In addition, decay of H^4 is expected to produce tritium and a neutron [132], not He^4, if conventional beliefs are correct. The question is, "Does the proposed H^4 made by LENR decay as expected or does it decay by beta decay?"

Before going to the next clue, let us see if the proposed process helps explain any observed behavior, assuming the reactions occur as summarized in Table 1. First, the presence of a few neutrons when tritium is produced now makes sense. As tritium accumulates, t + d + e fusion can occur, resulting in the very small but variable flux of neutrons with a n/T ratio less than 10^{-6}. Support for this reaction is given by Mosier-Boss et al. [133] using CR-39 detectors in

[1]See: http://media.caltech.edu/press_releases/13520

which neutrons having the energy expected from d + t fusion were found in small numbers. Unfortunately, the tritium content was not measured. Second, the expected energy from each reaction (Q) can be used to explain other behavior[m]. Note that energy from the p + p + e fusion reaction is much smaller than from the d + d + e reaction. Consequently, the former reaction would require many more NAE sites to achieve the same amount of detected power compared to when deuterium is used, thereby energy from the d + d + e reaction easier to detect. Consequently, failure to detect heat when hydrogen is used as a null test means only that too little NAE was present to make detectable energy from the weak p + p + e reaction. In fact, the claims for extra power made by Fleischmann and Pons during their null tests using H_2O can be understood to mean enough NAE was present on a few occasions to actually produce detectable heat. Consequently, light water would apparently act as a poison simply by reducing the amount of power compared to when D_2O is used, not by stopping LENR altogether. Third, the weak beta emission could produce the occasionally reported low-level Bremsstrahlung from cells containing D_2O [134].

What kind of mechanism and NAE would be consistent with observed behavior? The hot fusion process, as well as muon fusion, rely the nuclei getting close enough to engage the strong force. The resulting sudden release of energy naturally causes emission of energetic particles, which are not produced by LENR. Therefore, a different mechanism must be operating. To avoid detectable emission, the energy released by the nuclear reaction could involve many emitted atoms, with each carrying a small fraction of the energy. This idea, which has been suggested by other authors, requires a large collection of atoms ($>$10,000), all of which have the ability to take their required fraction of the total during a very fast process. Consequently, this method does not seem plausible, as previously concluded.

This paper proposes a resonance takes place in a string of hydrogen nuclei with each separated by an electron. As this resonance takes place, coherent photons (X-rays) are emitted, similar to what takes place in a laser. In this case, the energy does not come from outside sources, but from gradual conversion of the hydrogen nuclei into another element, with the intervening electron being absorbed into the final nucleus. As a result, mass is converted to energy as the two nuclei get closer together. Obviously, the relationship between the nuclei and the intervening electron is not conventional. This unconventional relationship is forced on the system by the walls of the crack in which the process occurs. A future paper by Brian Scanlan will explore this process in detail.

Other models might also describe the process. Sinha and Meulenberg [135] proposed a structure, called a Lochon, that might describe the unique relationship between the electron and the hydrogen nucleus. Kim and Ward [136] propose a resonance process between deuterons in a BEC when it forms on the surface of a nanoparticle of PdD, a process that might also function in a crack or nanotube. Chubb [137] uses the metaphor of particle to wave conversion, with the deuteron waves gradually converting to a helium wave as energy is lost from the wave structure. Clearly, the process is opened to several interpretations at this stage.

What evidence can be offered to suggest cracks are actually present? First, can cracks form in the materials being used? PdD is well known to form cracks [138,139]. Titanium, another successful metal, cracks readily when it reacts with hydrogen. When this metal is used as the cathode during electrolysis of D_2O, extra energy and transmutation are reported [140–144]. In addition, neutrons [145–147] are emitted when it is temperature cycled in D_2, further indicating active crack formation, but not necessarily producing LENR. Nickel does not form cracks easily when exposed to hydrogen, but thermal or pressure cycling in hydrogen [102,103] is expected to produce some cracks in the surface. The oxides that produce LENR by electromigration [148–150] all have the Perovskite crystal structure. This structure

[m]The effect of neutrino formation when an electron is added or ejected is ignored. Nevertheless, this would reduce the amount of measured energy by some unknown amount because energy added to the neutrino would not be converted to measured heat. The behavior of tritium decay can be used to estimate the fraction carried by the neutrino when the neutron decomposes. The energy expected is 529 keV, based on mass change, while the beta is measured to have 18.6 keV. This means only 3.5% of the expected energy can be recovered from the final decay process because the remainder is carried away by the neutrino. However, most of the detected energy results from initial formation of the final nucleus, not from its subsequent decay. As a result, the values listed in Table 1 are, in most cases, upper limits.

is susceptible to distortions as a result of small changes in component atom concentrations that could cause local cracks. The slight flow of hydrogen caused by applied voltage would move hydrogen atoms to these locations and help accelerate the LENR process. Layers of palladium applied to various materials, as used by Patterson [151] and later by Miley [92,152], are observed to crack when reacted with hydrogen. Layers containing possible cracks have also been applied to wires by Celani et al. [153]. In this case, a current flow through the wire is found to enhance the process, perhaps by making deuterons more readily available to cracks. Sonofusion [154] would be expected to cause cracks at the site of bubble collapse on a target metal. In addition, to cracks formed as a result of stress, all materials are known to contain imperfections unless efforts are made to remove them. While a large number of active cracks would produce obvious power, the small number in ordinary material might result in detectable amounts of unexpected LENR if enough deuterium ions were available and careful measurements were made. Nanotubes are expected to be more difficult to make, but might be present and occasionally active.

Other behaviors consistent with cracks being the NAE are observed on occasion, adding support to the idea. For example, placement of X-ray sensitive film near an active electrolytic cell has shown X-radiation having a very narrow beam width [155,156]. Gas discharge has also produced similarly tightly focused X-rays that act like a laser [157,158]. Such behavior requires emission only in favored directions, which requires a beam defining structure. As an example from conventional experience, small structures similar to cracks have been observed to produce laser emission [159]. Failure to detect radiation could result when most X-radiation is completely absorbed, or because most beams are pointed away from the detectors. A diffuse source could be produced when many cracks were pointed in random directions. Consequently, laser-like radiation would be rare and only observed when detectors are in the right place or the sources are all pointed in the same direction, which apparently has occasionally happened.

The study by Iwamura et al. [160] provides an opportunity to test the role of cracks in explaining transmutation. As explained previously, these workers deposited CaO + Pd layers on palladium, which was over-coated by 40 nm of palladium, after which various elements were applied to the surface. When deuterium diffused through this sandwich, the deposited nuclei were transmuted by addition of deuterons. Amazingly, only the deposited nuclei experienced transmutation, not the much larger concentration of palladium also present on the surface. In addition, the CaO layer was found to be essential for the process to work. This behavior can be explained if stress-cracks formed in the thin palladium layer between the CaO and the surface where the target element was deposited. The deposited material filled the mouths of the cracks, thereby sealing them and creating a cavity in which deuterons could accumulate and resonate. This resonance process is proposed to release energy and cause deuterons to enter those nuclei located at the end of the cavity, i.e. the deposited target. Only nuclei present at this exact location can be transmuted according to this model. Patterson [151] provided further support when he produced many cracks in layers of Pd and Ni applied to plastic beads. Many transmuted elements were found in these layers by Miley [152,161]. Obviously, the thickness of the crack would be important because at some width, the normal hydrogen molecule is known to form, which is not able to fuse. The difficulty in causing LENR is proposed be related to formation of a closed crack of exactly the right dimension, after which enough D or H ions might be present to fuel a fusion reaction. Naturally, these requirements would be very sensitive to conditions and treatment, thereby accounting for the difficulty in replicating the transmutation results.

The claim for nuclear reactions being possible in bacteria and other single-cell organisms is a challenge for any explanation [162]. Obviously, the chemical conditions are greatly different from these within inorganic crystals and the mechanisms applied to such crystal structures would not be expected to apply to a living cell. On the other hand, existence of voids created by complex protein molecules can be imagined to form in which the proposed resonance might take place provided hydrogen ions are available to the void. While this assumption has no evidence as yet, the suggestion can be tested.

No single observation provides a smoking gun. Nevertheless, a total analysis of all observations and patterns leads to one plausible conclusion – cracks or nanotubes of a particular size and shape are the only NAE that does not conflict with the known behavior of materials, allows a plausible mechanism to operate, and leads to testable predictions, many

of which are consistent with behavior already observed. The puzzle still lacks a clear description of the mechanism operating within the crack. Once a mechanism is found to apply, later mathematical analysis can be used to further support the model and generate other predictions.

2.5. Testable predictions

The model suggests the following testable predictions as a guide to future studies.

(1) X-ray radiation is produced at a wavelength determined partly by the mass of the nuclei in the crack and it is emitted in opposite directions among the axis of the crack. The process is proposed to have laser-like behavior. Some of this radiation would appear to result from Bremsstrahlung.
(2) Rate of tritium production is sensitive to the H/D ratio in the NAE.
(3) Rate of neutron production is sensitive to the D/T ratio in the NAE.
(4) Energy production from normal hydrogen results first in production of deuterium and then tritium, followed by a small but increasing neutron flux.
(5) Diffusion of H or D through a material containing suitable NAE causes detectable LENR because H or D would become available at the NAE. Increased applied pressure of D_2 or H_2 has the same effect.
(6) Laser light increases the rate of LENR as energy is added to the resonance process. Increased temperature would have the same effect, but would not be as localized and would have a counter effect by lowering the available concentration of H or D.
(7) Transmutation is occasionally experienced by nuclei located at the ends of active cracks or nanotubes.
(8) The rate of LENR using deuterium gradually decreases as active NAE sites became choked by immobile helium. This lifetime limiting process is less important when H is used because D and T can move out of the NAE or enter into subsequent fusion reactions without choking the site. Nevertheless, the growing concentration of D will increase the activation energy for resonance, thereby reducing its rate, and producing trapped helium.
(9) No difference exists between the conditions required to cause fusion involving pure D or pure H. However, many more NAE sites are required to obtain a detectable amount of energy when H is used compared to D.
(10) A mixture of D and H in a NAE makes LENR more difficult to start (increased activation energy) because the mixture, consisting of different masses, disrupts resonance. Apparent "poisoning" of the reaction is the result. Adding laser energy at the location of the crack can reduce the effect of this disruption.
(11) A material producing significant power will self-heat and reach a stable temperature determined by how effectively hydrogen can reach the NAE at that temperature. The greater the amount of NAE, the higher this temperature limit will be.
(12) Any metal or alloy able to catalyze decomposition of the hydrogen molecule into ions will support LENR once the NAE forms.

3. Summary

A model is described that summarizes all reported observations by using only a few assumptions. The LENR process is proposed not to take place in a lattice structure. Instead, a novel and rare structure must form in which the process occurs. This structure is common to all LENR reactions regardless of the reactants, nuclear products, or method used. The general structure is called the Nuclear Active Environment (NAE) and is proposed to take the form of a crack or gap that forms by stress relief in conventional structures.

Fusion reactions involving isotopes of hydrogen are proposed to occur in the same NAE. Deuterium is made by p + p + e fusion, tritium by d + p + e fusion, and helium by d + d + e fusion followed by beta emission, with the relative rates being determined by the relative concentrations of the hydrogen isotopes in the NAE. Occasional neutrons can

result from the t + d + e fusion reaction when tritium is produced. The number of active sites in a material, the temperature and/or applied energy, and the concentration of hydrogen isotopes determine the rate of each reaction. Energy is released to the surrounding environment by a resonance process between the hydrogen nuclei and the intervening electrons as many X-ray photons are emitted in a laser-like beam in opposite directions along the axis of the crack. Conditions required to create this resonance are forced on the hydrogen–electron combination by the structure in which they are located. This structure, consisting of cracks or nanotubes, must have a critically small size in the submicron range.

This model is based on observed behavior, not on the physical or mathematical models favored by modern science. While some of the proposed consequences of this behavior might conflict with what conventional science believes is possible, the paper identifies the important evidence required to resolve this conflict. If correct, the model places limits on the kind of mechanism causing the nuclear process, explains why energetic particles are not detected, and shows why such reactions are not "impossible" as conventional science believes. Analysis using mathematical tools will follow if the suggested model is found to be correct.

The model proposed in this paper has an immediate application to understanding the claims made by Rossi. He claims significant energy is made in a device he calls an E-Cat by conversion of nickel to copper. As discussed in the paper, this source of energy is not plausible. On the other hand, the other potential source based on the proposed p + e + p = d reaction would appear not to qualify as a source of useful energy because of energy loss to neutrino emission, as the Standard Model requires. Consequently, a careful study of the energy-producing reaction involving light hydrogen is important not only to understanding LENR but also to understanding the Standard Model.

Acknowledgements

I'm grateful to Brian Scanlan for helping make this analysis possible by his financial support and his insights into how electrons can be related to hydrogen nuclei under specials circumstances. This analysis would not have been possible without his contribution. Abd ul-Rahman Lomax and Bill Collis helped make the description easier to understand by repeated challenges to the idea. Carol Storms and Ruby Carat found the usual typos and made many suggestions that helped focus the arguments in the proper direction.

References

[1] Fleischmann, M., S. Pons, and M. Hawkins, Electrochemically induced nuclear fusion of deuterium. *J. Electroanal. Chem.* **261** (1989).: p. 301-308 and errata in Vol. 263, 187-188.
[2] Storms, E.K., *The science of low energy nuclear reaction*. 2007, Singapore: World Scientific. 312.
[3] Rothwell, J., *Cold fusion and the future*. 2007: www.LENR.org.
[4] Sheldon, E., *An overview of almost 20 years' research on cold fusion.* Contemp. Phys., 2009. **49**(5): p. 375.
[5] Krivit, S.B. and N. Winocur, *The rebirth of cold fusion; Real science, real hope, real energy*. 2004, Los Angeles, CA: Pacific Oaks Press.
[6] Simon, B., *Undead science: Science studies and the afterlife of cold fusion*. 2002, New Brunswick, NJ: Rutgers University Press. 252.
[7] Close, F., *Too hot to handle. The race for cold fusion*. second ed. 1992, New York: Penguin, paperback.
[8] Mallove, E., *Fire from ice*. 1991, NY: John Wiley.
[9] Peat, F.D., *Cold fusion: The making of a scientific controversy.* 1989, Chicago: Contempory Books. 188.
[10] Camp, W.J., *Helium detrapping and release from metal tritides.* J. Vac. Sci. Technol., 1977. **14**: p. 514-517.
[11] Storms, E.K. and C. Talcott-Storms, *The effect of hydriding on the physical structure of palladium and on the release of contained tritium.* Fusion Technol., 1991. **20**: p. 246.
[12] Dash, J., G. Noble, and D. Diman. *Changes in surface topography and microcomposition of a palladium cathode caused by electrolysis in acidified light water*. in *International Symposium on Cold Fusion and Advanced Energy Sources*. 1994. Belarusian State University, Minsk, Belarus: Fusion Information Center, Salt Lake City. p. 172.

[13] Miguet, S. and J. Dash, *Microanalysis of palladium after electrolysis in heavy water.* J. New Energy, 1996. **1**(1): p. 23.
[14] Storms, E., *Ways to initiate a nuclear reaction in solid environments.* Infinite Energy, 2002. **8**(45): p. 45.
[15] McKubre, M.C.H., et al. *New hydrogen energy research at SRI*. in *Sixth International Conference on Cold Fusion, Progress in New Hydrogen Energy*. 1996. Lake Toya, Hokkaido, Japan: New Energy and Industrial Technology Development Organization, Tokyo Institute of Technology, Tokyo, Japan. p. 75.
[16] Storms, E.K., *The nature of the energy-active state in Pd-D.* Infinite Energy, 1995(#5 and #6): p. 77.
[17] Tanzella, F.L., et al. *Parameters affecting the loading of hydrogen isotopes into palladium cathodes*. in *Sixth International Conference on Cold Fusion, Progress in New Hydrogen Energy*. 1996. Lake Toya, Hokkaido, Japan: New Energy and Industrial Technology Development Organization, Tokyo Institute of Technology, Tokyo, Japan. p. 171.
[18] Storms, E.K. *Relationship between open-circuit-voltage and heat production in a Pons-Fleischmann cell*. in *The Seventh International Conference on Cold Fusion*. 1998. Vancouver, Canada: ENECO, Inc., Salt Lake City, UT. p. 356.
[19] McKubre, M.C.H., et al. *Concerning reproducibility of excess power production*. in *5th International Conference on Cold Fusion*. 1995. Monte-Carlo, Monaco: IMRA Europe, Sophia Antipolis Cedex, France. p. 17.
[20] Sarto, F., et al. *The Role of Cathode's Surface Properties in the Electrochemical Deuterium Loading of Pd Foils*. in *15th International Conference on Condensed Matter Nuclear Science*. 2009. Rome, Italy: ENEA, Italy. p. 148-153.
[21] Castagna, E., et al. *Metallurgical characterization of Pd electrodes employed in calorimetric experiments under electrochemical deuterium loading*. in *14th International Conference on Condensed Matter Nuclear Science*. 2008. Washington, DC: www.LENR.org. p. 444-450.
[22] Dardik, I., et al. *Report on electrolysis experiments at energetics technologies*. in *International Conference on Condensed Matter Nuclear Science , ICCF-13*. 2007. Sochi, Russia: Tsiolkovsky Moscow Technical University. p. 325.
[23] Zhang, W.-S. and J. Dash. *Excess heat reproducibility and evidence of anomalous elements after electrolysis in* $Pd/D_2O + H_2SO_4$ *electrolystic cells*. in *International Conference on Condensed Matter Nuclear Science , ICCF-13*. 2007. Sochi, Russia: Tsiolkovsky Moscow Technical University. p. 202.
[24] Chicea, D. *Comment on carbon production In deuterium-metal systems*. in *Tenth International Conference on Cold Fusion*. 2003. Cambridge, MA: World Scientific Publishing Co. p. 475.
[25] Chen, S.-K., et al., *The microstructure of electrolytically deuterium-loaded palladium rods.* Fusion Technol., 1996. **29**: p. 302.
[26] . Szpak, S., P.A. Mosier-Boss, and F. Gordon. *Precursors and the fusion reactions in polarized Pd/D-*D_2O *systems: Effect of an external electric field*. in *11th International Conference on Cold Fusion*. 2004. Marseilles, France: World Scientific Co. p. 359.
[27] Szpak, S., P.A. Mosier-Boss, and J.J. Smith, *Deuterium uptake during Pd-D codeposition.* J. Electroanal. Chem., 1994. **379**: p. 121.
[28] Mosier-Boss, P.A., et al., *Review of TwentyYears of LENR Research Using Pd/D Co-deposition.* J. Cond. Matter Nucl. Sci., 2011. **4**: p. 173-187.
[29] Sankaranarayanan, T.K., et al. *Evidence for tritium generation in self-heated nickel wires subjected to hydrogen gas absorption/desorption cycles.* in *5th International Conference on Cold Fusion*. 1995. Monte-Carlo, Monaco: IMRA Europe, Sophia Antipolis Cedex, France. p. 173.
[30] . Rout, R.K., et al., *Copious low energy emissions from palladium loaded with hydrogen or deuterium.* Indian J. Technol., 1991. **29**: p. 571.
[31] . Savvatimova, I.B. and A.B. Karabut, *Radioactivity of palladium cathodes after irradiation in a glow discharge.* Poverkhnost (Surface), 1996(1): p. 76 (in Russian).
[32] Arata, Y. and Y.C. Zhang, *Helium (*^4He*,* ^3He*) within deuterated Pd-black.* Proc. Jpn. Acad., Ser. B, 1997. **73**: p. 1.
[33] Case, L.C. *Catalytic fusion of deuterium into helium-4*. in *The Seventh International Conference on Cold Fusion*. 1998. Vancouver, Canada: ENECO, Inc., Salt Lake City, UT. p. 48.
[34] Kidwell, D.A., et al. *Yes, Virginia there is Heat, but It is Likely of Chemical Origin*. in *15th International Conference on Condensed Matter Nuclear Science*. 2009. Rome, Italy: ENEA, Italy. p. 100-109.
[35] Arata, Y. and Y.C. Zhang. *Picnonuclear fusion generated in "lattice-reactor" of metallic deuterium lattice within metal atom-clusters. II Nuclear fusion reacted inside a metal by intense sonoimplantion effect*. in *The 9th International Conference on Cold Fusion, Condensed Matter Nuclear Science*. 2002. Tsinghua Univ., Beijing, China: Tsinghua Univ. Press. p. 5.

[36] Arata, Y., Y.C. Zhang, and X.F. Wang. *Production of Helium and Energy in the "Solid Fusion"*. in *15th International Conference on Condensed Matter Nuclear Science*. 2009. Rome, Italy: ENEA, Italy. p. 72-81.

[37] Yamaura, S., et al. *Hydrogen absorption of nanoscale Pd particles embedded in ZrO2 matrix prepared from Zr–Pd amorphous alloys*. in *14th International Conference on Condensed Matter Nuclear Science*. 2008. Washington, DC: www.LENR.org. p.

[38] Takahashi, A., et al. *Anomalous Heat Generation in Charging of Pd Powders with High Density Hydrogen Isotopes, (II) Discussions on Experimental Results and Underlying Physics*. in *15th International Conference on Condensed Matter Nuclear Science*. 2009. Rome, Italy: ENEA, Italy. p. 297-302.

[39] Iwamura, Y., et al., *Detection of anomalous elements, X-ray and excess heat induced by continuous diffusion of deuterium through multi-layer cathode (Pd/CaO/Pd).* Infinite Energy, 1998. **4**(20): p. 56.

[40] Liu, B., et al. *"Excess heat" in a gas-loaded D/Pd system with pumping inside palladium tube*. in *8th International Workshop on Anomalies in Hydrogen/Deuterium Loaded Metals*. 2007. Catania, Sicily, Italy: The International Society for Condensed Matter Science. p. 204.

[41] . Biberian, J.-P. and N. Armanet. *Excess heat production during diffusion of deuterium through palladium tubes*. in *8th International Workshop on Anomalies in Hydrogen/Deuterium Loaded Metals*. 2007. Catania, Sicily, Italy: The International Society for Condensed Matter Science. p. 19.

[42] Preparata, G. *Fractofusion revisted*. in *Anomalous Nuclear Effects in Deuterium/Solid Systems, "AIP Conference Proceedings 228"*. 1990. Brigham Young Univ., Provo, UT: American Institute of Physics, New York. p. 840.

[43] Lipson, A.G., V.A. Kuznetsov, and B.V. Deryagin, *Scenarios of 'cold nuclear fusion' by concentration of elastic energy in crystals.* Dokl. Akad. Nauk SSSR Fiz. Khim., 1991. **318**(3): p. 636 (in Russian).

[44] Yasui, K., *Fractofusion mechanism.* Fusion Technol., 1992. **22**: p. 400.

[45] Jabon, V.D.D., G.V. Fedorovich, and N.V. Samsonenko, *Catalitically induced d-d fusion in ferroelectrics.* Braz. J. Phys., 1997. **27**: p. 515.

[46] Czerski, K., et al., *The 2H(d,p)3H reaction in metallic media at very low energies.* Europhys. Lett., 2004. **68**: p. 363.

[47] Kasagi, J. *Screening potential for nuclear reactions in condensed matter*. in *14th International Conference on Condensed Matter Nuclear Science*. 2008. Washington, DC: www.LENR.org. p. 318-325.

[48] Kitamura, A., et al. *D(d,p)t reaction rate enhancement in a mixed layer of Au and Pd*. in *Tenth International Conference on Cold Fusion*. 2003. Cambridge, MA: World Scientific Publishing Co. p. 623.

[49] Hagelstein, P.I. and I. Chaudhary. *Arguments for dideuterium near monovacancies in PdD*. in *15th International Conference on Condensed Matter Nuclear Science*. 2009. Rome, Italy: ENEA, Italy. p. 282-287.

[50] Flanagan, T.B., et al., *The effect of lattice defects on hydrogen solubility in palladium, I. Experimentally observed solubility enhancements and thermodynamics of absorption.* J. Less-Common Met., 1979. **49**: p. 13.

[51] McKubre, M.C. and F. Tanzella. *Using resistivity to measure H/Pd and D/Pd loading: Method and significance*. in *Condensed Matter Nuclear Science, ICCF-12*. 2005. Yokohama, Japan: World Scientific. p. 392.

[52] Norlander, P., et al., *Multiple deuterium occupancy of vacancies in Pd and related metals.* Phys. Rev. B, 1989. **40**: p. 1990.

[53] Kozima, H. and S. Watanabe. *Nuclear processes in trapped neutron catalyzed model for cold fusion*. in *5th International Conference on Cold Fusion*. 1995. Monte-Carlo, Monaco: IMRA Europe, Sophia Antipolis Cedex, France. p. 347.

[54] . Fisher, J.C., *Polyneutrons as agents for cold nuclear reactions.* Fusion Technol., 1992. **22**: p. 511.

[55] Oriani, R.A., *Anomalous heavy atomic masses produced by electrolysis.* Fusion Technol., 1998. **34**: p. 76.

[56] Widom, A. and L. Larsen, *Ultra low momentum neutron catalyzed nuclear reactions on metallic hydride surfaces.* Eur. Phys. J., 2006. **C46**: p. 107.

[57] Daddi, L., *Proton-electron reactions as precursors of anomalous nuclear events.* Fusion Technol., 2001. **39**: p. 249.

[58] Chatterjee, L., *Electrolysis in thin-film nickel coatings: mimicking supernova physics?* Fusion Technol., 1998. **34**: p. 147.

[59] Das, D. and M.K.S. Ray, *Fusion in condensed matter - a likely scenario.* Fusion Technol., 1993. **24**: p. 115.

[60] Moon, D., *Review of a cold fusion theory: Mechanisms of a disobedient science.* Infinite Energy, 1999. **5**(28): p. 33.

[61] Phipps Jr., T.E., *Neutron formation by electron penetration of the nucleus.* Infinite Energy, 1999. **5**(26): p. 58.

[62] Conte, E. and M. Pieralice, *An experiment indicates the nuclear fusion of a proton and electron into a neutron.* Infinite Energy, 1999. **4**(23): p. 67.

[63] Mills, R.L. and W.R. Good, *Fractional quantum energy levels of hydrogen.* Fusion Technol., 1995. **28**: p. 1697.

[64] Dufour, J., et al. *The Hydrex concept-effect on heavy nuclei*. in *8th International Conference on Cold Fusion*. 2000. Lerici

(La Spezia), Italy: Italian Physical Society, Bologna, Italy. p. 431.
[65] Dufour, J.J., J.H. Foos, and X.J.C. Dufour, *Formation and properties of hydrex and deutex.* Infinite Energy, 1998. **4**(20): p. 53.
[66] Liu, F.S., *The phonon mechanism of the cold fusion.* Mod. Phys. Lett. B, 1996. **10**: p. 1129.
[67] Hagelstein, P.L. *Phonon-exchange models: Some new results*. in *11th International Conference on Cold Fusion*. 2004. Marseilles, France: World Scientific Co. p. 743.
[68] Violante, V. and A. De Ninno. *Quantum mechanical description of a lattice ion trap*. in *Sixth International Conference on Cold Fusion, Progress in New Hydrogen Energy*. 1996. Lake Toya, Hokkaido, Japan: New Energy and Industrial Technology Development Organization, Tokyo Institute of Technology, Tokyo, Japan. p. 221.
[69] Kalman, P. and T. Keszthelyi, *Attractive d–d interaction via phonon exchange in deuterated Pd.* Nucl. Instr. and Meth. in Phys. Res. B, 2005. **240**: p. 781-789.
[70] Kucherov, Y. *Slow nuclear excitation model*. in *Sixth International Conference on Cold Fusion, Progress in New Hydrogen Energy*. 1996. Lake Toya, Hokkaido, Japan: New Energy and Industrial Technology Development Organization, Tokyo Institute of Technology, Tokyo, Japan. p. 502.
[71] Chubb, S.R. and T.A. Chubb. *Theoretical framework for anomalous heat and* ^{4}*He in transition metal systems*. in *8th International Conference on Cold Fusion*. 2000. Lerici (La Spezia), Italy: Italian Physical Society, Bologna, Italy. p. 385.
[72] Bazhutov, Y.N. *Erzion discovery in cosmic rays and its possible great role in nature in framework of Erzion model of cold nuclear transmutation*. in *8th International Conference on Cold Fusion*. 2000. Lerici (La Spezia), Italy: Italian Physical Society, Bologna, Italy. p. 269.
[73] Matsumoto, T., *'Nattoh' model for cold fusion.* Fusion Technol., 1989. **16**: p. 532.
[74] McKibben, J.L., *Evidence for three primordially created particles and can one of them catalyze cold fusion?* 1989.
[75] Rafelski, J., et al., *Nuclear reactions catalyzed by a massive negatively charged particle. How Cold Fusion Can Be Catalyzed.* Fusion Technol., 1990. **18**: p. 136.
[76] Shoulders, K., *Projectiles from the dark side.* Infinite Energy, 2006. **12**(70): p. 39-40.
[77] Preparata, G. *Theoretical ideas on cold fusion*. in *The First Annual Conference on Cold Fusion*. 1990. University of Utah Research Park, Salt Lake City, Utah: National Cold Fusion Institute. p. 91.
[78] Fleischmann, M., S. Pons, and G. Preparata, *Possible theories of cold fusion.* Nuovo Cimento, 1994. **107A**(1): p. 143-156.
[79] Capek, V., *Tunnelling efficiency and the problem of cold fusion.* Czech. J. Phys., 1989. **B39**: p. 793.
[80] Turner, L., *Thoughts unbottled by cold fusion.* Phys. Today, 1989. **Sept.**: p. 140.
[81] Parmenter, R.H., *A possible scenario for the onset of cold fusion in deuterated metals.* Infinite Energy, 1998. **4**(21): p. 41.
[82] Fulvio, F. *Theoretical comparison between semi-classic and quantum tunneling effect any application coherence theory on the tumor*. in *Condensed Matter Nuclear Science, ICCF-12*. 2005. Yokohama, Japan: World Scientific. p. 494.
[83] Feng, S., *Enhancement of cold fusion rate by electron polarization in palladium deuterium solid.* Solid State Commun., 1989. **72**: p. 205.
[84] Li, X.Z., C.X. Li, and H.F. Huang, *Maximum value of the resonant tunneling current through the Coulomb barrier.* Fusion Technol., 1999. **36**: p. 324.
[85] Hora, H., G. Miley, and J. Kelly, *Low-energy nuclear reactions of protons in host metals at picometer distance.* Trans. Am. Nucl. Soc., 2000. **83**: p. 357.
[86] Hora, H., et al., *Proton-metal reactions in thin films with Boltzmann distribution similar to nuclear astrophysics.* Fusion Technol., 1999. **36**: p. 331.
[87] Hora, H., et al. *Shrinking of hydrogen atoms in host metals by dielectric effects and Inglis-Teller depression of ionization potentials.* in *The 9th International Conference on Cold Fusion, Condensed Matter Nuclear Science*. 2002. Tsinghua Univ., Beijing, China: Tsinghua Univ. Press. p. 135.
[88] Miley, G.H., H. Hora, and Y. X. *Condensed Matter "Cluster" Reactions in LENRs.* in *ICCF-14 International Conference on Condensed Matter Nuclear Science.* 2008. Washington, DC.: http://lenr-canr.org/acrobat/MileyGHcondensedm.pdf. p. 451-457.
[89] Miley, G.H. *Emerging physics for a breakthrough thin-film electrolytic power unit*. in *Space Technol. Applic. Int. Forum*. 1999. p. 1227.
[90] Miley, G., et al. *Cluster reactions in low energy nuclear reactions (LENR)*. in *8th International Workshop on Anomalies in*

Hydrogen/Deuterium Loaded Metals. 2007. Catania, Sicily, Italy: The International Society for Condensed Matter Science. p. 235-251.

[91] Badiei, S., P.U. Andersson, and L. Holmlid, *Laser-induced variable pulse-power TOF-MS and neutral time-of-flight studies of ultradense deuterium.* Phys. Scr., 2010. **81**(4).

[92] Miley, G., X. Yang, and H. Hora, *Ultra-High Density Deuteron-cluster Electrode for Low-energy Nuclear Reactions.* J. Cond. Matter Nucl. Sci., 2011. **4**: p. 256-268.

[93] Takahashi, A., et al., *Emission of 2.45 MeV and higher energy neutrons from D_2O-Pd cell under biased-pulse electrolysis.* J. Nucl. Sci. Technol., 1990. **27**: p. 663.

[94] Isobe, Y., et al. *Search for coherent deuteron fusion by beam and electrolysis experiments*. in *8th International Conference on Cold Fusion*. 2000. Lerici (La Spezia), Italy: Italian Physical Society, Bologna, Italy. p. 17-22.

[95] Iwamura, Y., et al., *Observation of Low Energy Nuclear Transmutation Reactions Induced by Deuterium Permeation through Multilayer Pd and CaO thin Film.* J. Cond. Matter Nucl. Sci., 2011. **4**: p. 132-144.

[96] Takahashi, A. *Tetrahedral and octahedral resonance fusion under transient condensation of deuterons at lattice focal points*. in *ICCF9, Ninth International Conference on Cold Fusion*. 2002. Beijing, China: Tsinghua University: Tsinghua Univ., China. p. 343.

[97] Hagelstein, P.I., *On the connection between Kαg-rays and energetic alpha particles in Fleischmann–Pons experiments.* J. Cond. Matter Nucl. Sci., 2010. **3**: p. 50-58.

[98] Kim, H.Y. *Bose-Einstein Condensation Nuclear Fusion: Theoretical Predictions and Experimental Tests*. in *15th International Conference on Condensed Matter Nuclear Science*. 2009. Rome, Italy: ENEA, Italy. p. 288-296.

[99] Kim, Y.E., *Bose–Einstein Condensate Theory of Deuteron Fusion in Metal.* J. Cond. Matter Nucl. Sci., 2011. **4**: p. 188-201.

[100] Cornell, E.A. and C.E. Wieman, *The Bose-Einstein Condensate.* Sci. Am., 1998. **278**(3): p. 40-45.

[101] Zwierlein, M.W., et al., *Observation of Bose–Einstein Condensation of Molecules.* Phys. Rev. Lett. 2003. **91**: p. 250401.

[102] Piantelli, F., *Energy generation and generator by means of anharmonic stimulated fusion*. 2010: World Property Organization.

[103] Campari, E.G., et al. *Nuclear reactions in Ni-H systems*. in *6th International Workship on Anomalies in Hydrogen/Deuterium Loaded Metals*. 2005. Siena, Italy. p.

[104] Campari, E.G., et al. *Surface analysis of hydrogen-loaded nickel alloys*. in *11th International Conference on Cold Fusion*. 2004. Marseilles, France: World Scientific Co. p. 414.

[105] Campari, E.G., et al. *Photon and particle emission, heat production and surface transformation in Ni-H system*. in *11th International Conference on Cold Fusion*. 2004. Marseilles, France: World Scientific Co. p. 405.

[106] Focardi, S., et al. *Evidence of electromagnetic radiation from Ni-H systems*. in *11th International Conference on Cold Fusion*. 2004. Marseilles, France: World Scientific Co. p. 70.

[107] Campari, E.G., et al. *Overview of H-Ni systems: Old experiments and new setup*. in *5th Asti Workshop on Anomalies in Hydrogen / Deuterium loaded Metals*. 2004. Asti, Italy. p.

[108] Campari, E.G., et al. *Ni-H systems*. in *8th International Conference on Cold Fusion*. 2000. Lerici (La Spezia), Italy: Italian Physical Society, Bologna, Italy. p. 69.

[109] Battaglia, A., et al., *Neutron emission in Ni-H systems.* Nuovo Cimento, 1999. **112 A**: p. 921.

[110] Focardi, S., et al., *Large excess heat production in Ni-H systems.* Nuovo Cimento, 1998. **111A**(11): p. 1233.

[111] Focardi, S., et al. *On the Ni-H system*. in *Asti Workshop on Anomalies in Hydrogen/Deuterium Loaded Metals*. 1997. Villa Riccardi, Italy: Societa Italiana Di Fisica. p. 35.

[112] Focardi, S., R. Habel, and F. Piantelli, *Anomalous heat production in Ni-H systems.* Nuovo Cimento, 1994. **107A**: p. 163.

[113] Rossi, A., *Journal of Nuclear Physics*. 2012, http://www.journal-of-nuclear-physics.com/.

[114] Rossi, A., *Method and apparatus for carrying out nickel and hydrogen exothermal reaction*. 2011: USA.

[115] Badiei, S., P.U. Andersson, and L. Holmlid, *Fusion reactions in high-density hydrogen: A fast route to small-scale fusion?* International J. Hydrogen Energy, 2009. **34**(1): p. 487.

[116] Badiei, S., P.U. Andersson, and L. Holmlid, *Production of ultradense deuterium: A compact future fusion fuel.* Appl. Phys. Lett., 2010. **96**: p. 124103.

[117] Arachi, Y., et al., *Structural analysis of nano-sized-Pd/ZrO2 composite after H(D) absorption.* Solid State Ionics, 2006. **177**: p. 1861.

[118] Takahashi, A., et al. *Deuterium Gas Charging Experiments with Pd Powders for Excess Heat Evolution (II). Discussions on*

Experimental Results and Underlying Physics. in *The 9th Meeting of Japan CF-Research Society.* 2009. Shizuoka, Japan: www.lenr.org. p.

[119] Celani, F., et al. *High temperature deuterium absorption in palladium nano-particles*. in *International Conference on Condensed Matter Nuclear Science , ICCF-13*. 2007. Sochi, Russia: Tsiolkovsky Moscow Technical University. p. 181.

[120] Mansoori, G.A., P.L. Barros de Araujo, and E. Silvano de Araujo, *Diamondoid molecules*. 2012: World Scientific, Impertial College Press.

[121] Dmitriyeva, O., et al. *Deuterium & hydrogen loading into nano-Pd on zeoliteand alumina matrices at low pressures*. in *ICCF-16*. 2011. Chenni, India. p.

[122] Frisone, F., *Theoretical model of the probability of fusion between deuterons within deformed crystalline lattices with microcracks at room temperature.* Fusion Sci. & Technol., 2001. **40**: p. 139.

[123] McIntyre, R. *Proposal for an experiment designed to seek evidence for cold fusion*. in *Tenth International Conference on Cold Fusion*. 2003. Cambridge, MA: World Scientific Publishing Co. p. 611.

[124] Liaw, B.Y., et al., *Elevated-temperature excess heat production in a Pd + D system.* J. Electroanal. Chem., 1991. **319**: p. 161.

[125] Harris, P.J.F., *Carbon nanotube science*. 2009, New York: Cambridege Univ. Press. 301.

[126] Mills, R., *The grand unified theory of classical quantum mechanics*. 2006, Ephrata, PA: Cadmus Professional Communications. 1450.

[127] Frisone, F. *Probability of deuteron plasmon fusion at room temperature within microcracks of crystalline lattices with deuterium loading*. in *8th International Conference on Cold Fusion*. 2000. Lerici (La Spezia), Italy: Italian Physical Society, Bologna, Italy. p. 443.

[128] Bockris, J.O.M. and P.K. Subramanyan, *The equivalent pressure of molecular hydrogen in cavities within metals in terms of the overpotential developed during the evolution of hydrogen.* Electrochim. Acta, 1971. **16**: p. 2169.

[129] Vigier, J.P. *New hydrogen energies in specially structured dense media: capillary chemistry and capillary fusion*. in *Third International Conference on Cold Fusion, "Frontiers of Cold Fusion"*. 1992. Nagoya Japan: Universal Academy Press, Inc., Tokyo, Japan. p. 325.

[130] Chien, C.-C., et al., *On an electrode producing massive quantities of tritium and helium.* J. Electroanal. Chem., 1992. **338**: p. 189-212.

[131] Schwinger, J., *Cold fusion: a hypothesis.* Z. Naturforsch., 1990. **45A**: p. 756.

[132] Fiarman, S. and W.E. Meyerhof, *Energy levels of light nuclei A=4.* Nucl. Phys. A, 1973. **206**(1): p. 1-64.

[133] Mosier-Boss, P.A., et al., *Comparison of Pd/D co-deposition and DT neutron generated triple tracks observed in CR-39 detectors.* Eur. Phys. J. Appl. Phys., 2010. **51**(2): p. 20901-20911.

[134] Swartz, M.R. and G. Verner, *Bremsstrahlung in hot and cold fusion.* J. New Energy 1999. **3**(4): p. 90-101.

[135] Sinha, K.P. and A. Meulenberg, *Lochon-mediated low-energy nuclear reactions.* J. Cond. Matter Nucl. Sci., 2012. **6** p. 55-63.

[136] Kim, Y.E. and T.E. Ward, *Bose–Einstein condensation nuclear fusion: Role of monopole transition.* J. Cond. Matter Nucl. Sci., 2012. **6**: p. 101-107.

[137] Chubb, S.R., *Resonant electromagnetic interaction in low-energy nuclear reactions*, in *ACS Symposium Series 998, Low-Energy Nuclear Reactions Sourcebook*, J. Marwan and S.B. Krivit, Editors. 2008, American Chemical Society: Washington, DC. p. 99.

[138] Storms, E.K., *A study of those properties of palladium that influence excess energy production by the Pons-Fleischmann effect.* Infinite Energy, 1996. **2**(8): p. 50.

[139] Bockris, J.O.M., D. Hodko, and Z. Minevski, *Fugacity of hydrogen isotopes in metals: degradation, cracking and cold fusion.* Proc. Electrochem. Soc, 1992. **1992**: p. 92.

[140] Kopecek, R. and J. Dash, *Excess heat and unexpected elements from electrolysis of heavy water with titanium cathodes.* J. New Energy, 1996. **1**(3): p. 46.

[141] Klopfenstein, M.F. and J. Dash. *Thermal imaging during electrolysis of heavy water with a Ti cathode*. in *The Seventh International Conference on Cold Fusion*. 1998. Vancouver, Canada: Eneco Inc. p. 98.

[142] Dash, J. and Q. Wang. *Anomalous Silver on the Cathode Surface after Aqueous Electrolysis*. in *15th International Conference on Condensed Matter Nuclear Science*. 2009. Rome, Italy: ENEA, Italy. p. 38-41.

[143] Bashkirov, Y.A., et al., *Observation of neutron emission from electrolysis of heavy water.* Pis'ma Zh. Tekh. Fiz., 1990. **16**(19):

p. 51 (in Russian).
[144] Lipson, A.G., et al., *Reproducible neutron emission by the combined effect of cavitation and electrolysis at the surface of a titanium cathode in electrolyte based on heavy water.* Pis'ma Zh. Teor. Fiz., 1991. **17**(21): p. 33 (in Russian).
[145] Izumida, T., et al., *A search for neutron emission from cold nuclear fusion in a titanium-deuterium system.* Fusion Technol., 1990. **18**: p. 641.
[146] Jianyu, H., et al. *Experimental study on anomalous neutron production in deuterium/solid system*. in *Anomalous Nuclear Effects in Deuterium/Solid Systems, "AIP Conference Proceedings 228"*. 1990. Brigham Young Univ., Provo, UT: American Institute of Physics, New York. p. 193.
[147] Bruschi, L., et al., *Search for neutron emission from a deuterium-titanium system".* Europhys. Lett., 1989. **10**(4): p. 303.
[148] Mizuno, T., et al. *Anomalous heat evolution from $SrCeO_3$-type proton conductors during absorption/desorption in alternate electric field*. in *Fourth International Conference on Cold Fusion*. 1993. Lahaina, Maui: Electric Power Research Institute 3412 Hillview Ave., Palo Alto, CA 94304. p. 14.
[149] Biberian, J.-P., et al. *Electrolysis of $LaAlO_3$ single crystals and ceramics in a deuteriated atmosphere*. in *The Seventh International Conference on Cold Fusion*. 1998. Vancouver, Canada: ENECO, Inc., Salt Lake City, UT. p. 27.
[150] Oriani, R.A., *An investigation of anomalous thermal power generation from a proton-conducting oxide.* Fusion Technol., 1996. **30**: p. 281.
[151] Patterson, J.A., *Method for electrolysis of water to form metal hydride*. 1994: US Patent # 5,318,675.
[152] Miley, G.H., et al. *Quantitative observations of transmutation products occuring in thin-film coated microspheres during electrolysis*. in *Sixth International Conference on Cold Fusion, Progress in New Hydrogen Energy*. 1996. Lake Toya, Hokkaido, Japan: New Energy and Industrial Technology Development Organization, Tokyo Institute of Technology, Tokyo, Japan. p. 629.
[153] Celani, F., et al., *Development of a high temperature hybrid CMNS reactor.* J. Cond. Matter Nucl. Sci., 2012. **6**: p. 24-33.
[154] Stringham, R., *When bubble cavitation becomes sonofusion.* J. Cond. Matter Nucl. Sci., 2012. **6**: p. 1-12.
[155] Szpak, S., P.A. Mosier-Boss, and J.J. Smith, *On the behavior of Pd deposited in the presence of evolving deuterium.* J. Electroanal. Chem., 1991. **302**: p. 255.
[156] Gozzi, D., et al., *Erratum to "X-ray, heat excess and ^4He in the D/Pd system".* J. Electroanal. Chem., 1998. **452**: p. 251-271.
[157] Karabut, A. *Research into powerful solid X-ray laser (wave length is 0.8-1.2 nm) with excitation of high current glow discharge ions*. in *11th International Conf. on Emerging Nuclear Energy Syst.* 2002. Albuquerque, NM. p. 374.
[158] Karabut, A.B., E.A. Karabut, and P.I. Hagelstein, *Spectral and Temporal Characteristics of X-ray Emission from Metal Electrodes in a High-current Glow Discharge.* J. Cond. Matter Nucl. Sci., 2012. **6**: p. 217-240.
[159] Khajavikhan, M. and Y. Fainman, *Thresholdless Nanoscale Coaxial Lasers.* Nature, 2012.
[160] Iwamura, Y., M. Sakano, and T. Itoh, *Elemental analysis of Pd complexes: effects of D_2 gas permeation.* Jpn. J. Appl. Phys. A, 2002. **41**(7): p. 4642-4650.
[161] Miley, G.H. and J.A. Patterson, *Nuclear transmutations in thin-film nickel coatings undergoing electrolysis.* J. New Energy, 1996. **1**(3): p. 5.
[162] Biberian, J.-P., *Biological Transmutations: Historical Perspective.* J. Cond. Matter Nucl. Sci., 2012. **7**: p. 11-15.

J. Condensed Matter Nucl. Sci. 9 (2012) 108–127

Research Article

Are Ni + H Nuclear Reactions Possible? *

Akito Takahashi †

Technova Inc., 1-1-1 Uchisaiwaicho, Chiyoda-ku, Tokyo 100-0011, Japan
also at
Osaka University, Yamadaoka, Suita, Osaka Prefecture 565-0871, Japan

Abstract

Various cases of possible orthodox nuclear reaction processes, including newly proposed 4H/TSC fusion by simultaneous weak and strong interactions, 4H/TSC + Ni induced fission products, Ni + p reactions and reaction by deuteron impurity, are comparatively discussed for feasibility.

(1) Ni + p nuclear reaction is impossibly difficult to make the Coulomb-field penetration of proton through so many inner electron shells (K, L, M), usually non-active in chemical reactions, of Ni-atom. Also the proton capture with Ni-nucleus, if any with kW level power, should emit lethal prompt gamma-rays which have never been observed. So, this type of nuclear reactions is unlikely.
(2) Deuteron impurity (1/6700 in H_2 gas usually) may induce (3H+D)/TSC fusion to be considered. Conditioning of 3-dimensional symmetry of QM-wave function for TSC is however of problem to condense into microscopic neutral entity small enough for causing any strong interactions.
(3) The newly proposed 4H/TSC WS (weak–strong interaction simultaneously) fusion is a plausible scenario to have clean products (^{3}He and proton, or deuterons) with significantly enhanced reaction rates in Ni nano-particles, for rare-conditioned (as discussed) visible heat generation with very weak secondary neutrons (10^{-13} order of ^{3}He primary product) and gamma-rays (10^{-11} order of ^{3}He primary product). Degrees of the generation rate of 4H/TSC ($t = 0$) transient clusters in Ni–H nano-particles and the life-time elongation of 4H/TSC-minimum state are speculatively studied. The auto-recovery capability of Ni nano-catalyst is considered as the key.
(4) The 4H/TSC + Ni-isotope capture-and-fission process, previously proposed in our paper of *JCMNS* **1** (2007) 86–96 is another plausible scenario, to result in generation of clean fission products in $A < 60$ mass region. More enhanced 4p + Ni to fission rates than the previous prediction is expected due to the possible elongation of 4H/TSC-minimum-state life time without complete nuclear break-up of the symmetric cluster under dynamic condensation.

Keywords: Clean fission, 4H/TSC WS fusion, Ni + H CF experiments, Ni + 4H/TSC capture, Nuclear reaction models

*Paper for 10th International Workshop on Anomalies in Hydrogen Loaded Metals, Siena , April 10–14, 2012

†E-mail: akito@sutv.zaq.ne.jp

© 2012 ISCMNS. All rights reserved. ISSN 2227-3123

1. Introduction

In the 23 years history of CMNS/CF (condensed matter nuclear science/cold fusion) experiments, unusual claims of finding excess heat and transmutation by nickel metal plus H_2 loading or H_2O electrolysis have been made by several researchers/research-groups. Most remarkable claims have been done by Siena-Bologna Group [1–3] and Miley group [4,5], about anomalously large excess heat and nuclear-like (transmutation-like) products. Recently, a demonstration of 10 kW 'commercial grade device' in January 2011 at Bologna (by Rossi et al.) has attracted great interest in the Internet debate/discussions. The scientific content as technical data of the Rossi demonstration has not been disclosed, and the CMNS community has to continue controversial opinion-exchanges about whether his claim is real or not. On the other side, the latest progress in CMNS experiments based on D(H)-gas loading method is significant with the usage of nano-fabricated metal samples such as nano-size (2–10 nm) Pd mono and Pd–Ni binary powders dispersed in ZrO_2 ceramic flakes by Arata group [6,7], Kobe University–Technova group [8–14], and NRL group. Reproducibility of these gas-loading experiments is almost 100% to show the existence of anomalously high (cf. known chemistry) heat generation with zero nominal input power and significant isotopic effect (D-loading gave larger heat). Takahashi et al. wrote [10,14] that about 70% of anomalous heat would be generated by 'new chemical absorption' on/into Pd-based nano-particles as 'mesoscopic catalyst' which would have deep GMPW (global mesoscopic potential well) and however about 30% could be nuclear heat by such fusion reaction as the 4D/TSC simultaneous 4-body fusion to produce helium-4 and clean heat (without neutrons as primary product). The 4D/TSC formation process was speculated to enhance on surface sub-nano-holes (SNH) of nano-particle and inside lattice points. The TSC theory was extended to predict that the 4H/TSC condensation on/in nano-nickel particle would have possibility of the 4H/TSC weak/strong fusion [15] and the clean fission by 4H/TSC capture into Ni isotope-nucleus [16]. These basic studies on observed phenomena in D(H)-gas loading experiments and explaining theoretical models as the TSC theory [17] will open a window to explore theoretical possibilities of 'feasible' nuclear reactions in Ni + H systems. The present paper discusses such possibilities.

As supporting data of anomalously large heat generation in nano-Ni/H-gas loading experiments, which is difficult to explain by known chemistry, Kobe–Technova group [18,19] and Celani group at INFN Frascati Italy (private communication) have been or will be reporting in latest/forthcoming meetings.

2. The Proton Capture Process into Ni Nucleus is Unlikely

As people would imagine first the Ni + p capture reaction to transmuted products, we briefly discuss that the process is unlikely to be feasible due to two main reasons: namely, the Coulomb barrier penetration of proton through 28 shell-electron layers of Ni for low energy seems impossible, and the lethal prompt gamma-rays by proton capture (if it were happened) to Ni-nucleus have never been observed.

Before discussing any nuclear reactions, we need to recall Fig. 1 that we have to treat substantially and quantitatively (as much as possible) the three steps of nuclear reactions, namely, (1) the initial state interactions where weak and/or strong nuclear interaction take place under the condensed matter conditioning (environment) of dynamic electro-magnetic (or Coulombic) interactions of protons (deuterons), metal nuclei (Ni in our case) and electrons, (2) the intermediate (sometimes virtual) compound nucleus state with excited energy (by mass defect energy, delta-$m - c^2$), spin-parity and isospin states, and (3) the final state interactions to going out with break-up particles (hadrons, photons, neutrino, and fission fragments). The mass defect by nuclear (strong/weak) interaction induces the shift of substructures (quarks–gluons bonding) of nuclei from the initial state particles to the intermediate compound nucleus, to be reflected in Ex, J-pi and isospin, and makes the returning path to the initial state impossible due to the drastic increment of system entropy (randomness). The situation of one-way process is same for the procedure from the intermediate compound state to the final state interactions. Such condition of nuclear reaction implies that the electro-magnetic interaction in the initial state interaction becomes 'adiabatic' to the nuclear strong/weak interactions.

Thus we can use satisfactorily the Born–Oppenheimer separation of wave functions between the QM (quantum

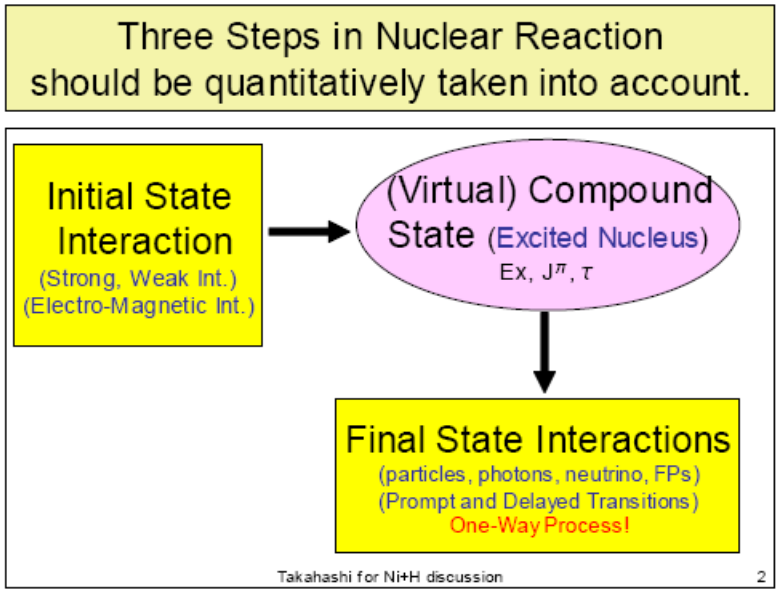

Figure 1. Three steps of nuclear interaction should be substantially treated in theory.

mechanical) wave function of EM (electromagnetic) field and the QM wave function in the strong/weak force field.

The first main problem is of extreme difficulty for low energy (<5 keV) proton to penetrate through the thick multiple QM electron-cloud layers (K shells to M shells) and to get close enough to make meaningful level strong interaction rate. We here have to remind that one watt power level heat needs huge reaction rate on the order of 10^{12} f/s by Ni + p capture reaction. One molar Ni metal (58.693 g) may absorb 1.8×10^{24} hydrogen-atoms at O-sites and T-sites, if at most. This means microscopic Ni–p fusion rate should exceed the level of 10^{-12} f/p–Ni-pair. Assuming that Ni–p strong interaction rate by 100% proton penetration through the barrier is written as $\nu S_{pNi}(0)/E$ per a p–Ni pair and $S_{pNi}(0)$ = ca. 10^5 kevb. At $E = 1$ keV (ν = ca. 2×10^7 cm/s), we get 2×10^{-12} f/s/(p–Ni-pair/cm^3) (here 1 b = 10^{-24} cm^2). There the required barrier factor is ca. 0.5 for a p–Ni pair. Assuming E = 0.025 eV (energy at room temperature), we get 1×10^{-9} f/s/ (p–Ni-pair/cm^3) for 100% penetration. So, the barrier factor 10^{-3} is required to the thermal proton injection into Ni-atom with many electron shells, to meet the 1 W/mol–Ni/cm^3 level heat level. Remembering the barrier factor for d–d pair of D_2 molecule [20] (d–e–e–d system) is 10^{-85}, for nucleus with only 1S electron, barrier penetration of 10^{-3} for a p–Ni pair is too difficult to realize. The feature of difficulty can be understood by Fig. 2, as we can imagine. Three steps of nuclear interaction should be substantially treated in theory

The inner most electron shell (K-shell) of nickel has about 1pm radius of 1S orbit with 8.3 keV binding energy. There are other 26 electron shells before the K shell. Bare incident proton nucleus should be trapped with the outer most (valence) electron shell to form NiH chemical compound, and should never approach to inside nucleus. Considering total ionization energy of Ni atom, the kinetic energy of incident proton should exceed 1 MeV to approach the Ni bare nucleus for making meaningful strong interaction with Ni nucleus having about 10 MeV barrier height at the contact surface of strong interactions between Ni and p. Therefore, low kinetic energy (KE) proton in Ni–H system, even at dynamic/transient condition, cannot overcome this very strong barrier of many electron shells.

It is obvious that only very small (as small as 0.1 pm in diameter or less) charge-neutral entity may penetrate

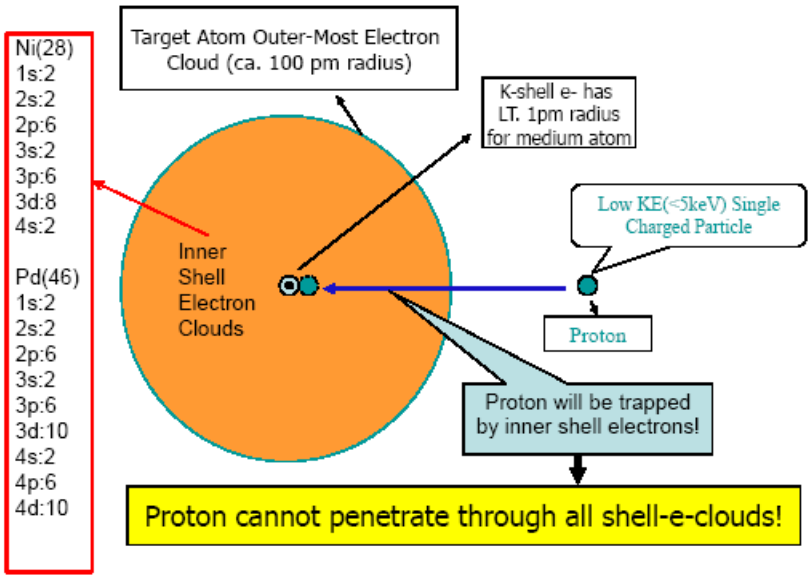

Figure 2. Procedure of Coulomb barrier penetration of proton through many layers of shell-electron clouds of Ni.

through the barrier of Fig. 2. Widom-Larsen has proposed [21] the generation of ultra-low momentum neutron (which can penetrate the Ni electron-shell-barrier) by 'heavy (more than 1MeV KE equivalent)' electron in metal-H lattice plasmon/surface-polariton state, although the assumed condition looks almost impossible and free neutrons leakage must be lethally observed, if at all [15]. Another idea might be a generation of sub-pm size mini-atom of H (p + e system), wishfully proposed by some models as hydrino [22] and lochon [23]. However, these mini-atom theories are based on non-QM (classical) mechanics, and therefore their existence in nature is very questionable or never observed. Y. Kim (private communication) is proposing Ni + 2p capture process, to avoid emission of prompt gamma-ray by p-capture, without showing how 2p pair can penetrate through the huge barrier (Fig. 2). The p–e–p three body and p–e–e–p 4-body dynamics have no sub-pm state QM solutions as discussed in [20].

The second main problem of Ni–p reaction is the fact that claimed large heat power has never associating lethal level prompt gamma-rays. The capture, intermediate compound state and decays (final state interactions) are shown in Fig. 3 for ^{58}Ni + p nuclear reaction.

The intermediate compound state ^{59}Cu*(Ex = 3.417MeV) emits, by no other means, EM-transition prompt gamma-rays (in a few fs) in its cascade excitation decay levels of ^{59}Cu. The initial explanation by Rossi–Focardi in their blog (*J. Nuclear Physics*) is wrong because of ignoring the prompt gamma-rays by proton capture before making transition to the ground state of ^{59}Cu which is radio-active positron-emitter. For all p-capture process for Ni isotopes (^{60}Ni, ^{61}Ni, ^{62}Ni, and ^{64}Ni), we should observe prompt gamma-rays in similar ways. Of course, in the following decay paths via positron emission, most energy is carried off by neutrino and 0.511 MeV annihilation gamma-rays should be observed, so that it is difficult to expect heat deposit in reaction chamber of Ni powder/bulk sample.

In summary, it seems extremely difficult (we can say impossibly) to propose any quantitatively proven mechanisms to overcome the Ni–p Coulomb barrier penetration obstacle of multi-layered shell electron clouds.

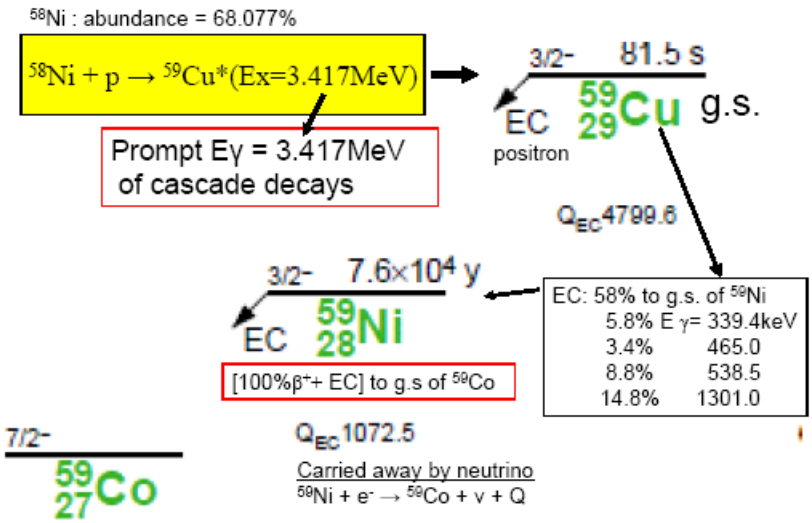

Figure 3. Ni + p reaction, its intermediate compound and decay scheme chart.

3. 4H/TSC Formation in Ni-contained Condensed Matter

We have proposed that the tetrahedral symmetric condensate (TSC) of four protons and four electrons, with orthogonal coupling of their 3-dimemsional QM wave-functions, will provide a dynamic chance of condensing into very small (as small as several fm in diameter) charge neutral entity for very short time interval (but enough long for self nuclear interaction and capture reaction to host metal nucleus). From the heat and D(H)-loading evolution of experiments with Pd–Ni binary nano-particle (PNZ2B) [13,14], we proposed a model for the catalytic effect of binary metal nano-particle as Pd_1Ni_7 in 2 nm size, as shown in Fig. 4. Pd ad-atoms may be replaced with other metal atoms as Cu, as we discuss later for the nano-catalyst effect (mesoscopic catalyst).

The formation of 4H/TSC is supposed to occur at SNHs (sub-nano-holes) on surface as explained with the inserted sentences in Fig. 4. One SNH with trapped D_2 image is shown in Fig. 5. First, a D_2 molecule will be trapped with active dangling electron bonds at SNH and be arranged at points illustrated. Before dissociation of D_2 and D-hopping into deeper site, next D_2 molecule may be trapped at the same SNH and arranged orthogonally, due to charge balance with the first trapped D_2, to form 4D(H)/TSC ($t = 0$) state. The second plausible mechanisms of 4D(H)/TSC formation is speculated [14] as the non-linear oscillation of D(H)-oscillators at O-sites of inner Bloch potential of GMPW (global mesoscopic potential well) of nano-catalyst to enhance TSC formation probability around T-sites of Ni inner local lattice. When ambient temperature of reaction chamber is elevated (300–500°C in experiments [18]), the TSC formation rate may be enhanced.

The image of GMPW is shown in Fig. 6, for the case of Ni-based nano-catalyst which experimentally [18] showed endothermic characteristics in lower temperature than 200°C (473 K) and exothermic characteristics in higher temperature than 250°C (523 K).

A simplified image of H(D) oscillator trapped in GMPW is shown in Fig. 7. The ambient temperature of reaction chamber is at the Outer Field Energy Level. Nano-catalyst with active dangling electron bonds works well to adsorb D_2 at room temperature (e.g., 300 K = 27°C) level ambient condition, but the weights of higher phonons ($n > 3$ phonons) oscillation in the phonon-frequency distribution are small at 300 K.

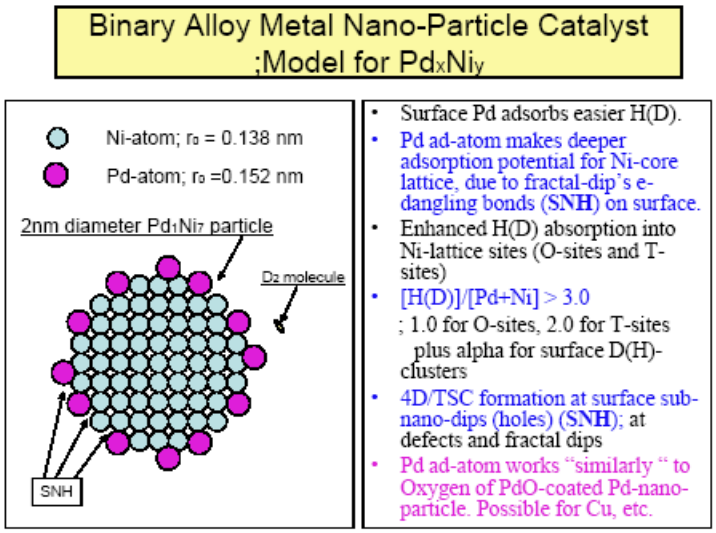

Figure 4. Working model of binary metal nano-particle as mesoscopic catalyst for D(H) gas[14].

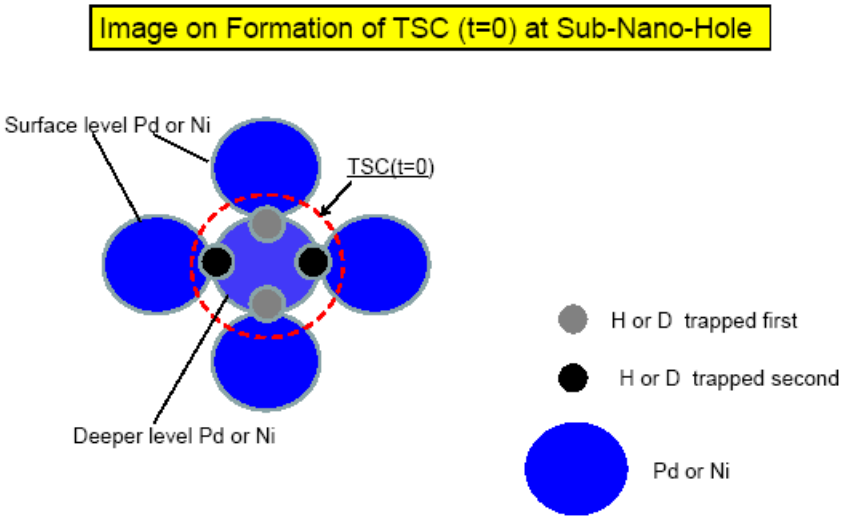

Figure 5. Image of 4H/TSC formation at a SNH (sub-nano hole) of Ni (Pd) nano-catalyst.

By elevating ambient temperature of reaction chamber, weights of higher phonon states are increased and the formation rate of TSC around inner T-sites is correspondingly enhanced by the non-linear QM oscillation in the coupled motion of long-pendulum oscillator of GMPW and short pendulum oscillators of inner O-sites of Bloch periodical (but local) potential. Image of such TSC enhancement process is illustrated in Fig. 8. However, proof quantitative QM

calculations by some simulation techniques are yet to be done.

Once a 4H(D)/TSC(t = 0) state forms, it makes very rapid condensation in about 1 fs to get to the 4H(D)/TSC-minimum state as calculated by the QM Langevin equation [20] as shown in Fig. 9. At 4H/TSC-minimum state, mean electron kinetic energy will exceed 600 keV within TSC trapping potential depth of –1 to –2 MeV and R_{pp} = 2.4 fm.

4. 4H/TSC Fusion by Simultaneous Weak and Strong Interactions in Ni–H System

We now show the first plausible model of clean heat generation by the self-nuclear interaction of four protons and condensed electrons in the dynamic condensation process of 4H/TSC. The theory of 4H/TSC fusion by the simultaneous weak/strong interaction is first reported in the latest work by the author [15].

The results of quantitative analyses of weak/strong interaction rates based on Fermi's golden rule are shown in simplified illustrations in Fig. 10 for 4H/TSC, and Fig. 11 for 4D/TSC for comparison purpose.

The detail of QM estimation procedure is given in [15]. In this paper, we discuss some ambiguous points in the first step dynamic condensation in Coulombic field, the weak interaction (electron capture to proton), the immediate strong interaction between just-produced neutron and three remained protons and the final state interaction (break up to ^{3}He + p).

In the case of 4D/TSC condensation/fusion reaction, 100% 4d fusion by strong interaction takes place in about 2×10^{-20} s time interval of the R_{dd} = ca. 20 fm (4D/TSC-minimum state) adiabatic time step with the 4D barrier factor of 1.98×10^{-3}. Thus 4D/TSC disappears for $R_{dd} < 20$ fm. Contrarily in the case of 4H/TSC condensation motion, there is no strong interaction fusion process among four protons. Therefore, the condensation motion of 4H/TSC continues further into very short R_{pp} distances. As proton behaves as a hard sphere with one positive electric charge in the EM (Coulombic) field of TSC, R_{pp}-minimum = 2× (proton radius: 1.2 fm) = 2.4 fm must be the end point of condensation, where the following weak interaction rate was estimated to be about 3×10^{-7} per 4H/TSC generation [15].

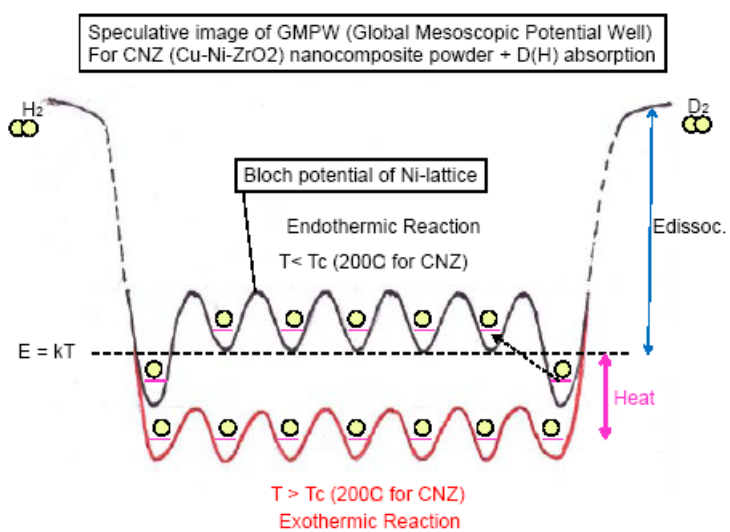

Figure 6. Image of global mesoscopic potential well (GMPW) of Ni nano-catalyst.

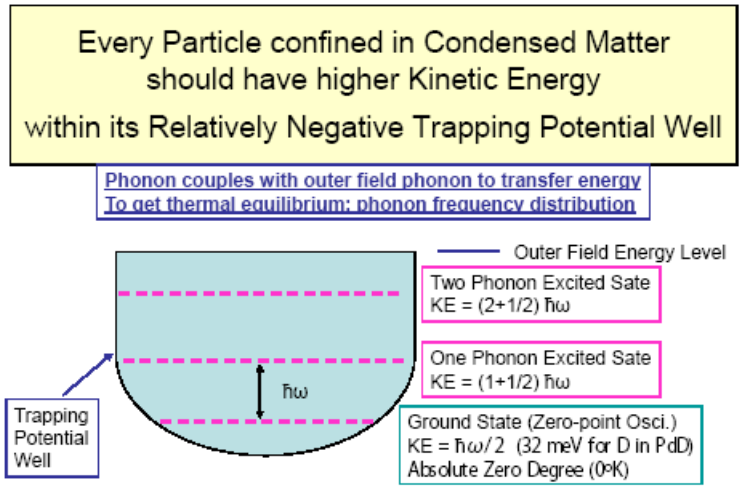

Figure 7. Image of phonon oscillator of trapped deuteron in GMPW.

$$\mathrm{p} + \mathrm{e}^- + E_{\mathrm{ke}} \rightarrow \mathrm{n} + \nu + (E_{\mathrm{ke}} - 272\,\mathrm{keV}). \tag{1}$$

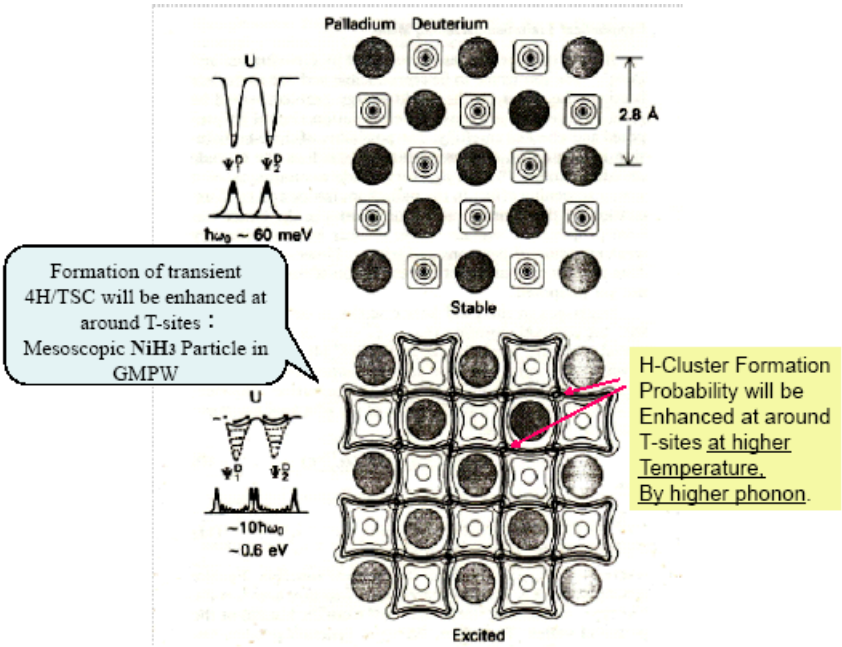

Figure 8. Image of the enhancement of TSC formation rate at elevated temperature of nano-catalyst.

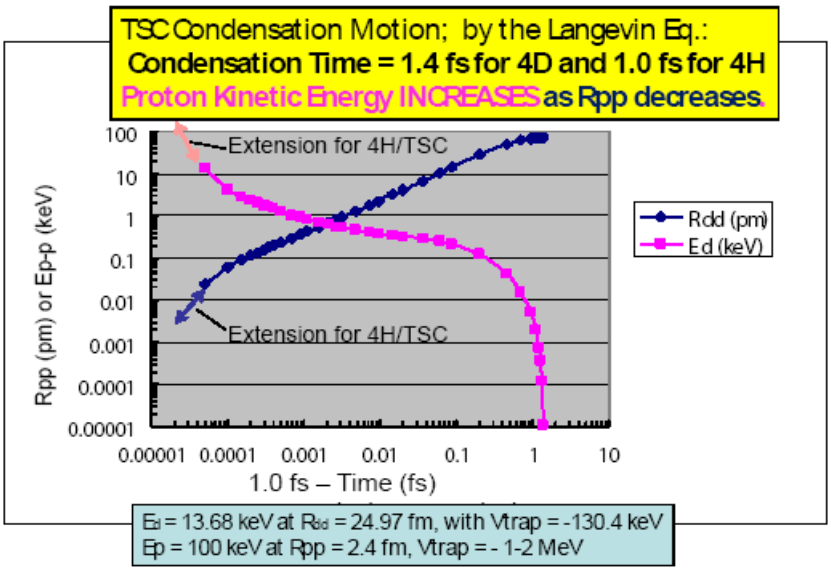

Figure 9. Rapid condensation of 4H/TSC, as shown with variation of p–p distance R_{pp} and relative kinetic energy of p–p pair of TSC.

We assumed the adiabatic time interval of 4H/TSC-minimum state is the same (namely 2×10^{-20} s) with that of the 4D/TSC-minimum adiabatic state, to calculate the weak interaction yield of 3×10^{-7}.

However, the adiabatic time interval of 4H/TSC-minimum can be very much longer than that, because the weak interaction rate is so small and the state does not disappear by the reason of weak interaction. How much is the actual life-time of 4H/TSC-minimum state is of important problem. We have not yet quantitatively estimated it. Considering that the electron kinetic energy (KE) of 4H/TSC-minimum (we supposed 0.6–1.2 MeV in the previous work [15]) is not stably kept because of dynamic state (non-ground state), we may imagine an oscillation state of R_{pp} values around 3 fm or so with ca. 0.6 fm amplitude. How much time may the oscillation last? We do not know at the moment. We need to study it further. By the way if we may assume the life time is on the order of a few fs (comparable to the condensation time), the following n + 3p simultaneous strong interaction (100% per n generation by the weak interaction [15]) fusion yield becomes a big value on the order of 10^{-2} (a few %);

$$\mathrm{n} + 3\mathrm{p} \rightarrow {}^{4}\mathrm{Li}^{*}(4.62\ \mathrm{MeV}) \rightarrow {}^{3}\mathrm{He} + \mathrm{p} + 7.72\ \mathrm{MeV}. \tag{2}$$

However, it is still 1/100 of the 4D fusion yield. The intermediate compound state ^{4}Li*(Ex = 4.62 MeV) may have another break-up channel as,

$${}^{4}\mathrm{Li}^{*}(\mathrm{Ex} = 4.62\ \mathrm{MeV}) \rightarrow \mathrm{d} + 2\mathrm{p} + 2.22\ \mathrm{MeV}. \tag{3}$$

We have presumed in [15] that Eq. (2) is predominant, but we do not know the branching ratio.

The high KE (5.79 MeV) proton by Eq. (2) should induce PIXE photons by ionization of the K-shell electron of Ni. The characteristic X-ray from Ni has K-alpha and beta peaks at around 8 keV, which must be a target of radiation measurement. The 5.79 MeV proton will slow down in sample powder and induce Ni(p,n) and Ni(p,γ) reactions.

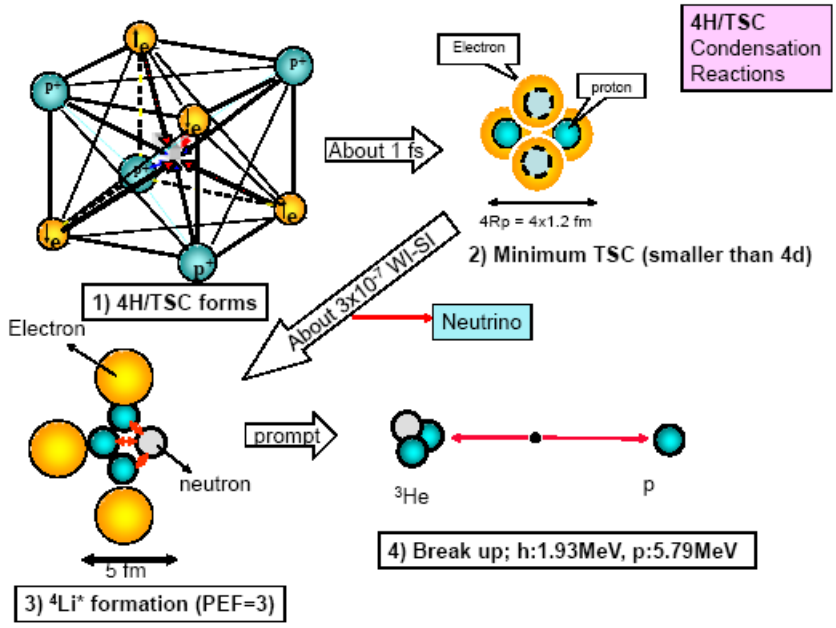

Figure 10. Illustration of 4H/TSC condensation motion and weak/strong fusion reaction [15].

Secondary neutron production by the Ni(p,n) is over threshold for higher mass isotopes (^{61}Ni, ^{62}Ni and ^{64}Ni) with yield of 10^{-13} n/p: this means 1MW 4H/TSC weak/strong fusion reactor will produce ca. 10^5 n/s that is very weak level as a level of weak checking neutron source. The yield of Ni (p,γ) will be two orders of magnitude greater than the neutron yield [15], but it is still very weak level to be well Pb-shielded for biological safety.

However, if the branch Eq. (3) were the major out-going channel, there were happening almost no emission of gamma-rays (nor neutrons) as secondary products, and weaker PIXE events by ca. 1 MeV proton may be searched in experiments.

Now we refer some typical experimental data of heat evolution by H(D)-gas loading with CNZ ($Cu_{0.08}Ni_{0.35}/Zr_{0.57}$) sample (Cu–Ni binary nano-particles dispersed into many ZrO_2 flakes), currently on-going at Kobe–Technova group [18,19]. Heat production is endothermic for $T < 200^{o}$C sample temperature, but exothermic for $T > 250^{o}$C and heat-enhancing trend for higher temperature. At 300°C, they have observed 1–1.5 W/g-Ni level average heat by H-gas-loading for a week of run continuously. The D-gas loading gave smaller level heat power (0.2–0.3 W/g-Ni) also continuously.

Total integrated heat data for one-week period were 380 eV/atom-Ni for H and 90 eV/atom-Ni for D, respectively. (They later found that the heat-power level of D-gas charging made catch-up with the level of H-gas charging in the later phase of several weeks of run-time.) These characteristic data of heat are anomalously large, compared with chemical reaction heat of several eV at most, and are very difficult to be explained by known chemical reactions. We need to consider if our nuclear reaction models discussing in this paper have feasibility rationally. Main issues are: (A) Why and how can H-system produce much higher heat than D-system, in the earlier weeks? (B) How can 1.0 W/g-Ni (or 60 W/mol-Ni) level nuclear heat be attained?

The quantitative results shown in [15] do not answer about questions A and B, clearly. In addition, some aspect

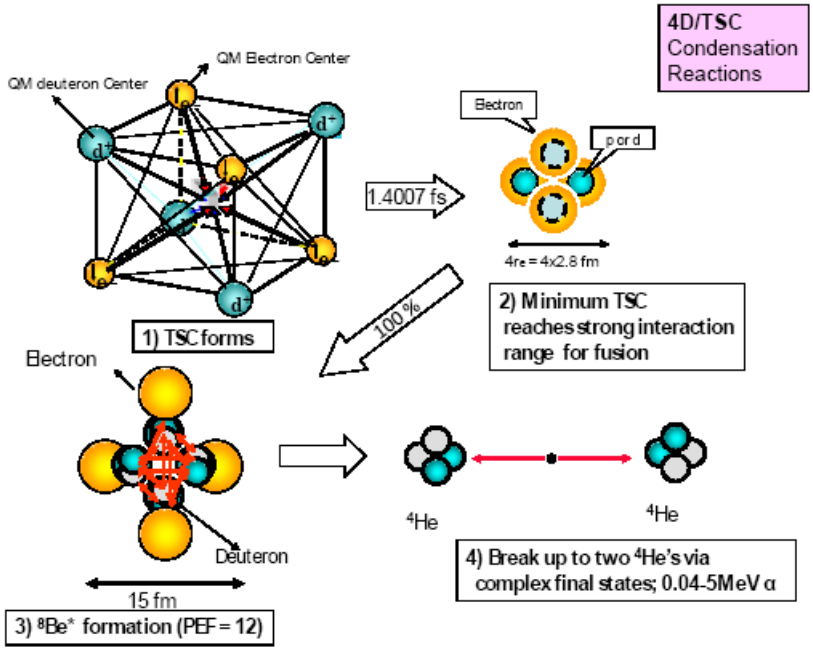

Figure 11. Illustration of 4D/TSC condensation motion and simultaneous 4d fusion [15].

on possible mechanisms to transit from the endothermic to exothermic heat evolution by elevating sample temperature should be discussed, concerning to Fig. 6. Namely, how GMPW shape has changed by changing sample temperature is of problem. The author is imagining the formation of auto-recovering nano-catalyst, similarly as Pd perovskite used for automobile exhaust gas cleaner (see Internet Googling), by cyclic damage/healing process under D(H)-gas charging at elevated temperature. If the CNZ binary Cu–Ni nano-particle (provided by Santoku Co.) were working in that way, it would be surprise. 4D fusion emits 47.6 MeV/f with alpha-particles and may damage harder CNZ sample than the case of 4H WS (weak/strong) fusion with 7.72 MeV, 75% energy of which are carried off by proton with several microns range of ionization/knock-on slowing down process in CNZ sample. Such damage mechanisms pertaining to the auto-recovery cycle of CNZ sample is of further interest to explore. For the t-phase (beginning phase of gas-pressure transition) of CNZ sample, D-gas loading gave larger heat release than H-gas, as is the case of Pd-based samples [8–14]. They have not yet done experiments with Pd-based samples at elevated temperatures. We shall wait for such results at higher temperature for Pd samples, to see the consistency with the case of Ni-based sample. We may speculate that the role of Cu ad-atoms on Ni nano-particle would be arranging SNHs in cyclic auto-recovery procedure.

One-watt heat-power by the 4H/TSC WS fusion events corresponds to the order of 10^{12} f/s. The observed power level of 60 W/mol-Ni corresponds to 10^{-22} W/atom-Ni. Our optimistic yield per TSC for the 4H/TSC WS fusion was on the order of 10^{-2}, so that the required 4H/TSC generation rate is $10^{12} \times 10^{-22}/10^{-2} = 10^{-8}$ TSC/s/atom-Ni: It is dissipative level events in dynamics of Ni–H condensed matter (or solid state physics/chemistry), and is too small fractional events to be visible in ordinary chemistry measures. Supposing the order of 10^4 displacements/WS-fusion of knocked-on Ni atoms from their 'lattice structure' in nano-catalyst, we obtain the damage-estimate of 100% displacements of all Ni atoms in $1/10^4/10^{-8} = 10^4$ s = 2.77 h.

This means that the proposed cyclic auto-recovery mechanism of CNZ nano-catalyst would be working with about 3 hours repetition period, which is not contradictory with the observed heat-power level fluctuations [18,19]. For the case of D-gas loading, observed heat-power level in average was about 20% of that for H-gas loading. One-watt power corresponds to 10^{11} 4D-fusions/s. The 4D fusion produces about 10-fold energy (47.6 MeV) of the 4H/TSC WS fusion, and damage rate will be on the order of 10^6 Ni-displacements/4D-fusion. In rough estimation, the proposed auto-recovery mechanism needs to work with about one hour repetition period that is 1/3 of the H-case: This condition might be the explanation of weaker heat-power of D-gas loading than that of H-gas loading, in the CNZ experiments [18,19]. F. Piantelli (Siena University, private communication), B. Ahern (in Boston, private communication) and F. Celani (INFN, Frascati, private communication) are reporting also weaker heat power data with D-gas loading, compared with significantly enhanced heat power data with H-gas loading. Any way, to provide nano-catalyst samples with the auto-recovery capability seems the key for long lasting (more than weeks can be expected) sustainable clean heat source with high heat power density.

One more discussion is for the possibility of D/H mixed TSC fusion [24]. As the natural H_2 gas contain 1/6700 portion of deuterium as impurity, strong interaction of (H+3D), (2H + 2D) and (3H + D) TSC fusion might take place with significant weight in considering Ni–H systems. Conventionally sold D-gas is 99.5% pure, and contains 0.5% H-gas also as impurity. However, our later study of TSC condensation by the QM Langevin equation [20] has suggested that asymmetric 3-dimensional configuration of centripetal force components for H/D mixed TSC will prohibit the continuous condensation as is seen in the cases of 4D/TSC and 4H/TSC. Therefore, we now consider the feasibility of H/D-mixed TSC fusion is very low.

5. Clean Fission of Ni + 4H/TSC Interaction

The author proposed TSC-induced fission process of host metal nuclei in CMNS experiments [16] to explain 'transmuted' elements observed in the Miley–Patterson experiments [4,5] using Ni-based electrodes in H_2O electrolysis. As we have discussed in the previous section, the life time of 4H/TSC-minimum may be much longer than the thought one in the previous work [16] and we may have more significant feasibility of heat generation and transmutation-products by Ni + 4H fission in currently on-going Ni–H gas-loading systems.

As 4H/TSC-minimum may be as small as 5 fm radius and charge neutral against many layers of shell electron clouds of Ni, it may rather easily penetrate through the Coulomb barrier to approach very close in several fm distance to Ni nucleus, as illustrated in Fig. 12, supposing momentum is given for TSC.

Since Ni K-shell is larger than that of Pd, TSC-induced Ni reaction is more plausible. And since 4H/TSC has much longer life-time than that of 4D/TSC-minimum, Ni + 4H/TSC fission process becomes more probable. Analysis of fission products of highly excited medium-heavy nuclei was proposed in [25]. Kobe–Technova group has made PIXE (particle induced X-ray emission) analysis of CNZ powder samples before and after use [18,19]. They have found visible increase of Ti and Zn in 'after' samples. Impurity was found also for Cr, Fe, and Ni, but these might be contaminants from reaction chamber made of SS304. In Fig. 13, we show typical clean fission products by,

$$^{62}\mathrm{Ni} + 4\mathrm{H} \rightarrow\ ^{66}\mathrm{Ge}^{*}(\mathrm{Ex} = 29\ \mathrm{MeV}) \rightarrow\ \text{Fission products}$$

and $^{64}\mathrm{Ni} + 4\mathrm{H} \rightarrow\ ^{68}\mathrm{Ge}^{*}(\mathrm{Ex} = 29\ \mathrm{MeV})$. ^{58}Ni + 4D/TSC will have similar FPs as Eq. (4).

If selective scission channels are dominant for near symmetric fragmentation channels, clean fission products by Ni + 4H induced fission are ^{20}Ne, ^{23}Na, ^{24}Mg, ^{27}Al, ^{28}Si, ^{32}S, ^{36}S, ^{38}Ar, ^{40}Ar, ^{39}K, ^{41}K, ^{42}Ca, ^{44}Ca, ^{45}Sc, ^{46}Ti, and ^{48}Ti; all are stable isotopes.

The sensitivity of PIXE is not enough for detecting lower Z element than Sc. As Kobe–Technova group [18,19] has found meaningful increase of Ti in CNZ samples after use, we shall wait for the analysis of sample by TOF-SIMS to search the lower Z elements, if any.

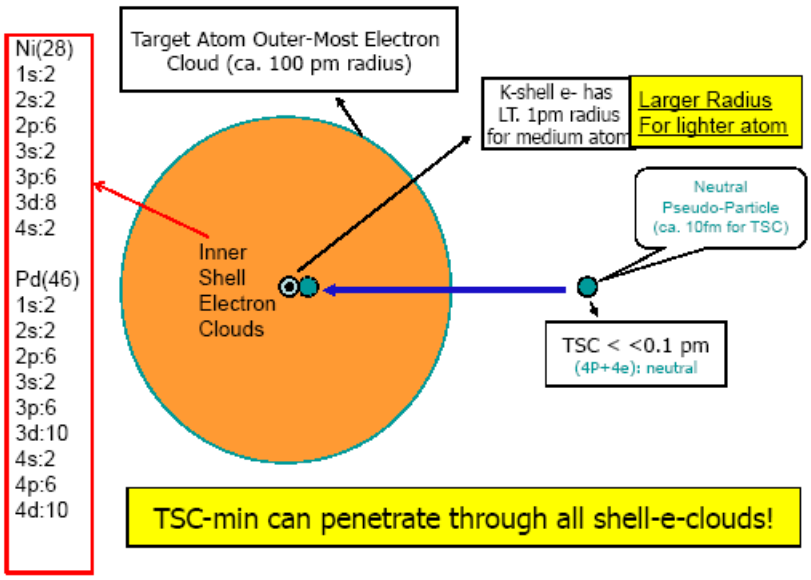

Figure 12. Image of barrier penetration of 4H/TSC-minimum through many layers of Ni shell electron clouds.

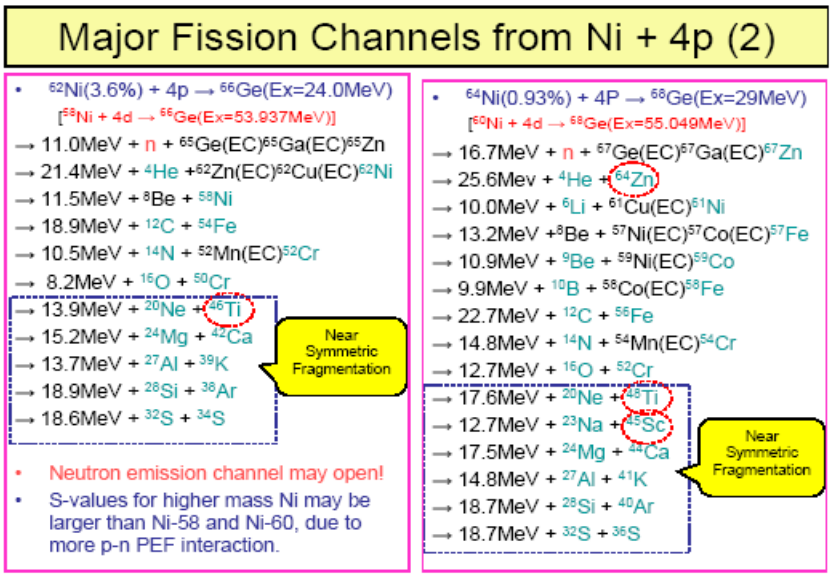

Figure 13. Typical radiation-less (clean) fission products by near symmetric fragmentation of ^{66}Ge*.

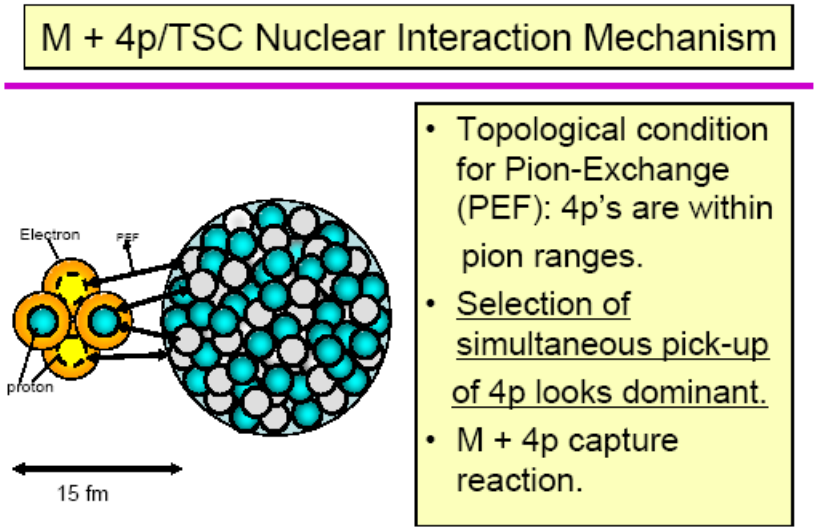

Figure 14. Image of strong interaction between 4H/TSC-minimum state and Ni nucleus.

In the previous paper [16], we considered 1p, 2p, 3p, and 4p pick-up processes in competition in the initial state nuclear interaction between 4H/TSC and Ni-nucleus. Now, we reconsider about the condition that simultaneous 4p capture to Ni is predominant because all four protons and surface nucleons of Ni-nucleus are within the range (1.4 fm of pion Compton wave length) of strong interaction (PEF) due to the further condensation of 4H/TSC to much smaller neutral entity (5 fm size) than the previous model. The image of such configuration is shown in Fig. 14. The nuclear reaction rate is estimated by the STTBA (sudden tall thin barrier approximation) method [16].

The clean fission process by Ni + 4H/TSC interaction is a plausible scenario for Ni–H systems, as 4H/TSC minimum has much longer life time than 4D/TSC-minimum.

Every fission event competes with the EM transition of deformed intermediate compound nucleus with high excited energy to emit cascade gamma-rays promptly. The ^{235}U + thermal-neutron fission (^{236}U* fission) competes with the ^{236}U* to ^{236}U (ground state) transition emitting gamma-rays, with [gamma]/[fission] = 98.7 b/585 b = 0.17 branching ratio [26]. Therefore, the gamma-ray emission level by U-fission is strong. Another example of fragmentation of lighter nuclei with high excited energy is the case of ^{6}Li + n to ^{7}Li* to t + α + 4.8 MeV competing with the EM channel ^{7}Li (gs) + γ. The branching ratio of [gamma]/[t] is 3.85×10^{-4} b/940.3 b = 4.1×10^{-7}: Very weak gamma emission in this case. In the case of ^{10}B + n to ^{11}B* to α+^{7}Li competing with the EM channel of ^{11}B (ground state) + γ, [γ]/[α] = 10^{-4}. We also know that the [γ]/[t] branching ratio for d–d fusion is ca. 10^{-7}. At the moment, we have no exact knowledge about [γ]/[fission] branching ratios for Ni-isotopes + 4H/TSC induced selective channel fragmentations.

The mystery of Iwamura claim of A-8 and Z-4 increased transmutation (Cs + 4d capture to Pr) [27] should be discussed, pertaining to the present discussions, but we will make it in other occasions.

There are other problems to study, e.g., such problem as how momentum (or velocity of the center-of-mass system) of 4H/TSC is generated at the TSC formation site to be able to approach a host metal nucleus locating nearby. The TSC formation at SNH on surface of nano-catalyst (see Fig. 5) may have a mechanism to generate TSC momentum.

6. Summary

The Ni + p nuclear reaction is impossibly difficult to make the Coulomb-field penetration of proton through so many inner electron shells (K, L, M), usually non-active in chemical reactions, of Ni-atom. And the proton capture with Ni-nucleus, if any, should emit lethal prompt gamma-rays which have never been observed. So, this type of nuclear reactions is unlikely.

Deuteron impurity (1/6700 in H_2 gas usually) may induce (3H+D)/TSC fusion to be considered. Conditioning of 3-dimesional symmetry of QM-wave function for TSC of H/D-mixed configuration is however of problem to make complete condensation into microscopic neutral entity small enough for causing any strong/weak nuclear interactions.

The newly proposed 4H/TSC WS (weak–strong interaction simultaneously) fusion is a plausible scenario to have clean products (^{3}He, deuteron and proton) with considerably enhanced reaction rates in Ni-nano-particles, for rare-conditioned (as discussed as 'dissipative') visible heat generation with very weak secondary neutrons (10^{-13} order of ^{3}He primary product) and gamma-rays (10^{-11} order of ^{3}He primary product). Degrees of the generation rate of 4H/TSC ($t = 0$) transient clusters in Ni–H nano-particles and the life-time elongation of 4H/TSC-minimum state are to be studied. Probably the damage of nano-catalyst by 4H/TSC WS fusion products is much lighter than that by 4D/TSC fusion products. This difference may make longer life of Cu–Ni binary nano-catalyst in cyclic auto-recovering of damaged catalyst, specifically for H-gas loading. So, this model may be explanation of clean heat for long time span as observed in CNZ samples to be the Ni–H nuclear effect. We shall wait for heat evolution data with Pd-based samples at elevated sample temperatures, whether the isotopic (D or H) difference is consistent with that with Ni-based samples or not.

The 4H/TSC + Ni-isotope capture-and-fission process, previously proposed in our paper [16] is another plausible scenario, to result in generation of clean fission products in $A < 60$ mass region. More enhanced 4p + Ni to fission rates than the previous prediction is expected due to the possible elongation of 4H/TSC-minimum-state life time without complete nuclear break-up of the symmetric cluster under dynamic condensation. However, we need further detailed analysis on predominant scission channels in Ni + 4H fission processes for Ni isotopes. Here, we need also the consistency search with experimental data of possible fission-like products by Pd + 4H systems, if any.

Acknowledgement

The author is grateful to Technova colleagues (A. Kitamura, R. Seto, and Y. Fujita) and Kobe University members (A. Taniike, Y. Miyoshi, H. Sakoh, and Y. Furuyama).

Appendix

A.1. Reviewer's Comments and Reply

Critical comments on the basic QM methodology on the TSC theory were thrown by a reviewer. This would raise a never-ending debate due to difference of individual approach. However, for the better understanding of readers, copy of commnets/reply is given below.

Thank you, reviewer for valuable comments. I (the author) reply as follows:

> Over the years Takahashi has been important contributions to the field, and we have great respect for him. He can take credit for numerous important experimental results; he has had a profound impact on the field in Japan; he has provided leadership for the International Society; and he continues to make an impact with new results, and with his contributions at conference meetings. Because of this, I take no satisfaction in drawing

attention in what follows to some issues in his theoretical approach to explaining the excess heat effect; it would be much preferred for his model to be free of such issues.

Right, albeit the compliment, the quality of original paper should be irrelevantly evaluated.

Basic issue

Takahashi and collaborators make use of Langevin equation for modeling the dynamics of atom clusters, which from our perspective should be able to give reliable answers in principle. We take issue with how this has been implemented in the models that Takahashi relies on. In particular, the electronic localization energy has not been properly accounted for. We can see this from a simple argument involving the scaling of the cluster size, which will take a few paragraphs in what follows to illustrate

The present paper discusses on how Ni + H nuclear reactions are possible. It uses the results of published papers in ACS LENRSB Vols. 1 and 2 by the author and extended to 4H/TSC condensation and possible nuclear reactions. The reviewer's comments are on the basis of these already published papers which made analysis with Langevin equations. As the author wrote in these published papers, the Langevin equations, quantum mechanically modified, have been solved for special geometric configurations of clusters constituted with deuterons and electrons, however using several steps of approximations. It has been done so because the immediate direct rigorous approach for the so many body dynamic problems is too complicated to solve.

This means that the rigor of the analyses should be checked by some proper ways later on. So the theory is not completed.

To this respect, comments by the reviewer are appreciated.

A.2. Classical Potential

If we first consider electrons and nuclei to be classical initially, then we could develop ai associated potential energy assuming fixed relative positions to obtain

$$V_{\text{tot}} = \left[\sum_{i<j} V\right]_{\text{nn}} + \left[\sum_{i<j} V_{ij}\right]_{\text{ee}} + \left[\sum_{ij} V_{ij}\right]_{\text{en}}, \tag{4}$$

where the first term is the (repulsive) Coulomb interaction between nuclei; the second is the (repulsive) Coulomb interaction between electrons; and the third is the (attractive) interaction between electrons and nuclei. This can be expanded out as

$$V_{\text{tot}} = \left[\sum_{i<j} \frac{Z_i Z_j e^2}{|R_i - R_j|}\right]_{\text{nn}} + \left[\sum_{i<j} \frac{e^2}{|r_i - r_j|}\right]_{\text{ee}} + \left[\sum_{ij} \frac{Z_i e^2}{|R_i - r_j|}\right]_{\text{en}}. \tag{5}$$

This gives the attractive interaction for the different cases considered by Takahashi and colleagues For example, in the case of d–e–d, we end up with

$$V_{\text{tot}} = -2\frac{e^2}{R_{\text{de}}} + \frac{e^2}{R_{\text{dd}}}, \tag{6}$$

which is in agreement with the result given in the ACS Volume 2 paper.

For tetrahedral symmetric condensation there are four D (or H) and four electrons assumed a the eight corners of a cube. If we assume that the distance between nearest neighbors is a then wh

$$V_{\text{tot}} = \left[6\frac{e^2}{\sqrt{2}a}\right]_{\text{ee}} - \left[4\left(3\frac{e^2}{a} + \frac{e^2}{\sqrt{3}a}\right)\right] = \left[6\sqrt{2} - \frac{4}{\sqrt{3}} - 12\right]\frac{e^2}{a} = -5.824\frac{e^2}{a} = -11.65IH\frac{a_0}{a}. \tag{7}$$

These classical attractive potentials appear in some of the models presented by Takahashi.

I agree.

A.3. Electronic Kinetic Energy

I remarked some years ago in the review of an earlier paper about the problem with the electronic kinetic energy in the models. To their credit, Takahashi and collaborators responded by including a contribution associated with the kinetic energy in their model. Unfortunately, their model does not appear to deal with localization properly as the collapse occurs in their model.

Consider for example an idealized version of the model where the electrons are localized at the corner of the cube (such localization is required, since delocalization will result in a severe reduction of the attractive term in the equation for V_{tot} above). Let us assume a simple Gaussian wave function for an electron at one corner of the form

$$\pi(\mathrm{r}) = \left[\frac{1}{\pi L^2}^{\frac{3}{2}}\right]\exp\left(-\frac{|\mathrm{r}-\mathrm{r}_0|^2}{2L^2}\right). \tag{8}$$

The associated kinetic energy for this electron is

$$\mathrm{KE} = \left\langle \pi(\mathrm{r}) \left| -\frac{\hbar^2\nabla^2}{2m_{\mathrm{e}}} \right| \pi(\mathrm{r}) \right\rangle = \frac{3\hbar^2}{4m_{\mathrm{e}}L^2}. \tag{9}$$

In order for the electron to remain localized as the collapse occurs, we require the size of the Gaussian to remain smaller than a

$$\sqrt{\langle \triangle x^2 \rangle} = \frac{L}{\sqrt{2}} \ll a. \tag{10}$$

If so, then the associate electronic kinetic energy must increase as a decreases

$$\mathrm{KE} \gg \frac{3\hbar^2}{4m_{\mathrm{e}}(2a^2)}. \tag{11}$$

I do not see what is a here. As written in my ACS papers, a synthesis of known electron wave functions (linear combination of coupled S-waves) for a d–e–e–d face of TSC was used as approximation, which however treated electron localization in QM way. I did not treat so far the electron wave functions as Gaussians. Gaussian wave-functions were employed only for deuterons (protons).

A.4. Potential and Kinetic Energy

If we augment the total classical potential with the electronic localization energy, then we may write for tetrahedral symmetric condensation an effective potential given by

$$V_{\text{eff}} = V_{\text{tot}} + 4\left(\frac{3\hbar^2}{4m_{\mathrm{e}}L^2}\right). \tag{12}$$

Next, let us pick a particular value for L which is the largest it could reasonably be consistent with some screening

$$L = \frac{a}{3}, \tag{13}$$

which leads to

$$\begin{aligned} V_{\text{eff}} &= V_{\text{tot}} + 27\frac{\hbar^2}{m_{\text{e}}a^2} \\ &= -5.824\frac{e^2}{a} + 27\frac{\hbar^2}{m_{\text{e}}a^2}. \end{aligned} \tag{14}$$

Well, this is a different approach from the author and seems less meaningful for me.

A.5. Equilibrium Condition

As the scale length a decreases, the kinetic energy increases faster than the Coulomb attraction. This suggests that there should be a minimum total Coulomb potential plus electron kinetic energy for some value of a. It seems interesting to solve for it. We find the minimum according to

$$\begin{aligned} \frac{\mathrm{d}}{\mathrm{d}a}V_{\text{eff}} &= \frac{\mathrm{d}}{\mathrm{d}a}\left[-5.824\frac{e^2}{a} + 27\frac{h^2}{m_{\text{e}}a^2}\right] \\ &= 5.824\frac{e^2}{a^2} - 54\frac{h^2}{m_{\text{e}}a^3} \\ &= 0 \end{aligned} \tag{15}$$

We solve to obtain

$$a = \frac{54}{5.824}\frac{\hbar^2}{m_{\text{e}}e^2} = 4.635a_0 = 2.45\ \text{Å} \tag{16}$$

This is not too far from the observed distance for tetra-hydrogen in a cryogenic argon matrix.

This is less meaningful, according to the ACS papers, as argued above. Argon has many inner shell electrons which should be properly treated in your case but not applicable to hydrogen isotopes which have 1S electron only and bare nucleus.

A.6. Discussion

Takahashrs model for the collapse of the tetrahedral symmetric arrangement of D or H and electrons would require electron localization commensurate with the size of the structure at any stage in the collapse. The electron kinetic energy associated with this electron localization very quickly becomes large, and makes the collapse energetically unfavorable below the Angstrom scale. Although Takahashi and collaborators have made an attempt to include the effect of the electronic kinetic energy in their formulation, this inclusion must be incomplete since they do not find what we might expect for the increase in the electronic kinetic energy as the spatial scale decreases.

I strongly encourage Takahashi to take this argument seriously, and to respond appropriately.

Discussion on this point is given in my paper at JCMNS Vol. 2: please see it: showing the dynamic TSC collapse is reasonable.

A. Takahashi, Dynamic mechanism of TSC condensation motion, *JCMNS* **2** (2009) 33–44. We have no stable (static) solutions there for TSC, as the reviewer argued in classical static way.

A.7. Other issue

There is one other issue that needs to be addressed in the paper. En many places Takahashi uses a language that seems to suggest that there is an issue for a proton to tunnel through electronic shells; for example:

> *The first main problem is of extreme difficulty for low energy (less than 5 keV) proton to penetrate through the thick multiple QM electron-cloud layers (K shells to M shells and) to get close enough to -make meaningful level strong interaction rate.*

I would think that the biggest issue is that the Coulomb repulsion between the proton charge and the charge of the metal nucleus is the big issue. The electrons provide screening, so that if you are outside many orbitals, the nuclear-nuclear interaction is screened. However, at close range when the proton is inside the outer shells, there can be essentially no screening from the outer electrons. In this case, the proton sees a very large repulsive potential.

This kind of wording appears several times in the paper, and would need to be fixed throughout.

Again, I have different view in atomic physics with inner shell electrons. The argued proton-nucleus Coulomb repulsion is irrelevant unless the proton passes through all the shell electrons surrounding nucleus. This is essential problem when people model Ni + H nuclear interaction, as simple plasma model for inner shell electrons is not rational in atomic physics and usual chemistry views.

Thank you for considerable comments. The essence of submitted paper is somewhat (or very much) off from the above discussions, however. It's pity.

(The second reviewer's comments and author's response are cut, for these contained unappropriate words for disclosure.)

References

[1] F. Piantelli, Hydrogen loading of nickel and related phenomena, Presentation 6th Int. Workshop on Anomalies in Hydrogen/Deuterium Loaded Metals, Siena 2005: http://www.iscmns.org/sien05/program.htm

[2] E. Campari et al:, Photon and particle emission, heat production and surface transformation in Ni–H system, Condensed Matter Nuclear Science, J. P. Biberian (Ed.), *Proc. ICCF11*, World Scientific, Singapore, pp. 405–413 (2004).

[3] S. Focardi et al., *Nuovo Cimento* **A111** (1998) 1233.

[4] G. Miley and J. Patterson, *J. New Energy* **1** (1996) 5.

[5] G. Miley and P. Shrestha, Overview of light water/hydrogen based low energy nuclear reactions, Condensed Matter Nuclear Science, *Proc. ICCF12*, A. Takahashi et al. (Eds.), World Scientific, Singapore, pp. 34−−43 (2005).

[6] Y. Arata and Y. Zhang, Special issue, *J. High Temp. Soc. Japan* **1** (2008).

[7] Y. Arata, Y. Zhang and X. Wang, Production of helium and energy in the 'solid fusion', *Proc. ICCF15*, Rome, Oct. 2009, V. Violante and F. Sarto (Eds.), ENEA, pp. 72–81.

[8] A. Kitamura, T. Nohmi, Y. Sasaki, A. Taniike, A. Takahashi, R. Seto and Y. Fujita, *Phys. Lett.* A **4** (2011) 3109–3112.

[9] A. Kitamura, A. Takahashi, R. Seto and Y. Fujita, *J. Condensed Matter Nucl. Sci.* **4** (2011) 56–68.

[10] A. Takahashi, R. Seto, Y. Fujita, A. Kitamura, Y. Sasaki, Y. Miyoshi and A. Taniike, *J. Condensed Matter Nucl. Sci.* **5** (2011) 17–33.

[11] A. Kitamura, Y. Miyoshi, H. Sakoh, A. Taniike, A. Takahashi, R. Seto and Y. Fujita, *J. Condensed Matter Nucl. Sci.* **5** (2011) 42–51.

[12] Y. Miyoshi et al., Hydrogen isotope absorption/adsorption characteristics of Pd–Zr oxide compounds, *Proc. JCF11*, pp. 10–15 (2011).
[13] H. Sakoh et al., Hydrogen absorption/adsorption characteristics of Ni–Pd binary nano-particles, *Proc. JCF11,* pp. 16–22 (2011).
[14] A. Takahashi et al., Mesoscopic catalyst and D-cluster fusion, *Proc. JCF11*, pp. .47–52 (2011).
[15] A. Takahashi, 4H/TSC fusion by simultaneous weak and strong interactions, *Proc. JCF12*, pp. 115–122 (2012).
[16] A. Takahashi, *JCNMS* 1 (2007) 86–96.
[17] A. Takahashi, *J. Condensed Matter Nucl. Sci.* 4 (2011) 269–281.
[18] Y. Miyoshi et al., Gas-phase hydrogen absorption/adsorption characteristics of a Ni-based sample, *Proc. JCF12*, pp. 1–9 (2012).
[19] A. Kitamura et al., Summary of the latest results of gas loading experiments, presented at 10th Int. Workshop on Anomalies in Hydrogen Loaded Metals, Siena, April 10–14, 2012 (see ISCMNS web-site Workshop/ppt presentations).
[20] A. Takahashi, The basics of deuteron cluster dynamics as shown by Langevin equation, American Chemical Society, Oxford University Press, LENRNET Sorcebook, Vol. 2, pp. 193–217 (2009).
[21] A. Widom and L. Larsen, *Eur. Phys. J.* **C46** (2006) 107.
[22] R. Mills, Identification of new hydrogen states, search his papers in internet.
[23] A. Muelenberg and K. Sinha, *J. Condensed Matter Nucl. Sci.* **4** (2011) 241–255.
[24] A. Takahashi, ^{3}He/^{4}He production ratios by tetrahedral symmetric condensation, Condensed Matter Nuclear Science, *Proc. ICCF11*, Marseille, J. Biberian (Ed.), World Scientific, Singapore, pp. 730–742 (2006).
[25] A. Takahashi, M. Ohta and T. Mizuno, *Japanese J. Appl. Phys.* **41** (2001) 7031.
[26] T. Nakagawa et al., Curves and Tables of Neutron Cross Sections in JENDL-3.3, JAERI-Data/Code 2002-020 Part-I and Part-II (2002).
[27] Y. Iwamura et al., *Japanese J. Appl. Phys*. **41** (2002) 4642.